



## 저작자표시-비영리-변경금지 2.0 대한민국

이용자는 아래의 조건을 따르는 경우에 한하여 자유롭게

- 이 저작물을 복제, 배포, 전송, 전시, 공연 및 방송할 수 있습니다.

다음과 같은 조건을 따라야 합니다:



저작자표시. 귀하는 원저작자를 표시하여야 합니다.



비영리. 귀하는 이 저작물을 영리 목적으로 이용할 수 없습니다.



변경금지. 귀하는 이 저작물을 개작, 변형 또는 가공할 수 없습니다.

- 귀하는, 이 저작물의 재이용이나 배포의 경우, 이 저작물에 적용된 이용허락조건을 명확하게 나타내어야 합니다.
- 저작권자로부터 별도의 허가를 받으면 이러한 조건들은 적용되지 않습니다.

저작권법에 따른 이용자의 권리는 위의 내용에 의하여 영향을 받지 않습니다.

이것은 [이용허락규약\(Legal Code\)](#)을 이해하기 쉽게 요약한 것입니다.

[Disclaimer](#)

약학박사 학위논문

**Insulin-mimetic and Neuroprotective  
Terpenoids from *Gynostemma longipes* and  
*Camellia japonica***

*Gynostemma longipes* 와 *Camellia  
japonica*로부터 인슐린 유사작용과  
뇌신경 세포보호 테페노이드 화합물

2019 년 2 월

서울대학교 대학원

약학과 생약학 전공

Ha Thi Kim Quy

**Insulin-mimetic and Neuroprotective Terpenoids  
from *Gynostemma longipes* and *Camellia japonica***

*Gynostemma longipes* 와 *Camellia  
japonica*로부터 인슐린 유사작용과 뇌신경 세포보호  
터페노이드 화합물

지도교수 오 원 근

이 논문을 약학박사 학위논문으로 제출함  
2019 년 1 월

서울대학교 대학원  
약학과 생약학전공  
Ha Thi Kim Quy

Ha Thi Kim Quy의 약학박사 학위논문을 인준함  
2019 년 1 월

위 원 장\_\_\_\_\_ (인)

부위원장\_\_\_\_\_ (인)

위 원\_\_\_\_\_ (인)

위 원\_\_\_\_\_ (인)

## Abstract

### **Insulin-mimetic and Neuroprotective Terpenoids from *Gynostemma longipes* and *Camellia japonica***

#### **Part 1**

Natural products are potential sources in the development of new classes for diabetes therapy. In the project of searching for antidiabetic substances from medicinal plants, a 95% ethanol fraction of *Gynostemma longipes*, an ethnomedicinal plant used to treat type 2 diabetes mellitus by local communities in Vietnam, was found to significantly increase glucose uptake using *in vitro* 2-NBDG assay. *Gynostemma longipes* (Cucurbitaceae family) was cultivated and collected in an herbal farm in the Ha Giang province of Vietnam. Recently, there are few studies on its chemical constituents and bioactivities. The chemical components of *G. longipes* are similar to species of *Gynostemma* genus which contain triterpenoids as major components. Therefore, the purpose of this research was performed the bioassay-guided fractionation and isolation of *G. longipes*. During this process, the purification of ten new triterpenes (**1–10**) were isolated, including three 3,4-*seco* dammarane (**1–3**), two hexanordammarane glycosides (**4** and **5**) and five other dammarane glycosides (**6–10**). All compounds were determined by the basis of spectroscopic analyses, including UV, IR, NMR, and MS/MS spectra. Isolated compounds (**1–10**) were then evaluated for their effect on glucose uptake in differentiated 3T3-L1 adipocyte cells using 2-NBDG,



as a fluorescent-tagged glucose probe. Among them, compounds **1**, **2**, **4**, and **8** showed particularly potent stimulatory effects through GLUT4 translocation. To investigate the underlying mechanism for the stimulation of 2-NBDG uptake into the cells by dammarane triterpenes from *G. longipes*, all isolates (**1–10**) were evaluated the stimulation effect on the AMPK pathway, which plays important role in glucose uptake regulation. It may be observed that compounds **1**, **2**, **4**, **8**, and **10** significantly up-regulated the expressions of phosphorylated AMPK and ACC in the mouse C2C12 myotubes. These results are consistent with ethnopharmacological report of *G. longipes* as a traditional medicine for treating diabetes.

## Part 2

*Camellia japonica* (Theaceae family) is an evergreen tree which widely cultivated in Korea, China, and Japan. Since the ancient times, the flower buds of *C. japonica* has been used for treating vomiting of blood and bleeding, tonic, anti-inflammatory. During *in vitro* screening of medicinal plants for neuroprotective effects on rotenone model of Parkinson's disease (PD), a 70% ethanol extract from the flowers of *C. japonica* was found as a potential hit. Accordingly, the goal of this study was successfully isolation of six new 3,4-seco-28-nor-oleanane triterpenoids (**11–16**) which based on bioassay-guided fractionation of this active extract. The molecular structures of these new triterpenoids were elucidated through extensive spectroscopic analyses, including UV, IR, high-resolution MS, NMR, and by spectral comparison with the published literature. Neuroprotective effect of isolated compounds was evaluated, and as a result, compounds **13–16** effectively protected against neurotoxicity in the human dopaminergic SH-SY5Y cell line. Among them, compound **15** was found to exhibit the strongest neuroprotective effect by suppressing of  $\alpha$ -synuclein expression and the intracellular production of reactive oxygen species (ROS) induced by rotenone treatment. Furthermore, this compound induced microtubule-associated protein 1A/1B-light chain 3 (LC3), a commonly used autophagy marker, and also reduced the condensation of chromosome induced by rotenone treatment. In conclusion, it was demonstrated that a new class of chemical entities for developing bioactive compounds for PD therapy.

---

**Keywords:** *Gynostemma longipes*, antidiabetic drugs, triterpenes, *Camellia japonica*, neuroprotective effects, Parkinson's disease.

**Student Number: 2015-30776**

# Table of Contents

<b>Abstract.....</b>	<b>i</b>
<b>List of Abbreviations .....</b>	<b>ix</b>
<b>List of Tables.....</b>	<b>i</b>
<b>List of Schemes.....</b>	<b>i</b>
<b>Part 1. Triterpenoid Constituents of <i>Gynostemma longipes</i> and Their Insulin Mimetic Activity.....</b>	<b>1</b>
1. Introduction.....	2
1.1. Diabetes disease .....	2
1.2. AMPK signaling pathway .....	6
1.3. <i>Gynostemma longipes</i> .....	11
1.4. Purpose of research.....	12
2. Materials and methods.....	13
2.1. Plant materials .....	13
2.2. Chemicals, reagents and chromatography .....	14
2.3. Extraction and isolation schemes .....	16
2.4. Chemical and spectral properties of isolated compounds .....	19
2.5. Differentiation of 3T3-L1 adipocytes .....	27
2.6. Measurement of cell viability.....	27
2.7. Measurement of 2-NBDG uptake.....	28
2.8. Measurement of GLUT4 translocation .....	29

2.9. Measurement of <i>p</i> -AMPK and <i>p</i> -ACC in C2C12 myotubes.....	30
2.10. Statistical analysis .....	30
3. Results and discussion.....	32
3.1. Structural elucidation of isolated compounds ( <b>1–10</b> ).....	32
3.2. Insulin mimetic activity of triterpenoids from <i>G. longipes</i> .....	84
4. Conclusions.....	102
<b>Part 2. Neuroprotective Effects of Triterpenes from <i>Camellia japonica</i> in a Rotenone Model of Parkinson’s Disease.....</b>	<b>104</b>
1. Introduction.....	105
1.1. Parkinson’s disease.....	105
1.2. Rotenone-induced Parkinson’s disease model .....	106
1.3. Structure and aggregation of $\alpha$ -synuclein in PD .....	108
1.4. The role of light chain 3 (LC3) in autophagy.....	110
1.5. <i>Camellia japonica</i> .....	112
1.6. Purpose of research.....	114
2. Materials and methods.....	115
2.1. Plant materials .....	115
2.2. Chemicals, reagents and chromatography .....	115
2.3. Extraction and isolation schemes .....	115
2.4. Chemical and spectral properties of isolated compounds .....	118
2.5. Cytotoxicity assay .....	122

2.6. Quantitative real-time PCR.....	123
2.7. Western blot analysis.....	124
2.8. Measurement of intracellular ROS levels .....	124
2.9. Confocal immunostaining.....	125
2.10. Statistical analysis .....	125
3. Results and discussion.....	126
3.1. Structural elucidation of isolated compounds ( <b>11–16</b> ).....	126
3.2. Neuroprotective effect of compounds <b>11–16</b> on rotenone-induced neurotoxicity of SH-SY5Y cells .....	146
3.3. Effects of compounds <b>15</b> on $\alpha$ -synuclein expression induced by rotenone treatment .....	148
3.4. Effects of compound <b>15</b> on intracellular ROS production in a rotenone treatment model .....	153
3.5. Compound <b>15</b> reduced the condensation of chromosome induced by rotenone treatment.....	154
4. Conclusions.....	157
<b>References .....</b>	<b>158</b>
<b>국문초록 .....</b>	<b>169</b>

## List of Abbreviations

2-NBDG: 2-[N-(7-nitrobenz-2-oxa-1,3-diazol-4-yl)amino]-2-deoxy-D-glucose

$[\alpha]_D^{25}$ : Specific rotation at 25 Celsius degrees

AMPK: AMP-activated protein kinase

Akt/PKB: Protein kinase B

CC: column chromatography

$\text{CDCl}_3$ : deuteriochloroform

$\text{CH}_3\text{CN}$ : acetonitrile

CNS: Central nervous system

d: doublet

DAPI: 4',6-diamidino-2-phenylindole

DCFDA: 2',7'-dichlorofluorescein diacetate

dd: double of doublet

DM: Diabetes mellitus

DMEM: Dulbecco's modified Eagle's medium

DMSO: dimethyl sulfoxide

EDTA: ethylenediaminetetraacetic acid

EtOAc: ethyl acetate

EtOH: ethanol

FBS: Fetal bovine serum

GLP: *Gynostemma longipes* precipitated

GLS: *Gynostemma longipes* soluble

GLUT4: Glucose transporter 4

HMBC: Heteronuclear Multiple Bond Correlation

HPLC: High Performance Liquid Chromatography

HRESIMS: High-resolution electrospray ionization mass spectrometry

HSQC: Heteronuclear Single Quantum Coherence

Hx: Hexane

Hz: Hertz

IHD: Indices of hydrogen deficiency

IR: Infrared (spectrum)

KBNMB: Korea Bioactive Natural Material Bank

LC3: Light chain 3

m: multiplet

MeOH: methanol

MTT: 3-(4,5-dimethyl-2-thiazolyl)-2,5-diphenyl-2*H*-tetrazolium bromide



*m/z*: Mass to charge ratio

NaF: Sodium fluoride

NMR: Nuclear magnetic resonance

NOESY: Rotating frame nuclear Overhauser Effect Spectroscopy

NP: Normal-phase (silica gel)

PBS: Phosphate buffered saline

PD: Parkinson's disease

PI3K: Phosphatidylinositol 3-kinase

PVDF: Polyvinylidene fluoride

ROS: Reactive oxygen species

RP-C<sub>18</sub>: C<sub>18</sub>-reversed phase silica gel

s: singlet

t: triplet

T1DM: Type 1 diabetes mellitus

T2DM: Type 2 diabetes mellitus

TLC: Thin-layer chromatography

*t<sub>R</sub>*: Retention time

UV: Ultraviolet (spectrum, detector)



## List of Figures

Figure 1. The global epidemic of diabetes from 2010 to 2030.....	2
Figure 2. The therapeutic targets in type 2 diabetes mellitus organized per tissue...	5
Figure 3. Functional domains of three AMPK subunits.....	7
Figure 4. Role of AMPK in regulation of energy homeostasis in whole-body. ....	9
Figure 5. Authentication of <i>G. longipes</i> based on morphology.....	12
Figure 6. <sup>1</sup> H and <sup>13</sup> C NMR of compound <b>1</b> (pyridine- <i>d</i> <sub>5</sub> , 500 MHz/125 MHz).....	34
Figure 7. HSQC (H→C) of compound <b>1</b> (pyridine- <i>d</i> <sub>5</sub> , 500 MHz).....	35
Figure 8. HMBC (H→C) of compound <b>1</b> (pyridine- <i>d</i> <sub>5</sub> , 500 MHz).....	36
Figure 9. COSY (H↔H) of compound <b>1</b> (pyridine- <i>d</i> <sub>5</sub> , 500 MHz). ....	37
Figure 10. NOESY (H↔H) of compound <b>1</b> (pyridine- <i>d</i> <sub>5</sub> , 500 MHz).....	38
Figure 11. <sup>1</sup> H and <sup>13</sup> C NMR of compound <b>2</b> (pyridine- <i>d</i> <sub>5</sub> , 500 MHz/125 MHz)....	40
Figure 12. HSQC (H→C) of compound <b>2</b> (pyridine- <i>d</i> <sub>5</sub> , 500 MHz).....	41
Figure 13. HMBC (H→C) of compound <b>2</b> (pyridine- <i>d</i> <sub>5</sub> , 500 MHz).....	42
Figure 14. COSY (H↔H) of compound <b>2</b> (pyridine- <i>d</i> <sub>5</sub> , 600 MHz). ....	43
Figure 15. NOESY (H↔H) of compound <b>2</b> (pyridine- <i>d</i> <sub>5</sub> , 600 MHz).....	44
Figure 16. <sup>1</sup> H and <sup>13</sup> C NMR of compound <b>3</b> (pyridine- <i>d</i> <sub>5</sub> , 500 MHz/125 MHz)....	46
Figure 17. HMBC (H→C) of compound <b>3</b> (pyridine- <i>d</i> <sub>5</sub> , 500 MHz).....	47
Figure 18. HSQC (H→C) of compound <b>3</b> (pyridine- <i>d</i> <sub>5</sub> , 500 MHz).....	48

Figure 19. $^1\text{H}$ and $^{13}\text{C}$ NMR of compound <b>4</b> (pyridine- $d_5$ , 600 MHz/150 MHz)....	51
Figure 20. HMBC (H $\rightarrow$ C) of compound <b>4</b> (pyridine- $d_5$ , 500 MHz).....	52
Figure 21. HSQC (H $\rightarrow$ C) of compound <b>4</b> (pyridine- $d_5$ , 600 MHz).....	53
Figure 22. $^1\text{H}$ and $^{13}\text{C}$ NMR of compound <b>5</b> (pyridine- $d_5$ , 600 MHz/150 MHz)....	55
Figure 23. HMBC (H $\rightarrow$ C) of compound <b>5</b> (pyridine- $d_5$ , 500 MHz).....	56
Figure 24. HSQC (H $\rightarrow$ C) of compound <b>5</b> (pyridine- $d_5$ , 600 MHz).....	57
Figure 25. $^1\text{H}$ and $^{13}\text{C}$ NMR of compound <b>6</b> (pyridine- $d_5$ , 600 MHz/150 MHz)....	59
Figure 26. HMBC (H $\rightarrow$ C) of compound <b>6</b> (pyridine- $d_5$ , 600 MHz).....	60
Figure 27. HSQC (H $\rightarrow$ C) of compound <b>6</b> (pyridine- $d_5$ , 600 MHz).....	61
Figure 28. $^1\text{H}$ and $^{13}\text{C}$ NMR of compound <b>7</b> (pyridine- $d_5$ , 600 MHz/150 MHz)....	63
Figure 29. HMBC (H $\rightarrow$ C) of compound <b>7</b> (pyridine- $d_5$ , 600 MHz).....	64
Figure 30. HSQC (H $\rightarrow$ C) of compound <b>7</b> (pyridine- $d_5$ , 600 MHz).....	65
Figure 31. $^1\text{H}$ and $^{13}\text{C}$ NMR of compound <b>8</b> (pyridine- $d_5$ , 800 MHz/200 MHz)....	67
Figure 32. HMBC (H $\rightarrow$ C) of compound <b>8</b> (pyridine- $d_5$ , 800 MHz).....	68
Figure 33. HSQC (H $\rightarrow$ C) of compound <b>8</b> (pyridine- $d_5$ , 800 MHz).....	70
Figure 34. $^1\text{H}$ and $^{13}\text{C}$ NMR of compound <b>9</b> (pyridine- $d_5$ , 500 MHz/125 MHz)....	72
Figure 35. HMBC (H $\rightarrow$ C) of compound <b>9</b> (pyridine- $d_5$ , 500 MHz).....	73
Figure 36. HSQC (H $\rightarrow$ C) of compound <b>9</b> (pyridine- $d_5$ , 500 MHz).....	74

Figure 37. $^1\text{H}$ and $^{13}\text{C}$ NMR of compound <b>10</b> (pyridine- $d_5$ , 600 MHz/150 MHz)..	76
Figure 38. HMBC (H $\rightarrow$ C) of compound <b>10</b> (pyridine- $d_5$ , 600 MHz).....	77
Figure 39. HSQC (H $\rightarrow$ C) of compound <b>10</b> (pyridine- $d_5$ , 600 MHz).....	78
Figure 40. COSY (H $\leftrightarrow$ H) of compound <b>10</b> (pyridine- $d_5$ , 600 MHz).....	79
Figure 41. NOESY (H $\leftrightarrow$ H) of compound <b>10</b> (pyridine- $d_5$ , 600 MHz). ....	80
Figure 42. Structures of ten compounds isolated from <i>G. longipes</i> . ....	81
Figure 43. Key COSY and HMBC correlations of compounds <b>1</b> , <b>2</b> , <b>4</b> , <b>7</b> , <b>8</b> , and <b>10</b> . .....	82
Figure 44. Key NOESY correlations of the dammarane skeletons of compounds <b>1</b> , <b>4</b> , <b>8</b> , and <b>10</b> . ....	83
Figure 45. The cytotoxicity effect of compounds <b>1–10</b> 40 $\mu\text{M}$ (A) and compound <b>10</b> at different concentrations (B) in 3T3-L1 adipocytes.....	85
Figure 46. The cytotoxicity effect of all isolates <b>1–10</b> at 40 $\mu\text{M}$ (A) and <b>10</b> at various concentrations (B) on C2C12 myoblasts. ....	86
Figure 47. Stimulation effect of isolates from <i>G. longipes</i> on 2-NBDG uptake in 3T3-L1 adipocytes. ....	88
Figure 48. Enhancement of glucose uptake by compounds <b>1–10</b> in 3T3-L1 adipocytes using a fluorescent analogue of glucose (2-NBDG). ....	89
Figure 49. Concentration-response relationships of the effects of several compounds on 2-NBDG in 3T3-L1 adipocytes. ....	90
Figure 50. Effect of strong candidates ( <b>1</b> , <b>2</b> , <b>4</b> , and <b>8</b> ) on the translocation of GLUT4 into the plasma membrane of adipocytes.....	92

Figure 51. Isolated compounds from <i>G. longipes</i> induced the translocation of GLUT4 to the plasma membrane of 3T3-L1 adipocytes; original uncropped blots. ....	93
Figure 52. Effect of isolated compounds <b>1–10</b> on <i>p</i> -AMPK (Thr <sup>172</sup> ) and <i>p</i> -ACC (Ser <sup>79</sup> ) in differentiated mouse C2C12 skeletal myoblasts. ....	96
Figure 53. The effect of compounds <b>1–10</b> on <i>p</i> -AMPK Thr <sup>172</sup> and <i>p</i> -ACC Ser <sup>79</sup> in mouse C2C12 myotubes; original uncropped blots. ....	97
Figure 54. The effect of compounds <b>1, 2, 4, and 8</b> at different concentrations (5 and 10 $\mu$ M) on the phosphorylation of AMPK (Thr <sup>172</sup> ) and ACC (Ser <sup>79</sup> ) in differentiated mouse C2C12 skeletal myoblasts. ....	99
Figure 55. Activation effects of compounds <b>1, 2, 4, and 8</b> from <i>G. longipes</i> on the phosphorylation of AMPK Thr <sup>172</sup> and ACC Ser <sup>79</sup> in C2C12 myotubes; original uncropped blots. ....	100
Figure 56. The etiology of Parkinson's disease. ....	107
Figure 57. Mechanism of rotenone induced apoptosis. ....	108
Figure 58. Schematic diagram illustrating the steps of autophagy. ....	111
Figure 59. <i>Camellia japonica</i> Linnaeus var. <i>japonica</i> . ....	113
Figure 60. <sup>1</sup> H and <sup>13</sup> C NMR of compound <b>11</b> (pyridine- <i>d</i> <sub>5</sub> , 500 MHz/125 MHz). ....	128
Figure 61. HMBC of compound <b>11</b> (pyridine- <i>d</i> <sub>5</sub> , 500 MHz). ....	129
Figure 62. Key HMBC (H→C) and ROESY correlations for compounds <b>11, 14, and 16</b> . ....	130
Figure 63. <sup>1</sup> H and <sup>13</sup> C NMR of compound <b>12</b> (methanol- <i>d</i> <sub>4</sub> , 500 MHz/125 MHz). ....	132

Figure 64. HMBC of compound <b>12</b> (methanol- <i>d</i> <sub>4</sub> , 500 MHz).....	133
Figure 65. <sup>1</sup> H and <sup>13</sup> C NMR of compound <b>13</b> (methanol- <i>d</i> <sub>4</sub> , 600 MHz/150 MHz). .....	135
Figure 66. HMBC of compound <b>13</b> (methanol- <i>d</i> <sub>4</sub> , 600 MHz).....	136
Figure 67. <sup>1</sup> H and <sup>13</sup> C NMR of compound <b>14</b> (acetone- <i>d</i> <sub>6</sub> , 500 MHz/125 MHz).	138
Figure 68. HMBC of compound <b>14</b> (acetone- <i>d</i> <sub>6</sub> , 500 MHz). ....	139
Figure 69. <sup>1</sup> H and <sup>13</sup> C NMR of compound <b>15</b> . ....	141
Figure 70. HMBC of compound <b>15</b> (methanol- <i>d</i> <sub>4</sub> , 600 MHz).....	142
Figure 71. <sup>1</sup> H and <sup>13</sup> C NMR of compound <b>16</b> (acetone- <i>d</i> <sub>6</sub> , 500 MHz/125 MHz).	144
Figure 72. HMBC of compound <b>16</b> (acetone- <i>d</i> <sub>6</sub> , 500 MHz). ....	145
Figure 73. Six 3,4- <i>seco</i> -28-nor-oleanane triterpenoids ( <b>11–16</b> ) from <i>C. japonica</i> . .....	146
Figure 74. Effects of compounds <b>11–16</b> on rotenone-induced cytotoxicity in SH-SY5Y cells.....	147
Figure 75. Relative mRNA and protein expression levels of $\alpha$ -synuclein against SH-SY5Y cells.....	149
Figure 76. Effects of compound <b>13</b> and <b>15</b> on the protein expressions of $\alpha$ -synuclein; original uncropped blots. ....	151
Figure 77. Inhibition of intracellular ROS production by compound <b>15</b> . SH-SY5Y cells were pre-treated with or without compound <b>15</b> for 24 h. ....	153
Figure 78. Compound <b>15</b> reduced the condensation of chromosome induced by rotenone treatment in HEK293 cells stably expressing GFP-LC3 measured by the immunocytochemistry method.....	155

Figure 79. Compound <b>15</b> (20 $\mu$ M) reduced the condensation of chromosome induced by rotenone treatment in HEK293 cells. ....	156
--	-----



## List of Tables

Table 1. Staging of type 1 diabetes.....	3
Table 2. AMPK activators from natural products.....	10
Table 3. <sup>1</sup> H NMR spectroscopic data for compounds <b>1–10</b> . ....	22
Table 4. <sup>13</sup> C NMR spectroscopic data for compounds <b>1–10</b> . ....	25
Table 5. The functions of $\alpha$ -synuclein .....	109
Table 6. NMR spectroscopic data for compounds <b>11–13</b> . ....	120
Table 7. NMR spectroscopic data for compounds <b>14–16</b> . ....	121

## List of Schemes

Scheme 1. The bio-guided isolation strategy of <i>G. longipes</i> plant. ....	13
Scheme 2. Extraction and fractionation of <i>G. longipes</i> . ....	17
Scheme 3. Isolation scheme of 95% EtOH fraction of <i>G. longipes</i> . ....	19
Scheme 4. The bio-guided isolation strategy of <i>C. japonica</i> flowers. ....	114
Scheme 5. Extraction and fractionation of <i>C. japonica</i> . ....	116
Scheme 6. Isolation scheme of <i>n</i> -BuOH fraction of <i>C. japonica</i> . ....	117

**Part 1. Triterpenoid Constituents of *Gynostemma*  
*longipes* and Their Insulin Mimetic Activity**

# 1. Introduction

## 1.1. Diabetes disease

### 1.1.1. Diabetes mellitus

Diabetes mellitus (DM) is one of the most serious metabolic diseases and rapidly increases in the population aging (Zimmet et al., 2001). During the past three decades, the number of patients across the world rise more than doubled. In 2010, it is estimated that more than 285 million people worldwide suffered from diabetes in the 20-79 year age group and 90% of whom have type 2 diabetes mellitus (Chen et al., 2012; Danaei et al., 2011). In particular, it also projected that around 439 million people could be afflicted with diabetes in 2030 (Figure 1) (Chen et al., 2012). Therefore, future research for the treatment of type 2 diabetes mellitus is necessary to develop the program of health promotion and disease prevention in the community.

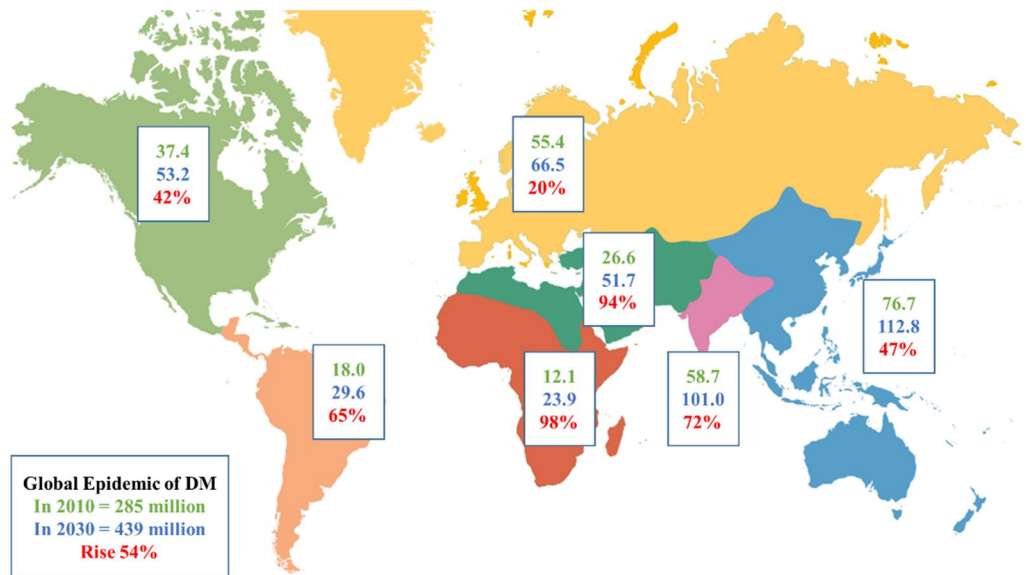


**Figure 1.** The global epidemic of diabetes from 2010 to 2030 (Chen et al., 2012).

### 1.1.2. Classification of diabetes

Recently, diabetes is classified into three main types: type 1 diabetes (also called as insulin-dependent diabetes), type 2 diabetes (known as non-insulin-dependent diabetes), and gestational diabetes (ADA, 2017; Bellamy et al., 2009). In addition, there have other specific types of diabetes which could be known as monogenic diabetes syndromes including neonatal diabetes, maturity-onset diabetes of the young, diseases of the exocrine pancreas, and drug- or chemical-induced diabetes (ADA, 2017).

Firstly, type 1 diabetes mellitus (T1DM), also known as juvenile-onset diabetes, results from the destruction of autoimmune  $\beta$ -cells in the pancreas. Eventually, the pancreas no longer secretes enough insulin and then glucose level in the bloodstream significantly increases. Therefore, many organ systems of the body could be damaged during three stages of disease (Table 1). Nowadays, several studies demonstrated that T1D presents not only in children with typical symptoms of polyuria/polydipsia and diabetic ketoacidosis but also in adults with classic symptoms similar to children. Even though the methods for distinguishing the type of diabetes still complicated, recent advances in diagnosis are developed over time (ADA, 2017).

**Table 1.** Staging of type 1 diabetes (ADA, 2017).

Stage 1	Stage 2	Stage 3
Autoimmunity	Autoimmunity	New-onset hyperglycemia

Symptom	Normoglycemia	Dysglycemia	Symptomatic
	Presymptomatic	Presymptomatic	

---

Secondly, type 2 diabetes mellitus (T2DM), also called adult-onset diabetes, which is the most common form of the disease. At diagnosis, T2DM affects around 90% of all patients with diabetes. This disease is caused by both genetic and lifestyle factors. However, the lifestyle factors such as inactivity, excess weight gain, sleep deprivation, dietary fat, and carbohydrates play an important role in the development of T2D with some symptoms (insulin resistance, hypertension, hyperglycaemia, and dyslipidaemia) (Ardisson Korat et al., 2014; Marín-Peñalver et al., 2016). Recently, several novel medications are in development based on different tissues (Figure 2) (DeFronzo et al., 2015). Therefore, the clinical treatment approach for T2D includes some methods:

- Lifestyle changes.
- Oral agents: (1) metformin – activation of AMP-activated protein kinase (AMPK) pathway; (2) insulin secretagogues (sulfonylureas and meglitinides) – increasing insulin secretion; (3)  $\alpha$ -glucosidase inhibitors – reducing postprandial triglycerides; (4) thiazolidinediones – increasing insulin sensitivity; (5) dipeptidyl peptidase-4 inhibitors – enhancing islet function and glycaemic control; (6) sodium glucose co-transporter-2 inhibitor – reducing the reabsorption of glucose.
- Injectable agents: exenatide, lixisenatide, liraglutide, albiglutide, dulaglutide.

Especially, older people with diabetes have a risk of death by hypoglycaemia than other age groups. Therefore, the treatment for elderly patients is similar to that of younger patients, but preventing the side effects is an important part of diabetic treatment, ensuring a better quality of life, and reducing the risk of falls (Marín-Peñalver et al., 2016).

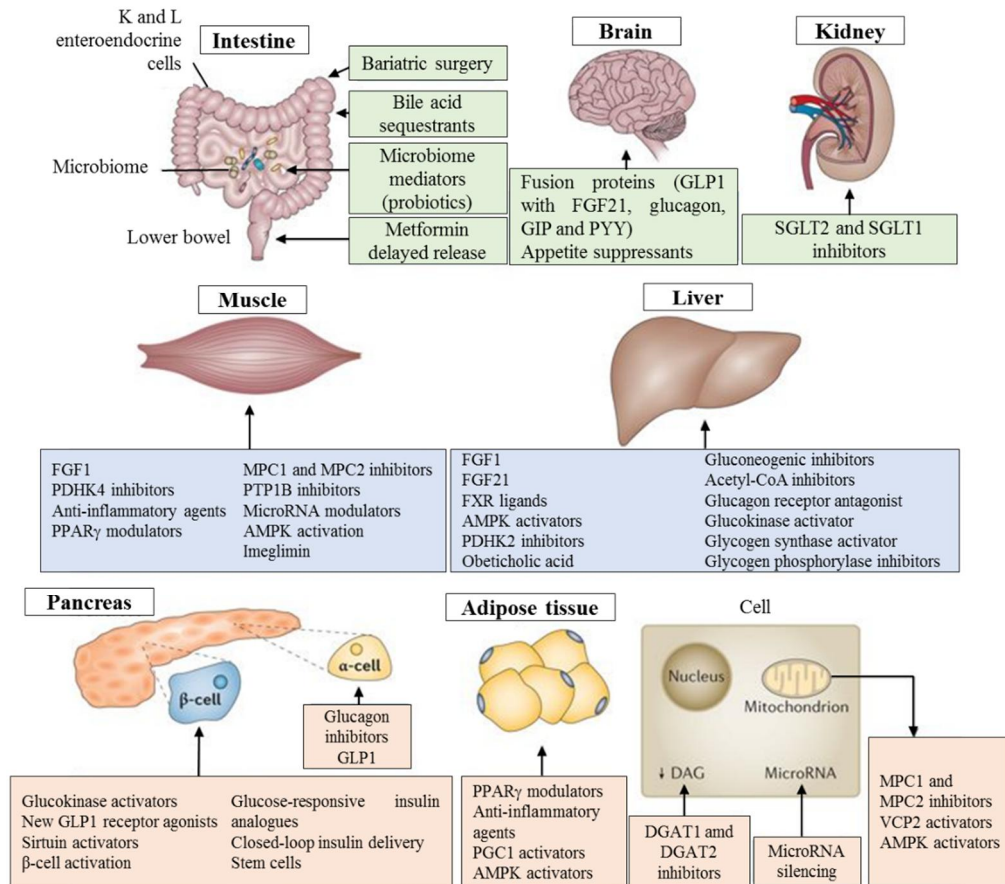


**Figure 2.** The therapeutic targets in type 2 diabetes mellitus organized per tissue (DeFronzo et al., 2015).

Finally, gestational diabetes only occurs during pregnancy. Glucose homeostasis of women could be restored to non-pregnancy levels after delivery. However, patients with gestational diabetes can develop to T2DM if the self-care and overall diet are not considered (Bellamy et al., 2009).

## 1.2. AMPK signaling pathway

### 1.2.1. AMPK protein

AMPK is one of the central regulators of cellular and it plays a critical role in the balance of systemic energy (Mihaylova and Shaw, 2012). In eukaryotes, AMPK protein contains a catalytic  $\alpha$ -subunit ( $\alpha 1$  and  $\alpha 2$ ) and two regulatory  $\beta$ - and  $\gamma$ -subunits ( $\beta 1$ ,  $\beta 2$  and  $\gamma 1$ ,  $\gamma 2$ ,  $\gamma 3$ ) (Figure 3) (Hardie et al., 2012a; Kim et al., 2016; Ruderman et al., 2013). AMPK regulates multiple metabolic pathways in whole-body (including skeletal muscle, heart, liver, adipose cells, pancreatic  $\beta$  cells, the brain) that can control the uptake/storage/utilization of glucose and lipid (Figure 4) (Kahn et al., 2005). Many studies demonstrated that AMPK pathway plays a potential role in the treatment of T2D and metformin widely used for activation of AMPK in clinical therapy (Hardie et al., 2012b). Thus, it is necessary to search new anti-diabetic drugs through the activation of the AMPK pathway.



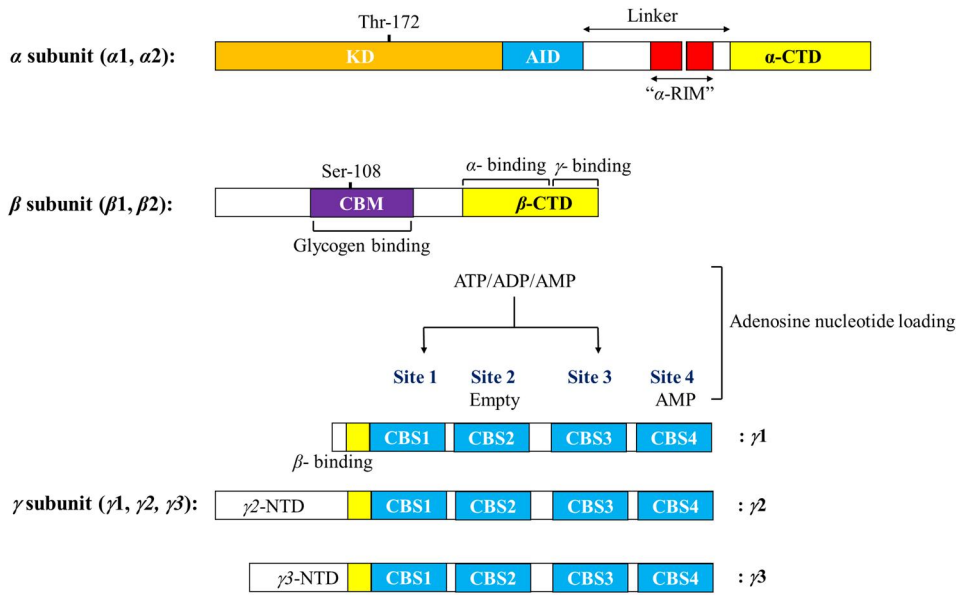


**Figure 3.** Functional domains of three AMPK subunits (Kim et al., 2016).

### 1.2.2. AMPK regulates glucose transporter 4 (GLUT4) translocation

The mechanism for stimulation the glucose uptake in peripheral tissues is necessary to decrease the glucose level in the bloodstream for management of T2DM (Krook et al., 2004). GLUT4 is a major mediator which is responsible for insulin-regulated glucose uptake into muscle and adipose tissue. The decreased expression and translocation of GLUT4 is a characteristic of patients with T2DM. Therefore, increasing the translocation and expression of GLUT4 is the potential approaches for anti-diabetic drug discovery (Huang and Czech, 2007). Both insulin receptor signaling and exercise are essential for recruitment of GLUT4 of the cell surface of adipocytes and muscles. (Herman and Kahn, 2006; Stanford and Goodyear, 2014). Moreover, in the insulin signal transduction pathway, the secretion of insulin from the pancreas and it is bound to a plasma-membrane-localized receptor. This complex activates the downstream signaling pathways,

including (i) phosphatidylinositol 3-kinase (PI3K) - an intracellular signaling pathway which regulates the cell survival, proliferation, and differentiation; (ii) protein kinase B (Akt/PKB) - a regulator of cell survival and apoptosis. The activation of Akt/PKB pathway plays an important role for stimulation of glucose uptake and the translocation of GLUT4 transporter in 3T3-L1 adipocytes because it stimulates the membrane translocation of the glucose transporter, GLUT4, to increase glucose uptake in 3T3-L1 adipocytes (Kim and Wands, 2010). In addition, the strong link between the physical exercise and caloric restriction have found to induce glucose transport through the AMPK signaling pathway.

Therefore, the activation AMPK signaling pathway is successfully used for treatment the deficiency of insulin, the disorder of insulin receptor, and metabolic syndrome-related diseases (Richter and Ruderman, 2009; Ruderman et al., 2013). Finally, the stimulation of AMPK rapidly promotes the glucose uptake via the translocation of GLUT1 and GLUT4 and enhances the GLUT4 expression (Newman and Cragg, 2016; O'Neill, 2013).

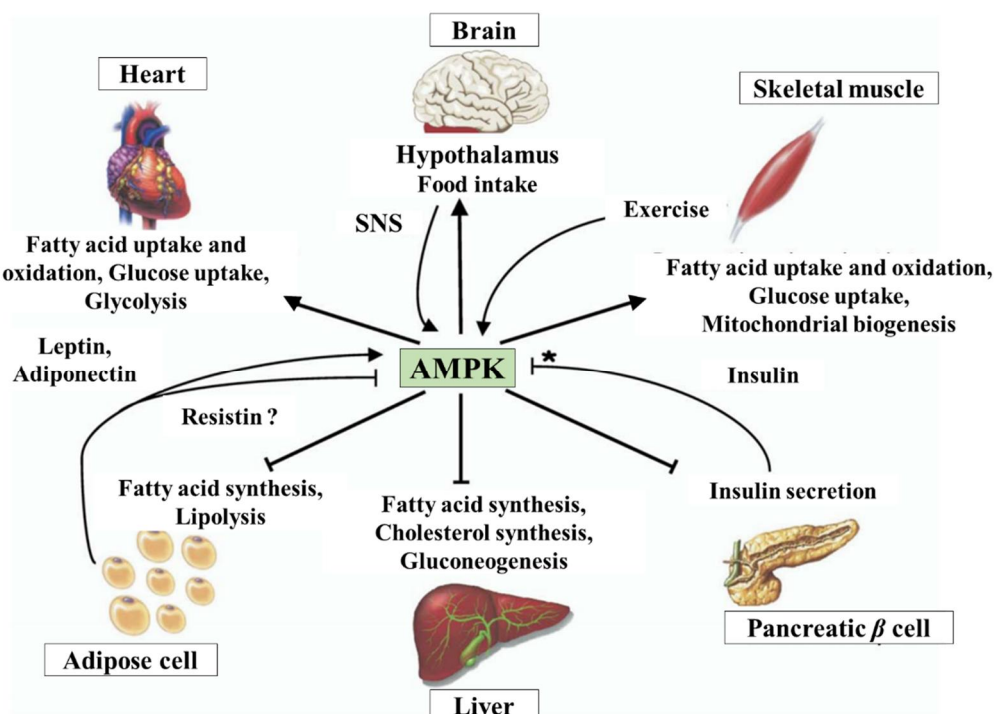


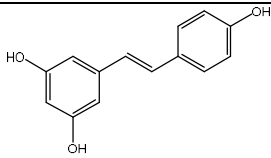
**Figure 4.** Role of AMPK in regulation of energy homeostasis in whole-body (Newman and Cragg, 2016).

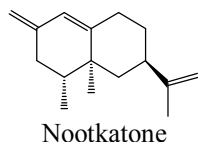
### 1.2.3. AMPK activators from natural products

Natural products are rich sources of antidiabetic drugs that play significant roles in the development of new antidiabetic agents (Table 2) (Nasir Uddin et al., 2013). Especially, triterpene class is known as a potential agent due to the stimulating the glucose uptake through enhancing GLUT4 translocation and AMPK activation. Among them, platyconic acid, a triterpene glycoside from the roots of *Platycodon*

*grandiflorum*, significantly increased the level of glucose uptake in adipocyte cell model and enhanced glucose homeostasis in T2D of mice (Kwon et al., 2012). Several studies indicated that damulins A and B, dammarane triterpenoids, which isolated from *Gymnostemma pentaphyllum* significantly enhanced the 2-deoxyglucose uptake and GLUT4 translocation to the cell membrane of L6 myotube cells (Nguyen et al., 2011). Recently, around 150 dammarane triterpenoids were successfully isolated from the genus *Gynostemma*. However, there are just two dammarane compounds were reported from *Gynostemma pentaphyllum*, including 21-norgypenoside A and B (Yang et al., 2013).

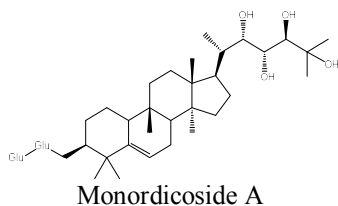
**Table 2.** AMPK activators from natural products (Nasir Uddin et al., 2013).

Compound	Plant source	Proposed Therapeutic Use
 Resveratrol	<i>Vitis amurensis</i>	Effect on anti-diabetic and anti-obesity



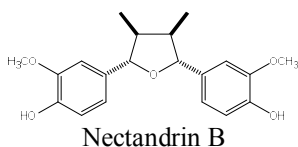
*Citrus paradisi*

Treatment of anti-diabetic, anti-obesity as well as exercise substituting agent



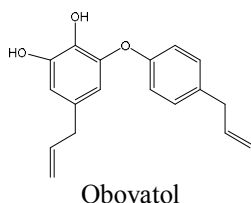
*Momordica charanita*

To prevent and treat diabetes and obesity



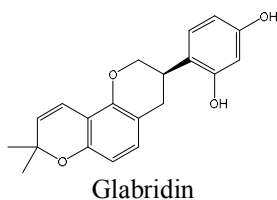
*Myristica fragrans*

Treating metabolic syndrome (obesity, diabetes, and hyperlipidemia)



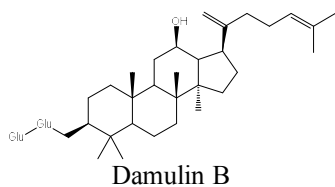
*Magnolia obovata*

Treating high blood sugar (hyperlipidemia)



*Glycyrrhiza glabra*

Treatment the excessive accumulation of surplus calories in the body



*Gynostemma pentaphyllum*

Anti-diabetes and anti-obesity

### 1.3. *Gynostemma longipes*

*Gynostemma longipes*, also known as “That diep dom”, is a traditional Vietnamese herb for treating diabetes, tonic, and health strengthening. Major secondary metabolites of this plant contain dammarane-type triterpenoids (Anh et al., 2015; Guo et al., 1997) which are similar to other species of *Gynostemma* genus (Lee et

al., 2015; Nguyen et al., 2011). To the best of our knowledge, there is no evidence about the anti-diabetes activity of *G. longipes*. Therefore, in this study, ten new triterpenes (1–10) were isolated using the bioassay-guided fractionation. All compounds were measured the glucose uptake in 3T3-L1 adipocytes using 2-[N-(7-nitrobenz-2-oxa-1,3-diazol-4-yl)amino]-2-deoxy-D-glucose (2-NBDG) as a fluorescent glucose molecule. In addition, all isolates were also evaluated the AMPK activation using mouse C2C12 myotubes.

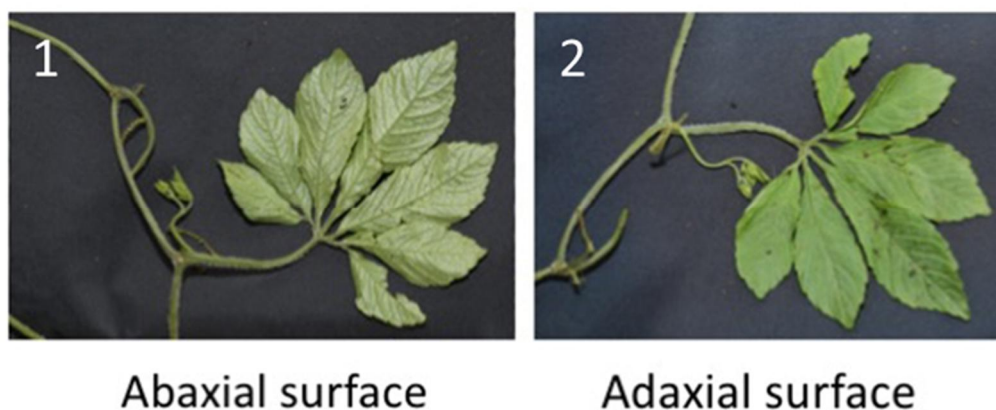
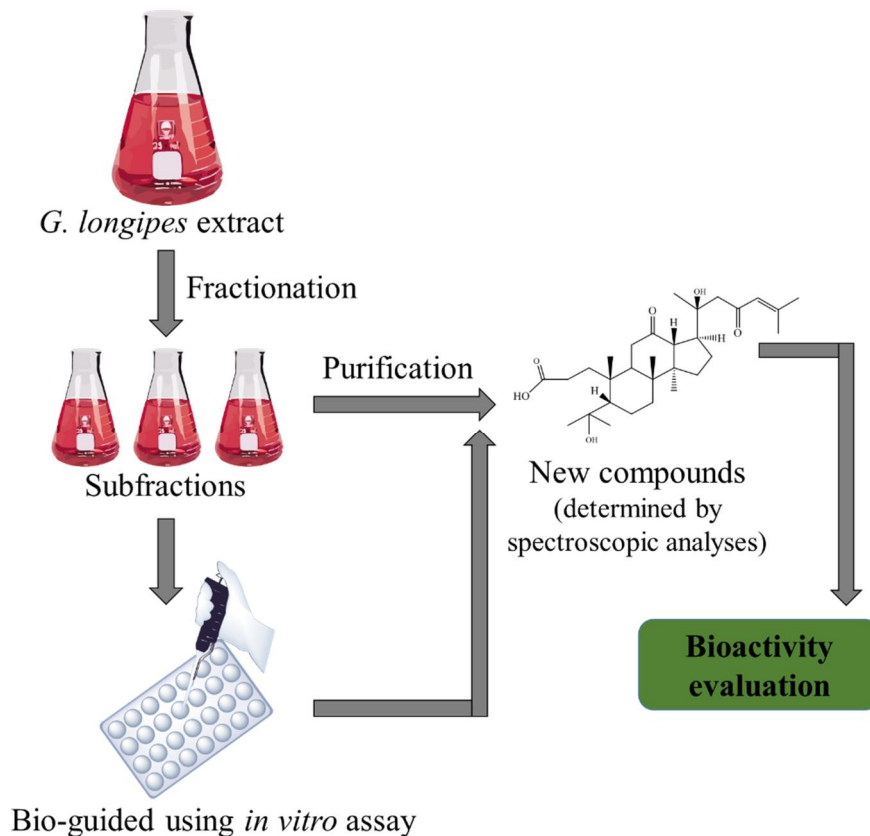


**Figure 5.** Authentication of *G. longipes* based on morphology: (1) whole plant with abaxial leaf and (2) adaxial leaf.

#### 1.4. Purpose of research

This study was discovery of new active constituents applying the bio-guided strategy. We have screened thousands of plant extracts for anti-diabetes activity using *in vitro* assay. During this process, the faction from *G. longipes* showed potential effects on glucose uptake in 3T3L1 adipocytes. A class of

chemotaxonomic marker metabolite of *G. longipes*, triterpenoid, was selected as a target compound because it was most well-known and widely for treatment T2DM. The schematic representation of bio-guided isolation strategy is shown in Scheme 1.



**Scheme 1.** The bio-guided isolation strategy of *G. longipes* plant.

## 2. Materials and methods

### 2.1. Plant materials

*Gynostemma longipes* was collected in Ha Giang province of Vietnam (GPS 23°08'34.9"N 105°25'42.6"E) in August 2016 and the authentication of this plant was carried out by Prof. Tran Van On, Head of Department of Botany, Hanoi

University of Pharmacy, Hanoi, Vietnam. The specimen voucher accession number of this plant was coded as HNIP.18505/16 and it was stored in the Medicinal Herbarium of Hanoi University of Pharmacy.

## 2.2. Chemicals, reagents and chromatography

### 2.2.1. Chemistry reagents

- Normal-phase silica gel (ZEOPrep 60 40-63  $\mu\text{m}$ ) and Reversed-phase silica gel (Cosmosil 75C<sub>18</sub>-PREP) were purchased from Merck (Darmstadt, Germany).
- Sephadex<sup>TM</sup> LH-20 (a bead-formed dextran medium for gel filtration) from Sigma-Aldrich (St. Louis, MO, USA) was used for column chromatography (CC).
- TLC Silica gel 60 F<sub>254</sub> (20 × 20 cm plate) and TLC Silica gel 60 RP-18 F<sub>254S</sub> (20 × 20 cm plate) from Merck (Darmstadt, Germany).
- Solvents for extraction and isolation were purchased from Dae Jung Pure Chemical Engineering Co. Ltd. (Siheung, Korea).
- Solvents (ACN, MeOH) for HPLC chromatography were bought from HoneyWell Burdick & Jackson<sup>®</sup>, USA.
- NMR solvents were purchased from Cambridge Isotope Laboratories, Inc., USA.

### 2.2.2. Bioassay reagents

- 2-NBDG (Invitrogen, Eugene, OR, USA)
- BCA protein assay kit (Bio-Rad Laboratories, Inc., Hercules, CA, USA)
- Chemiluminescence Western blot detection kit (Thermo sci., Rockford, IL, USA)



- Dexamethasone, 3-isobutyl-1-methyl-xanthine, MTT (Sigma, St. Louis, MO, USA)
- DMEM, FBS, Trypsin (Hyclone, Logan, UT, USA)
- Dimethyl sulfoxide (DMSO) (Junsei Chemical Co. Ltd., Tokyo, Japan)
- GLUT4 antibody (Santa Cruz, CA, USA)
- Insulin (Roche, Mannheim, Germany)
- Na<sup>+</sup>/K<sup>+</sup> ATPase  $\alpha$ 1 antibody (Cell signaling Technology, Inc., Beverly, MA, USA)
- *p*-ACC Ser<sup>79</sup>, ACC, *p*-AMPK $\alpha$  Thr<sup>172</sup>, AMPK $\alpha$  antibodies (Cell signaling Technology, Inc., Beverly, MA, USA)
- Penicillin (100 U/mL), and streptomycin (100  $\mu$ g/mL), calf serum, horse serum (Gibco, NY, USA)
- Phosphate-buffered saline (PBS) (Takara, Shiga, Japan)
- Polyvinylidene fluoride (PVDF) membranes (PVDF 0.45  $\mu$ m, Immobilon-P., USA)
- Ethylene Diamine Tetra Acetic acid (EDTA) (Sigma-Aldrich Co., St Louis, MO, USA).

### 2.2.3. Experimental instruments

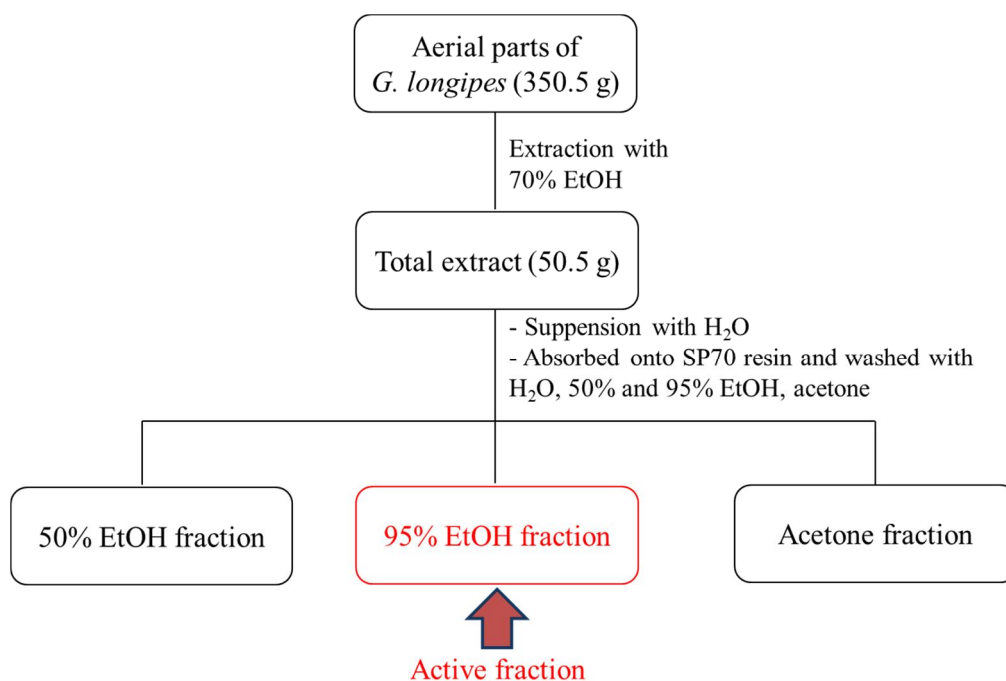
- Clean bench: Class II Biological Safety Cabinet, ESCO<sup>®</sup>
- CO<sub>2</sub> incubator: Forma Series II water jacketed CO<sub>2</sub> incubator, THERMO

- Evaporator: EYELA KSB-202, Japan
- ESIMS spectrometer: Agilent Technologies 6130 Quadrupole LC/MS spectrometer equipped with an Agilent Technologies 1260 Infinity LC system (Agilent Technologies, Inc., Santa Clara, CA, USA)
- Fluorescence microplate reader: Spectra Max Gemini XPS, Molecular Devices, San Jose, CA, USA
- Fluorescence microscope: Olympus ix70 Fluorescence Microscope, Olympus Corporation, Tokyo, Japan
- HPLC system: Gilson 321 pump and Gilson UV/VIS 151 detector, USA.
- LAS 4000 luminescent image analyzer: Fuji Film, Tokyo, Japan
- IR spectrometer: JASCO, FT/IR-4200, USA
- Microscope: Promo vert, China
- NMR spectrometers:
  - Bruker 500 MHz spectrometer (Bruker, Billerica, MA USA)
  - JNM-ECA 600 MHz spectrometer (JEOL Ltd., Tokyo, Japan)
- Optical rotations: JASCO P-2000 polarimeter (JASCO International Co. Ltd., Tokyo, Japan).

### 2.3. Extraction and isolation schemes

The powdered aerial parts (350.5 g) of *G. longipes* were extracted with 70% EtOH using the ultrasonication method. The crude ethanolic extract (50.5 g) was

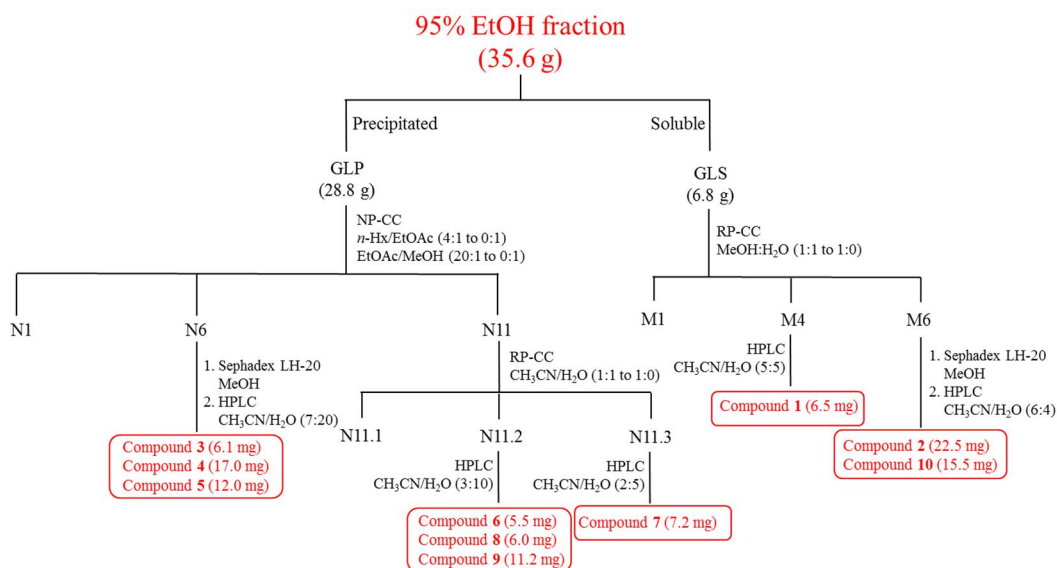
suspended in water and then absorbed onto Sepabeads SP70 resin. It was first washed with H<sub>2</sub>O, and then eluted with 50% EtOH, 95% EtOH, and acetone, progressively (Scheme 2).



**Scheme 2.** Extraction and fractionation of *G. longipes*.

The active fraction, 95% EtOH fraction (35.6 g), was separated using centrifugation into two parts, including the precipitated portion named GLP (28.8 g)

and the soluble portion named GLS (6.8 g). Then, the GLS part was applied to reversed-phase silica gel column chromatography using mobile phase MeOH/H<sub>2</sub>O with a step gradient of 50% to 100% to divide into six sub-fractions from GLS-M1 to GLS-M6. Among them, GLS-M4 fraction was applied to semi-preparative HPLC (Optima Pak C<sub>18</sub> column) with mobile phase system: CH<sub>3</sub>CN/H<sub>2</sub>O (5:5), flow rate 2 mL/min, to obtain compound **1** (6.5 mg). Another fraction (GLS-M6) was first subjected to Sephadex LH-20 column using MeOH solvent and then separated again by HPLC (Optima Pak C<sub>18</sub> column) with solvent condition as follow: CH<sub>3</sub>CN/H<sub>2</sub>O (6:4), flow rate 2 mL/min, to yield compounds **2** (22.5 mg) and **10** (15.5 mg). The GLP portion was successfully applied to silica gel CC (10 × 35 cm; 63–200 μm particle size) using different mobile phase systems: (1) *n*-hx/EtOAc from 4:1 to 0:1, (2) EtOAc/MeOH from 20:1 to 0:1. Eleven fractions (N1-N11) were obtained which based on the thin-layer chromatography (TLC) profile. Sub-fraction N11 was subjected to C<sub>18</sub>-reversed phase silica gel (RP-C<sub>18</sub>) column using CH<sub>3</sub>CN/H<sub>2</sub>O (1:1 to 1:0) to give three sub-fractions: GLP.N11-1 to GLP.N11-3. From fraction GLS.N11-2, three compounds [**6** (5.5 mg), **8** (6.0 mg), and **9** (11.2 mg)] were yielded by HPLC (Optima Pak C<sub>18</sub> column) with CH<sub>3</sub>CN/H<sub>2</sub>O (3:10) solvent system. Another fraction (GLP.N11-3) was applied to semi-preparative HPLC with mobile phase system: CH<sub>3</sub>CN/H<sub>2</sub>O (2:5) to give compound **7** (7.2 mg). Final fraction (GLP.N6) was separated by Sephadex LH-20 column (MeOH) and then purified again using semi-preparative HPLC [Optima Pak C<sub>18</sub>, CH<sub>3</sub>CN/H<sub>2</sub>O (7:20)], to yield three compounds [**3** (6.1 mg), **4** (17.0 mg), and **5** (12.0 mg)] (Scheme 3).



**Scheme 3.** Isolation scheme of 95% EtOH fraction of *G. longipes*.

## 2.4. Chemical and spectral properties of isolated compounds

### 2.4.1. Secolongipengenin S1 (**1**)

Compound **1** was obtained as a white amorphous powder;  $[\alpha]_{\text{D}}^{25}$  13.5 (*c* 0.2, MeOH); UV (MeOH)  $\lambda_{\text{max}}$  (log  $\epsilon$ ) 254 (3.8); IR (KBr)  $\nu_{\text{max}}$  3402, 2972, 2923, 1711, 1053, 1008  $\text{cm}^{-1}$ ;  $^1\text{H}$  and  $^{13}\text{C}$  NMR data, Tables 3 and 4; HRESIMS  $m/z$  503.3382  $[\text{M} - \text{H}]^-$  (calcd for  $\text{C}_{30}\text{H}_{47}\text{O}_6$ , 503.3378).

### 2.4.2. Secolongipengenin S2 (**2**)

Compound **2** was obtained as a white amorphous powder;  $[\alpha]_{\text{D}}^{25}$  4.9 (*c* 0.2, MeOH); IR (KBr)  $\nu_{\text{max}}$  3398, 2972, 2361, 1701, 1051, 1013  $\text{cm}^{-1}$ ;  $^1\text{H}$  and  $^{13}\text{C}$  NMR data, Tables 3 and 4; HRESIMS  $m/z$  521.3496  $[\text{M} - \text{H}]^-$  (calcd for  $\text{C}_{30}\text{H}_{49}\text{O}_7$ , 521.3484).

#### 2.4.3. Secolongipengenin S3 (**3**)

Compound **3** was obtained as a white amorphous powder;  $[\alpha]_D^{25}$  5.5 (*c* 0.2, MeOH); IR (KBr)  $\nu_{\max}$  3400, 2970, 2938, 1698, 1617, 1069, 1053, 1008  $\text{cm}^{-1}$ ;  $^1\text{H}$  and  $^{13}\text{C}$  NMR data, Tables 3 and 4; HRESIMS  $m/z$  405.2647  $[\text{M} - \text{H}]^-$  (calcd for  $\text{C}_{24}\text{H}_{37}\text{O}_5$ , 405.2646).

#### 2.4.4. Longipenoside ND1 (**4**)

Compound **4** was obtained as a white amorphous powder;  $[\alpha]_D^{25}$  2.7 (*c* 0.2, MeOH); IR (KBr)  $\nu_{\max}$  3709, 2971, 2870, 1698, 1617, 1069, 1053, 1013  $\text{cm}^{-1}$ ;  $^1\text{H}$  and  $^{13}\text{C}$  NMR data, Tables 3 and 4; HRESIMS  $m/z$  873.4525  $[\text{M} + \text{HCOO}]^-$  (calcd for  $\text{C}_{43}\text{H}_{69}\text{O}_{18}$ , 827.4489).

#### 2.4.5. Longipenoside ND2 (**5**)

Compound **5** was obtained as a white amorphous powder;  $[\alpha]_D^{25}$  5.9 (*c* 0.2, MeOH); IR (KBr)  $\nu_{\max}$  3403, 2935, 1704, 1388, 1134, 1048, 1005  $\text{cm}^{-1}$ ;  $^1\text{H}$  and  $^{13}\text{C}$  NMR data, Tables 3 and 4; HRESIMS  $m/z$  1019.5104  $[\text{M} + \text{HCOO}]^-$  (calcd for  $\text{C}_{49}\text{H}_{79}\text{O}_{22}$ , 1019.5068).

#### 2.4.6. Longipenoside GL1 (**6**)

Compound **6** was obtained as a white amorphous powder;  $[\alpha]_D^{25}$  -1.5 (*c* 0.2, MeOH); IR (KBr)  $\nu_{\max}$  3401, 2971, 2923, 2371, 2320, 1053, 1008  $\text{cm}^{-1}$ ;  $^1\text{H}$  and  $^{13}\text{C}$  NMR data, Tables 3 and 4; HRESIMS  $m/z$  1135.5946  $[\text{M} + \text{HCOO}]^-$  (calcd for  $\text{C}_{55}\text{H}_{91}\text{O}_{24}$ , 1135.5906).

#### 2.4.7. Longipenoside GL2 (**7**)

Compound **7** was obtained as a white amorphous powder;  $[\alpha]_{\text{D}}^{25}$  -1.6 (*c* 0.2, MeOH); UV (MeOH):  $\lambda_{\text{max}}$  ( $\log \epsilon$ ) 280 (3.7), 250 (3.8) nm; IR (KBr)  $\nu_{\text{max}}$  3400, 2972, 2942, 2371, 2320, 1053, 1013  $\text{cm}^{-1}$ ;  $^1\text{H}$  and  $^{13}\text{C}$  NMR data, Tables 3 and 4; HRESIMS  $m/z$  1099.5730  $[\text{M} + \text{HCOO}]^-$  (calcd for  $\text{C}_{55}\text{H}_{87}\text{O}_{22}$ , 1099.5694).

#### 2.4.8. Longipenoside GL3 (**8**)

Compound **8** was obtained as a white amorphous powder;  $[\alpha]_{\text{D}}^{25}$  -2.5 (*c* 0.2, MeOH); IR (KBr)  $\nu_{\text{max}}$  3400, 2971, 2921, 2346, 2313, 1053, 1008  $\text{cm}^{-1}$ ;  $^1\text{H}$  and  $^{13}\text{C}$  NMR data, Tables 3 and 4; HRESIMS  $m/z$  973.5414  $[\text{M} + \text{HCOO}]^-$  (calcd for  $\text{C}_{49}\text{H}_{81}\text{O}_{19}$ , 973.5378).

#### 2.4.9. Longipenoside GL4 (**9**)

Compound **9** was obtained as a white amorphous powder;  $[\alpha]_{\text{D}}^{25}$  -0.5 (*c* 0.2, MeOH); IR (KBr)  $\nu_{\text{max}}$  3400, 2982, 2372, 2320, 1052, 1037  $\text{cm}^{-1}$ ;  $^1\text{H}$  and  $^{13}\text{C}$  NMR data, Tables 3 and 4; HRESIMS  $m/z$  1119.6008  $[\text{M} + \text{HCOO}]^-$  (calcd for  $\text{C}_{55}\text{H}_{91}\text{O}_{23}$ , 1119.5957).

#### 2.4.10. Longipenoside GL5 (**10**)

Compound **10** was obtained as a white amorphous powder;  $[\alpha]_{\text{D}}^{25}$  -0.8 (*c* 0.2, MeOH); UV (MeOH):  $\lambda_{\text{max}}$  ( $\log \epsilon$ ) 225 nm (2.8); IR (KBr)  $\nu_{\text{max}}$  3390, 2971, 1057, 1013  $\text{cm}^{-1}$ ;  $^1\text{H}$  and  $^{13}\text{C}$  NMR data, Tables 3 and 4; HRESIMS 811.4872  $[\text{M} + \text{HCOO}]^-$  (calcd for  $\text{C}_{43}\text{H}_{71}\text{O}_{14}$ , 811.4849).

**Table 3.**  $^1\text{H}$  NMR spectroscopic data for compound **1–10** (in pyridine- $d_5$ ).

	<b>1</b>	<b>2</b>	<b>3</b>	<b>4</b>	<b>5</b>	<b>6</b>	<b>7</b>	<b>8</b>	<b>9</b>	<b>10</b>
Position	$\delta_{\text{H}}$ ( $J$ in Hz)	$\delta_{\text{H}}$ ( $J$ in Hz)	$\delta_{\text{H}}$ ( $J$ in Hz)	$\delta_{\text{H}}$ ( $J$ in Hz)	$\delta_{\text{H}}$ ( $J$ in Hz)	$\delta_{\text{H}}$ ( $J$ in Hz)	$\delta_{\text{H}}$ ( $J$ in Hz)	$\delta_{\text{H}}$ ( $J$ in Hz)	$\delta_{\text{H}}$ ( $J$ in Hz)	$\delta_{\text{H}}$ ( $J$ in Hz)
	500 MHz	500 MHz	500 MHz	600 MHz	600 MHz	600 MHz	600 MHz	500 MHz	500 MHz	600 MHz
1	3.21, ddd (4.7, 11.5, 15.5)	3.21, ddd (4.7, 11.5, 15.5)	3.17, ddd (4.7, 11.5, 15.5)	1.45, overlap	1.46, overlap	1.24, m	1.22, overlap	1.21, overlap	1.21, overlap	1.20, overlap
	1.95, ddd (4.6, 11.8, 15.5)	1.94, ddd (4.6, 11.8, 15.5)	1.92, ddd (4.6, 11.8, 15.5)							
	2.56, overlap	2.54, overlap	2.51, ddd (4.7, 11.8, 15.6)	2.23, overlap	2.25, overlap	2.15, m	2.22, overlap	2.22, overlap	2.21, overlap	2.21, overlap
	3.00, overlap	2.98, overlap	2.98, ddd (4.6, 11.5, 15.6)	1.77, overlap	1.79, overlap	1.75, m	1.75, overlap	1.75, overlap	1.78, overlap	1.77, overlap
3				3.24, overlap	3.29, overlap	3.26, dd (11.7, 4.1)	3.32, overlap	3.27, dd (11.9, 4.3)	3.27, dd (11.9, 4.3)	3.29, overlap
5	1.69, overlap	1.67, overlap	1.67, overlap	0.69, m	0.72, m	0.72, m	0.68, overlap	0.67, overlap	0.70, overlap	0.67, overlap
6	1.67, overlap	1.69, overlap	1.65, overlap	1.50, m	1.50, overlap	1.54, m	1.52, m	1.53, overlap	1.51, overlap	1.49, overlap
	1.65, overlap	1.65, overlap	1.63, overlap	1.40, m	1.40, overlap	1.41, m	1.42, m	1.42, overlap	1.42, overlap	1.40, overlap
7	1.29, m	1.29, m	1.29, m	1.40, m	1.40, overlap	1.41, m	1.45, m	1.45, overlap	1.40, overlap	1.40, overlap
	1.28, m	1.26, m	1.28, m	1.20, m	1.20, overlap	1.27, m	1.27, m	1.26, overlap	1.27, overlap	1.26, overlap
9	2.20, dd (13.4, 3.3)	2.19, dd (13.4, 3.3)	2.16, dd (14.2, 3.3)	1.70, m	1.71, overlap	1.66, overlap	1.67, m	1.67, overlap	1.66, overlap	1.66, overlap
11	2.60, dd (13.4, 3.3)	2.59, dd (13.4, 3.3)	2.58, dd (14.2, 3.3)	2.23, overlap	2.27, overlap	2.24, overlap	2.27, overlap	2.27, t (13.0)	2.23, overlap (2H)	2.22, overlap (2H)
	2.39, t (13.4)	2.35, t (13.4)	2.30, t (14.2)	2.15, overlap	2.14, t (13.0)	2.22, overlap	2.22, overlap	2.22, dd (13.0, 4.0)		
13	3.33, d (9.7)	3.27, d (9.7)	3.31, d (9.7)	3.21, d (9.7)	3.19, d (9.7)	3.17, d (9.7)	3.02, d (10.5)	3.36, d (9.6)	3.33, d (9.6)	3.30, overlap
15	1.85, m	1.83, m	1.74, m	1.69, overlap	1.70, overlap	1.80, m	1.85, m	1.87, m	1.86, m	1.86, overlap
	1.17, overlap	1.16, overlap	1.53, overlap	1.10, overlap	1.09, overlap	1.14, m	1.23, m	1.17, m	1.14, m	1.17, overlap



Position	1	2	3	4	5	6	7	8	9	10
	$\delta_{\text{H}}$ ( <i>J</i> in Hz)	$\delta_{\text{H}}$ ( <i>J</i> in Hz)	$\delta_{\text{H}}$ ( <i>J</i> in Hz)	$\delta_{\text{H}}$ ( <i>J</i> in Hz)	$\delta_{\text{H}}$ ( <i>J</i> in Hz)	$\delta_{\text{H}}$ ( <i>J</i> in Hz)	$\delta_{\text{H}}$ ( <i>J</i> in Hz)	$\delta_{\text{H}}$ ( <i>J</i> in Hz)	$\delta_{\text{H}}$ ( <i>J</i> in Hz)	$\delta_{\text{H}}$ ( <i>J</i> in Hz)
	500 MHz	500 MHz	500 MHz	600 MHz	600 MHz	600 MHz	600 MHz	500 MHz	500 MHz	600 MHz
16	2.10, overlap	2.06, overlap	2.00, m	2.00, overlap	1.96, overlap	2.02, m	2.07, m	2.14, m	2.10, m	2.08, m
	1.92, overlap	1.89, overlap	1.76, overlap	1.70, overlap	1.72, overlap	1.88, m	1.91, m	1.90, m	1.89, m	1.90, m
17	2.79, td (10.2, 5.2)	2.80, td (10.2, 5.2)	3.38, m	3.35, m	3.30, m	2.74, td (10.1, 10.0, 5.3)	3.17, ddd (17.0, 10.6, 6.7)	2.76, m	2.72, m	2.73, td (10.0, 5.3)
18	1.26, s	1.24, s	1.15, s	1.00, s	1.01, s	1.09, s	1.14, s	1.13, s	1.11, s	1.11, s
19	1.19, s	1.18, s	1.16, s	0.77, s	0.75, s	0.75, s	0.82, s	0.78, s	0.77, s	0.78, s
21	1.52, s	1.52, s	2.22, s	2.23, s	2.21, s	1.46, s	2.33, s	1.45, s	1.42, s	1.42, s
	2.92, d (14.2)	3.12, d (14.2)				3.10, d (15.6)	6.44, s	2.59, dd (13.8, 6.5)	2.57, dd (13.8, 6.5)	1.76, overlap (2H)
22	2.70, d (14.2)	2.83, d (14.2)						2.53, dd (13.8, 8.6)	2.51, dd (13.8, 8.3)	
								6.25, ddd (15.1, 8.3, 6.5)	6.21, ddd (15.1, 8.3, 6.5)	2.41, m
23										2.28, m
24	6.31, br s	3.00, br s				2.94, br s	6.16, s	5.99, d (15.1)	5.97, d (15.1)	5.27, m
26	1.72, s	1.50, s				1.44, s	1.70, s	1.52, s	1.51, s	1.66, s
27	2.18, s	1.50, s				1.45, s	2.22, s	1.52, s	1.51, s	1.62, s
28	1.46, s	1.46, s	1.45, s	1.07, s	1.09, s	1.18, s	1.24, s	1.19, s	1.21, s	1.23, s
29	1.50, s	1.50, s	1.49, s	1.15, s	1.19, s	1.12, s	1.10, s	1.14, s	1.11, s	1.17, s
30	0.86, s	0.85, s	0.81, s	0.71, s	0.78, s	0.78, s	0.88, s	0.86, s	0.83, s	0.89, s
1'				4.76, d (7.7)	4.73, d (8.0)	4.72, d (7.5)	4.80, d (7.5)	4.83, d (7.5)	4.79, d (7.5)	4.92, d (7.2)
2'				3.97, overlap	3.94, t (8.0)	4.01, overlap	4.02, overlap	4.09, overlap	4.00, overlap	4.28, overlap
3'				4.07, overlap	4.06, t (8.0)	4.11, overlap	4.13, overlap	4.18, overlap	4.12, overlap	4.26, overlap
4'				3.84, overlap	3.80, overlap	3.86, overlap	3.87, overlap	3.89, overlap	3.84, overlap	4.13, t (9.3)
5'				3.84, overlap	3.90, overlap	3.94, overlap	3.95, overlap	4.07, overlap	3.95, overlap	3.95, ddd (9.3, 5.4, 2.6)
6'				4.59, overlap	4.48, overlap	4.53, overlap	4.53, overlap	4.53, overlap	4.49, overlap	4.57, dd (11.8,

Position	1	2	3	4	5	6	7	8	9	10
	$\delta_{\text{H}} (J \text{ in Hz})$	$\delta_{\text{H}} (J \text{ in Hz})$	$\delta_{\text{H}} (J \text{ in Hz})$	$\delta_{\text{H}} (J \text{ in Hz})$	$\delta_{\text{H}} (J \text{ in Hz})$	$\delta_{\text{H}} (J \text{ in Hz})$	$\delta_{\text{H}} (J \text{ in Hz})$	$\delta_{\text{H}} (J \text{ in Hz})$	$\delta_{\text{H}} (J \text{ in Hz})$	$\delta_{\text{H}} (J \text{ in Hz})$
	500 MHz	500 MHz	500 MHz	600 MHz	600 MHz	600 MHz	600 MHz	500 MHz	500 MHz	600 MHz
				4.47, overlap	4.08, overlap	4.13, overlap	4.13, overlap	4.38, overlap	4.14, overlap	2.6)
										4.37, dd (11.8, 5.4)
1''				5.88, br s	5.89, br s	5.86, br s	5.96, br s	5.99, br s	6.00, br s	6.56, br s
2''				4.68, overlap	4.68, overlap	4.66, overlap	4.68, overlap	4.71, overlap	4.68, overlap	4.84, dd (3.0, 1.3)
3''				4.50, overlap	4.50, overlap	4.45, overlap	4.50, overlap	4.50, overlap	4.49, overlap	4.66, dd (9.4, 3.0)
4''				4.25, overlap	4.29, overlap	4.27, overlap	4.33, overlap	4.30, overlap	4.33, overlap	4.33, t (9.4)
5''				4.64, overlap	4.62, overlap	4.60, overlap	4.62, overlap	4.66, overlap	4.62, overlap	4.79, dq (9.4, 6.2)
6''				1.63, d (4.6)	1.63, d (6.3)	1.61, d (6.3)	1.68, d (6.3)	1.68, d (6.3)	1.67, d (6.3)	1.70, d (6.2)
1'''				5.67, br s	5.69, br s	5.65, br s	5.75, br s	5.76, br s	5.74, br s	
2'''				4.84, overlap	4.87, overlap	4.86, overlap	4.92, overlap	4.93, overlap	4.92, overlap	
3'''				4.51, overlap	4.53, overlap	4.50, d (9.3)	4.52, d (9.3)	4.58, overlap	4.52, d (9.3)	
4'''				4.31, overlap	4.28, overlap	4.25, overlap	4.28, overlap	4.32, overlap	4.28, overlap	
5'''				4.68, overlap	4.70, overlap	4.67, overlap	4.70, overlap	4.74, overlap	4.70, overlap	
6'''				1.60, d (4.6)	1.62, overlap	1.57, d (6.3)	1.64, d (6.3)	1.64, d (6.3)	1.62, d (6.3)	
1''''					5.39, br s	5.37, br s	5.44, br s		5.43, br s	
2''''					4.53, overlap	4.50, overlap	4.53, overlap		4.52, overlap	
3''''					4.62, overlap	4.59, overlap	4.62, overlap		4.63, overlap	
4''''					4.35, overlap	4.32, overlap	4.35, overlap		4.35, overlap	
5''''					4.34, overlap	4.31, overlap	4.34, overlap		4.34, overlap	
6''''					1.64, overlap	1.59, d (6.3)	1.65, d (6.3)		1.64, d (6.3)	

**Table 4.**  $^{13}\text{C}$  NMR spectroscopic data for compounds **1–10** (in pyridine- $d_5$ ).

	<b>1</b>	<b>2</b>	<b>3</b>	<b>4</b>	<b>5</b>	<b>6</b>	<b>7</b>	<b>8</b>	<b>9</b>	<b>10</b>
Position	$\delta_{\text{C}}$ , type 125 MHz	$\delta_{\text{C}}$ , type 125 MHz	$\delta_{\text{C}}$ , type 125 MHz	$\delta_{\text{C}}$ , type 150 MHz	$\delta_{\text{C}}$ , type 150 MHz	$\delta_{\text{C}}$ , type 150 MHz	$\delta_{\text{C}}$ , type 150 MHz	$\delta_{\text{C}}$ , type 125 MHz	$\delta_{\text{C}}$ , type 125 MHz	$\delta_{\text{C}}$ , type 150 MHz
1	35.8, CH <sub>2</sub>	35.9, CH <sub>2</sub>	35.7, CH <sub>2</sub>	39.2, CH <sub>2</sub>	39.1, CH <sub>2</sub>	39.3 CH <sub>2</sub>	39.3, CH <sub>2</sub>	39.4, CH <sub>2</sub>	39.3, CH <sub>2</sub>	39.3, CH <sub>2</sub>
2	30.0, CH <sub>2</sub>	30.0, CH <sub>2</sub>	30.0, CH <sub>2</sub>	28.1, CH <sub>2</sub>	28.0, CH <sub>2</sub>	26.8, CH <sub>2</sub>	27.0, CH <sub>2</sub>	27.0, CH <sub>2</sub>	27.0, CH <sub>2</sub>	27.1, CH <sub>2</sub>
3	177.4, C	177.3, C	177.3, C	88.6, CH	88.8, CH	89.2, CH	89.0, CH	88.6, CH	89.1, CH	88.7, CH
4	75.1, C	75.1, C	75.1, C	39.3, C	39.2, C	39.9, C	39.8, C	41.0, C	39.9, C	40.0, C
5	52.6, CH	52.6, CH	52.5, CH	56.5, CH	56.5, CH	56.7, CH	56.6, CH	56.6, CH	56.7, CH	56.7, CH
6	23.2, CH <sub>2</sub>	23.3, CH <sub>2</sub>	23.1, CH <sub>2</sub>	18.7, CH <sub>2</sub>	18.8, CH <sub>2</sub>	18.7, CH <sub>2</sub>	19.0, CH <sub>2</sub>	18.9, CH <sub>2</sub>	18.4, CH <sub>2</sub>	18.8, CH <sub>2</sub>
7	34.1, CH <sub>2</sub>	34.1, CH <sub>2</sub>	34.0, CH <sub>2</sub>	34.6, CH <sub>2</sub>	34.6, CH <sub>2</sub>	34.8, CH <sub>2</sub>	34.7, CH <sub>2</sub>	34.9, CH <sub>2</sub>	34.8, CH <sub>2</sub>	34.9, CH <sub>2</sub>
8	40.8, C	40.8, C	40.5, C	40.7, C	40.6, C	41.0, C	41.0, C	41.4, C	41.0, C	41.0, C
9	47.1, CH	47.1, CH	46.1, CH	53.8, CH	53.6, CH	54.7, CH	54.0, CH	54.7, CH	54.7, CH	54.8, CH
10	42.2, C	42.2, C	42.1, C	37.5, C	37.6, C	37.8, C	37.8, C	37.7, C	37.8, C	37.7, C
11	40.0, CH <sub>2</sub>	40.0, CH <sub>2</sub>	39.2, CH <sub>2</sub>	39.8, CH <sub>2</sub>	39.8, CH	40.2, CH	40.0, CH <sub>2</sub>	40.2, CH <sub>2</sub>	40.2, CH <sub>2</sub>	40.2, CH <sub>2</sub>
12	211.8, C	211.8, C	209.8, C	210.3, C	209.9, C	212.5, C	210.0, C	212.2, C	212.3, C	212.1, C
13	56.8, CH	57.0, CH	58.5, CH	58.5, CH	58.4, CH	56.8, CH	59.0, CH	56.9, CH	56.8, CH	56.9, CH
14	56.6, C	56.6, C	55.1, C	54.8, C	54.6, C	56.7, C	55.2, C	56.2, C	56.2, C	56.7, C
15	32.3, CH <sub>2</sub>	32.3, CH <sub>2</sub>	31.9, CH <sub>2</sub>	31.8, CH <sub>2</sub>	31.7, CH <sub>2</sub>	32.3, CH <sub>2</sub>	32.1, CH <sub>2</sub>	32.3, CH <sub>2</sub>	32.2, CH <sub>2</sub>	32.3, CH <sub>2</sub>
16	25.3, CH <sub>2</sub>	25.3, CH <sub>2</sub>	26.3, CH <sub>2</sub>	26.1, CH <sub>2</sub>	26.0, CH <sub>2</sub>	25.2, CH <sub>2</sub>	28.8, CH <sub>2</sub>	24.8, CH <sub>2</sub>	24.7, CH <sub>2</sub>	24.8, CH <sub>2</sub>
17	45.3, CH	45.4, CH	48.0, CH	47.9, CH	47.9, CH	45.1, CH	45.7, CH	44.4, CH	44.3, CH	44.4, CH
18	15.8, CH <sub>3</sub>	15.8, CH <sub>3</sub>	15.7, CH <sub>3</sub>	15.9, CH <sub>3</sub>	15.9, CH <sub>3</sub>	16.1, CH <sub>3</sub>	16.1, CH <sub>3</sub>	16.1, CH <sub>3</sub>	16.1, CH <sub>3</sub>	16.1, CH <sub>3</sub>
19	21.2, CH <sub>3</sub>	21.2, CH <sub>3</sub>	20.9, CH <sub>3</sub>	16.2, CH <sub>3</sub>	16.2, CH <sub>3</sub>	16.6, CH <sub>3</sub>	16.4, CH <sub>3</sub>	16.5, CH <sub>3</sub>	16.6, CH <sub>3</sub>	17.2, CH <sub>3</sub>
20	74.1, C	73.9, C	210.2, C	210.0, C	210.2, C	73.9, C	159.8, C	74.0, C	73.8, C	73.6, C
21	27.1, CH <sub>3</sub>	26.8, CH <sub>3</sub>	30.2, CH <sub>3</sub>	30.2, CH <sub>3</sub>	30.2, CH <sub>3</sub>	26.8, CH <sub>3</sub>	17.7, CH <sub>3</sub>	27.5, CH <sub>3</sub>	27.5, CH <sub>3</sub>	26.9, CH <sub>3</sub>
22	54.8, CH <sub>2</sub>	55.1, CH <sub>2</sub>				55.2, CH <sub>2</sub>	126.2, CH	45.8, CH <sub>2</sub>	45.8, CH <sub>2</sub>	42.3, CH <sub>2</sub>
23	201.9, C	213.1, C				212.9, C	191.7, C	123.2, CH	123.1, CH	23.9, CH <sub>2</sub>
24	126.6, CH	57.8, CH <sub>2</sub>				57.7, CH <sub>2</sub>	127.4, CH	143.1, CH	143.0, CH	126.2, CH
25	154.9, C	70.0, C				70.1, C	154.0, C	70.1, C	70.1, C	131.2, C
26	27.7, CH <sub>3</sub>	30.8, CH <sub>3</sub>				30.7, CH <sub>3</sub>	27.7, CH <sub>3</sub>	31.1, CH <sub>3</sub>	31.0, CH <sub>3</sub>	26.1, CH <sub>3</sub>
27	21.0, CH <sub>3</sub>	30.5, CH <sub>3</sub>				30.3, CH <sub>3</sub>	20.8, CH <sub>3</sub>	31.0, CH <sub>3</sub>	31.0, CH <sub>3</sub>	18.0, CH <sub>3</sub>
28	28.6, CH <sub>3</sub>	28.6, CH <sub>3</sub>	28.6, CH <sub>3</sub>	28.1, CH <sub>3</sub>	28.0, CH <sub>3</sub>	28.1, CH <sub>3</sub>	28.2, CH <sub>3</sub>	28.1, CH <sub>3</sub>	28.1, CH <sub>3</sub>	28.1, CH <sub>3</sub>

	1	2	3	4	5	6	7	8	9	10
Position	$\delta_c$ , type 125 MHz	$\delta_c$ , type 125 MHz	$\delta_c$ , type 125 MHz	$\delta_c$ , type 150 MHz	$\delta_c$ , type 150 MHz	$\delta_c$ , type 150 MHz	$\delta_c$ , type 150 MHz	$\delta_c$ , type 125 MHz	$\delta_c$ , type 125 MHz	$\delta_c$ , type 150 MHz
29	34.5, CH <sub>3</sub>	34.5, CH <sub>3</sub>	34.5, CH <sub>3</sub>	16.9, CH <sub>3</sub>	16.8, CH <sub>3</sub>	16.8, CH <sub>3</sub>	16.9, CH <sub>3</sub>	17.0, CH <sub>3</sub>	16.6, CH <sub>3</sub>	16.5, CH <sub>3</sub>
30	17.3, CH <sub>3</sub>	17.3, CH <sub>3</sub>	17.2, CH <sub>3</sub>	17.4, CH <sub>3</sub>	17.4, CH <sub>3</sub>	17.5, CH <sub>3</sub>	17.7, CH <sub>3</sub>	17.6, CH <sub>3</sub>	17.6, CH <sub>3</sub>	17.6, CH <sub>3</sub>
1'				105.3, CH	105.2, CH	105.3, CH	105.3, CH	105.4, CH	105.3, CH	105.8, CH
2'				78.3, CH	78.4, CH	78.5, CH	78.5, CH	78.3, CH	78.4, CH	77.6, CH
3'				87.5, CH	87.0, CH	87.1, CH	87.3, CH	87.6, CH	87.2, CH	80.2, CH
4'				70.6, CH	70.5, CH	71.0, CH	70.7, CH	70.7, CH	70.8, CH	72.5, CH
5'				78.3, CH	76.2, CH	76.4, CH	76.4, CH	78.5, CH	76.4, CH	78.6, CH
6'				62.8, CH <sub>2</sub>	68.1, CH <sub>2</sub>	68.4, CH <sub>2</sub>	68.4, CH <sub>2</sub>	62.9, CH <sub>2</sub>	68.3, CH <sub>2</sub>	63.2, CH <sub>2</sub>
1''				102.5, CH	102.4, CH	102.5, CH	102.6, CH	102.6, CH	102.6, CH	102.1, CH
2''				72.3, CH	72.1, CH	72.2, CH	72.1, CH	72.4, CH	72.1, CH	72.5, CH
3''				72.7, CH	72.1, CH	72.5, CH	72.3, CH	72.8, CH	72.3, CH	72.9, CH
4''				74.0, CH	73.7, CH	73.7, CH	73.9, CH	74.1, CH	73.9, CH	74.5, CH
5''				70.1, CH	70.0, CH	70.2, CH	70.2, CH	70.2, CH	70.2, CH	69.9, CH
6''				18.9, CH <sub>3</sub>	18.9, CH <sub>3</sub>	19.0, CH <sub>3</sub>	19.0, CH <sub>3</sub>	18.9, CH <sub>3</sub>	18.9, CH <sub>3</sub>	19.0, CH <sub>3</sub>
1'''				104.0, CH	103.8, CH	103.9, CH	104.0, CH	104.1, CH	104.0, CH	
2'''				72.7, CH	72.4, CH	72.7, CH	72.8, CH	72.8, CH	72.8, CH	
3'''				72.9, CH	72.6, CH	72.8, CH	73.1, CH	73.0, CH	73.0, CH	
4'''				73.8, CH	73.8, CH	73.9, CH	74.1, CH	74.0, CH	74.0, CH	
5'''				71.0, CH	70.9, CH	70.8, CH	70.7, CH	71.1, CH	70.6, CH	
6'''				18.7, CH <sub>3</sub>	18.8, CH <sub>3</sub>	18.9, CH <sub>3</sub>	19.0, CH <sub>3</sub>	18.8, CH <sub>3</sub>	19.0, CH <sub>3</sub>	
1''''					102.6, CH	102.8, CH	102.8, CH		102.8, CH	
2''''					72.9, CH	73.0, CH	72.9, CH		73.0, CH	
3''''					72.6, CH	72.8, CH	72.8, CH		72.9, CH	
4''''					74.0, CH	74.1, CH	74.2, CH		74.2, CH	
5''''					70.6, CH	70.8, CH	70.8, CH		70.8, CH	
6''''					18.6, CH <sub>3</sub>	18.7, CH <sub>3</sub>	18.7, CH <sub>3</sub>		18.7, CH <sub>3</sub>	

## 2.5. Differentiation of 3T3-L1 adipocytes

3T3-L1 myoblasts were maintained at 37°C in an atmosphere of 5% CO<sub>2</sub> using Dulbecco's modified Eagle's medium (DMEM) (HyClone, Logan, UT, USA) supplemented with 10% calf serum, penicillin (100 U/mL), and streptomycin (100 µg/mL) (Gibco, Grand Island, NY, USA). The procedure of differentiation was carried out following two steps: (1) the cells firstly incubated for 2 days with medium containing 10% fetal bovine serum (FBS) (HyClone), 1 µM dexamethasone (Sigma, MO, USA), 520 µM 3-isobutyl-1-methyl-xanthine (Sigma) and 1 µg/mL insulin (Roche, Mannheim, Germany); (2) the cells were continually incubated with fresh DMEM containing 10% FBS, 1 µg/mL insulin, 100 U/mL penicillin and 100 µg/mL streptomycin. The cultures were changed the fresh medium every 1.5-2 days until the adipogenesis induction. After 4-6 days of incubation, lipid droplets significantly accumulated in the 3T3-L1 adipocytes.

## 2.6. Measurement of cell viability

To evaluate the cell viability, 3-(4,5-dimethyl-2-thiazolyl)-2,5-diphenyl-2*H*-tetrazolium bromide (MTT) assay was used as a simple and common method. Briefly, the cells (C2C12 myoblasts or 3T3-L1 adipocytes) were seeded into 96-well plates with DMEM containing 10% FBS. After 24 h of incubation, the cells were exposed to test samples which were dissolved in the serum-free medium. The cultures were continuously incubated for 24 h at 37°C in an atmosphere of 5% CO<sub>2</sub> and then the MTT solution (Sigma) (20 µL of the 2 mg/mL) were added to each well. After 4 h of incubation in the dark, the formazan product was dissolved in dimethyl sulfoxide (DMSO) and measured at 550 nm using a microplate reader (VersaMax, PA, USA).

## 2.7. Measurement of 2-NBDG uptake

The glucose uptake into the cells was evaluated using a fluorescent derivative of glucose 2-NBDG (Invitrogen, Eugene, OR, USA), which was commonly used for *in vitro* studies. The glucose uptake assay using the 2-NBDG probe was performed as previously described (Pham et al., 2018). Briefly, 3T3-L1 adipocytes were seeded into 96-well plates using a glucose-free medium supplemented with 10% FBS for 24 h. The cells were then treated with insulin (as a positive control) and test samples in the presence or absence of 2-NBDG probe and continuously incubated for 1 h. After that, the cultures were washed with cold phosphate buffered saline (PBS). To measure the fluorescent intensity, a fluorescence microplate reader (Spectra Max Gemini XPS, Molecular Devices, San Jose, CA, USA) was applied at 450/535 nm excitation/emission wavelengths. Moreover, the transport of 2-NBDG into adipocytes was also confirmed using a fluorescence microscopy method. Briefly, the cells were grown on sterilized glass coverslips using the glucose-free medium (10% FBS) for 1 day. The following steps were carried out as described above. After that, coverslips were washed with cold PBS and fluorescent images were obtained using a fluorescence microscope (Olympus ix70 Fluorescence Microscope, Olympus Corporation, Tokyo, Japan).

## 2.8. Measurement of GLUT4 translocation

The translocation of GLUT4 protein to the plasma membrane of adipocytes was evaluated using the Western blot method. 3T3-L1 adipocytes were grown on 6-well plates with DMEM containing 10% FBS. The cells were then exposed to insulin for 2 h and the test samples for 24 h using the serum-free medium. The fractions of the plasma membrane were isolated as previously described with several modifications (Yamamoto et al., 2016). The concentrations of protein were measured using a BCA protein assay kit (Bio-Rad Laboratories, Inc., Hercules, CA, USA). The equal amount of proteins were loaded on 12% SDS-polyacrylamide gels. The gels were then transferred to polyvinylidene fluoride (PVDF) membranes (PVDF 0.45  $\mu\text{m}$ , Immobilon-P., USA). After blocking with 5% skim milk solution for 1 h, the membranes were incubated overnight with primary antibodies for GLUT4 (Santa Cruz, CA, USA),  $\text{Na}^+/\text{K}^+$  ATPase  $\alpha 1$  (Cell Signaling, Danvers, MA, USA). The blots were continuously incubated with secondary antibodies for 2 h and the bands were detected using a LAS 4000 luminescent image analyzer (Fuji Film, Tokyo, Japan).

## 2.9. Measurement of *p*-AMPK and *p*-ACC in C2C12 myotubes

For differentiating C2C12 myoblasts to myotubes, the procedure was performed using differentiation media [DMEM supplemented with 2% horse serum (Gibco), penicillin (100 U/mL), and streptomycin (100  $\mu$ g/mL)]. The medium was changed with fresh differentiation medium until the formation of myotubes. To evaluate the expression of *p*-AMPK and *p*-ACC proteins, Western blot analysis was used. Myotubes were incubated with compounds for 1 h and the cell lysates were then collected using a lysis buffer [50 mM Tris-HCl (pH 7.6), 120 mM NaCl, 1 mM EDTA, 0.5% NP-40, 50 mM NaF]. The BCA protein assay was used for determining the protein concentrations. Proteins were electrophoresed on 8% or 12% SDS-polyacrylamide gels and then transferred to PVDF membranes. The blots were continuously incubated with primary antibodies, including *p*-ACC Ser<sup>79</sup>, ACC, *p*-AMPK $\alpha$  Thr<sup>172</sup>, AMPK $\alpha$  (Cell Signaling) or  $\beta$ -actin (Thermo Fisher Scientific, Rockford, IL, USA). After 24 h of incubation, the membranes were then incubated with secondary antibodies for 2 h. An enhanced chemiluminescence Western blot detection kit (Thermo Fisher Scientific) was used for detection of membranes.

## 2.10. Statistical analysis

Data are presented by the mean  $\pm$  SD of three independent experiments. For quantitative analysis of Western blotting, ImageJ software was applied. The one-way analysis of variance (ANOVA) was used to determine the significant differences between groups following Tukey's or Duncan's post



hoc test as appropriate, which conducted in SPSS Statistics 23 (SPSS, Inc., Chicago, IL, USA). Statistical significance was accepted at \*  $p < 0.05$ , \*\*  $p < 0.01$ , and \*\*\*  $p < 0.001$ .

### 3. Results and discussion

#### 3.1. Structural elucidation of isolated compounds (**1–10**)

##### 3.1.1. Compound **1**

Compound **1** was acquired as an amorphous powder with  $[\alpha]_D^{25}$  13.5 (*c* 0.2, MeOH). Its molecular formula was obtained as  $C_{30}H_{48}O_6$  by HRESIMS with an ion peak at  $m/z$  503.3382  $[M - H]^-$  (calcd for  $C_{30}H_{47}O_6$ , 503.3378). The existence of  $\alpha,\beta$ -unsaturated carbonyl groups were confirmed at  $1711\text{ cm}^{-1}$  in the IR spectrum and at 254 nm in the UV absorption. In addition, the presence of hydroxy groups significantly recorded at  $3402\text{ cm}^{-1}$  and  $1053\text{ cm}^{-1}$ . In the  $^1\text{H}$  NMR spectrum, it showed six methyl singlets in the most upfielded resonances at  $\delta_H$  1.52, 1.50, 1.46, 1.26, 1.19, and 0.86 (each 3H) and other two methyl singlets at  $\delta_H$  2.18, 1.72 were connected to an olefin functionality. In the most downfielded resonances, the presence of olefinic proton was confirmed at  $\delta_H$  6.31 (1H, br s) (Table 3 and Figure 6). Besides, the positions of two oxygenated quaternary carbons were determined based on the  $^{13}\text{C}$  NMR and HSQC spectra at  $\delta_C$  75.1 and 74.1. From the molecular formula ( $C_{30}H_{47}O_6$ ) and  $^{13}\text{C}$  NMR spectrum, compound **1** was suggested seven indices of hydrogen deficiency (IHD), which included three rings of the modified triterpenoid skeleton with an open ring, two  $\text{sp}^2$  carbons ( $\delta_C$  154.9 and 126.6), one carboxylic acid carbon ( $\delta_C$  177.4), and two carbonyl carbons ( $\delta_C$  211.8 and 201.9) (Table 4 and Figures 6, 7). In the HMBC spectrum, the presences of an oxygenated carbon (C-4), C-23 (C=O), and a  $\Delta^{24,25}$  olefin system were identified by the HMBC cross peaks from H-28 ( $\delta_H$  1.46) and H-29 ( $\delta_H$  1.50) to C-4 ( $\delta_C$  75.1), from H-22 ( $\delta_H$  2.92 and 2.70), H-24 ( $\delta_H$  6.31) to C-23 ( $\delta_C$  201.9) and from H-26 ( $\delta_H$  1.72), H-27

( $\delta_{\text{H}}$  2.18) to C-24 ( $\delta_{\text{C}}$  126.6) and C-25 ( $\delta_{\text{C}}$  154.9) (Figure 8). Its COSY data revealed the key correlations between methylene protons H-1 at  $\delta_{\text{H}}$  3.21 [1H, ddd (4.7, 11.5, 15.5)] and  $\delta_{\text{H}}$  1.95 [1H, ddd (4.6, 11.8, 15.5)] to the protons H-2 ( $\delta_{\text{H}}$  2.56, 3.00) (Figure 9). For confirming the carboxylic acid moiety, the HMBC experiment was applied to determine the ring cleavage occurred between C-3 and C-4. The HMBC spectrum showed the cross-peaks between H-2 and C-3 without any correlation from H-28 and H-29 to C-3. The relative configuration of compound **1** was obtained using NOESY experiment. Based on its result, the key correlation between H-5 ( $\delta_{\text{H}}$  1.69) and H-19 ( $\delta_{\text{H}}$  1.19) indicated the  $\beta$  orientation of H-5 and H-19. In addition, protons H-17 ( $\delta_{\text{H}}$  2.79) showed correlations to H-21 ( $\delta_{\text{H}}$  1.52) and H-30 ( $\delta_{\text{H}}$  0.86) which were determined as the  $\alpha$  orientation (Figure 10). The side chain of **1** was elucidated by comparison with the chemical shifts of Gypentonoside A (Fang and Zeng, 1996). Besides, the position at C-21 ( $\delta_{\text{C}}$  27.1) is similar to the chemical shift of 20(*S*) dammarane analogues (Lee et al., 2013). Finally, compound **1** was determined as 4,20(*S*)-dihydroxy-3,4-*seco*-dammar-24-en-12,23-dione-3-oic acid, which also called as Secolongipegenin S1. Especially, 3,4-*seco*-dammarane triterpenoid is firstly isolated from the genus *Gynostemma*.

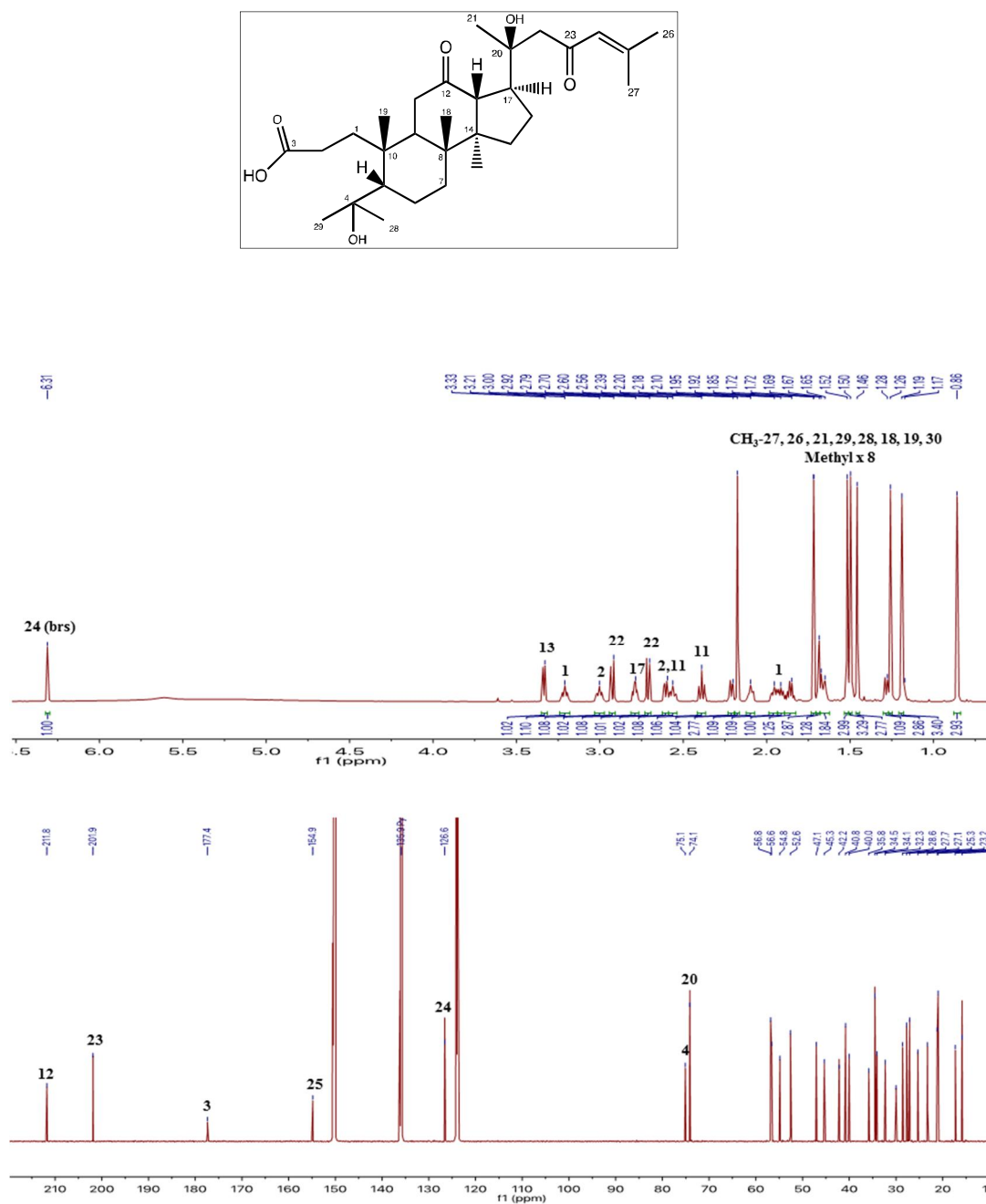


**Figure 6.**  $^1\text{H}$  and  $^{13}\text{C}$  NMR of compound 1 ( $\text{pyridine-}d_5$ , 500 MHz/125 MHz).

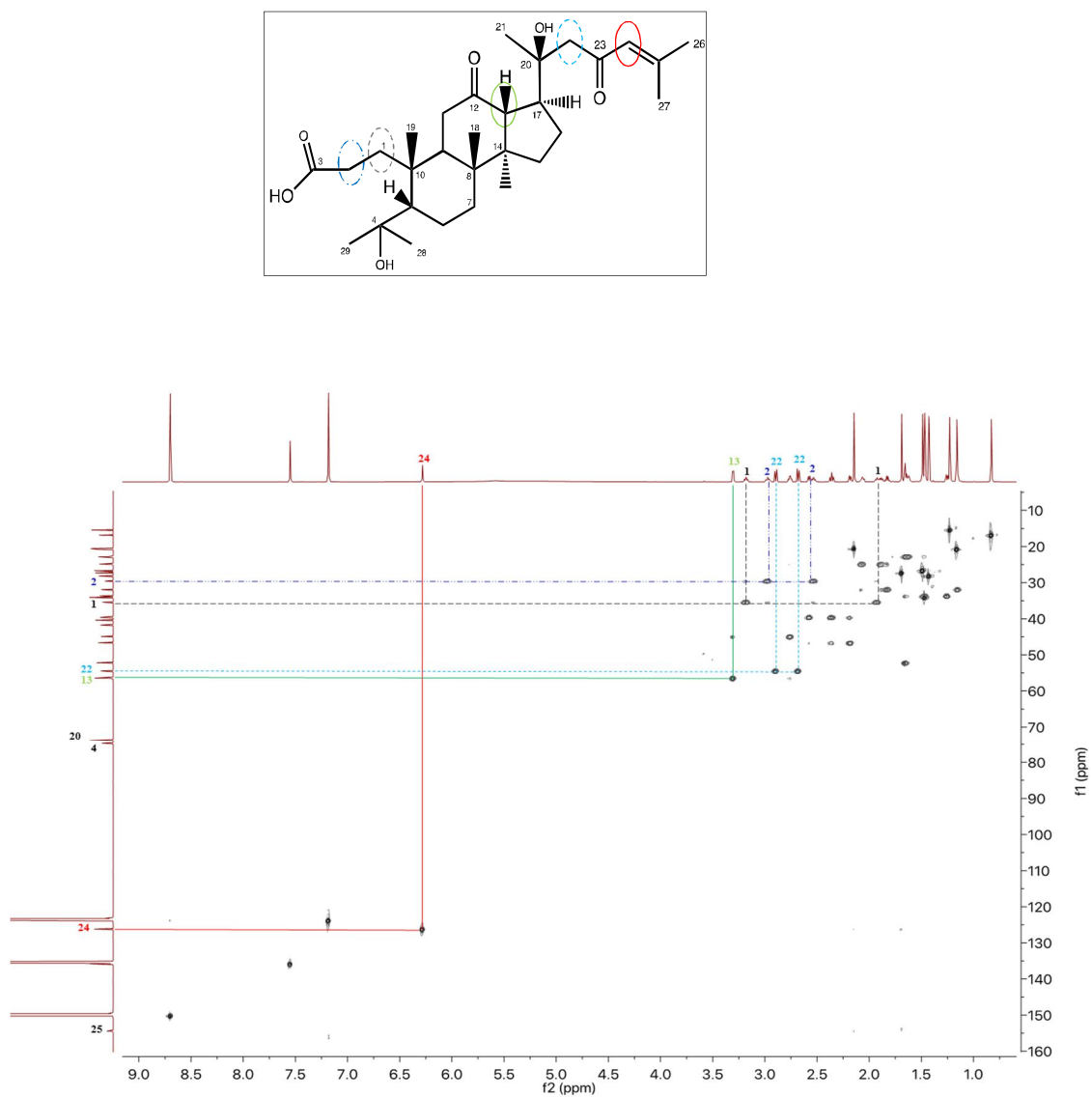


**Figure 7.** HSQC (H→C) of compound **1** (pyridine-*d*<sub>5</sub>, 500 MHz).

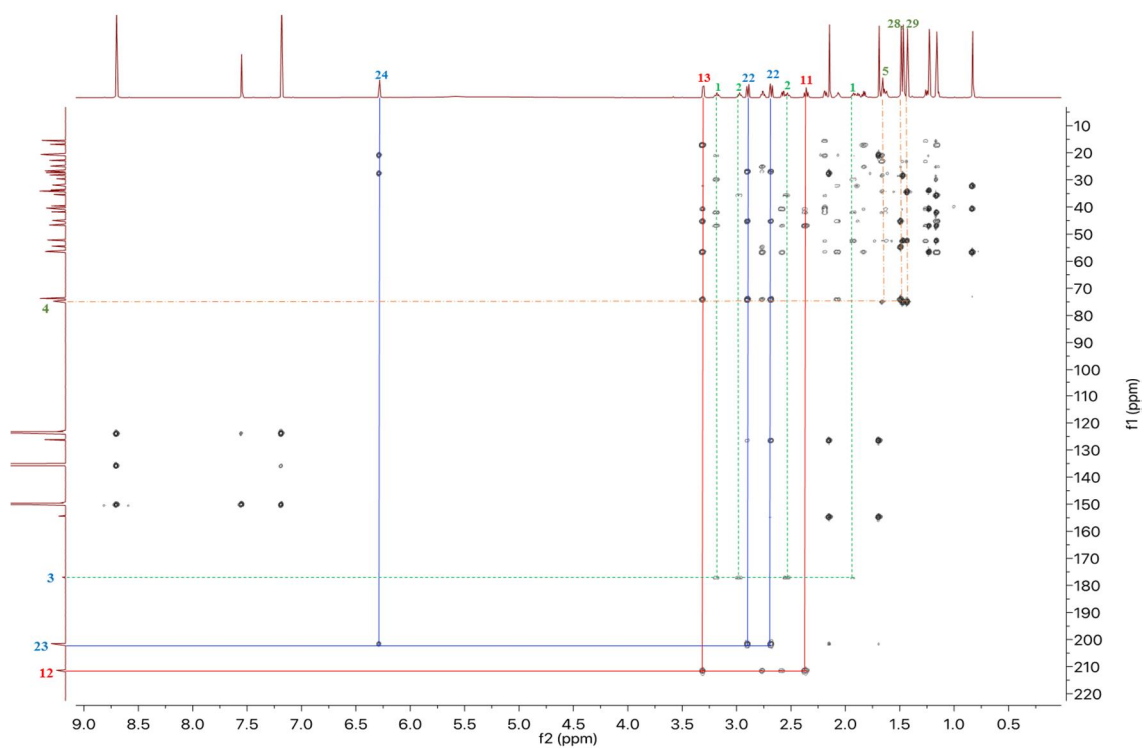
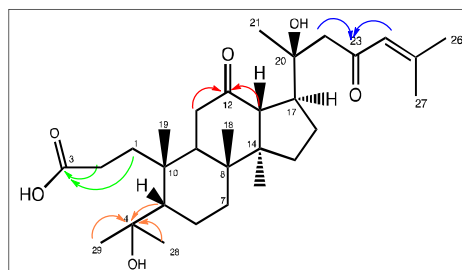


**Figure 8.** HMBC (H→C) of compound **1** (pyridine- $d_5$ , 500 MHz).

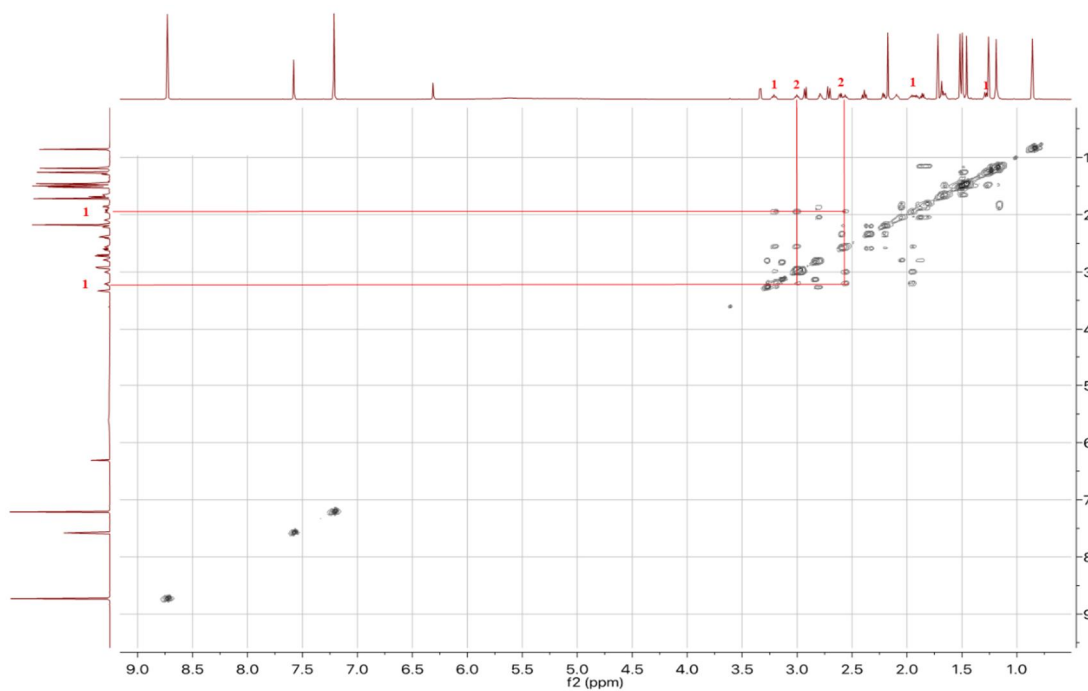
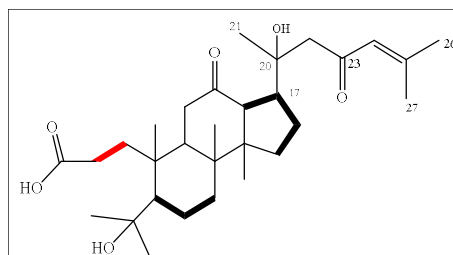


**Figure 9.** COSY (H↔H) of compound **1** (pyridine- $d_5$ , 500 MHz).

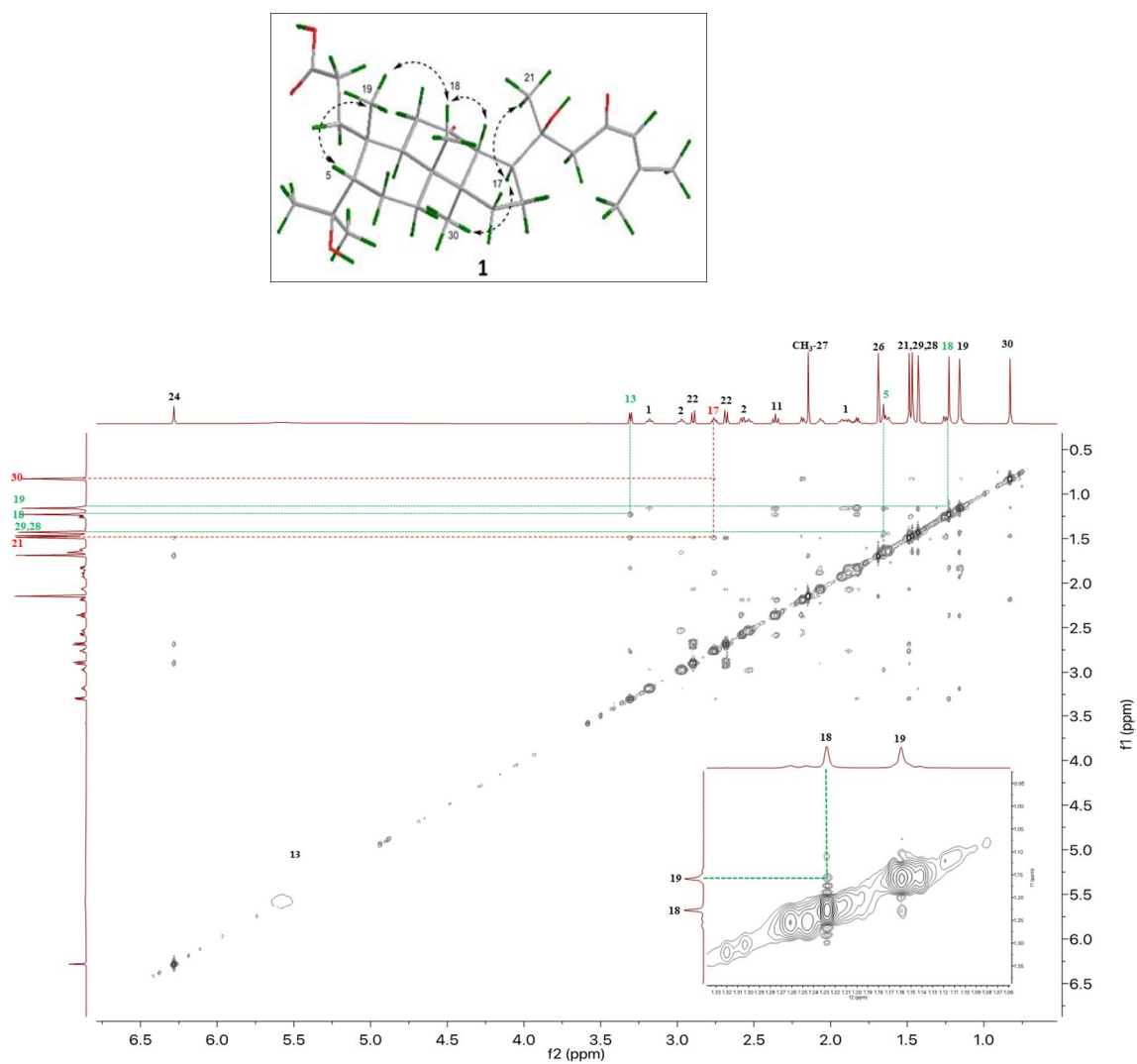


**Figure 10.** NOESY (H↔H) of compound **1** (pyridine-*d*<sub>5</sub>, 500 MHz).



### 3.1.2. Compound 2

Triterpenoid **2** was obtained as an amorphous powder with  $[\alpha]_D^{25}$  4.9 (*c* 0.2, MeOH). Its molecular formula of **2** was identified as  $C_{30}H_{50}O_7$  based on an ion peak at  $m/z$  521.3496  $[M - H]^-$  HRESIMS (calcd for  $C_{30}H_{49}O_7$ , 521.3484). The calculation of IHD for this compound was recorded as 6 indices. A comparison with the  $^1H$  and  $^{13}C$  NMR spectroscopic data of **1** (Tables 3 and 4), triterpenoid **2** also demonstrated similarly chemical shifts. However, the absence of the  $\Delta^{24,25}$  olefinic linkage and the appearance of one more hydroxy moiety were clearly confirmed by  $^{13}C$  NMR and HMBC experiment. The presence of C-24 ( $\delta_C$  57.8, -68.8 ppm), C-25 ( $\delta_C$  70.0, -84.9 ppm), and C-23 ( $\delta_C$  213.1, +11.2 ppm) compared with these chemical shifts of compound **1**. In addition, the HMBC cross peaks from Me-26 and Me-27 to C-25 were also obtained. These results strongly indicated the hydroxy group attached at C-25. Hence, compound **2** was assigned as 4,20(*S*),25-trihydroxy-3,4-*seco*-dammaran-12,23-dione-3-oic acid which also named as Secolongipegenin S2 (Figures 11-15).

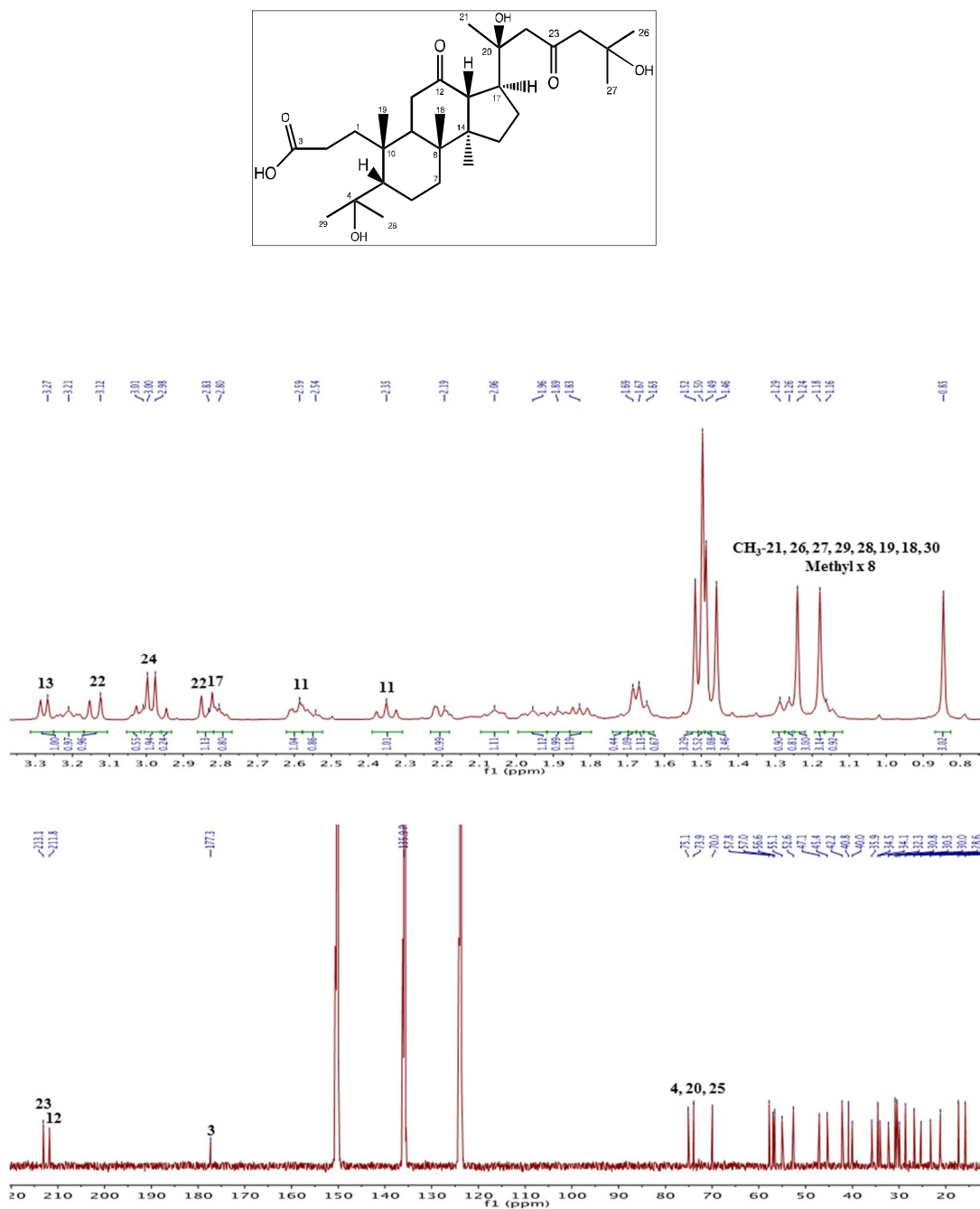


**Figure 11.**  $^1\text{H}$  and  $^{13}\text{C}$  NMR of compound **2** ( $\text{pyridine-d}_5$ , 500 MHz/125 MHz).

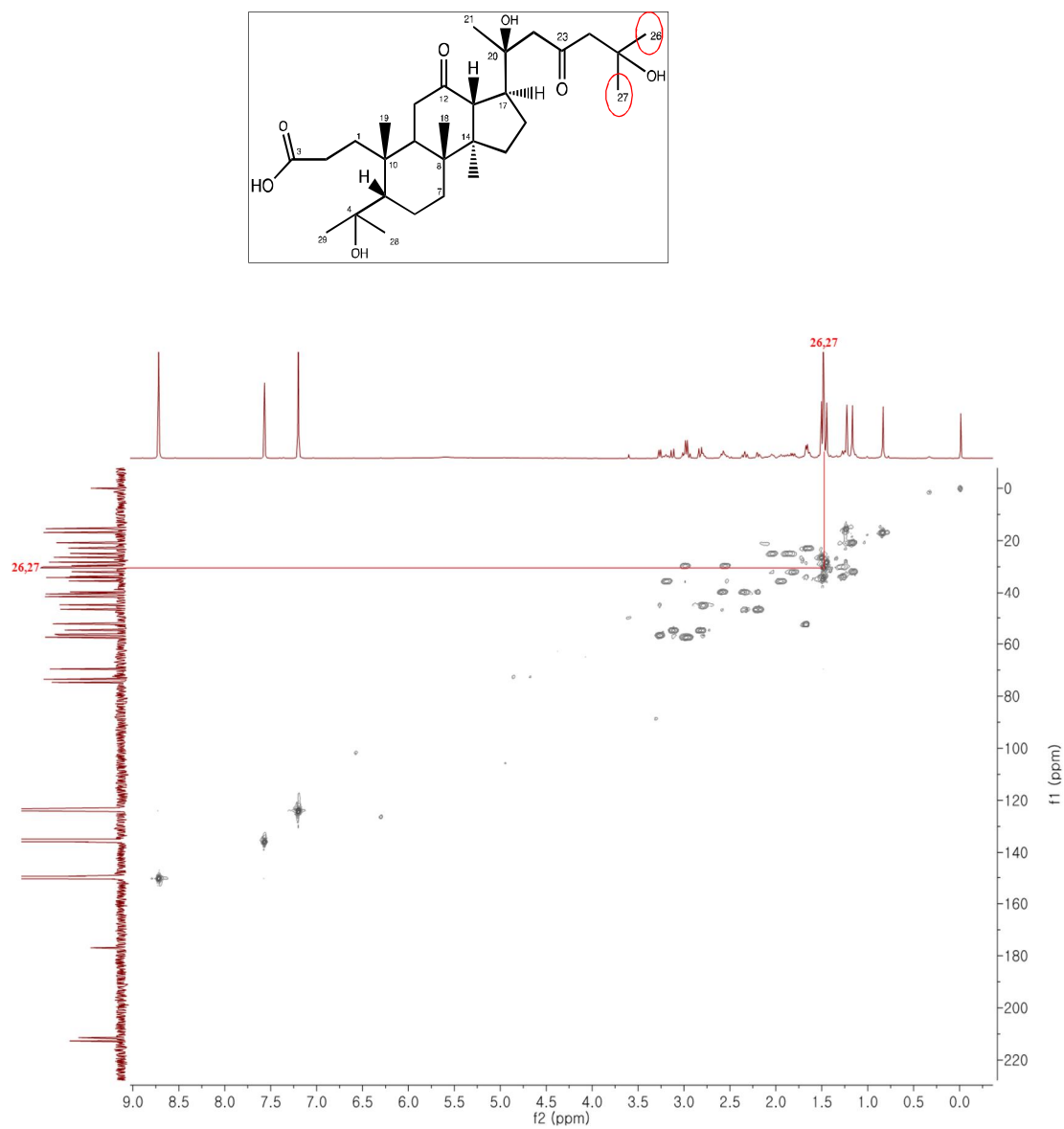


**Figure 12.** HSQC (H→C) of compound **2** (pyridine-*d*<sub>5</sub>, 500 MHz).

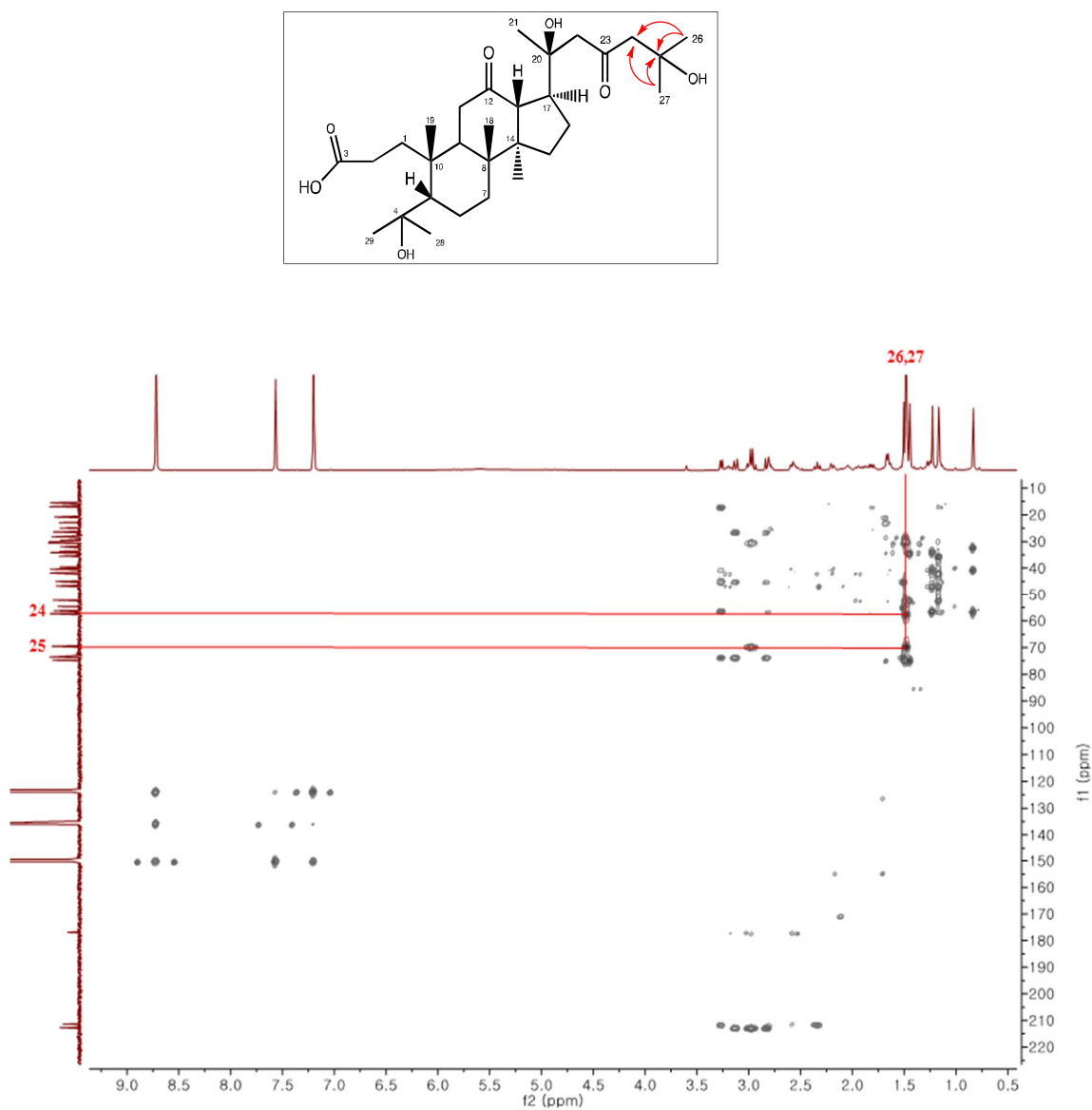


**Figure 13.** HMBC (H→C) of compound 2 (pyridine- $d_5$ , 500 MHz).

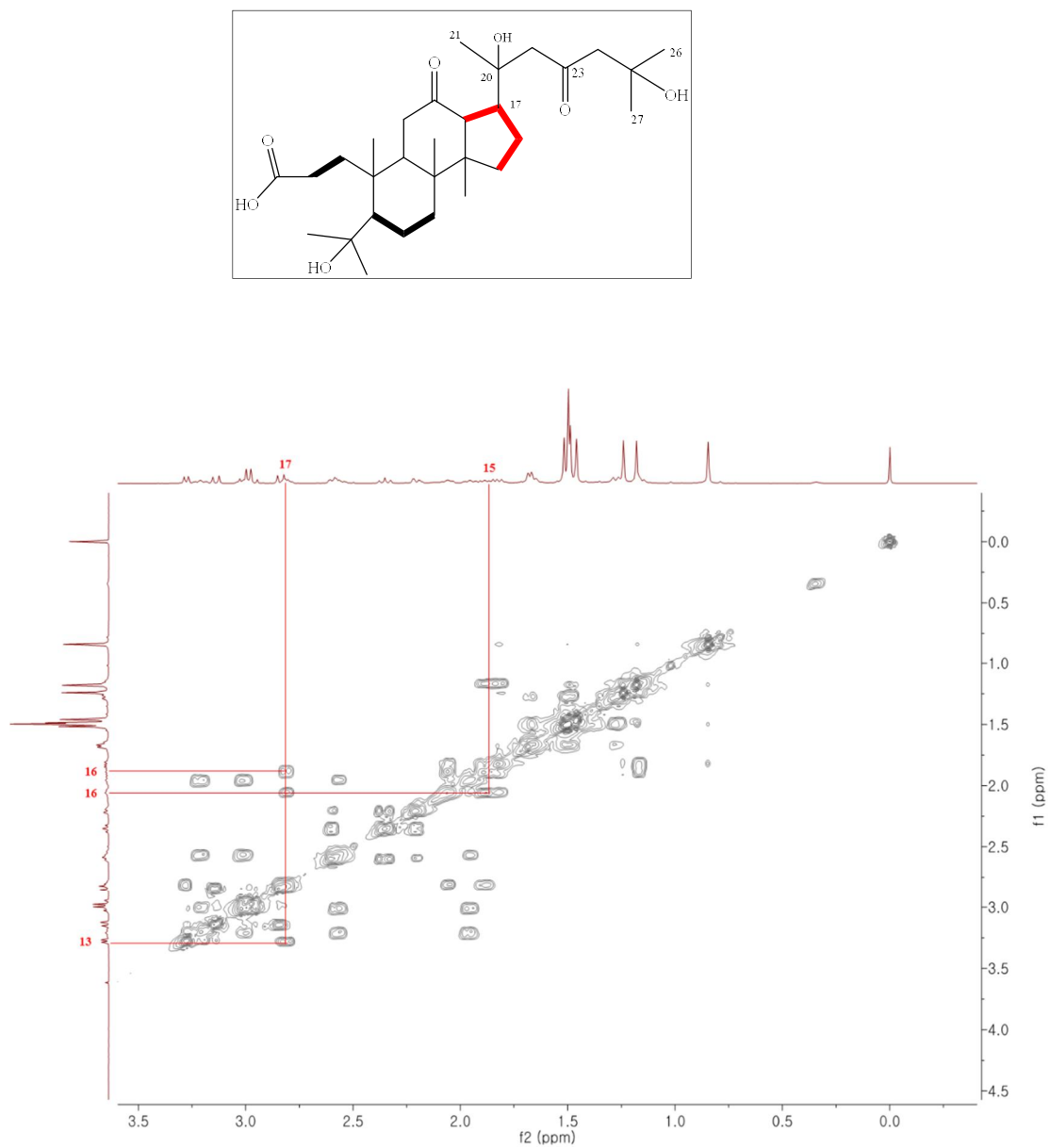


**Figure 14.** COSY (H $\leftrightarrow$ H) of compound 2 (pyridine-*d*<sub>5</sub>, 600 MHz).

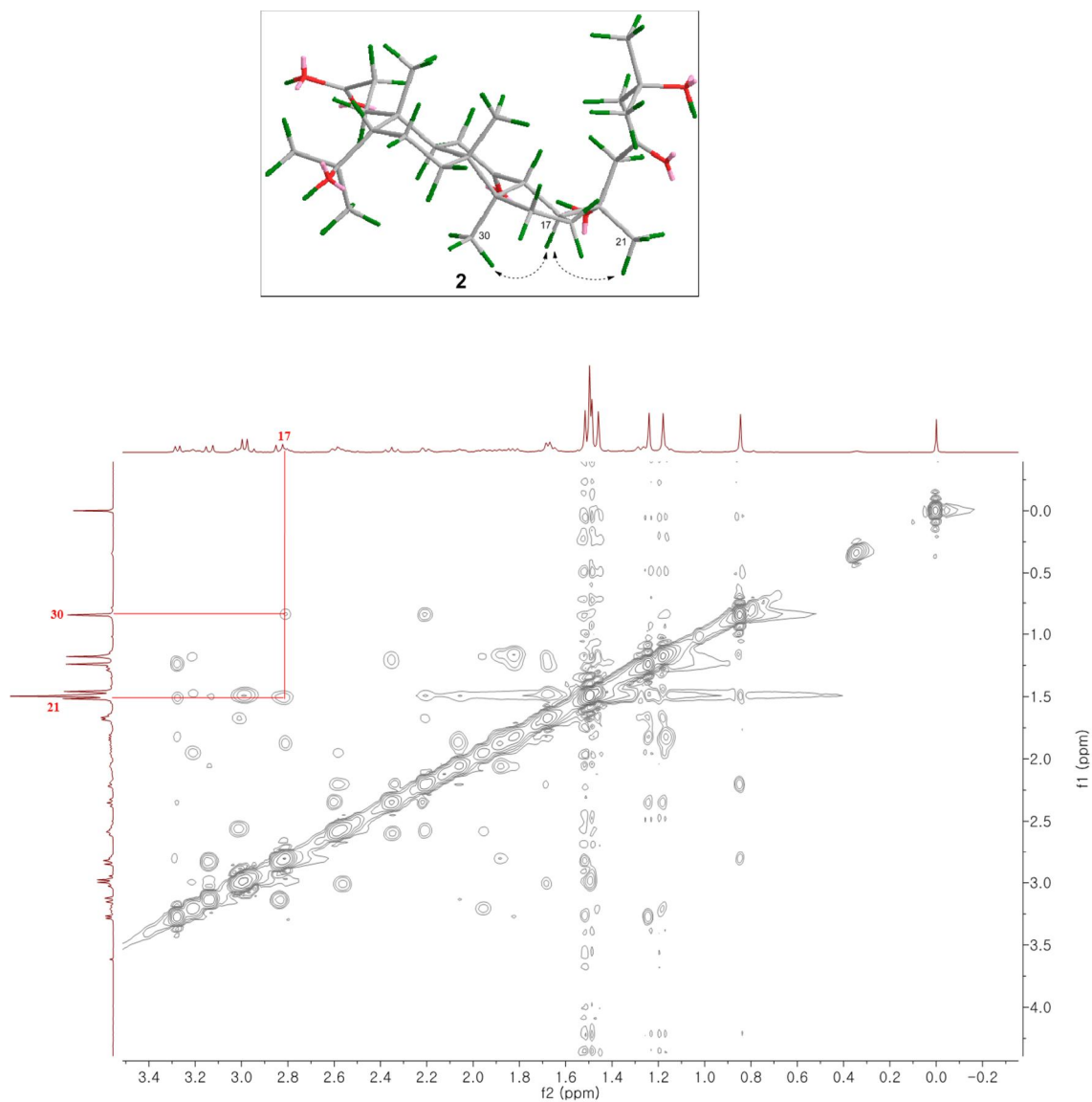


**Figure 15.** NOESY (H↔H) of compound **2** ( $\text{pyridine-}d_5$ , 600 MHz).

### 3.1.3. Compound **3**

Secolongipegenin S3 (**3**) was purified as an amorphous powder with  $[\alpha]_{\text{D}}^{25}$  5.5 ( $c$  0.2, MeOH). Its molecular formula was identified as  $\text{C}_{24}\text{H}_{38}\text{O}_5$  and based on the HRESIMS with an ion peak at  $m/z$  405.2647  $[\text{M} - \text{H}]^-$  (calcd for  $\text{C}_{24}\text{H}_{37}\text{O}_5$  405.2646). The IHD of this compound was calculated as six indices. According to NMR experiment (Tables 3 and 4), compound **3** clearly demonstrated a similar skeleton with **1** in *seco* rings A and B. In addition, the HMBC spectrum showed the cross-peaks between H-17 and Me-21 to C-20. Therefore, compound **3** was determined as 4-hydroxy-3,4-*seco*-22,23,24,25,26,27-hexanordammaran-12,20-dion-3-oic acid (Figures 16-18).

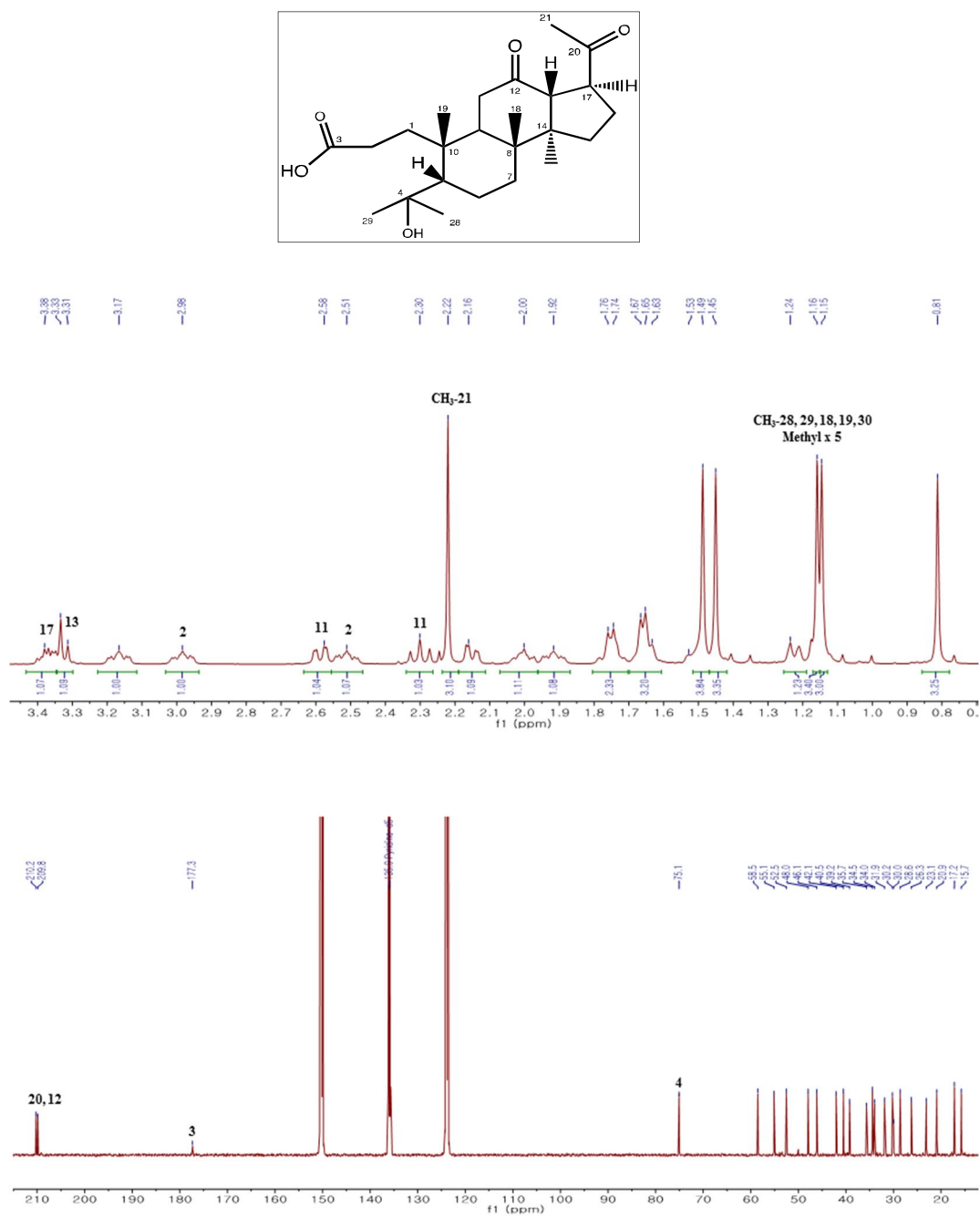


**Figure 16.** <sup>1</sup>H and <sup>13</sup>C NMR of compound 3 (pyridine-*d*<sub>5</sub>, 500 MHz/125 MHz).



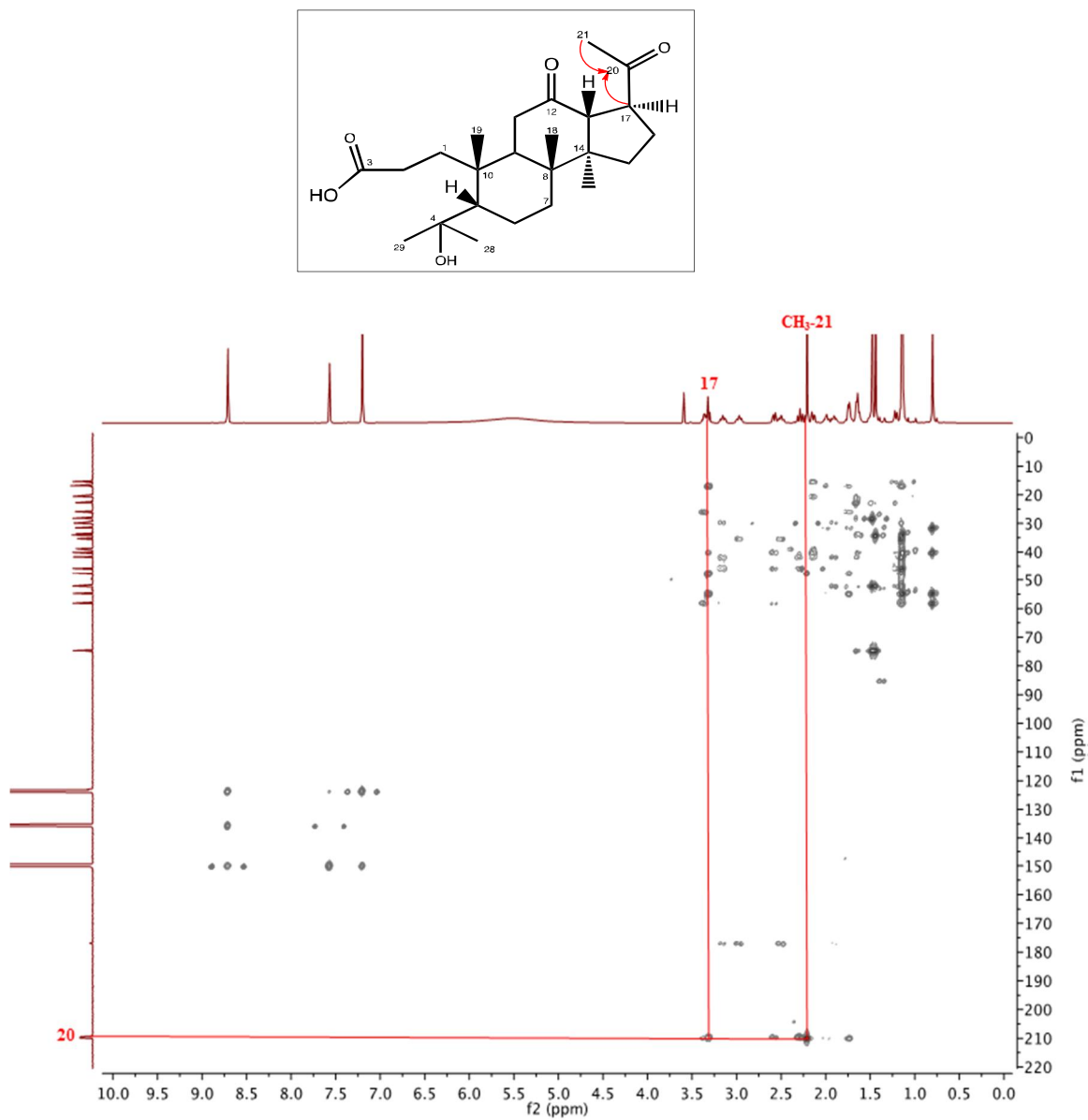


**Figure 17.** HMBC (H→C) of compound 3 (pyridine-*d*<sub>5</sub>, 500 MHz).

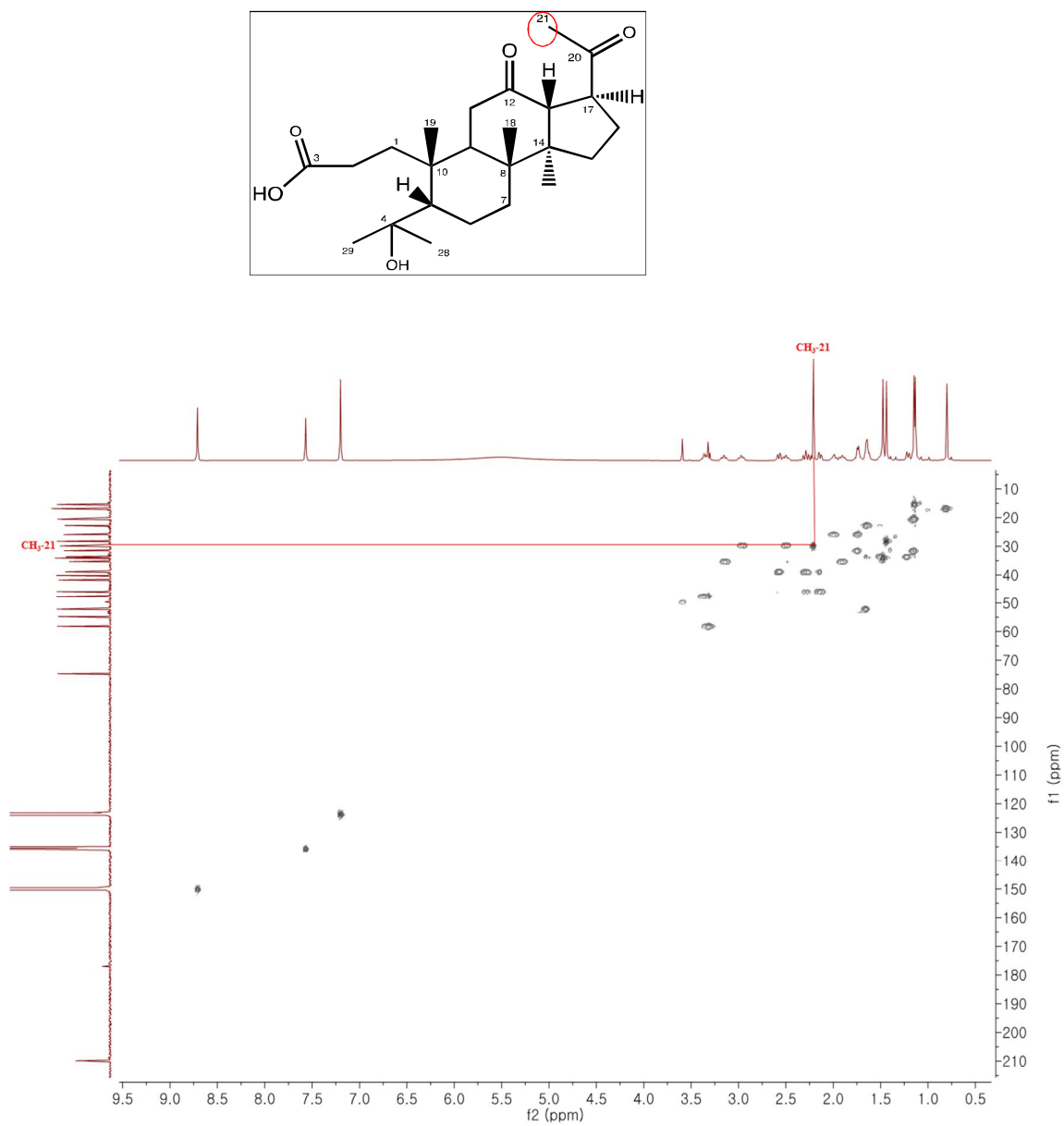


**Figure 18.** HSQC (H $\rightarrow$ C) of compound **3** (pyridine-*d*<sub>5</sub>, 500 MHz).

#### 3.1.4. Compound 4

Triterpenoid **4** was isolated as an amorphous powder with  $[\alpha]_D^{25}$  2.7 (*c* 0.2, MeOH). The HRESIMS presented a pseudomolecular ion peak at  $m/z$  873.4525  $[M + HCOO]^-$  (calcd for  $C_{43}H_{69}O_{18}$ , 873.4489), which suggested this compound had the molecular formula of  $C_{42}H_{68}O_{16}$  and the presence of nine IHD. The  $^1H$  NMR data revealed six methyl singlets ( $\delta_H$  2.23, 1.15, 1.07, 1.00, 0.77, and 0.71) (each 3H, s) (Figure 19). The presence of two carbonyl groups ( $\delta_C$  210.3 and 210.0), three anomeric carbons ( $\delta_C$  105.3, 104.0, 102.5), and 17 oxygenated carbons ( $\delta_C$  62.8 to 88.6) were indicated by the  $^{13}C$  NMR data (Figure 19). Based on the comparison of the NMR data between compound **4** with 3 $\beta$ -hydroxy-hexanordammaran-20-one (Tu et al., 2008), the structures of two compounds were similar. However, compound **4** was substituted with one carbonyl group and possessed one more sugar. In the HMBC spectrum, the presences of carbonyl groups C-12 and C-20 were determined by the HMBC cross peaks from H-11 ( $\delta_H$  2.23 and 2.15) and H-13 ( $\delta_H$  3.21) to C-12 ( $\delta_C$  210.3), from H-17 ( $\delta_H$  3.35) and H-21 ( $\delta_H$  2.22) to C-20 ( $\delta_C$  210.0) (Figure 20). The relative configuration of compound **4** was identified using NOESY experiment. The key correlations of H-3 ( $\delta_H$  3.24) and H-5 ( $\delta_H$  0.69) indicated an  $\alpha$  orientation for H-3 (Figure 44). Hence, the aglycone of **4** revealed unequivocally as 3 $\beta$ -hydroxy-22,23,24,25,26,27-hexanordammarane-12,20-dione. In the sugar moieties of compound **4**, all NMR data demonstrated the appearance of three sugars units, including a  $\beta$ -glucopyranosyl unit [ $\delta_H$  4.76, d (7.7);  $\delta_C$  105.3] and two  $\alpha$ -rhamnopyranosyl units [( $\delta_H$  5.88, br s;  $\delta_C$  102.5) and ( $\delta_H$  5.67, br s;  $\delta_C$  104.0)] (Figure 21). In addition, compound **4** also successfully hydrolyzed with HCl to obtain D-glucose and L-rhamnopyranose. After reaction with L-cysteine

methyl ester hydrochloride and TMS derivatization, the mixtures were measured using gas chromatographic analysis. Result of the positive mode in HPLC-MS indicated fragment ions at 829  $[M + H]^+$ , 683  $[M + H - \text{rha} (146)]^+$ , 536  $[M + H - \text{rha} - \text{rha} (146)]^+$ , and 375  $[M + H - \text{H}_2\text{O} - 2 \times \text{rha} - \text{glc} (162)]^+$ , which suggested the existence of two rhamnose and one glucose moieties. The positions of three sugars were also identified based on a HMBC experiment (Figure 20). This data was demonstrated the presence of key HMBC correlations between H-1' ( $\delta_{\text{H}}$  4.76) and C-3 ( $\delta_{\text{C}}$  88.6), H-1'' ( $\delta_{\text{H}}$  5.88) and C-2' ( $\delta_{\text{C}}$  78.3), H-1''' ( $\delta_{\text{H}}$  5.67) and C-3' ( $\delta_{\text{C}}$  87.5). Therefore, compound **4** was determined as 3 $\beta$ -hydroxy-22,23,24,25,26,27-hexanordammaran-12,20-dione-3-*O*- $\alpha$ -L-rhamnopyranosyl-(1 $\rightarrow$ 2)-[ $\alpha$ -L-rhamnopyranosyl-(1 $\rightarrow$ 3)]- $\beta$ -D-glucopyranoside which also called as Longipenoside ND1.

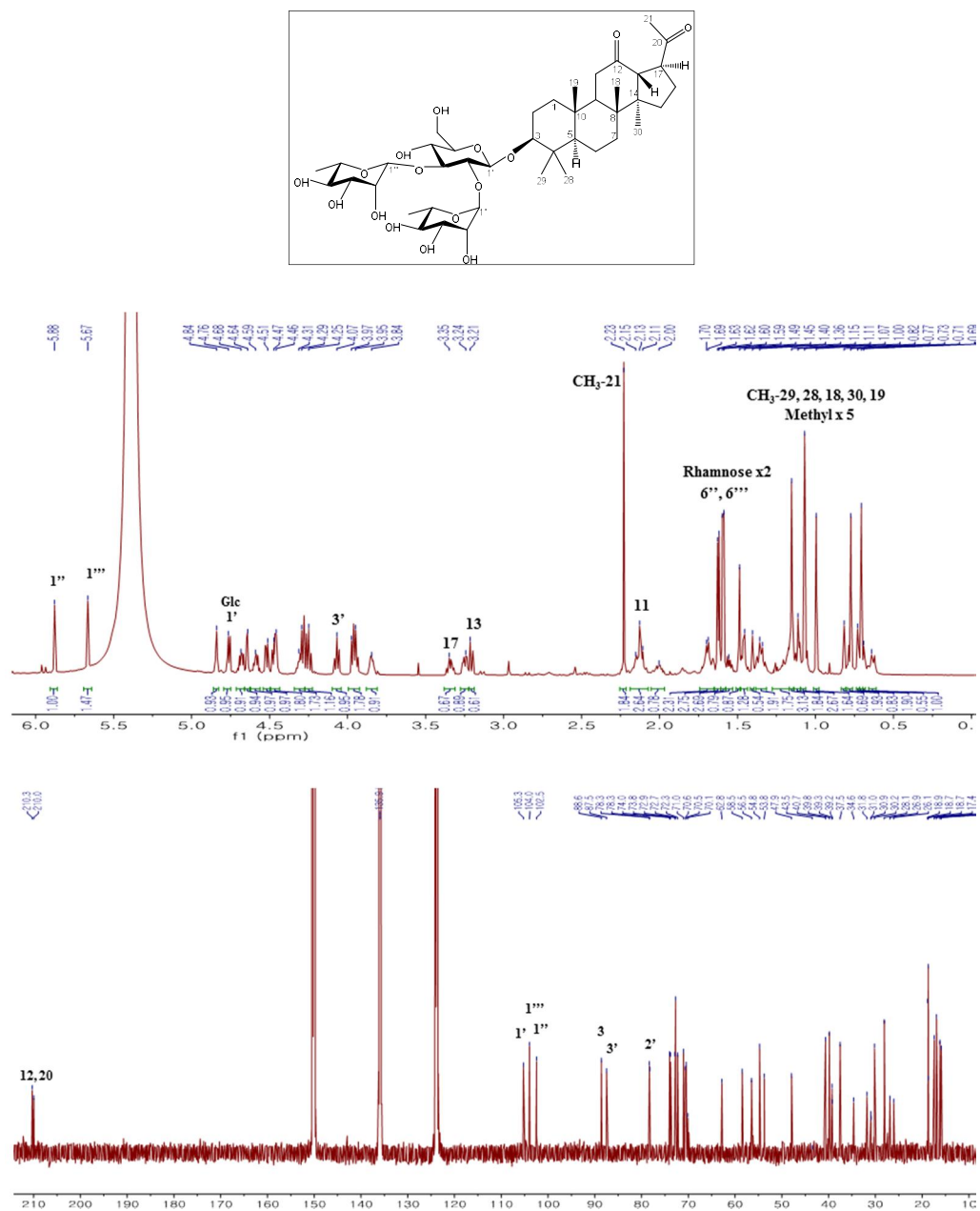


**Figure 19.** <sup>1</sup>H and <sup>13</sup>C NMR of compound 4 (pyridine-*d*<sub>5</sub>, 600 MHz/150 MHz).

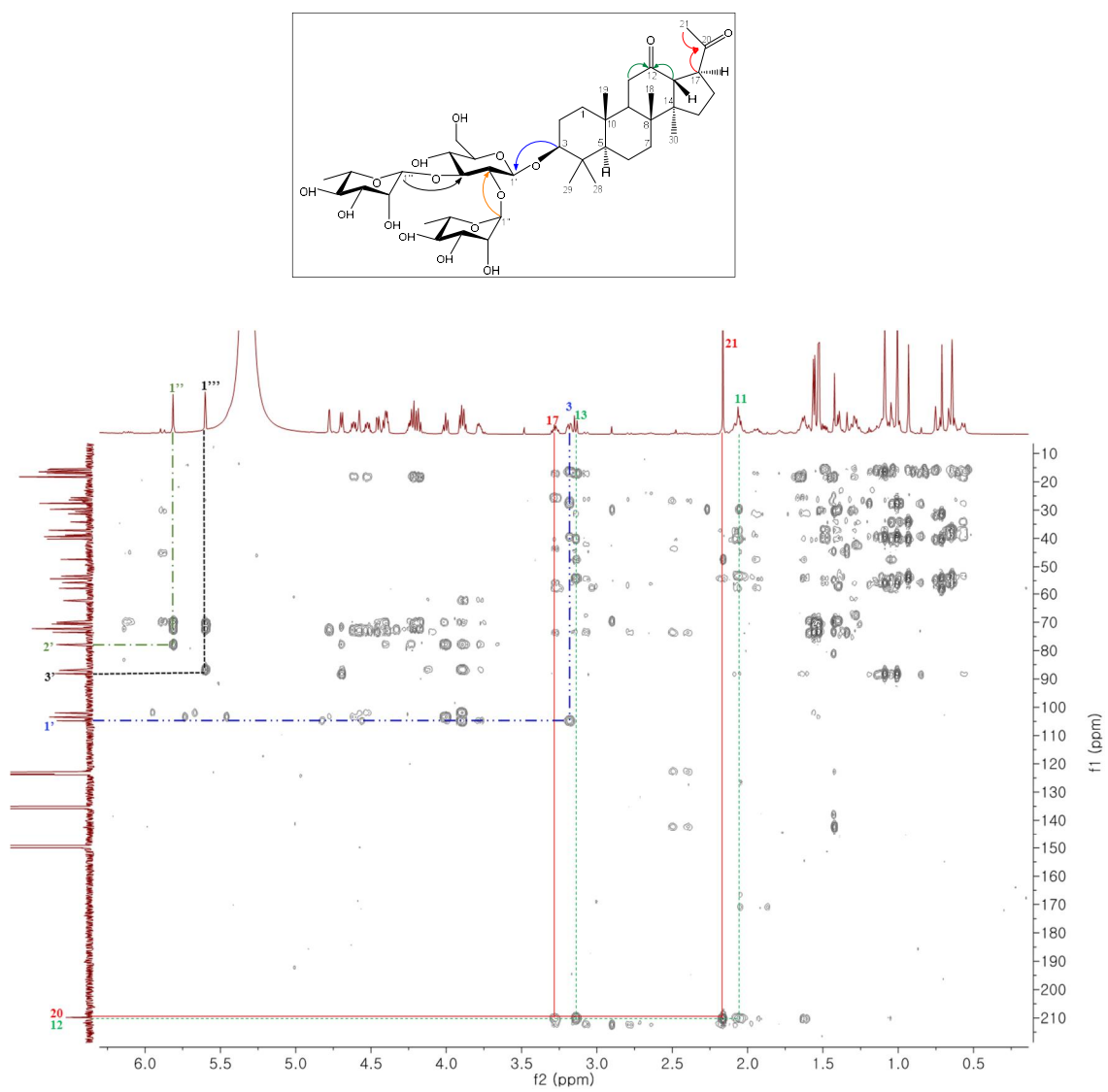


**Figure 20.** HMBC (H→C) of compound **4** (pyridine- $d_5$ , 500 MHz).

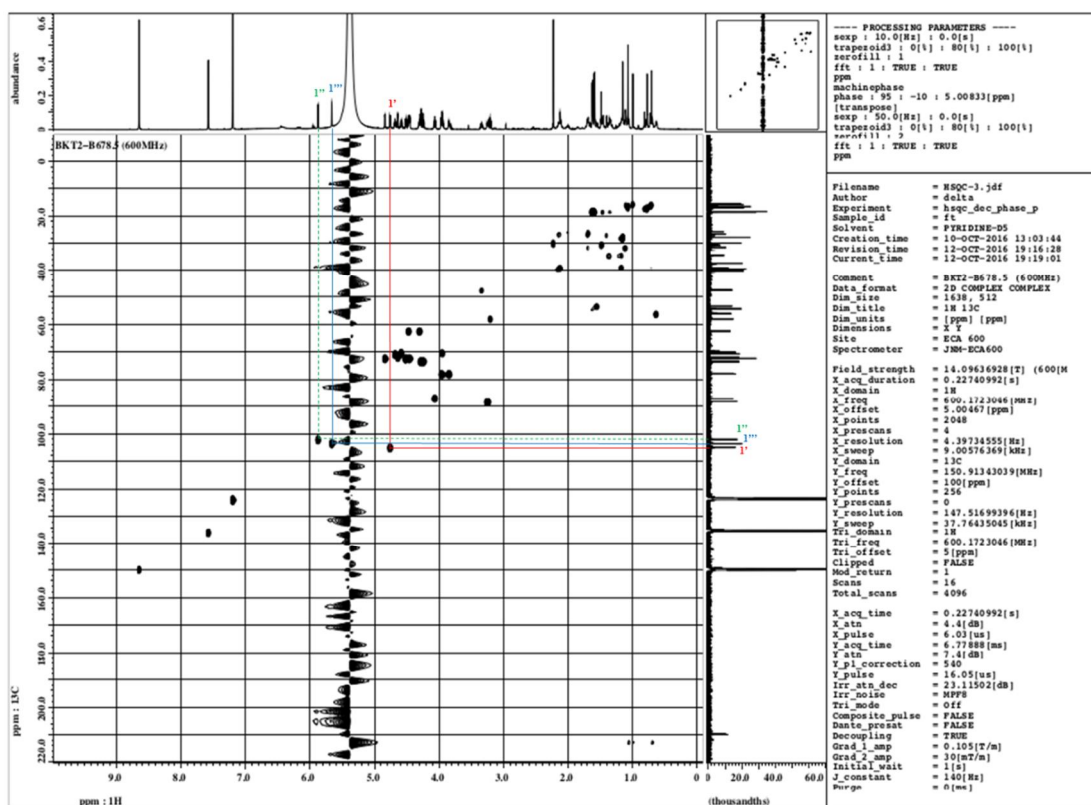
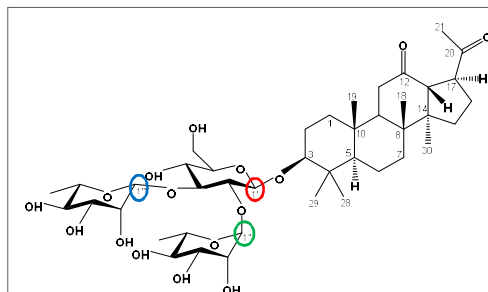
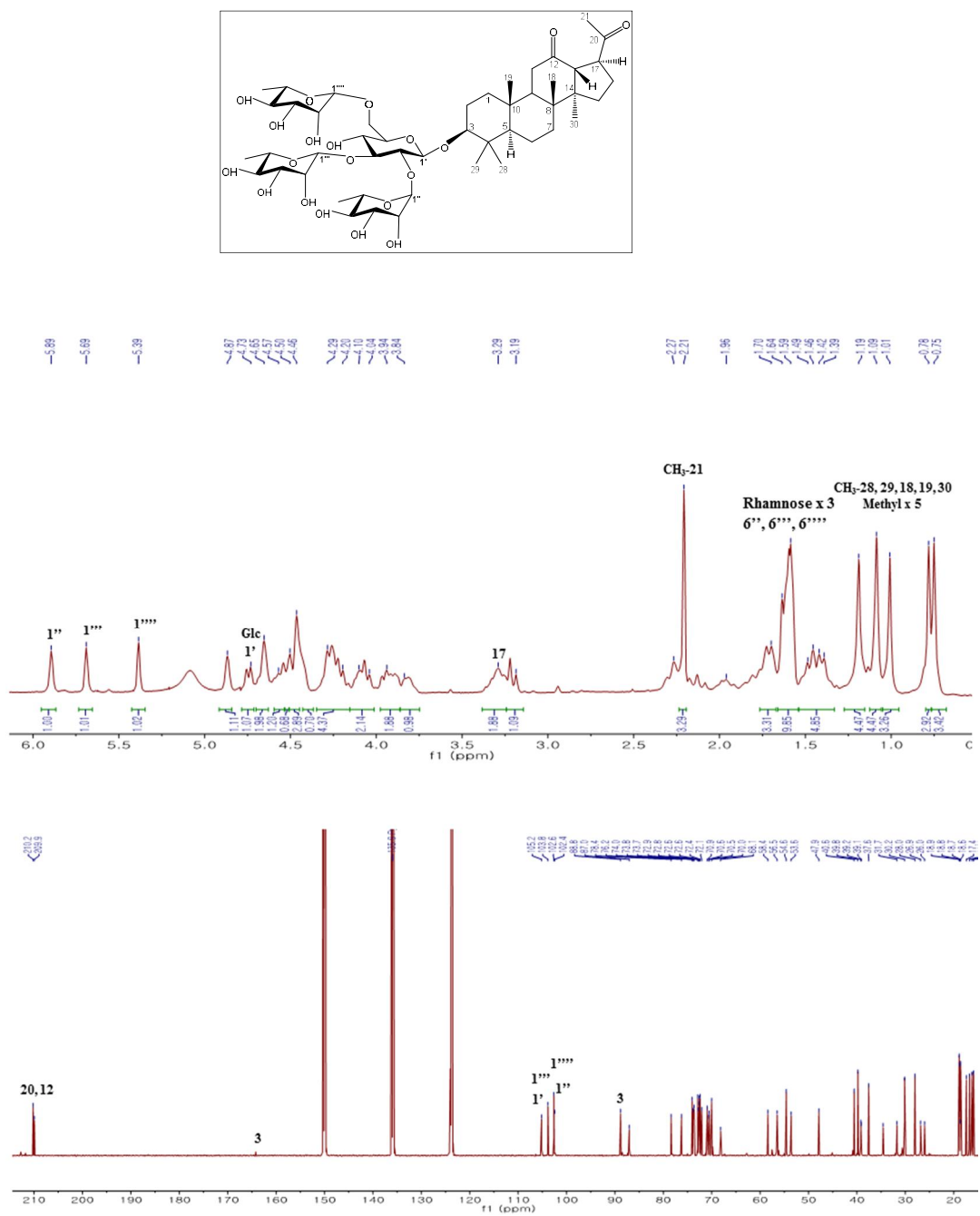


Figure 21. HSQC (H→C) of compound 4 (pyridine- $d_5$ , 600 MHz).

### 3.1.5. Compound **5**

Longipenoside ND2 (**5**) was isolated as an amorphous powder with  $[\alpha]_D^{25}$  5.9 (c 0.2, MeOH). The HRESIMS of this compound revealed an ion peak at  $m/z$  1019.5104  $[M + HCOO]^-$  (calcd for  $C_{49}H_{79}O_{22}$ , 1019.5068). It suggested a molecular formula  $C_{48}H_{78}O_{20}$  and indicated the presence of ten IHD. All NMR data of compound **5** showed similarly the chemical shifts with compound **4**. The difference was appearance of a rhamnose glycosyl unit at C-6', which was identified by a downfield chemical shift of C-6' ( $\delta_C$  68.1, +5.3 ppm) and the strong HMBC correlation from H-1''' ( $\delta_H$  5.39, br s) to C-6'. In addition, compound **5** was reacted with acid HCl, L-cysteine methyl ester hydrochloride and TMS derivatization, progressively. The products of D-glucose and L-rhamnose were analyzed using gas chromatography method. The positive mode of HPLC-MS experiment clearly showed the existence of one glucose and three rhamnose units based on fragment ions at  $m/z$  975  $[M + H]^+$ , 829  $[M + H - rha (146)]^+$ , 682  $[M + H - rha - rha (146)]^+$ , 535  $[M + H - H_2O - 2 \times rha - rha (146)]^+$  and 375  $[M + H - H_2O - 3 \times rha - glc (162)]^+$ . Finally, the structure of **5** was identified as 3 $\beta$ -hydroxy-22,23,24,25,26,27-hexanordammaran-12,20-dione-3-*O*- $\alpha$ -L-rhamnopyranosyl-(1 $\rightarrow$ 2)-[ $\alpha$ -L-rhamnopyranosyl-(1 $\rightarrow$ 3)]-[ $\alpha$ -L-rhamnopyranosyl-(1 $\rightarrow$ 6)]- $\beta$ -D-glucopyranoside (Figures 22-24).





**Figure 22.** <sup>1</sup>H and <sup>13</sup>C NMR of compound **5** (pyridine-*d*<sub>5</sub>, 600 MHz/150 MHz).

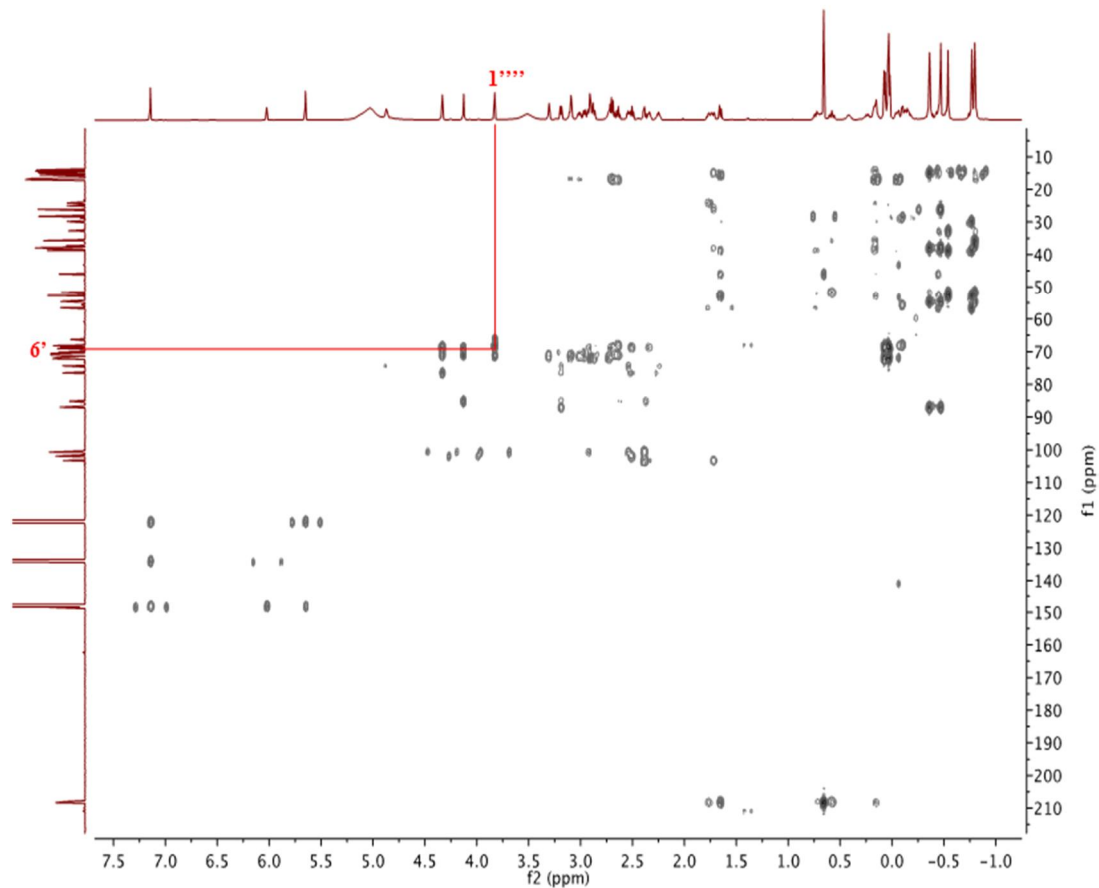
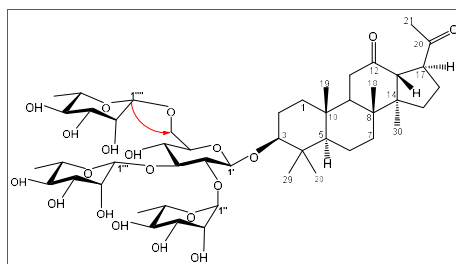


**Figure 23.** HMBC (H→C) of compound **5** (pyridine-*d*<sub>5</sub>, 500 MHz).

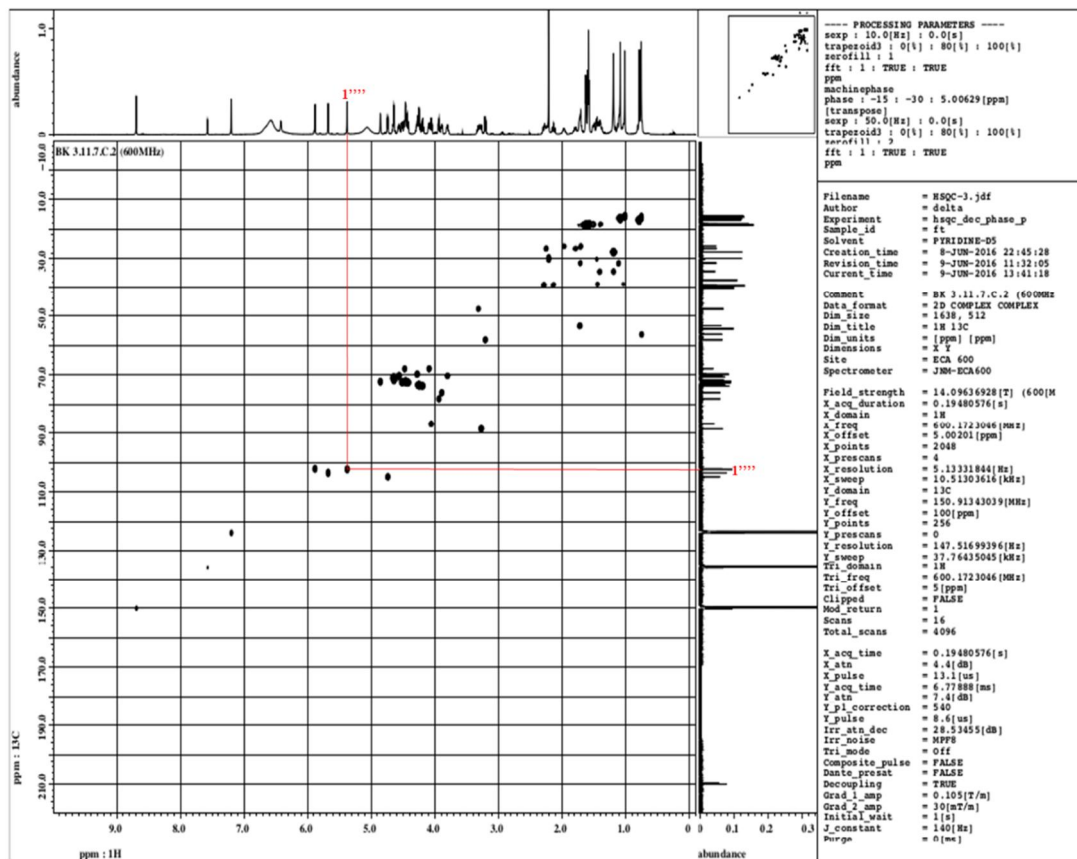
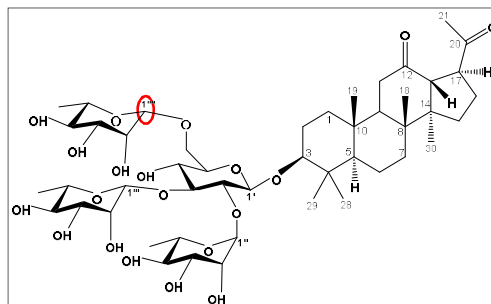


**Figure 24.** HSQC (H→C) of compound **5** (pyridine- $d_5$ , 600 MHz).

### 3.1.6. Compound **6**

Compound **6** was purified as an amorphous powder with  $[\alpha]_D^{25}$  -1.5 (*c* 0.2, MeOH). Its molecular formula was identified as C<sub>54</sub>H<sub>90</sub>O<sub>22</sub> based on the negative ion peak at *m/z* 1135.5946 [M + HCOO]<sup>-</sup> (calcd for C<sub>55</sub>H<sub>91</sub>O<sub>24</sub>, 1135.5906). According to the HPLC-MS experiment, the positive mode of **6** suggested the appearance of a glycoside chain similar to compound **5** and the aglycone was substituted by two hydroxy groups. The <sup>1</sup>H and <sup>13</sup>C NMR spectroscopic data of **6** (Tables 3 and 4) showed the same skeleton with **5**, excepted of the side chain at C-17 which had the similar resonances to those of **1**. The disappearance of olefinic linkage at Δ<sup>24,25</sup> and the attachment of a hydroxyl group at C-25 were confirmed by <sup>13</sup>C NMR spectrum via C-24 (δ<sub>C</sub> 57.7, -68.9 ppm), C-25 (δ<sub>C</sub> 70.1, -84.8 ppm), and C-23 (δ<sub>C</sub> 212.9, +11.0 ppm) compared to **1**. In the HMBC experiment, the key correlations were established from Me-26 (δ<sub>H</sub> 1.44, s) and Me-27 (δ<sub>H</sub> 1.45, s) to C-25 (δ<sub>C</sub> 70.1). Hence, compound **6** was elucidated as 3β,20(*S*),25-trihydroxydammaran-12,23-dione-3-*O*-α-L-rhamnopyranosyl-(1→2)-[α-L-rhamnopyranosyl-(1→3)]-[α-L-rhamnopyranosyl-(1→6)]-β-D-glucopyranoside which also named as Longipenoside GL1 (Figures 25-27).

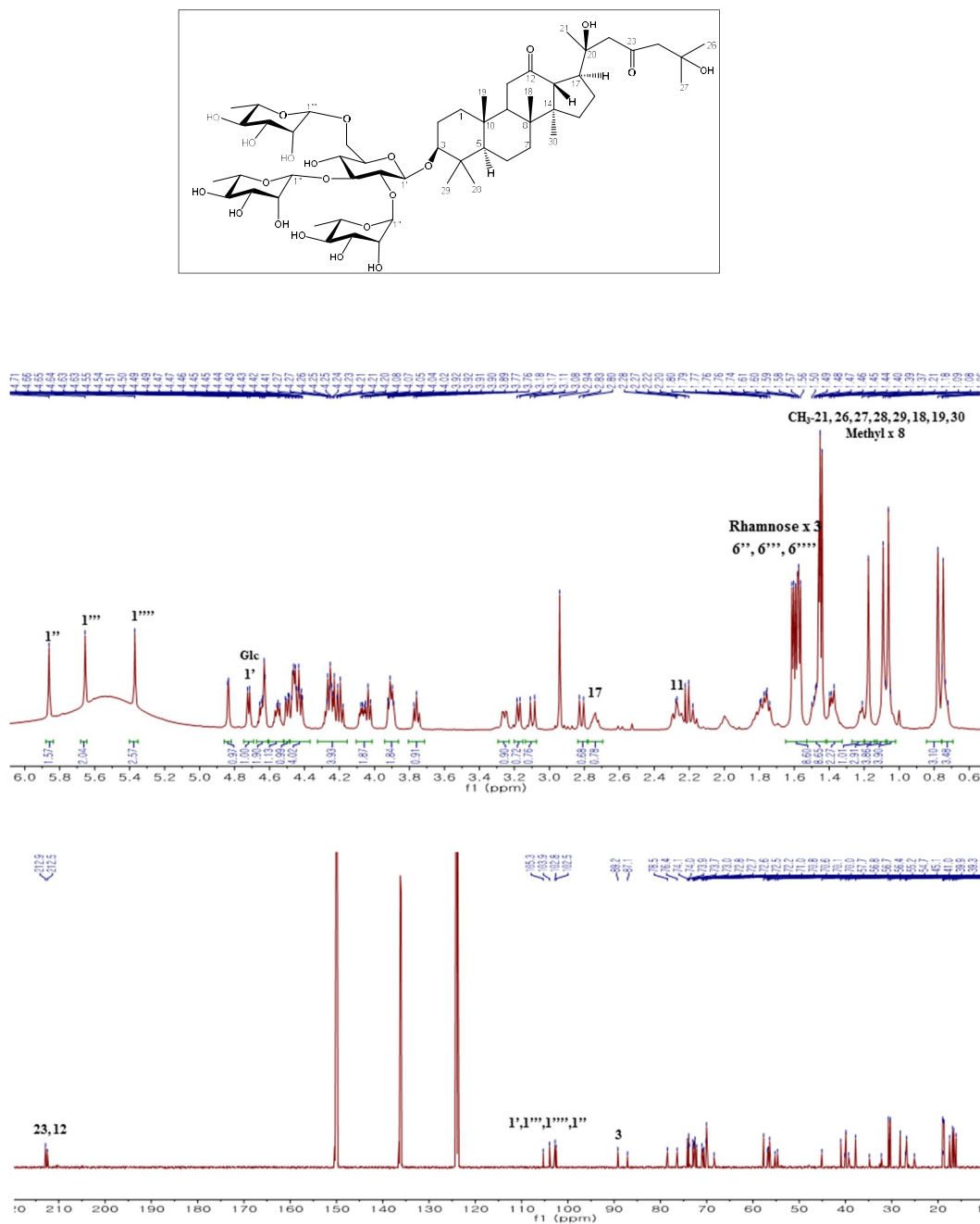


**Figure 25.**  $^1\text{H}$  and  $^{13}\text{C}$  NMR of compound 6 ( $\text{pyridine-}d_5$ , 600 MHz/150 MHz).

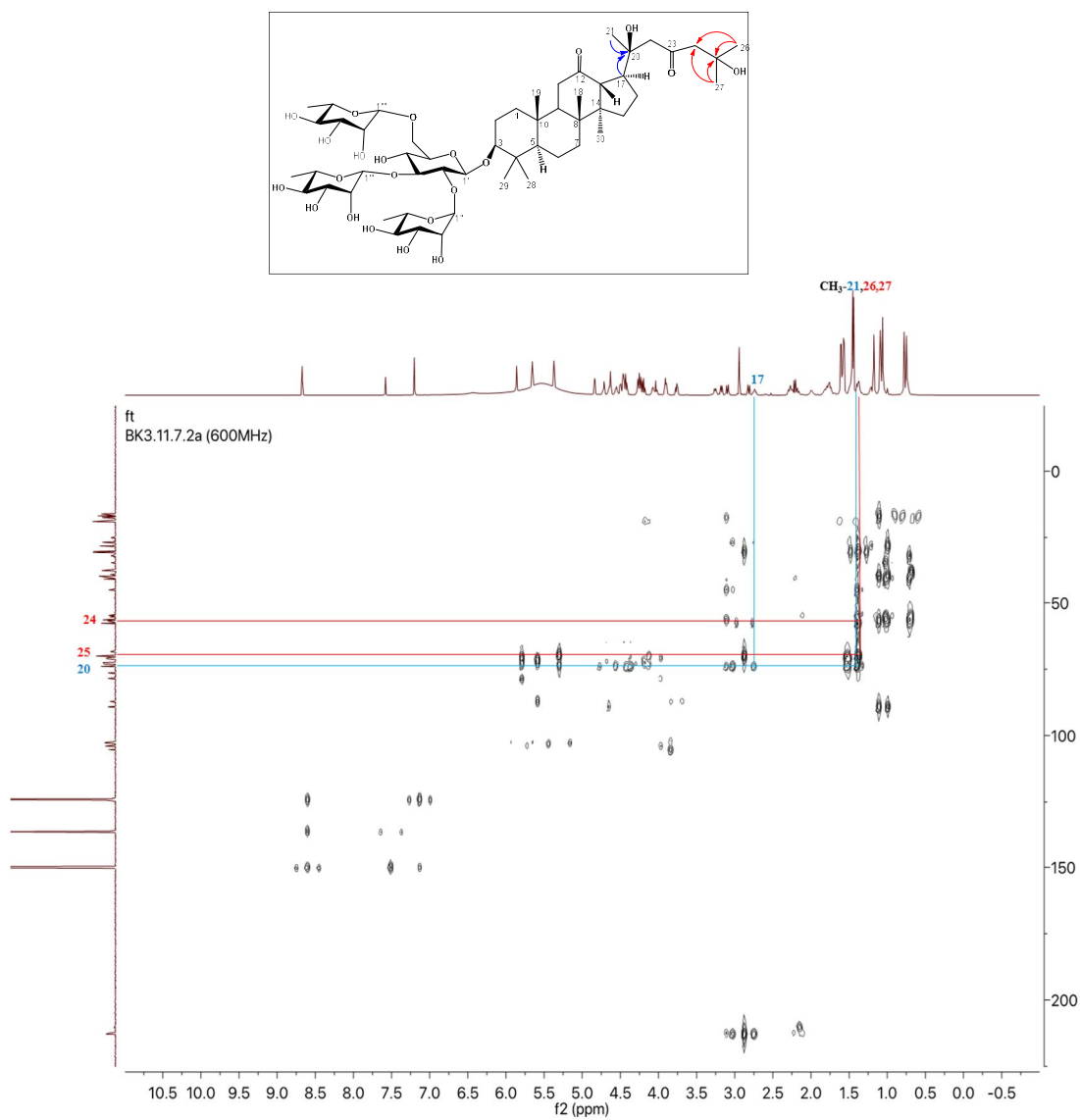


**Figure 26.** HMBC (H→C) of compound **6** (pyridine- $d_5$ , 600 MHz).

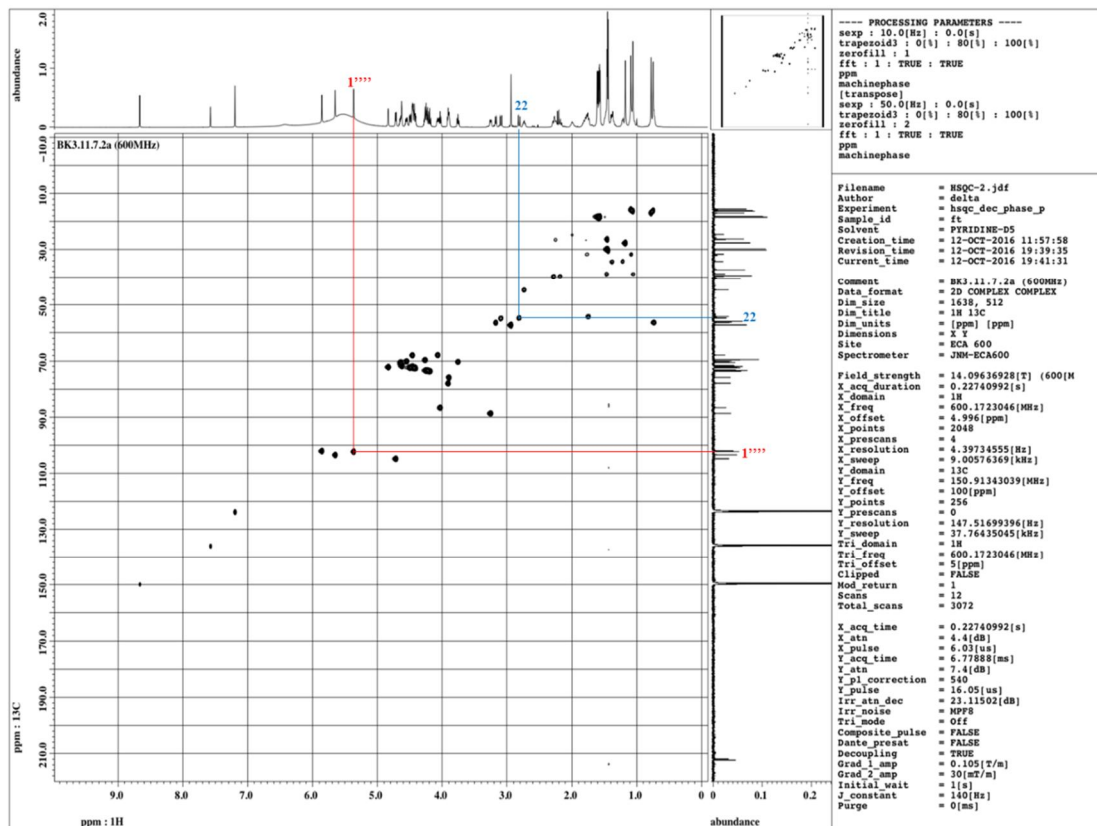
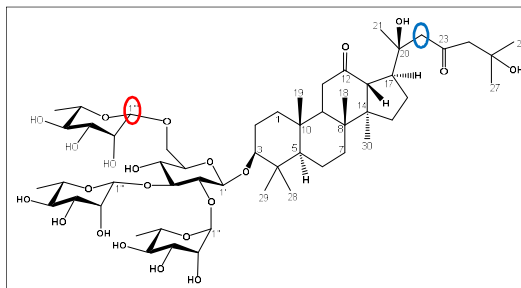
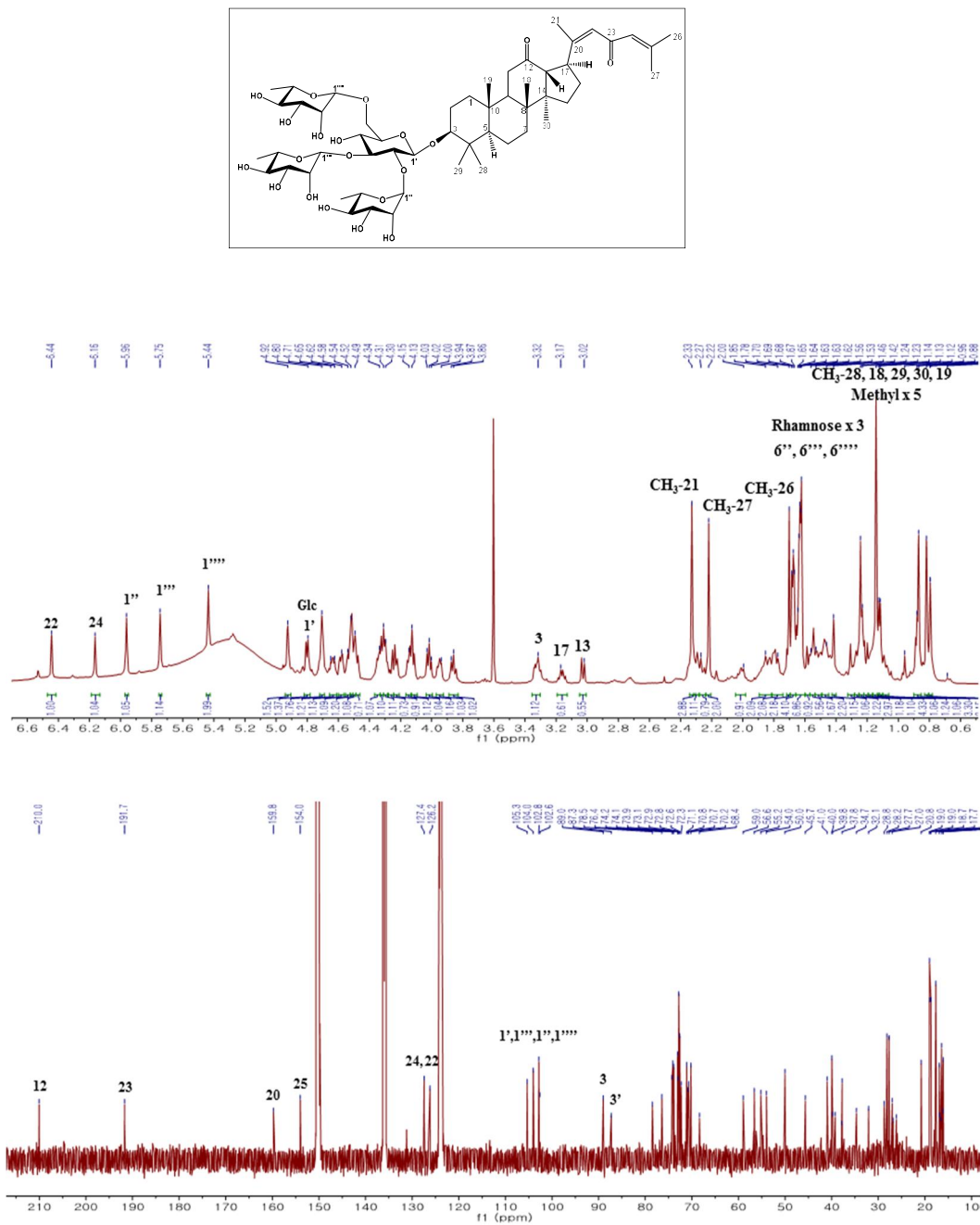


Figure 27. HSQC (H→C) of compound 6 (pyridine- $d_5$ , 600 MHz).

### 3.1.7. Compound 7

Longipenoside GL2 (**7**), isolated as an amorphous powder with  $[\alpha]_D^{25}$  -1.6 (*c* 0.2, MeOH), showed a molecular formula of  $C_{54}H_{86}O_{20}$  based on an ion peak at  $m/z$  1099.5730  $[M + HCOO]^-$  (calcd for  $C_{55}H_{87}O_{22}$ , 1099.5694). The positive-ion mode in HPLC-MS spectrum indicated the presence of a glycoside chain which is similar to that of compound **5**. The  $^1H$  and  $^{13}C$  NMR data of **7** (Tables 3 and 4) revealed the similar connectivity as **6**, except for the disappearance of two hydroxy group signals (C-20 and C-25) and the replacement by two olefinic linkages ( $\Delta^{20,22}$  and  $\Delta^{24,25}$ ). The dehydration of **7** at C-20 and C-25 was identified when compared with **6** using  $^{13}C$  NMR data: C-21 ( $\delta_C$  17.7, -9.1 ppm), C-20 ( $\delta_C$  159.8, +85.9 ppm), C-22 ( $\delta_C$  126.2, +71.0 ppm), C-24 ( $\delta_C$  127.4, +72.3 ppm), and C-25 ( $\delta_C$  154.0, +83.9 ppm). In addition, the olefinic moieties were also confirmed from HMBC correlation between H-21 and H-17 to C-20, C-22, and H-26, H-27 to C-24, C-25, respectively. Hence, compound **7** was elucidated as 3 $\beta$ -hydroxydammar-20,24-dien-12,23-dione-3-*O*- $\alpha$ -L-rhamnopyranosyl-(1 $\rightarrow$ 2)-[ $\alpha$ -L-rhamnopyranosyl-(1 $\rightarrow$ 3)]-[ $\alpha$ -L-rhamnopyranosyl-(1 $\rightarrow$ 6)]- $\beta$ -D-glucopyranoside (Figures 28-30).





**Figure 28.** <sup>1</sup>H and <sup>13</sup>C NMR of compound 7 (pyridine-*d*<sub>5</sub>, 600 MHz/150 MHz).

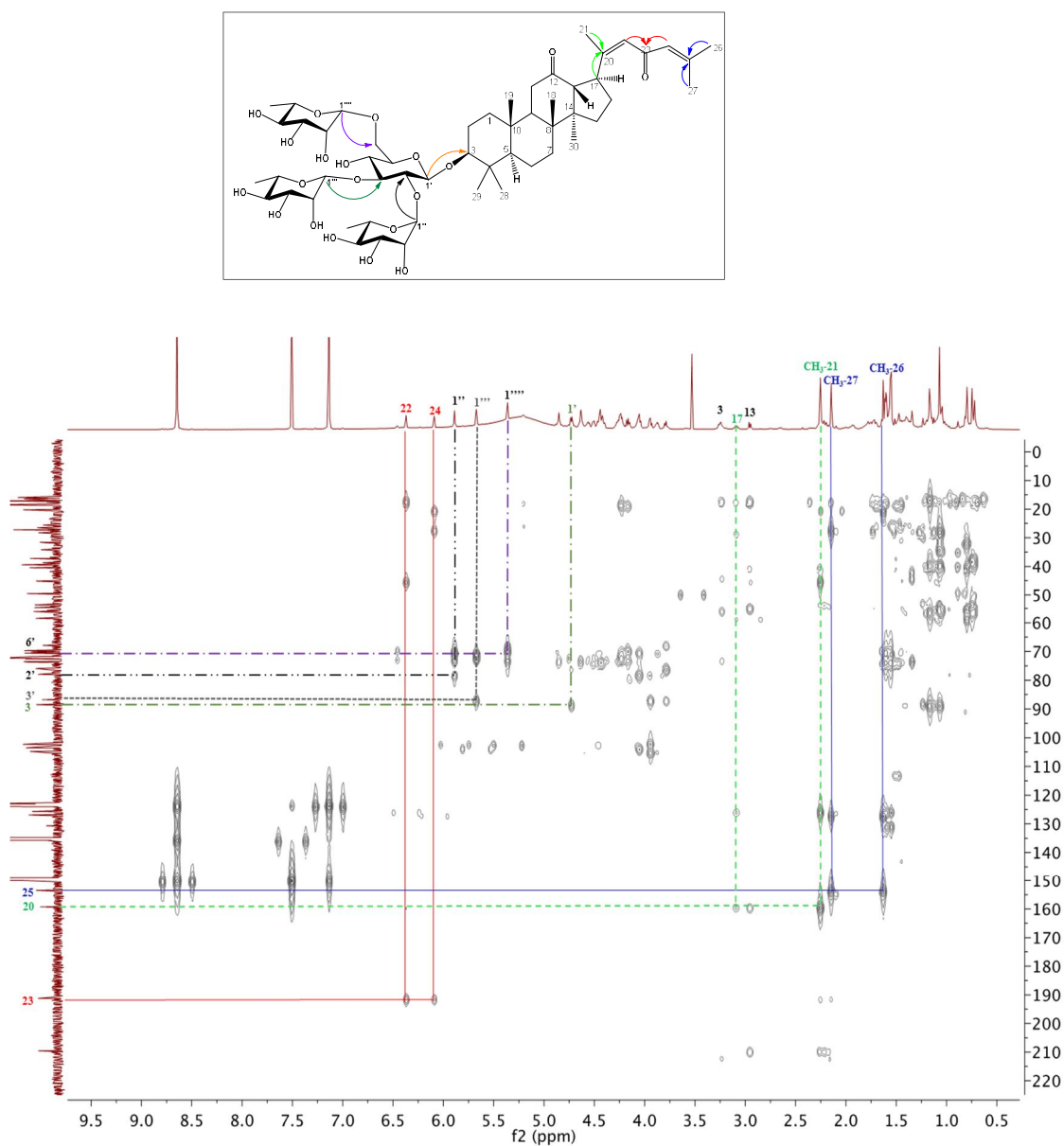


**Figure 29.** HMBC (H→C) of compound 7 (pyridine-*d*<sub>5</sub>, 600 MHz).

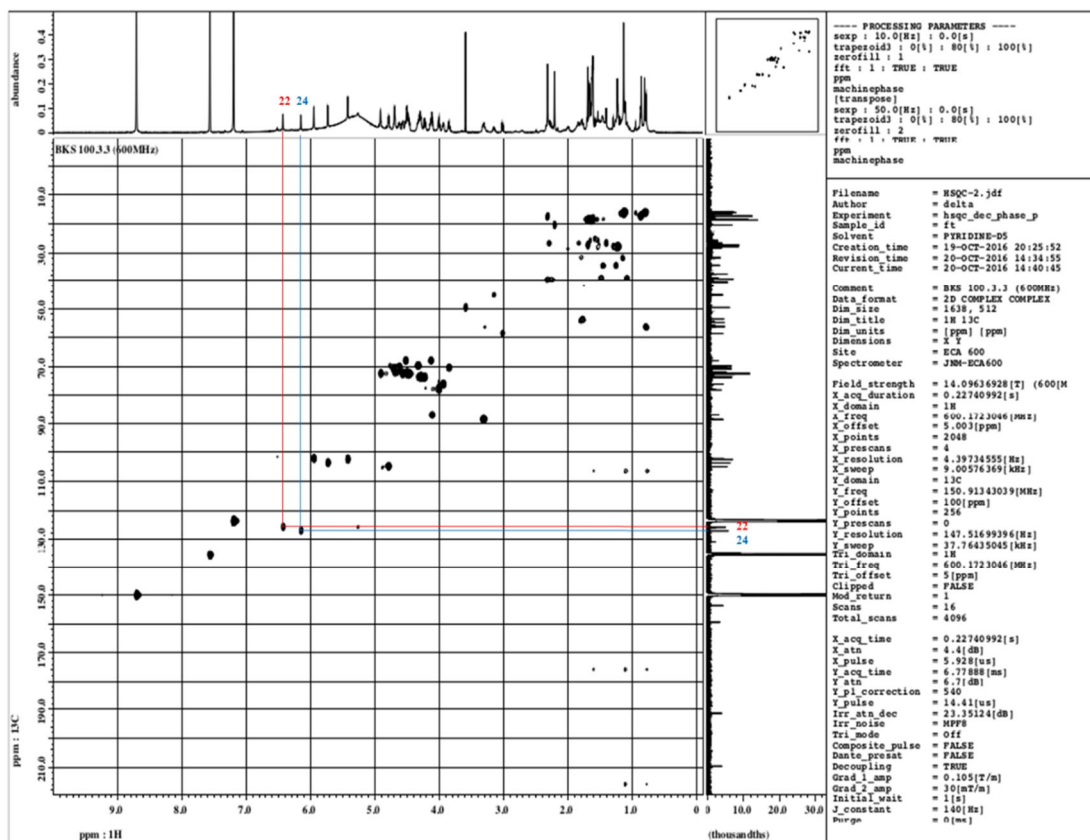
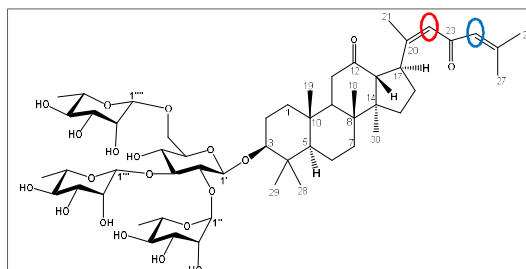
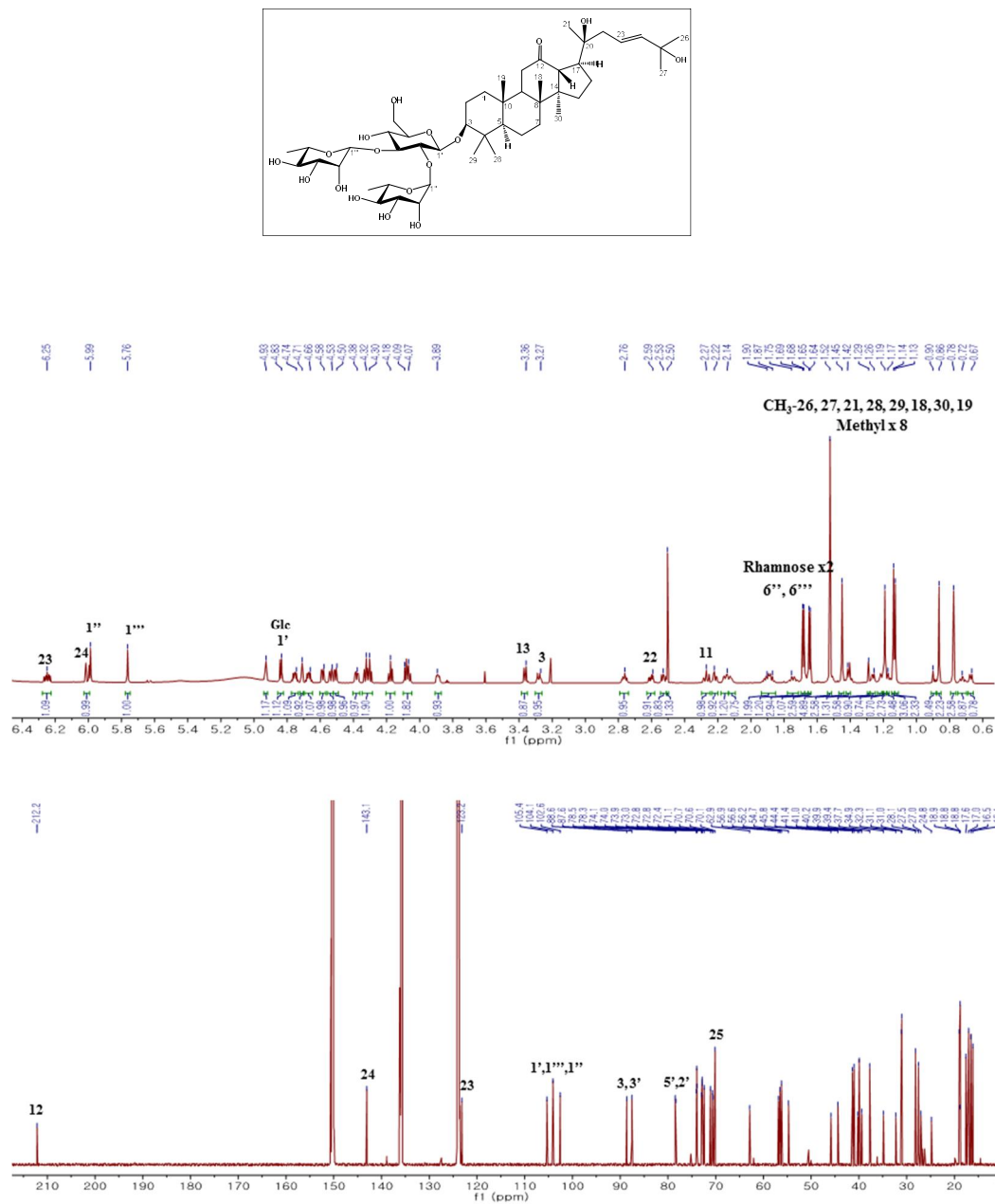


Figure 30. HSQC (H→C) of compound 7 (pyridine- $d_5$ , 600 MHz).

### 3.1.8. Compound **8**

Compound **8** was isolated as an amorphous powder with  $[\alpha]_D^{25}$  -2.5 (*c* 0.2, MeOH). Its molecular formula was assigned as  $C_{48}H_{80}O_{17}$  based on a negative ion peak  $[M + HCOO]^-$  at  $m/z$  973.5414 (calcd for  $C_{49}H_{81}O_{19}$ , 973.5378). Analysis and comparison of the NMR spectra between compounds **4** and **8**, results demonstrated that the glycoside chain and the main dammarane skeleton of two compounds were similar. However, differences of these compounds appeared at the side chain. Compound **8** contained two oxygen-bearing carbons at C-20 and C-25 ( $\delta_C$  74.0 and 70.1), two olefinic methine signals at C-23 and C-24 ( $\delta_C$  123.2 and 143.1). These result indicated its side chain was similar to the structure of notoginsenoside ST-5 (Liao et al., 2008). According to HMBC experiment, the positions of the side chain were confirmed by correlations from H-21 to C-17, C-20 and C-22; from H-23, H-24 to C-22, C-25; from H-26, H27 to C-23, C-24, and C-25. The large coupling constant ( $J = 15.1$  Hz) between H-23 and H-24 provided the evidence that the *E* geometry of the  $\Delta^{23,24}$  olefinic bond. Therefore, compound **8** was elucidated as 3 $\beta$ ,20(*S*),25-trihydroxydammar-23(*E*)-en-12-one-3-*O*- $\alpha$ -L-rhamnopyranosyl-(1 $\rightarrow$ 2)-[ $\alpha$ -L-rhamnopyranosyl-(1 $\rightarrow$ 3)]- $\beta$ -D-glucopyranoside which also named as Longipenoside GL3 (Figures 31-33).



**Figure 31.**  $^1\text{H}$  and  $^{13}\text{C}$  NMR of compound **8** ( $\text{pyridine-}d_5$ , 800 MHz/200 MHz).

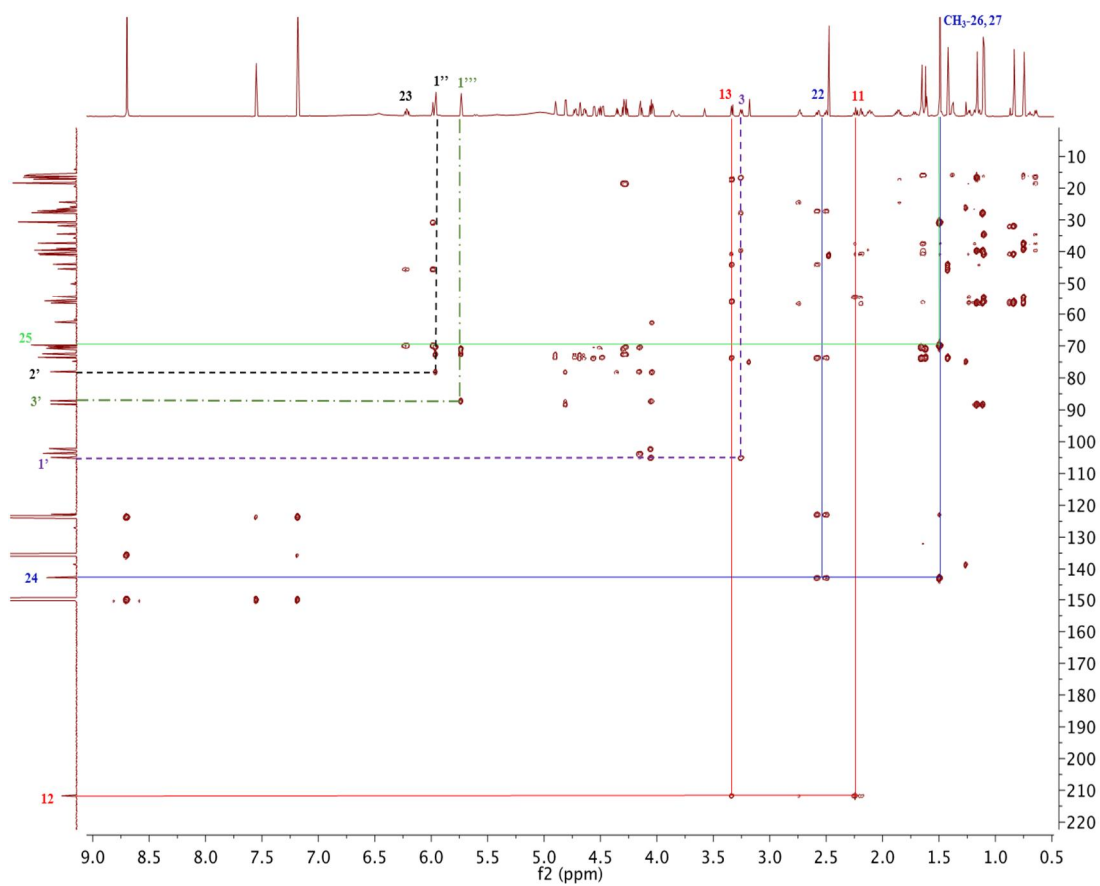
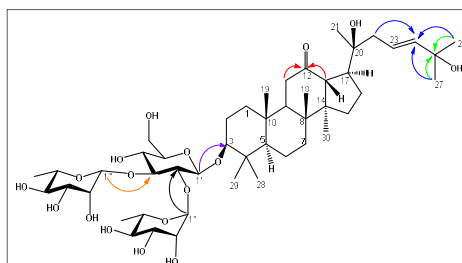


**Figure 32.** HMBC (H→C) of compound **8** (pyridine- $d_5$ , 800 MHz).

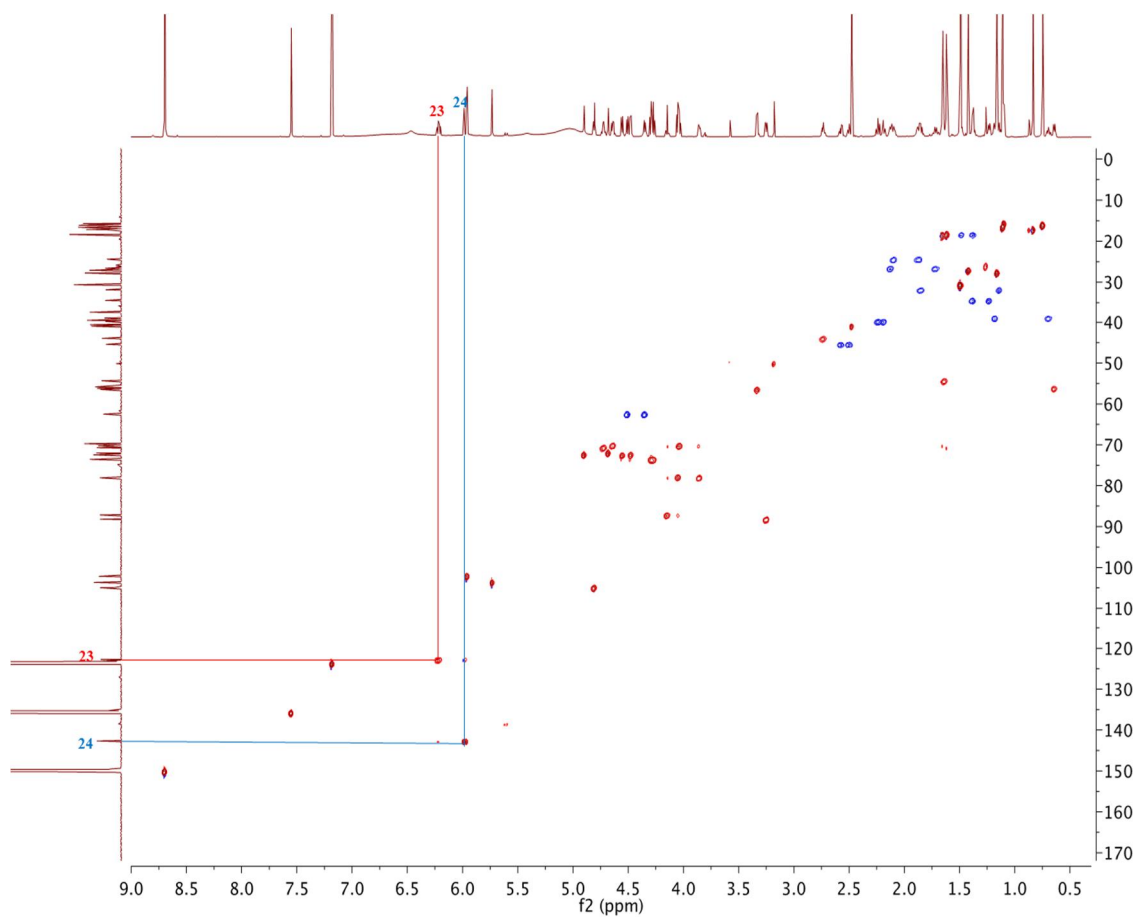
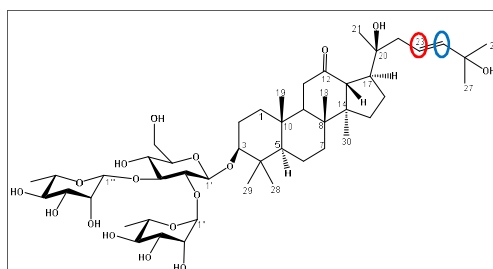
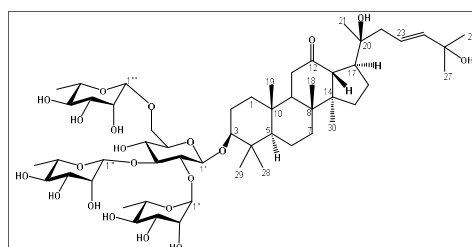


**Figure 33.** HSQC (H→C) of compound **8** (pyridine-*d*<sub>5</sub>, 800 MHz).

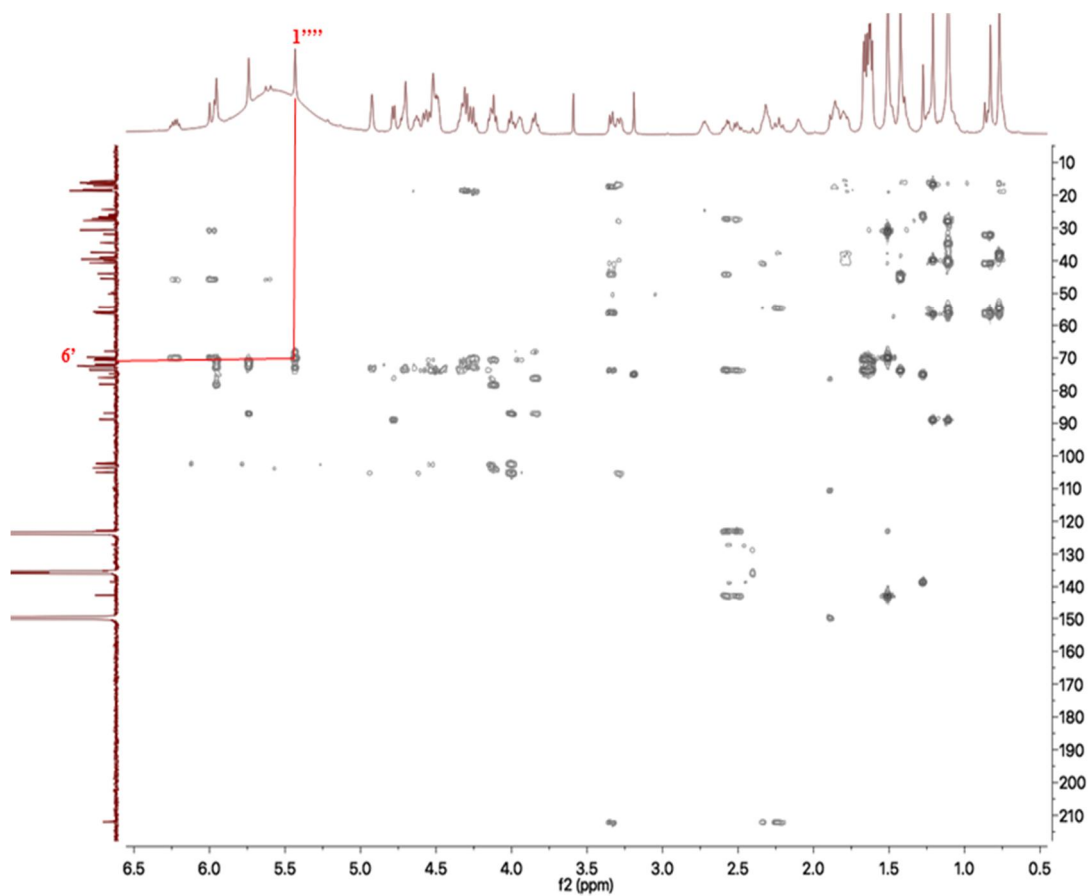
### 3.1.9. Compound **9**

Longipenoside GL4 (**9**) was identified as an amorphous powder with  $[\alpha]_{\text{D}}^{25} -0.5$  (*c* 0.2, MeOH). Its molecular formula was assigned as C<sub>54</sub>H<sub>90</sub>O<sub>21</sub> through the negative ion peak  $[\text{M} + \text{HCOO}]^-$  at *m/z* 1119.6008 (calcd for C<sub>55</sub>H<sub>91</sub>O<sub>23</sub>, 1119.5957), and it had ten indices of hydrogen deficiency. Similar with the NMR of compound **8**, those of **9** showed generally the same resonances. However, the difference of these compounds appeared at the additional rhamnose substituent at C-6'. According to NMR spectroscopic data, the presence of C-6' ( $\delta_{\text{C}}$  68.3, + 5.4 ppm) and HMBC correlation from H-1''' anomeric proton ( $\delta_{\text{H}}$  5.43) to C-6' were strongly observed. Therefore, the structure of **9** was determined as 3 $\beta$ ,20(*S*),25-trihydroxydammar-23(*E*)-en-12-one-3-*O*- $\alpha$ -L-rhamnopyranosyl-(1→2)-[ $\alpha$ -L-rhamnopyranosyl-(1→3)]-[ $\alpha$ -L-rhamnopyranosyl-(1→6)]- $\beta$ -D-glucopyranoside (Figures 34-36).

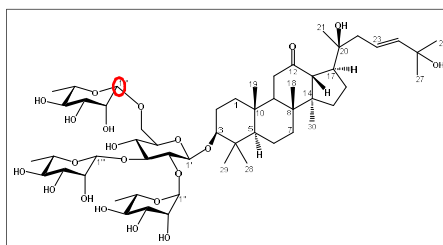








**Figure 35.** HMBC (H→C) of compound **9** (pyridine-*d*<sub>5</sub>, 500 MHz).



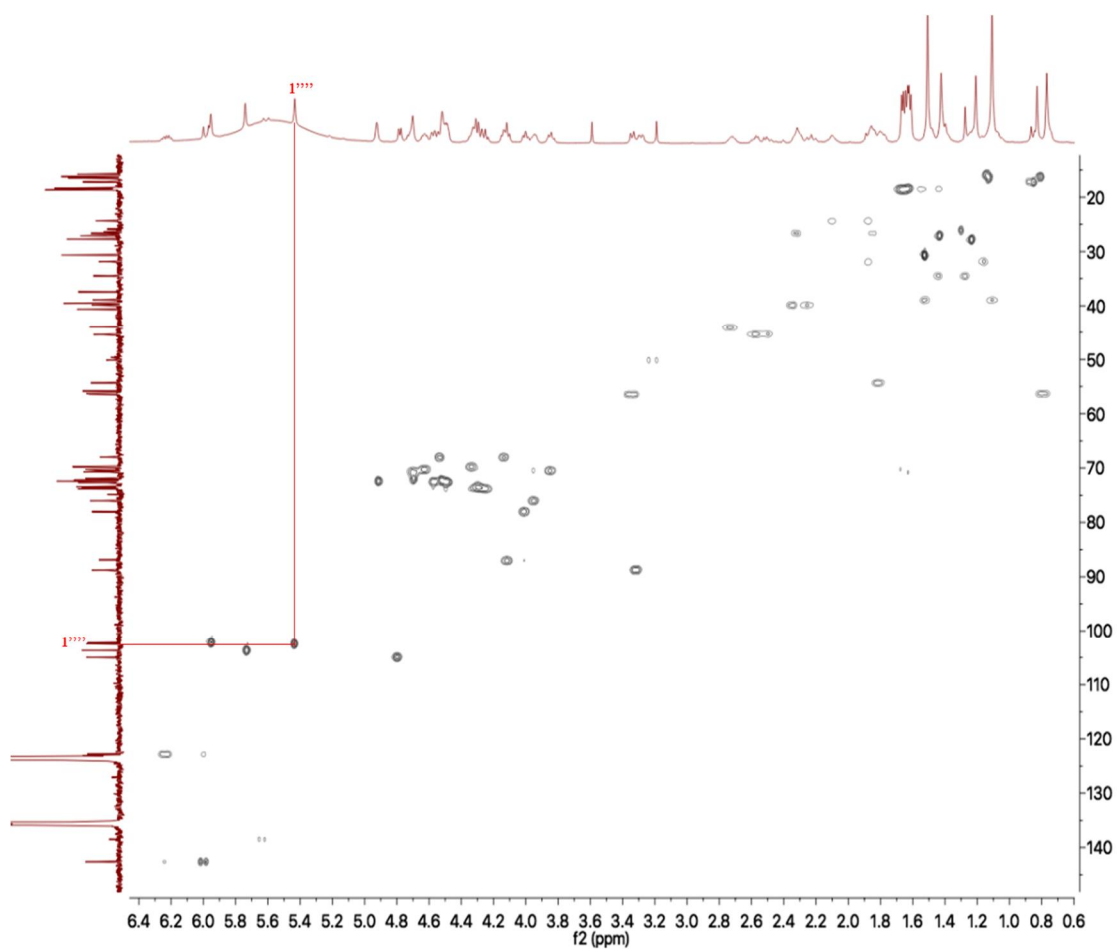
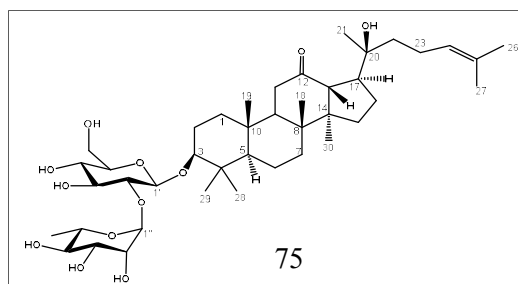


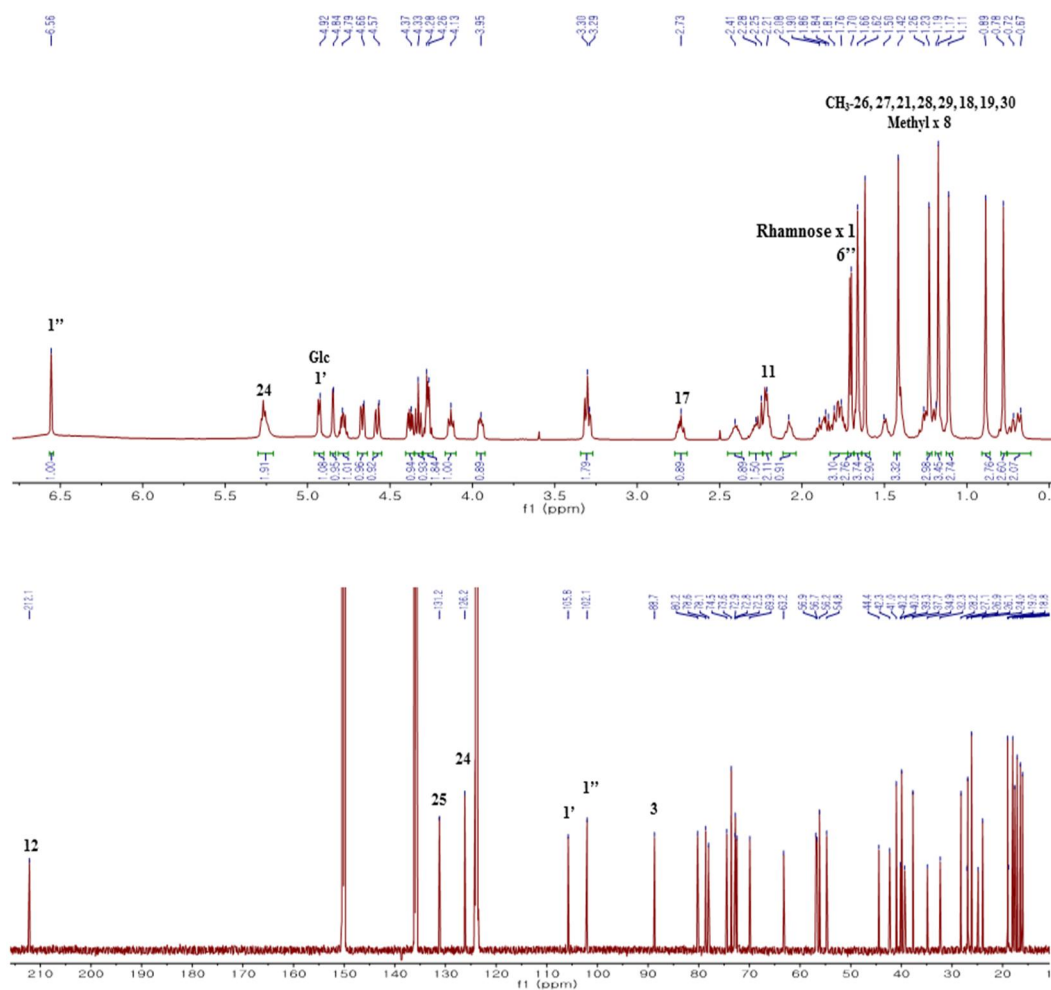
**Figure 36.** HSQC (H→C) of compound **9** (pyridine-*d*<sub>5</sub>, 500 MHz).

### 3.1.10. Compound **10**

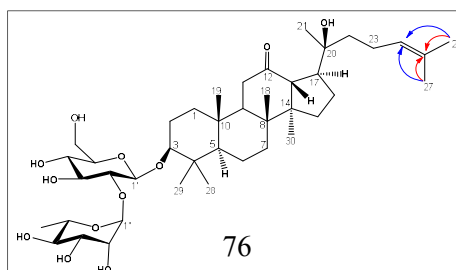
Triterpene **10** was obtained as a white amorphous powder with  $[\alpha]_{\text{D}}^{25}$  -0.8 (*c* 0.2, MeOH). Its molecular formula was identified as C<sub>42</sub>H<sub>70</sub>O<sub>12</sub> through an ion peak at *m/z* 811.4872 [M + HCOO]<sup>-</sup> (calcd for C<sub>43</sub>H<sub>71</sub>O<sub>14</sub>, 811.4849). The IR spectrum of

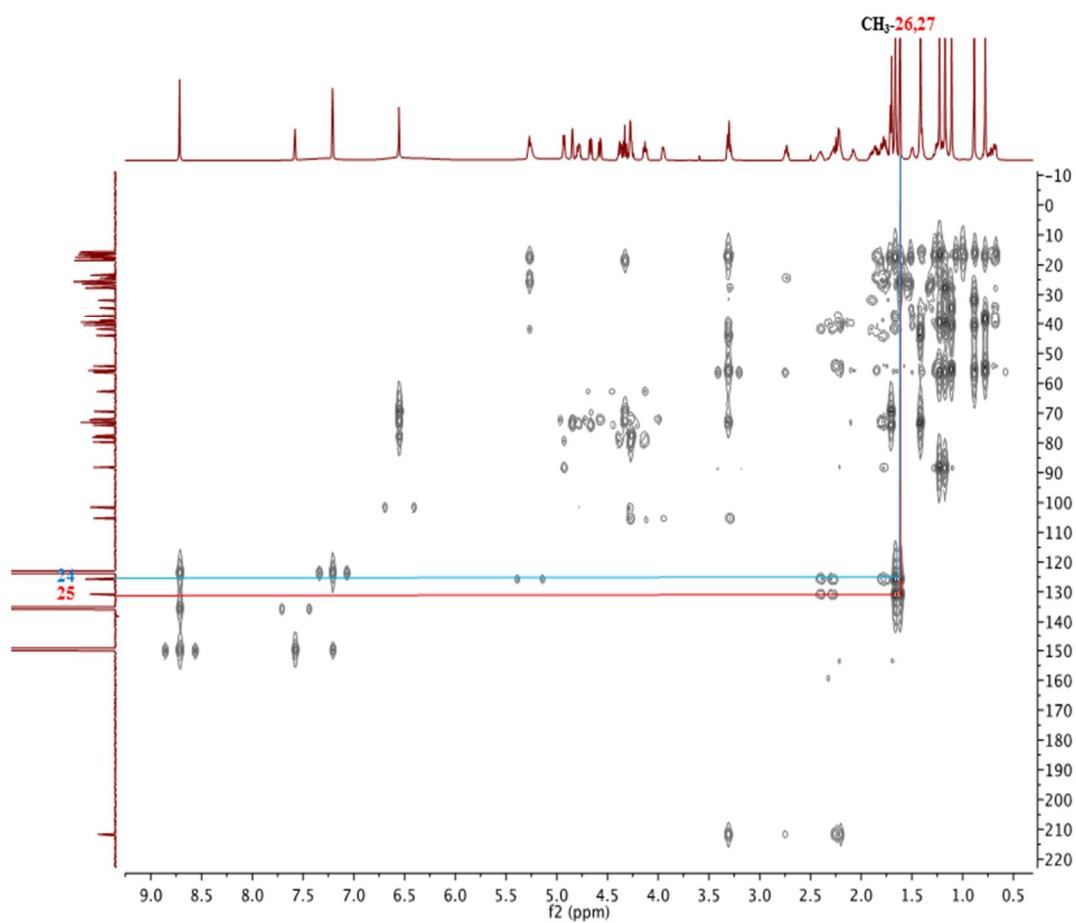
**10** exhibited the absorption bands for several functionalities, including hydroxyl, carbonyl, and olefinic groups. The  $^1\text{H}$  NMR data revealed eight methyl groups ( $\delta_{\text{H}}$  1.66, 1.62, 1.42, 1.23, 1.17, 1.11, 0.89, 0.78), an oxygenated methine proton ( $\delta_{\text{H}}$  3.29), and an olefinic proton ( $\delta_{\text{H}}$  5.27). In addition, total 42 carbon signals were apparent in the  $^{13}\text{C}$  NMR spectrum, corresponding to a carbonyl carbon ( $\delta_{\text{C}}$  212.1), an oxymethine carbon ( $\delta_{\text{C}}$  88.7), and an oxygenated quaternary carbon ( $\delta_{\text{C}}$  73.6). This result indicated that dammarane **10** contained one carbonyl group and two hydroxyl groups. The HMBC spectrum revealed the correlations from H-11 ( $\delta_{\text{H}}$  2.22), H-13 ( $\delta_{\text{H}}$  3.30), H-17 ( $\delta_{\text{H}}$  2.73) to C-12 ( $\delta_{\text{C}}$  212.1), from H-26 ( $\delta_{\text{H}}$  1.66), H-27 ( $\delta_{\text{H}}$  1.62) to C-24 and C-25, indicating the presence of the carbonyl group and  $\Delta^{24,25}$  olefin system. The relative configuration of **1** was determined based on the NOESY experiment. The  $\alpha$ -orientations of H-3, H-5, and H-28 were established through the correlations from H-3 ( $\delta_{\text{H}}$  3.29) to H-5 ( $\delta_{\text{H}}$  0.67) and H-28 ( $\delta_{\text{H}}$  1.23). To determine the sugar moieties, the NMR data revealed the presence of two anomeric protons, including a glucopyranosyl unit (d,  $J = 7.7$  Hz) with the  $\beta$ -configuration and a rhamnopyranosyl unit (bbs) with the  $\alpha$ -configuration. In addition, the connection of these sugars was identified based on the HMBC correlations from H-1'' ( $\delta_{\text{H}}$  6.56) and C-2' ( $\delta_{\text{C}}$  77.6). Therefore, the structure of compound **10** was elucidated as 3 $\beta$ ,20(*S*)-dihydroxydammar-24-en-12-one-3-*O*- $\alpha$ -L-rhamnopyranosyl-(1 $\rightarrow$ 2)- $\beta$ -D-glucopyranoside which was also named as Longipenoside GL5 (Figures 37-41).



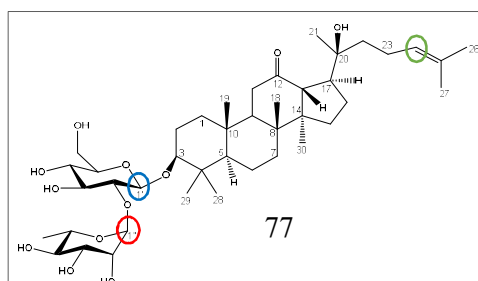


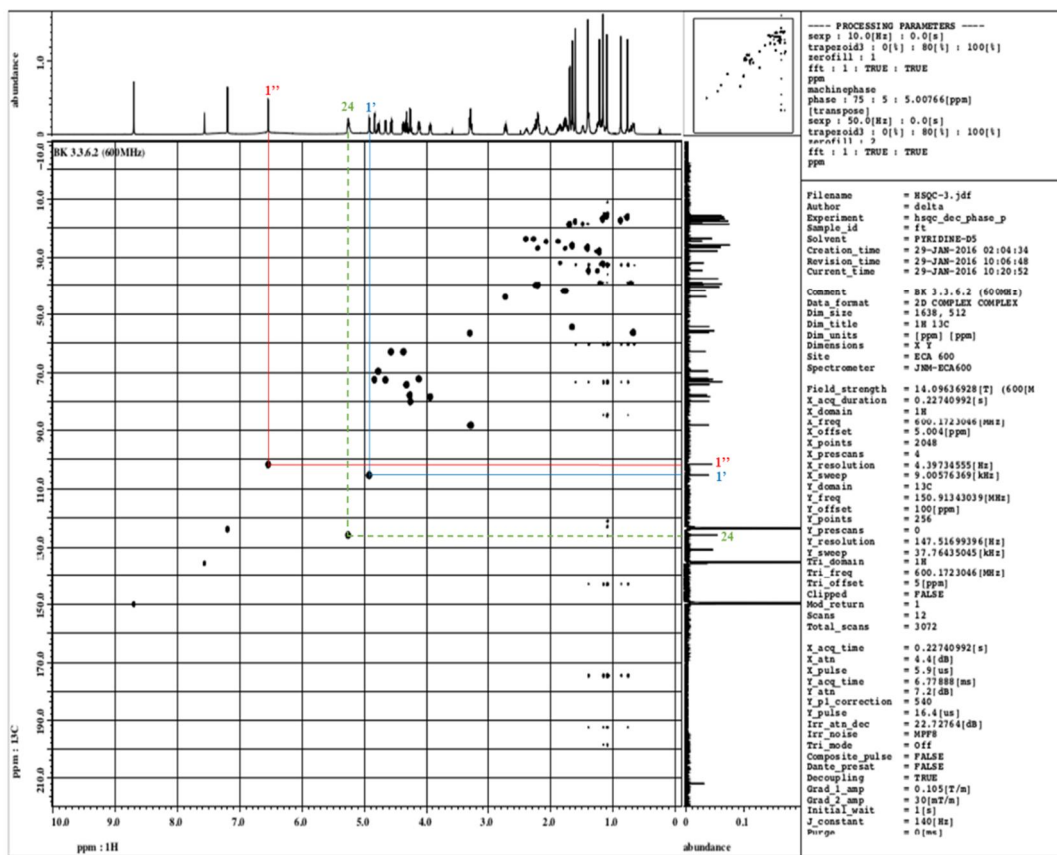
**Figure 37.**  $^1\text{H}$  and  $^{13}\text{C}$  NMR of compound **10** ( $\text{pyridine-}d_5$ , 600 MHz/150 MHz).



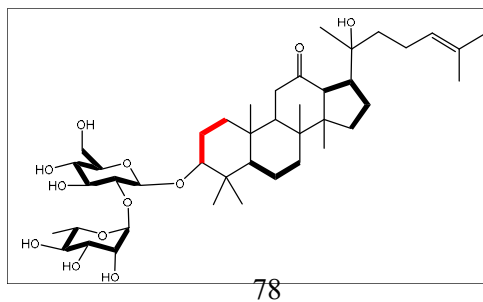


**Figure 38.** HMBC (H→C) of compound **10** (pyridine-*d*<sub>5</sub>, 600 MHz).

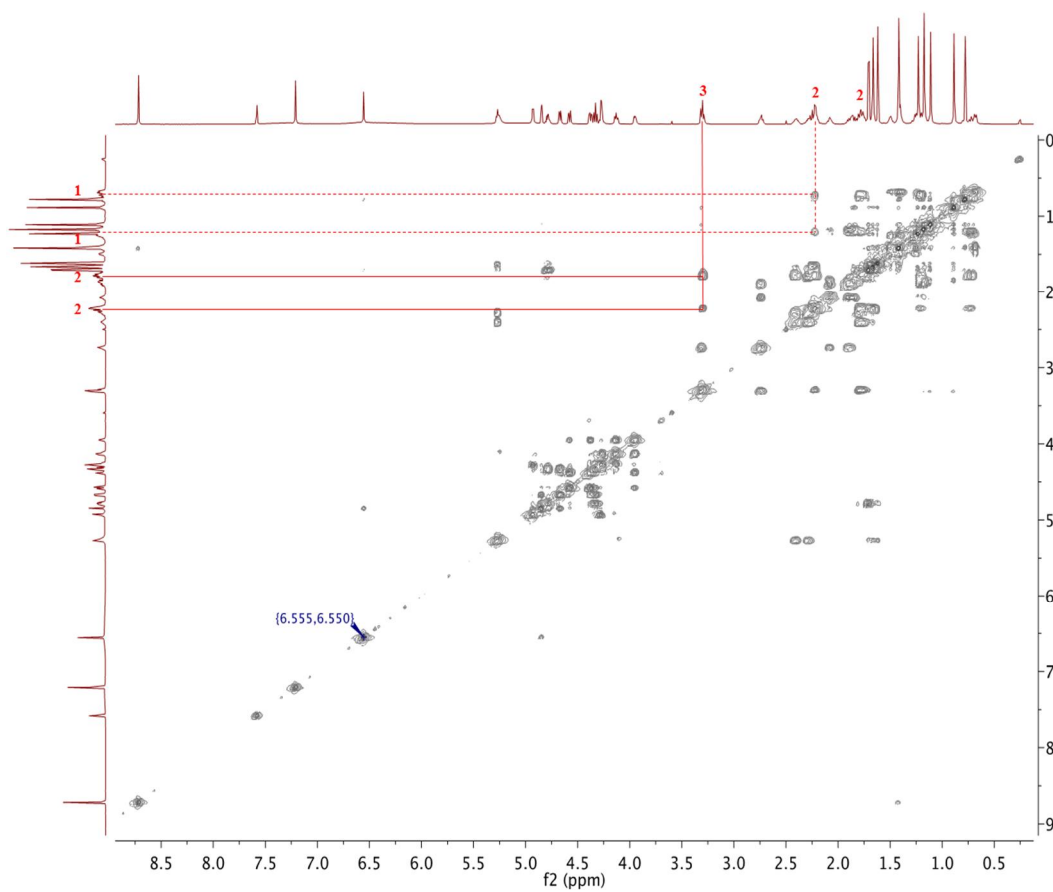




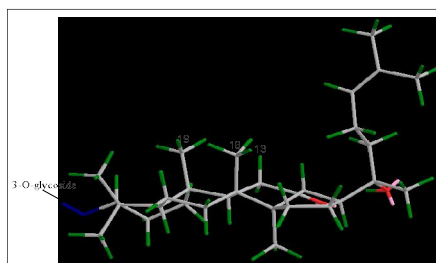
**Figure 39.** HSQC (H→C) of compound **10** (pyridine-*d*<sub>5</sub>, 600 MHz).







**Figure 40.** COSY (H↔H) of compound **10** (pyridine- $d_5$ , 600 MHz).



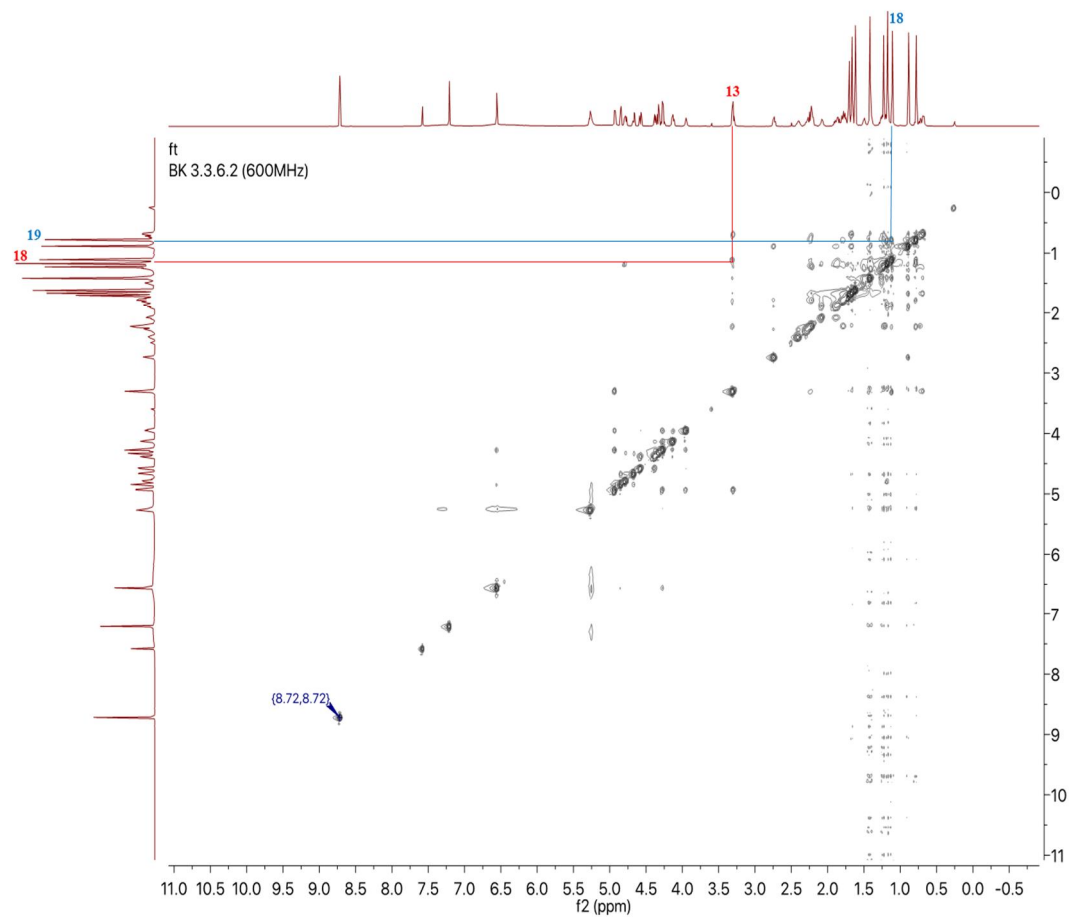
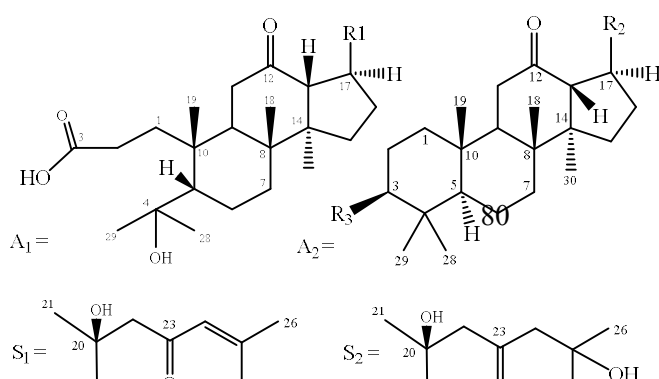


**Figure 41.** NOESY (H↔H) of compound **10** (pyridine-*d*<sub>5</sub>, 600 MHz).



		<b>R<sub>1</sub></b>	<b>R<sub>2</sub></b>	<b>R<sub>3</sub></b>
<b>1</b>	A <sub>1</sub>	S <sub>1</sub>	—	—
<b>2</b>	A <sub>1</sub>	S <sub>2</sub>	—	—
<b>3</b>	A <sub>1</sub>	S <sub>3</sub>	—	—
<b>4</b>	A <sub>2</sub>	—	S <sub>3</sub>	G <sub>2</sub>
<b>5</b>	A <sub>2</sub>	—	S <sub>3</sub>	G <sub>3</sub>
<b>6</b>	A	—	S	G

**Figure 42.** Structures of ten compounds isolated from *G. longipes*.

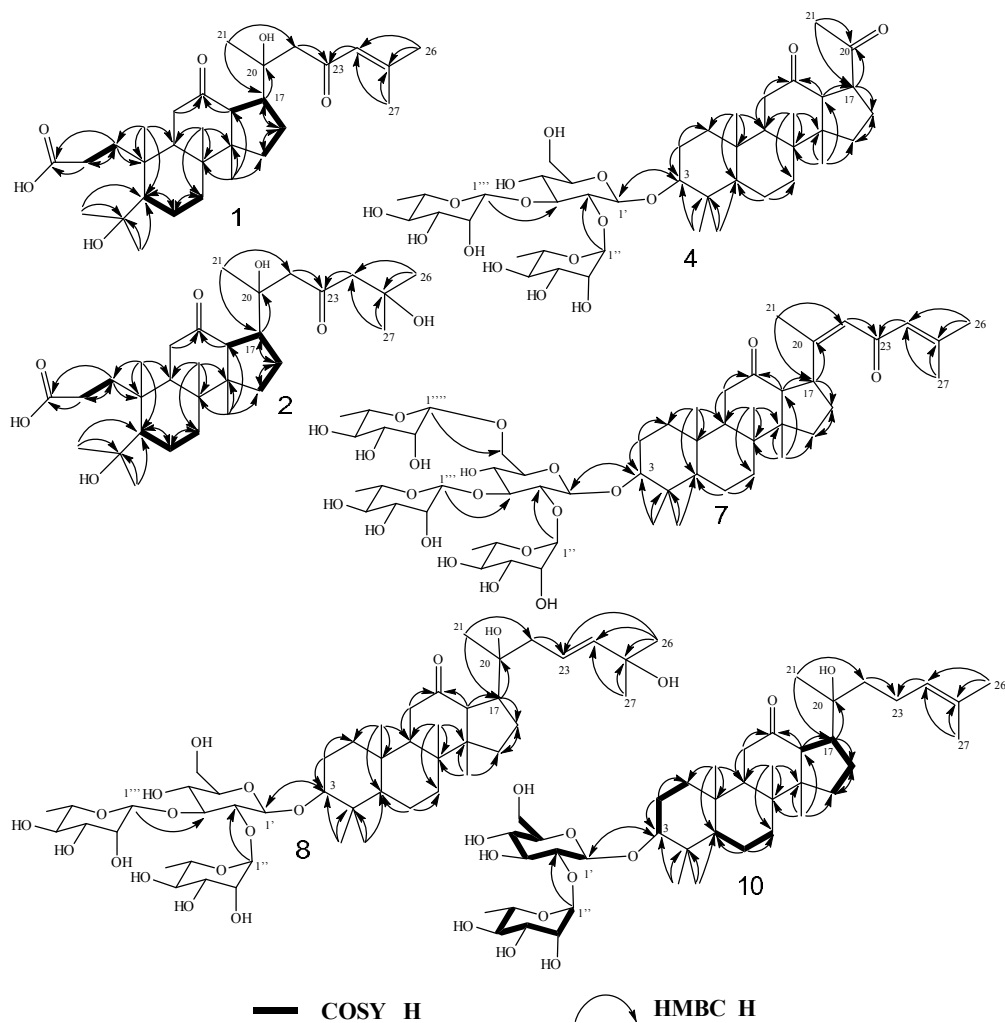


**Figure 43.** Key COSY and HMBC correlations of compounds **1**, **2**, **4**, **7**, **8**, and **10**.

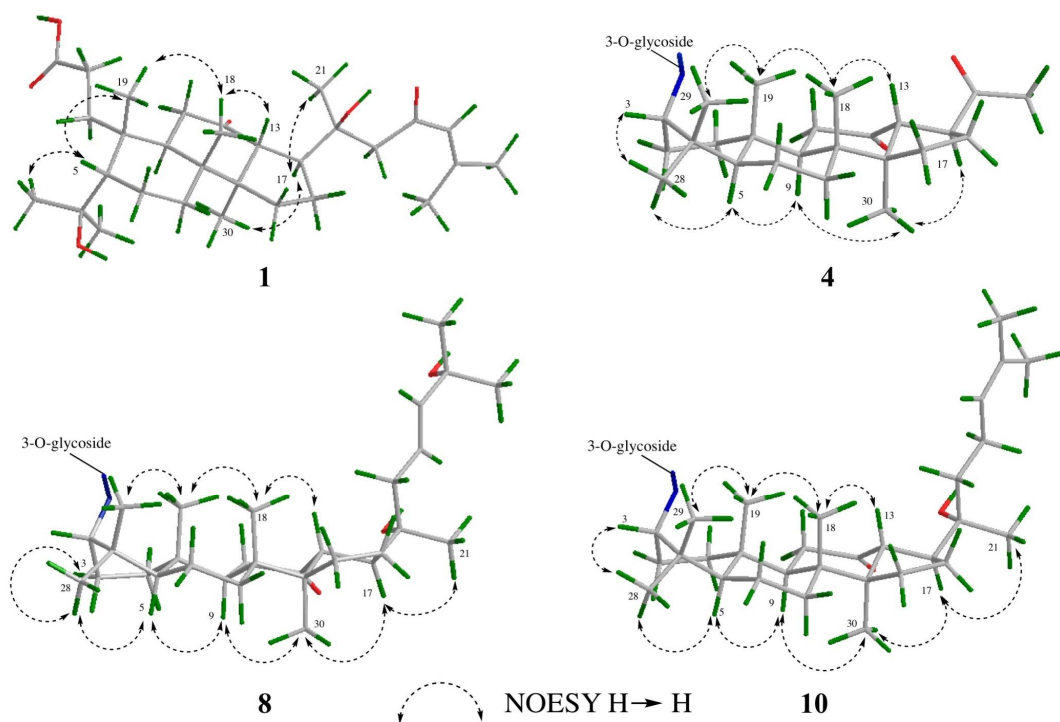


**Figure 44.** Key NOESY correlations of the dammarane skeletons of compounds **1**, **4**, **8**, and **10**.

### 3.2. Insulin mimetic activity of triterpenoids from *G. longipes*

#### 3.2.1. Cytotoxic effects of all isolated compounds on 3T3-L1 adipocytes and mouse C2C12 cells

Triterpenoids (**1–10**) (Figure 42) were measured cytotoxic effects in 3T3-L1 adipocytes using the MTT method. Firstly, the cells were incubated with all compounds at 40  $\mu$ M for 24 h, result in Figure 45A indicated compounds **1–9** showed no cytotoxic effects, but **10** dramatically reduced the percentage of cell viability. Then, compound **10** was performed another experiment at various concentrations (10, 20, and 30  $\mu$ M). As shown in Figures 45B, compound **10** exhibited no toxicity only at 10  $\mu$ M and its concentration was applied for the 2-NBDG assay.

In the C2C12 myoblast model, all isolated compounds were also evaluated the cytotoxic effects using the MTT method as described above. Similarly with the result in Figure 45, compounds **1–9** (40  $\mu$ M) did not show any toxic to C2C12 myoblast, except for compound **10** no cytotoxicity at 10  $\mu$ M (Figure 46).

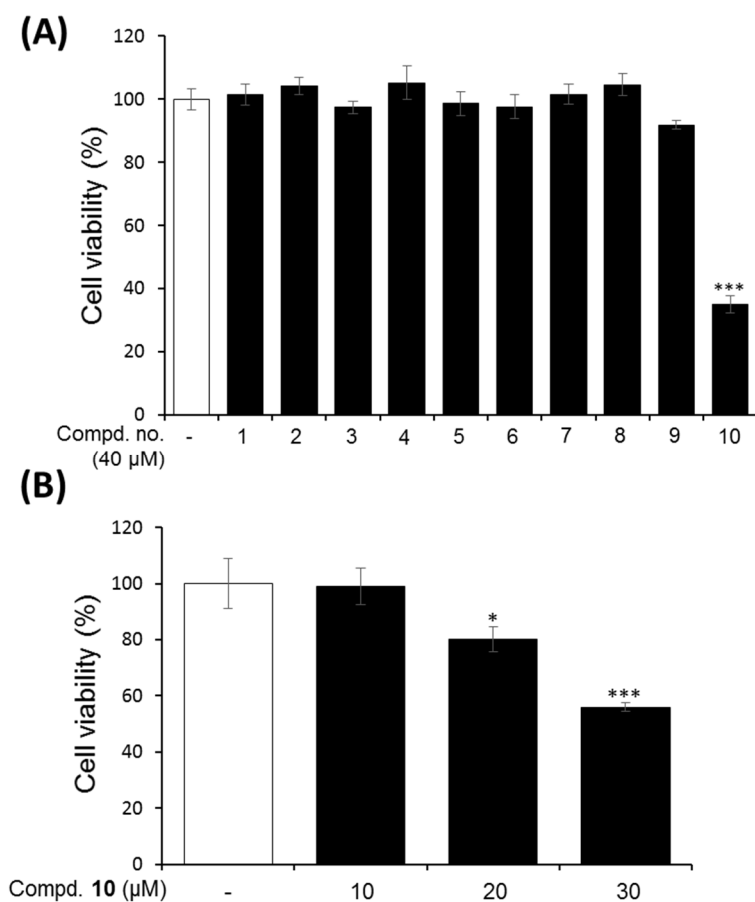


**Figure 45.** The cytotoxicity effect of compounds **1–10** 40  $\mu$ M (A) and compound **10** at different concentrations (B) in 3T3-L1 adipocytes. After 24 h of incubation with test compounds, the MTT assay was carried out as described in the experimental section. Data are presented as the mean  $\pm$  SD ( $n = 3$ ), \*  $p < 0.05$ , and \*\*\*  $p < 0.001$ , compared to the negative group.

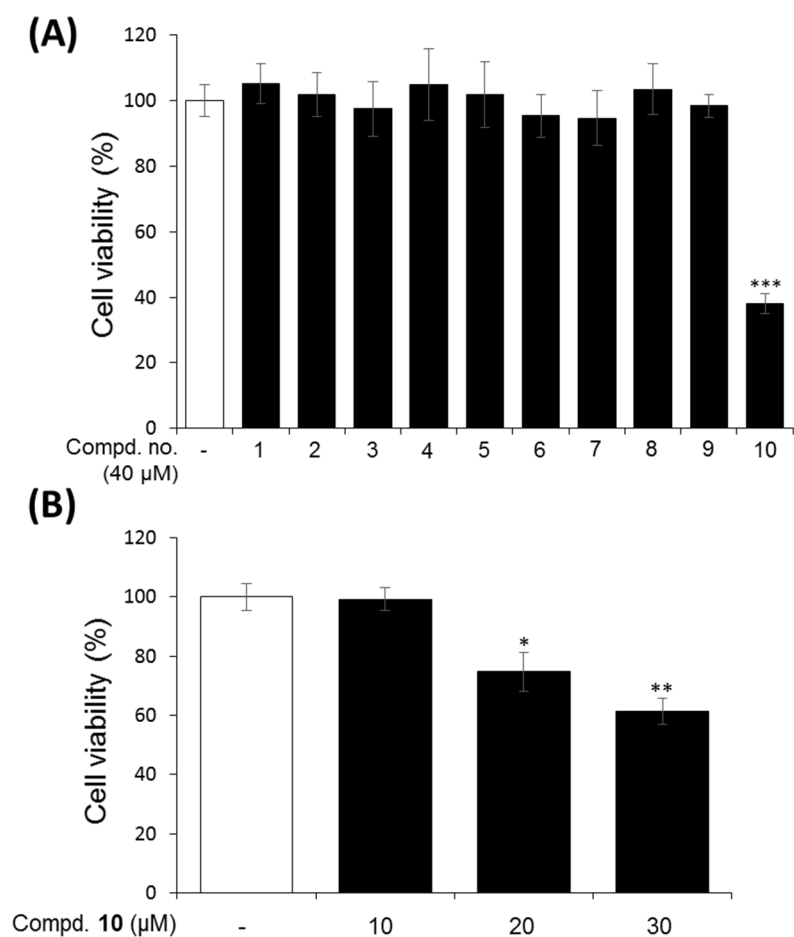


**Figure 46.** The cytotoxicity effect of all isolates 1–10 at 40  $\mu$ M (A) and 10 at various concentrations (B) on C2C12 myoblasts. After the cells were treated with compounds for 1 day, the percentage of cell viability was evaluated using the MTT method. Result are presented as the mean  $\pm$  SD ( $n = 3$ ), \*  $p < 0.05$ , \*\*  $p < 0.01$ , and \*\*\*  $p < 0.001$ , compared to the negative control.



### 3.2.2. Stimulation effects of dammarane triterpenes from *G. longipes* on 2-NBDG uptake into the cells

To measure glucose uptake into the cells, a fluorescent-tagged glucose analogue, 2-[*N*-(7-nitrobenz-2-oxa-1,3-diazol-4-yl)amino]-2-deoxy-D-glucose (2-NBDG), was applied as a common method for *in vitro* study. In this research, triperpenoids **1–10** were evaluated for their stimulatory effects on glucose uptake using 3T3-L1 adipocytes, which are more sensitive to insulin and more potential than other cell lines. Based on the fluorescence microscope method, the efficiency of 2-NBDG transport into cells was identified successfully by the fluorescent intensities in the adipocytes, comparison with that of the absence of 2-NBDG (Figure 47). In the presence of 2-NBDG, the fluorescent signals clearly induced when the cells were treated with compounds **1**, **2**, **4**, **5**, **8**, and **10** (Figure 47, 48A). In addition, several compounds (**1**, **2**, **4**, and **8**) were selected for further investigation the glucose uptake at different concentrations. Results in Figures 48B and 49 demonstrated these compounds significantly increased the 2-NBDG uptake into adipocytes in a dose-dependent manner.

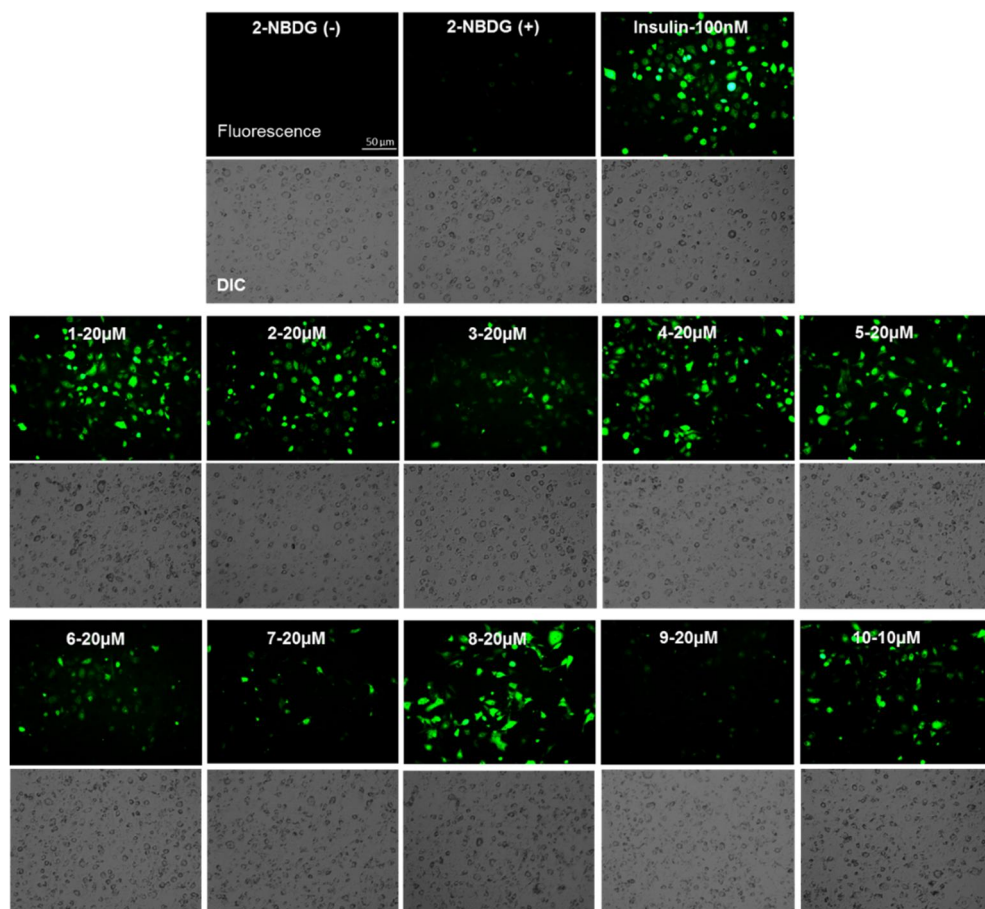


**Figure 47.** Stimulation effect of isolates from *G. longipes* on 2-NBDG uptake in 3T3-L1 adipocytes. The cells were exposed to insulin (100 nM) as a positive control, compounds **1–9** (20  $\mu$ M), and **10** (10  $\mu$ M). After incubation for 1 h, the images of cells were then captured using a fluorescence microscope. The intensity of green fluorescence significantly induced, which suggested the successful 2-NBDG transport into adipocytes.

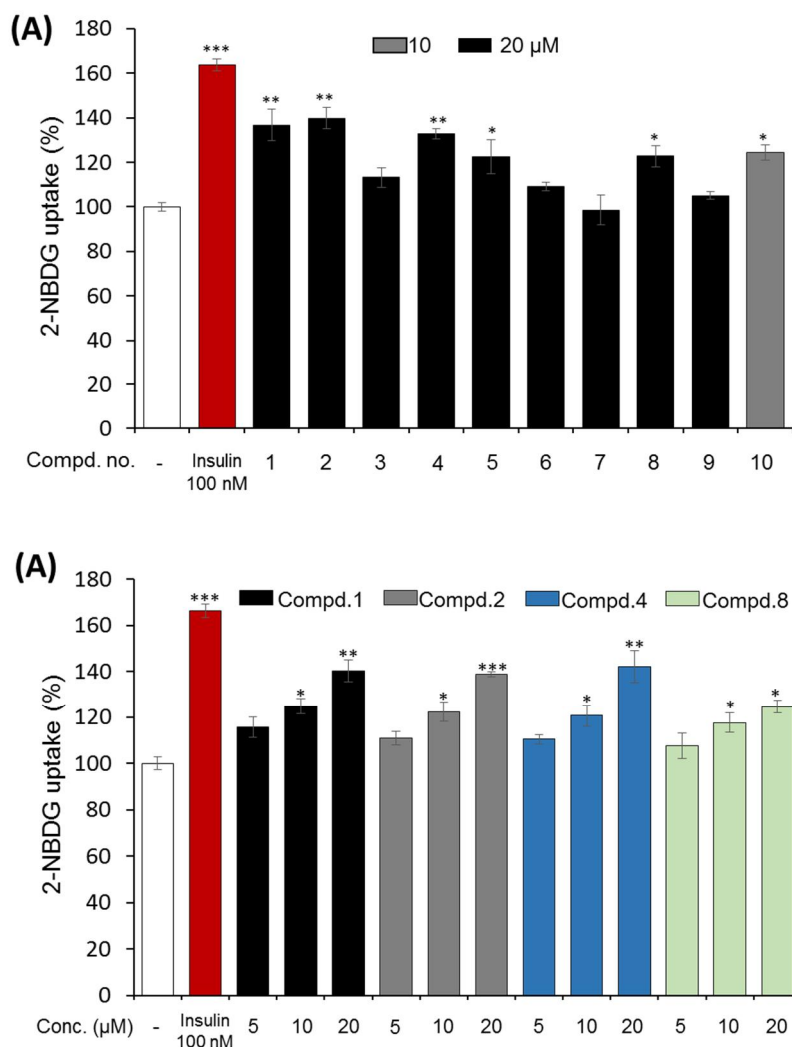


**Figure 48.** Enhancement of glucose uptake by compounds **1–10** in 3T3-L1 adipocytes using a fluorescent analogue of glucose (2-NBDG). (A, B) The cells were treated with insulin (100 nM) and compounds at various concentrations in the presence or absence of 2-NBDG. After 1 h of incubation, the fluorescent intensity was evaluated at Ex/Em = 450/535 nm using a fluorescence microplate reader. Each experiment was carried out in triplicate. Data are presented as the means  $\pm$  SD ( $n = 3$ ); \*  $p < 0.05$ , \*\*  $p < 0.01$ , and \*\*\*  $p < 0.001$ , compared to vehicle.

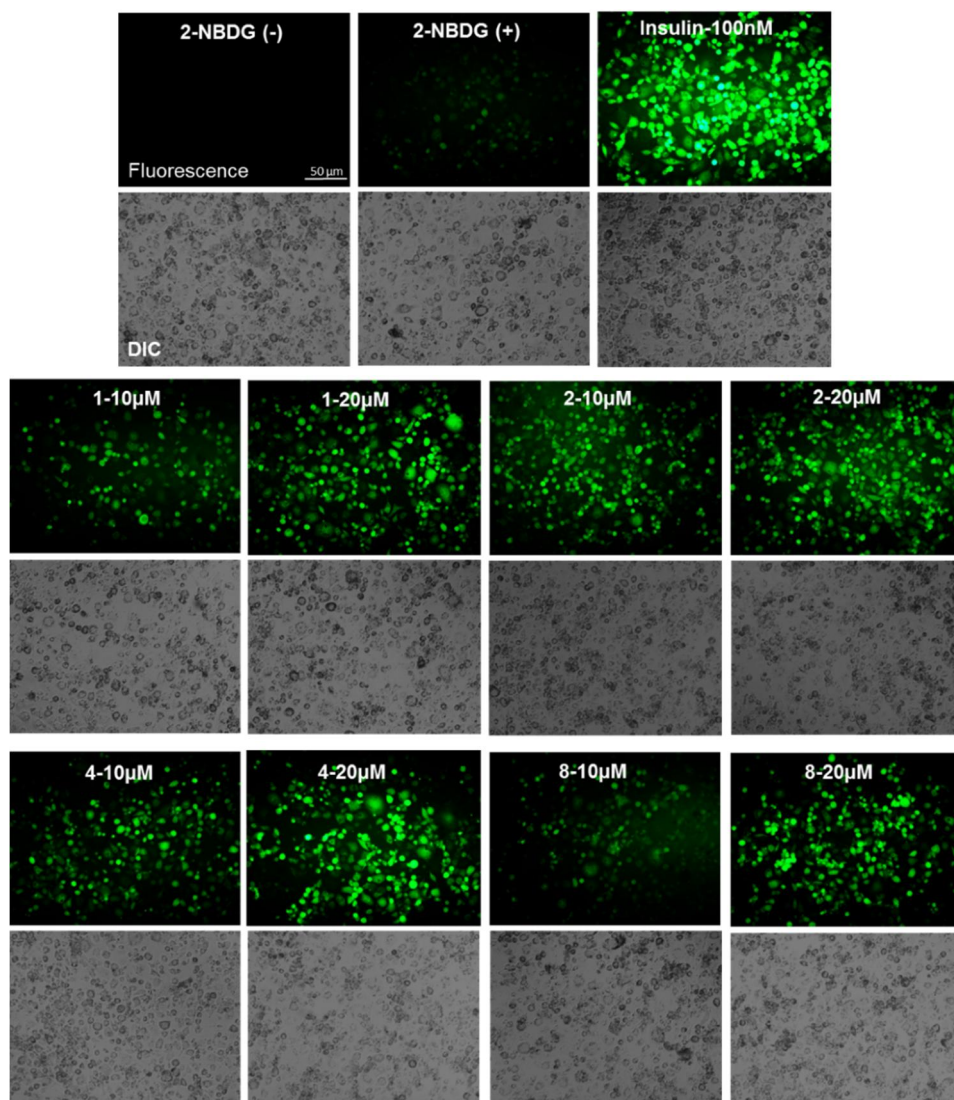


**Figure 49.** Concentration-response relationships of the effects of several compounds on 2-NBDG in 3T3-L1 adipocytes. After incubation with compounds **1**, **2**, **4**, and **8** (10 and 20  $\mu\text{M}$ ) or insulin (100 nM) in the presence of 2-NBDG for 1 h, the fluorescence and bright-field images were obtained using a fluorescence microscope.

### 3.2.3. Evaluation of compounds **1**, **2**, **4**, and **8** glucose uptake through GLUT4 translocation

GLUT4 recently is a potential therapeutic target to treat T2DM. The regulation of GLUT4 translocation is necessary for the glucose absorption across the plasma membrane of adipocytes. According to previous studies, dammarane triterpenoids (damulins A and B) from *G. pentaphyllum* have been reported as potential candidates for enhancing 2-deoxyglucose uptake and the translocation of GLUT4 into the plasma membrane of skeletal L6 myotubes in a dose-dependent manner (Nguyen et al., 2011). Therefore, in this study, compounds **1**, **2**, **4**, and **8** were also evaluated stimulation effects on the GLUT4 translocation to the plasma membrane of 3T3-L1 adipocytes. Data in Figures 50 and 51 revealed the increasing of GLUT4 translocation by these compounds as well as insulin (as a positive control). These results indicated that the effect of these compounds on glucose uptake was stimulated by the translocation of GLUT4 protein. Our data suggested that dammarane triterpenoids from *G. longipes* might be promising candidates for the development of antidiabetic drugs.

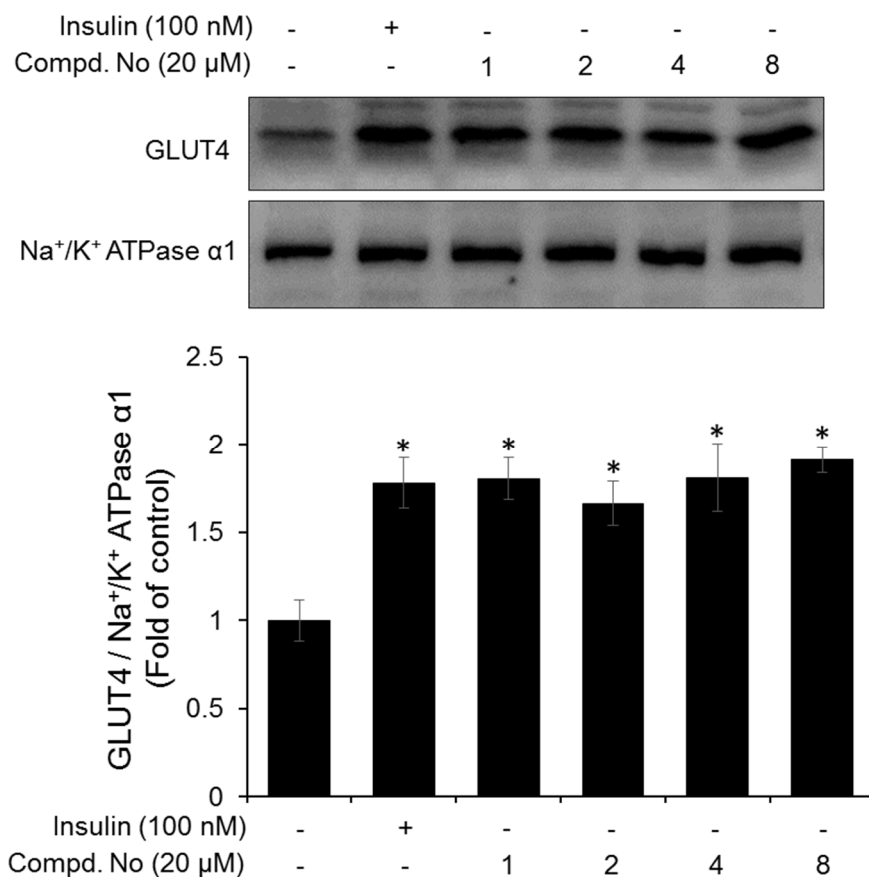


**Figure 50.** Effect of strong candidates (**1**, **2**, **4**, and **8**) on the translocation of GLUT4 to the plasma membrane of adipocytes. The cells were exposed to test compounds (20  $\mu$ M) for 24 h or insulin (100 nM) for 2 h. The GLUT4 expression in the plasma membranes was measured using the Western blot method. Data are presented as the means  $\pm$  SD ( $n = 3$ ), \*  $p < 0.05$ , compared to the negative group.

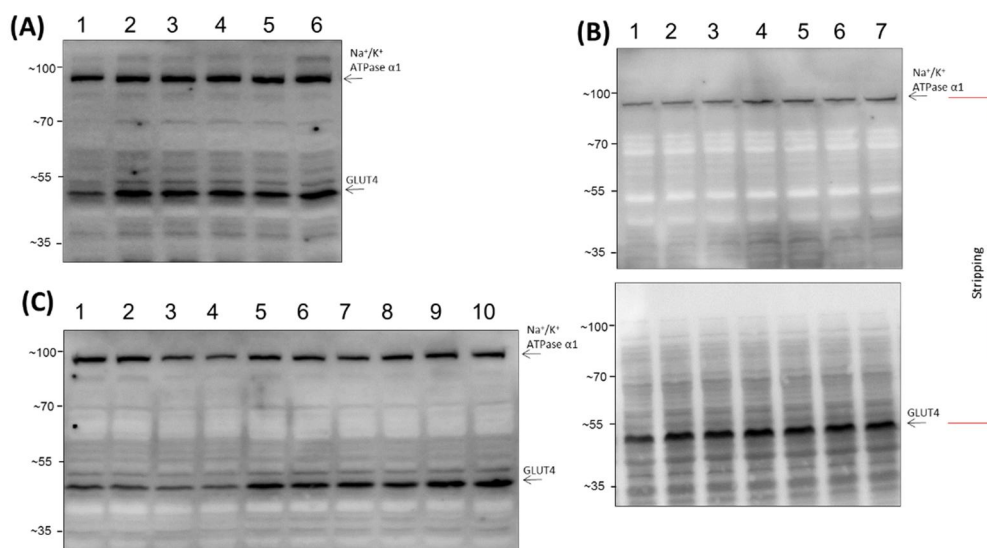


**Figure 51.** Isolated compounds from *G. longipes* induced the translocation of GLUT4 to the plasma membrane of 3T3-L1 adipocytes; original uncropped blots.

3T3-L1 adipocytes were exposed to compounds **1**, **2**, **4**, and **8** (20 μM) for 24 h or insulin (100 nM) for 2 h. Then, the cells were collected at same time point and the fractions of plasma membrane fractions were isolated as described in experimental sections. The GLUT4 translocation was evaluated using Western blot analysis. Equal amounts of proteins were heated up to 37°C for 10 min and then loaded on SDS-polyacrylamide gels. After transferred to PVDF membranes, the blot was co-incubated with GLUT4 and Na<sup>+</sup>/K<sup>+</sup> ATPase α1 antibodies. (A) Sample names were from 1-6 as follows: Ctrl, insulin 100 nM, compounds **1**, **2**, **4**, and **8** (20 μM). (B) Similarly, the membrane was also carried as above procedure. However, the blot was first detected the Na<sup>+</sup>/K<sup>+</sup> ATPase α1 protein. Then, using a Restore<sup>TM</sup> Western blot stripping buffer (Thermo Sci.) for removing bound primary and secondary antibodies, the band was continually incubated with GLUT4 antibody. Sample

names were from 1–7 as follows: Ctrl, insulin 100 nM, compounds **1**, **2**, **4**, and **8** (20  $\mu$ M), reload **8** (20  $\mu$ M). (C) Collected cells (control and insulin groups) at different time points were also carried out. Sample names were from 1-10 as follows: Ctrl1 and Ctrl2 (collected after 24 h of experiment procedure), Ctrl3 and Ctrl4 (collected after 2 h of experiment procedure), insulin 100 nM-1 (treated at 22 h point and collected after 24 h of experiment procedure), insulin 100 nM-2 (collected after 2 h of experiment procedure), compounds **1**, **2**, **4**, and **8** (20  $\mu$ M) (collected after 24 h of experiment procedure). All bands were detected using LAS 4000 luminescent image analyzer. Figure A was included in final analysis (Figure 50).



#### 3.2.4. Effects of dammarane triterpenes on AMPK signaling pathway

To investigate the underlying mechanism for the stimulation of 2-NBDG uptake into the cells by dammarane triterpenes from *G. longipes*, the effects of all compounds were evaluated on the AMPK pathway, which plays a key role in glucose uptake regulation. The effects of all isolated compounds on phosphorylation of AMPK were evaluated using mouse C2C12 myotubes. According to the Western blot evidence in Figures 52-55, it may be observed that compounds **1**, **2**, **4**, **8**, and **10** up-regulated significantly ( $p < 0.01$ ) the expression of phosphorylated AMPK ( $p$ -AMPK). Weaker stimulation effects were observed in compounds **3** and **5** ( $p < 0.05$ ). However, no significant activity was found for compounds **6**, **7**, and **9**. Phosphorylated acetyl-CoA carboxylase ( $p$ -ACC) is a downstream signal of the AMPK signaling pathway that plays an important role in metabolic regulation. The function of AMPK is associated with fatty acid oxidation and regulation of the skeletal muscle metabolism via the phosphorylation of ACC1 at Ser<sup>79</sup>. Thus, the level of  $p$ -ACC was measured by Western blot analysis with phosphorylated ACC antibody to better understand AMPK action in ACC phosphorylation. As shown in Figures 52-55, compounds **1**, **2**, **4**, **8**, and **10** also up-regulated the expression of phosphorylated ACC. The results suggested that isolated compounds **1**, **2**, **4**, **8**, and **10** enhanced glucose uptake by regulating the AMPK signaling pathway. These results are consistent with the ethnopharmacological report of *G. longipes* as a traditional medicine for treating diabetes.

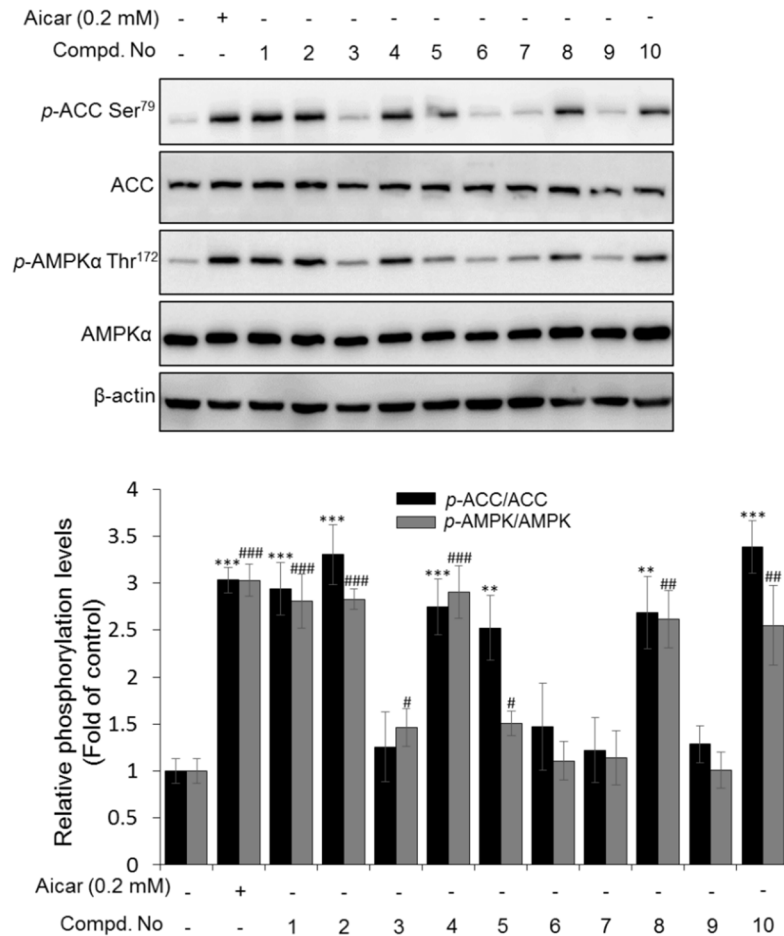


**Figure 52.** Effect of isolated compounds **1–10** on *p*-AMPK (Thr<sup>172</sup>) and *p*-ACC (Ser<sup>79</sup>) in differentiated mouse C2C12 skeletal myoblasts. The cells were treated with compounds **1–9** (20  $\mu$ M), and **10** (10  $\mu$ M) or Aicar (0.2 mM) as an AMPK activator. After 1 h of incubation, the phosphorylation of AMPK and ACC proteins were evaluated using the Western blot method. The results were expressed as the means  $\pm$  SD ( $n = 3$ ), \*  $p < 0.05$ , \*\*  $p < 0.01$ , and \*\*\*  $p < 0.001$  compared to the negative control, *p*-ACC; #  $p < 0.05$ , ##  $p < 0.01$ , and ###  $p < 0.001$ , compared to the negative control of *p*-AMPK.

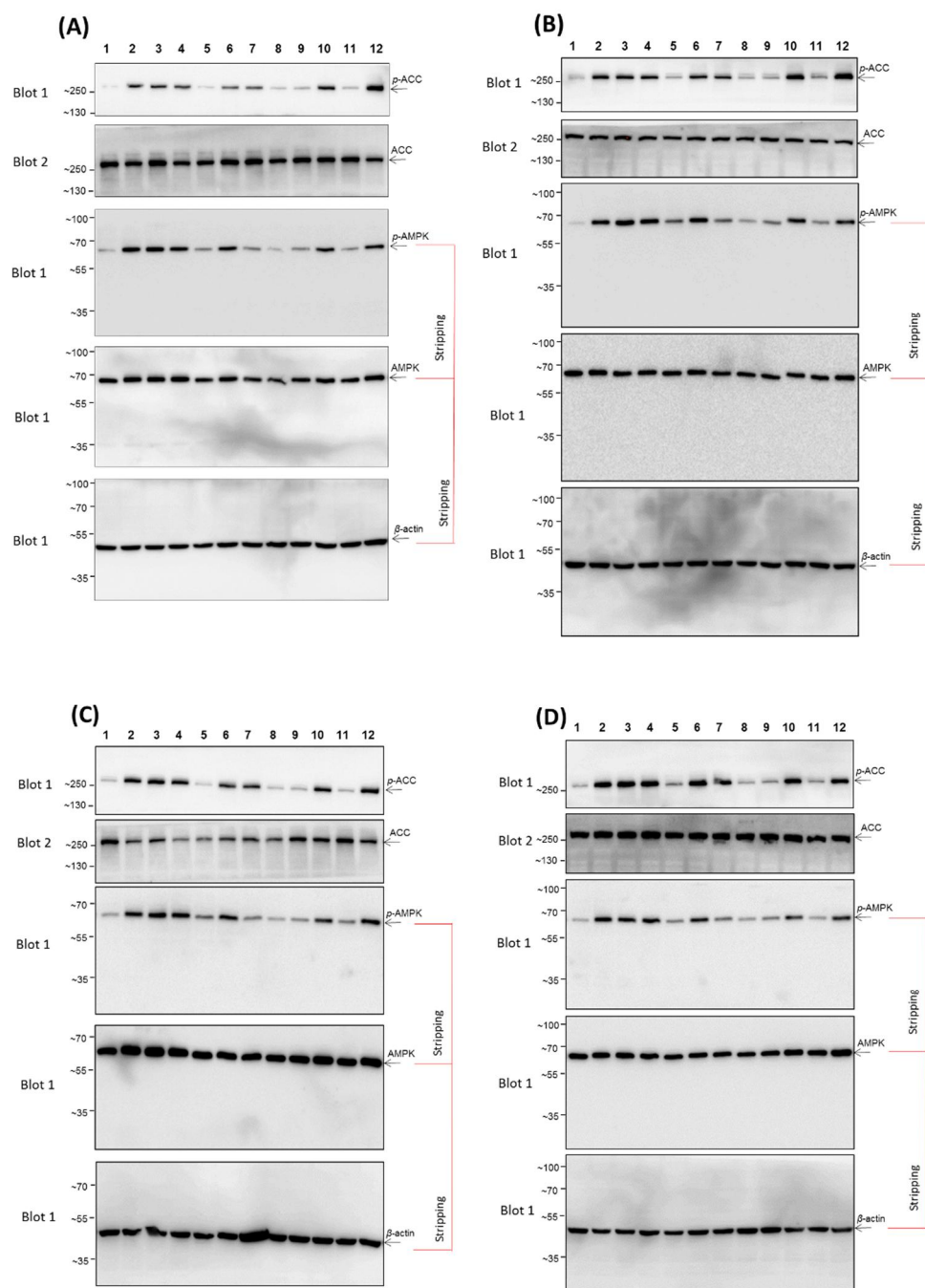


**Figure 53.** The effect of compounds 1–10 on *p*-AMPK Thr<sup>172</sup> and *p*-ACC Ser<sup>79</sup> in mouse C2C12 myotubes; original uncropped blots.

The cells were incubated with compounds **1–9** (20  $\mu$ M), compound **10** (10  $\mu$ M) or Aicar (0.2 mM) for 1 h. The cell lysates were then collected and the target proteins were measured using Western blotting method. Equal amounts of proteins were electrophoresed on 8% or 12% SDS-polyacrylamide gels and transferred to PVDF membranes. For detecting *p*-ACC Ser<sup>79</sup> and ACC proteins, the 1X transfer buffer was added 0.5% SDS solution. Different membranes were cut based on protein sizes and incubated with primary antibodies for *p*-ACC Ser<sup>79</sup>, ACC. However, to measure the phosphorylation of AMPK protein, the blot was first detected *p*-AMPK $\alpha$  Thr<sup>172</sup> protein. Then, using a Restore<sup>TM</sup> Western blot stripping buffer (Thermo Sci.) for removing bound primary and secondary antibodies, the blot was continually incubated with AMPK $\alpha$  and  $\beta$ -actin antibodies, respectively. All membranes were detected using a LAS4000 luminescent image analyzer. (A-D) Sample names were from 1-12 as follows: Ctrl, Aicar 0.2 mM, **1–9** (20  $\mu$ M), **10** (10  $\mu$ M). Figure D was included in the final analysis (Figure 52).

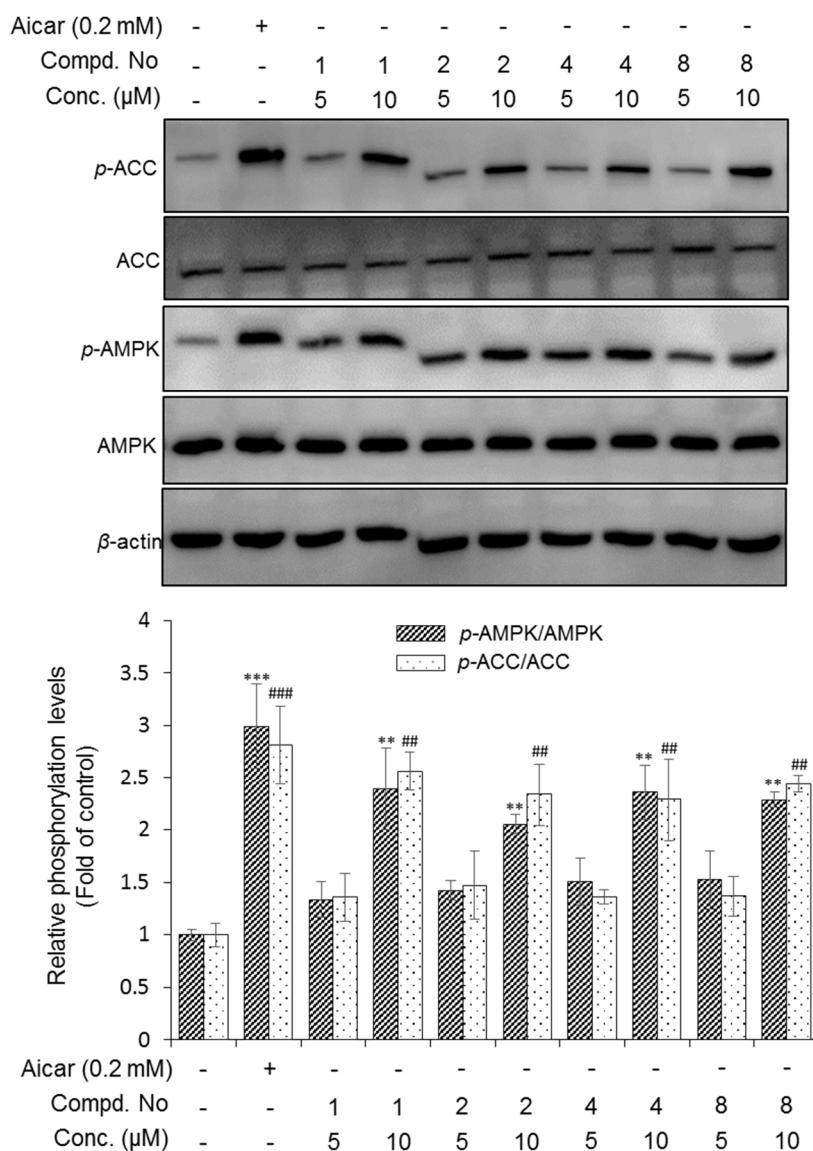


**Figure 54.** The effect of compounds **1**, **2**, **4**, and **8** at different concentrations (5 and 10  $\mu$ M) on the phosphorylation of AMPK (Thr<sup>172</sup>) and ACC (Ser<sup>79</sup>) in differentiated mouse C2C12 skeletal myoblasts. The results were calculated as the mean  $\pm$  SD (n = 3), \* p < 0.05, \*\* p < 0.01, and \*\*\* p < 0.001.

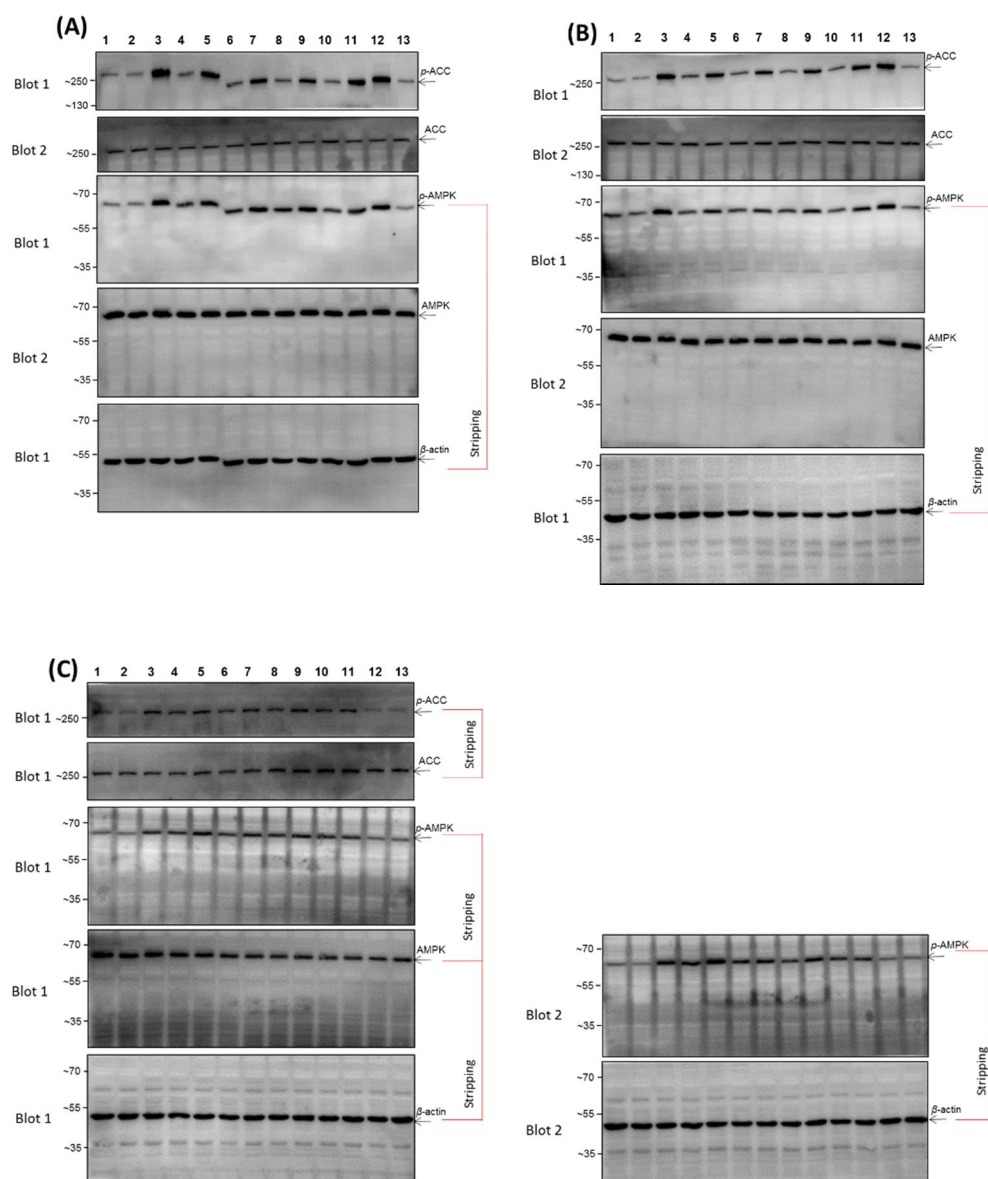


**Figure 55.** Activation effects of compounds 1, 2, 4, and 8 from *G. longipes* on the phosphorylation of AMPK Thr<sup>172</sup> and ACC Ser<sup>79</sup> in C2C12 myotubes; original uncropped blots.

The cells were exposed with tested compounds at different concentrations (5 and 10  $\mu$ M) or Aicar (0.2 mM) for 1 h. The phosphorylation of target proteins was evaluated using Western blot analysis. Equal amounts of proteins were loaded on

SDS-polyacrylamide gel. The gel was cut based on protein sizes and then transferred to PVDF membranes with different conditions (the 1X transfer buffer was added 0.5% SDS solution for detecting *p*-ACC Ser<sup>79</sup> and ACC proteins). The blots were firstly detected with *p*-AMPK $\alpha$  Thr<sup>172</sup> and *p*-ACC Ser<sup>79</sup> proteins. Then, using a Restore<sup>TM</sup> Western blot stripping buffer (Thermo Sci.), the membrane was further incubated  $\beta$ -actin antibody and detected by the LAS4000 luminescent image analyzer. Other gel was also cut and transferred as above described. The membranes were then incubated with AMPK and ACC antibodies and evaluated using a LAS4000 luminescent image analyzer. (A-B) Sample names were from 1-13 as follows: Ctrl1, Ctrl2, Aicar (0.2 mM), **1** (5, 10  $\mu$ M), **2** (5, 10  $\mu$ M), **4** (5, 10  $\mu$ M), **8** (5, 10  $\mu$ M), reload Aicar (0.2 mM), reload Ctrl1, respectively. (C) Similarly, the cut-membranes were firstly detected the *p*-AMPK $\alpha$  Thr<sup>172</sup> and *p*-ACC Ser<sup>79</sup> proteins (blot 1). Then, these blots were further incubated with ACC, AMPK and  $\beta$ -actin antibodies. In addition, these samples were reloaded again on other SDS-polyacrylamide gel. After transferred to PVDF membrane, the blot was detected the *p*-AMPK $\alpha$  Thr<sup>172</sup> and  $\beta$ -actin proteins (blot 2). Sample names were from 1-13 as follows: Ctrl1, Ctrl2, Aicar (0.2 mM), **1** (5, 10  $\mu$ M), **2** (5, 10  $\mu$ M), **4** (5, 10  $\mu$ M), **8** (5, 10  $\mu$ M), reload Ctrl1, reload Ctrl2, respectively. Figure A was included in the final analysis (Figure 54).

#### 4. Conclusions

A 70% EtOH extract of *G. longipes* was subjected to various chromatographic columns and then to purification by preparative HPLC to afford ten new dammarane triterpenes (**1–10**) with two 3,4-*seco* dammarane analogues, secolongipegenins S1-S2 (**1** and **2**), a 3,4-*seco* hexanordammarane, secolongipegenin S3 (**3**), two hexanordammarane glycosides, longipenosides ND1-ND2 (**4** and **5**) and five other dammarane glycosides, longipenosides GL1-GL5 (**6–10**). There are included (**1**) 4,20(*S*)-dihydroxy-3,4-*seco*-dammar-24-en-12,23-dion-3-oic acid, (**2**) 4,20(*S*),25-trihydroxy-3,4-*seco*-dammaran-12,23-dion-3-oic acid, (**3**) 4-hydroxy-3,4-*seco*-22,23,24,25,26,27-hexanordammaran-12,20-dion-3-oic acid, (**4**) 3 $\beta$ -hydroxy-22,23,24,25,26,27-hexanordammaran-12,20-dione-3-*O*-[ $\alpha$ -L-rhamnopyranosyl (1 $\rightarrow$ 2)]-[ $\alpha$ -L-rhamnopyranosyl(1 $\rightarrow$ 3)]- $\beta$ -D-glucopyranoside, (**5**) 3 $\beta$ -hydroxy-22,23, 24,25,26,27-hexanordammaran-12,20-dione-3-*O*-[ $\alpha$ -L-rhamnopyranosyl(1 $\rightarrow$ 2)]-[ $\alpha$ -L-rhamnopyranosyl(1 $\rightarrow$ 3)]-[ $\alpha$ -L-rhamnopyranosyl(1 $\rightarrow$ 6)]- $\beta$ -D-glucopyranoside, (**6**) 3 $\beta$ ,20(*S*),25-trihydroxydammaran-12,23-dione-3-*O*-[ $\alpha$ -L-rhamnopyranosyl (1 $\rightarrow$ 2)]-[ $\alpha$ -L-rhamnopyranosyl(1 $\rightarrow$ 3)]-[ $\alpha$ -L-rhamnopyranosyl(1 $\rightarrow$ 6)]- $\beta$ -D-glucopyranoside, (**7**) 3 $\beta$ -hydroxydammar-20,24-dien-12,23-dione-3-*O*-[ $\alpha$ -L-rhamnopyranosyl (1 $\rightarrow$ 2)]-[ $\alpha$ -L-rhamnopyranosyl(1 $\rightarrow$ 3)]-[ $\alpha$ -L-rhamnopyranosyl(1 $\rightarrow$ 6)]- $\beta$ -D-glucopyranoside, (**8**) 3 $\beta$ ,20(*S*),25-trihydroxydammar-23(*E*)-en-12-one-3-*O*-[ $\alpha$ -L-rhamnopyranosyl(1 $\rightarrow$ 2)]-[ $\alpha$ -L-rhamnopyranosyl(1 $\rightarrow$ 3)]- $\beta$ -D-glucopyranoside, (**9**) 3 $\beta$ ,20(*S*),25-trihydroxydammar-23(*E*)-en-12-one-3-*O*-[ $\alpha$ -L-rhamnopyranosyl(1 $\rightarrow$ 2)]-[ $\alpha$ -L-rhamnopyranosyl(1 $\rightarrow$ 3)]-[ $\alpha$ -L-rhamnopyranosyl(1 $\rightarrow$ 6)]- $\beta$ -D-glucopyranoside,



(10) 3 $\beta$ ,20(*S*)-hydroxydammar-24-en-12-one-3-*O*- $\alpha$ -L-rhamnopyranosyl(1 $\rightarrow$ 2)- $\beta$ -D-glucopyranoside.

Compounds **1**, **2**, **4**, and **8** enhanced 2-NBDG uptake in a concentration dependent manner and stimulated the translocation of GLUT4 protein to the plasma membrane of 3T3-L1 adipocytes.

It also observed that dammarane triterpenes (**1**, **2**, **4**, **8**, and **10**) significantly up-regulated the expressions of phosphorylated AMPK and ACC using mouse C2C12 myotubes. These results suggested that *G. longipes* may be a potential therapeutic agent for treating diabetes.

**Part 2. Neuroprotective Effects of Triterpenes from**  
***Camellia japonica* in a Rotenone Model of**  
**Parkinson's Disease**

## 1. Introduction

### 1.1. Parkinson's disease

Neurological disorders are the leading cause of death and disability in the world (Feigin et al., 2017). These disorders include Alzheimer disease, Parkinson's disease (PD), epilepsy, and cerebrovascular diseases,... Among them, PD is the second most common neurodegenerative disorder of the central nervous system (CNS) worldwide (Dawson and Dawson, 2003; Kwon et al., 2014; Lotharius and Brundin, 2002). Recently, PD is surpassing growth than Alzheimer disease (Dorsey and Bloem, 2018; Feigin et al., 2017). According to the Global Burden of Disease Study, the number of PD patients will increase to around 6.9 million in 2015 to 14.2 million in 2040 (Dorsey and Bloem, 2018).

PD is physiologically caused by dopamine deficits in the brain and the diminution of dopaminergic neurons in substantia nigra (Lin et al., 2012; Sashidhara et al., 2014). PD patients present clinical symptoms such as rigidity, tremors, bradykinesia, and postural instability (Zhang et al., 2014). Diagnosing this disease has long been a challenge due to the complicated and progressive symptoms among different stages and the confusion with the symptoms of other CNS disorders (Jackson-Lewis and Przedborski, 2007). The drugs used clinically for treating PD mainly include dopamine agonists and monoamine oxidase inhibitors (Meissner et al., 2011). However, these approaches only relieve the PD symptoms; they do not inhibit or reverse the neurodegeneration (Hsieh and Chiang, 2014).

## 1.2. Rotenone-induced Parkinson's disease model

Nowadays, there are two types of PD including sporadic and familial PD. However, the most common form of this disease is sporadic PD which is caused by genetic susceptibility and environmental factors (Figure 56). Even though aging is an important risk factor for patients with sporadic PD, evidence has indicated that toxins exposure (such as rotenone, paraquat,...) is also associated with PD in humans (Exner et al., 2012; Wrangel et al., 2015).

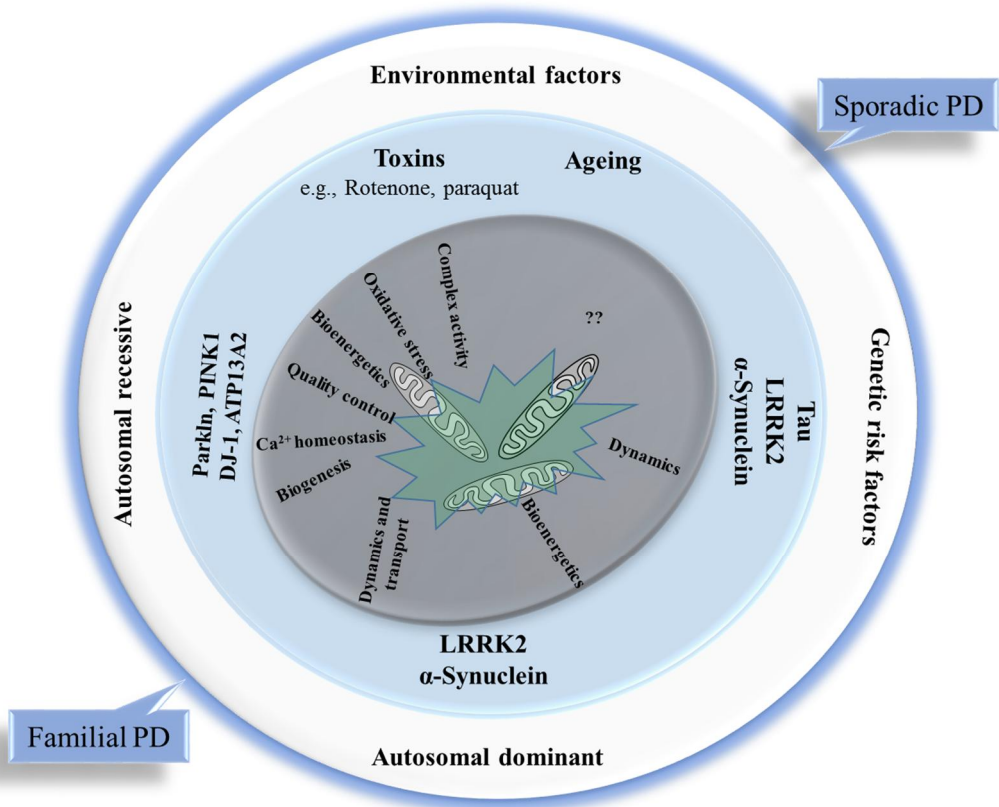


**Figure 56.** The etiology of Parkinson's disease (Exner et al., 2012).

Rotenone, an inhibitor for mitochondrial complex I, is able to induce  $\alpha$ -synuclein oligomerization and is able to produce intracellular reactive oxygen species (ROS) (Figure 57) (Dadakhujiev et al., 2010; Luk et al., 2012; N. et al., 2017). Through this function, rotenone has been reported to be an effective reagent for mimicking the biochemical process of PD, and this model has been used to screen potential active compounds for PD treatment (Ryu et al., 2013). Considering the interrelationship between natural products and PD therapy, our group attempted to screen the Korea Bioactive Natural Material Bank (KBNMB) using a rotenone-induced Parkinson's disease model to search for new bioactive natural products with the potential for treating PD.

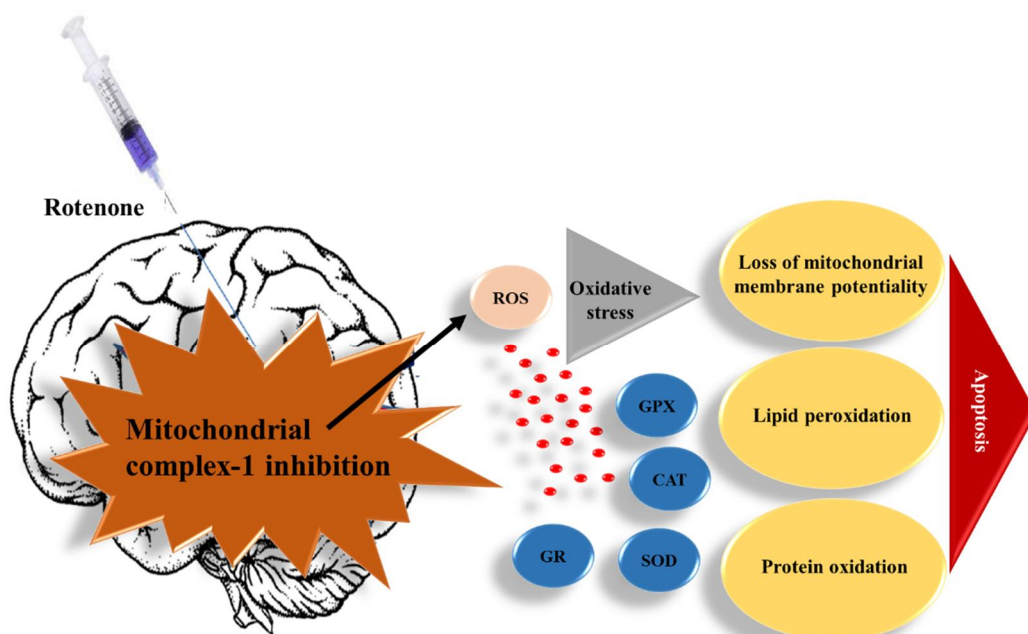


**Figure 57.** Mechanism of rotenone induced apoptosis (N. et al., 2017).

### 1.3. Structure and aggregation of $\alpha$ -synuclein in PD

Human  $\alpha$ -synuclein protein was encoded by the NG\_011851 (*SNCA*) gene that consists of 6 exons (from 42 to 1110 bp).  $\alpha$ -synuclein is a small acidic protein which contains 140 amino acid. It has been divided into three domains including a positively charged N-terminal region, a central hydrophobic region, and a highly acidic C-terminal domain (Emamzadeh, 2016; Rocha et al., 2018). Recently, the functional role of  $\alpha$ -synuclein is not fully understood, but several functions are successfully identified and summarized in Table 5 (Emamzadeh, 2016). Especially, soluble  $\alpha$ -synuclein aggregates, known as oligomers, play an important role in the development of PD through impairing many subcellular functions (Choi et al., 2013; Colla et al., 2012). Substantial evidence indicates the phosphorylation of  $\alpha$ -synuclein at residue Serine-129 could enhance the aggregation of oligomeric  $\alpha$ -synuclein (Anderson et al., 2006; Rocha et al., 2018). Moreover, high levels of soluble oligomeric form induced cell death in both *in vitro* and *in vivo* models (Rocha et al., 2018). Therefore,  $\alpha$ -synuclein might be considered as a potential biomarker for PD.

**Table 5.** The functions of  $\alpha$ -synuclein (Emamzadeh, 2016).

<b><math>\alpha</math>-synuclein function</b>	<b>Target</b>	<b>Mechanism</b>
Suppression of apoptosis	Protein kinase C	Deactivation of nuclear factor $\kappa$ B (NF $\kappa$ B)
Regulation of glucose levels	G-protein-couple-receptor	Increase tissue glucose uptake
	The pancreatic $\beta$ -cell	Inhibition of insulin secretion
	KATP channel	
Modulation of calmodulin activity	Calmodulin (CaM)	Conversion of CaM from an inhibitor to an activator
Chaperone activity	Presynaptic membranes	Maintenance of sensitive factor attachment protein receptor
Maintenance of PUFA levels	Acyl-coA synthetase	Modulation of lipid synthesis
Antioxidation	Cytochrome c oxidase	Prevention of Caspases activation
	c-Jun N-terminal kinase (JNK) interacting protein	Inhibition of JNK pathway
Neuronal differentiation	Rab3a	Activation of ERK/MAPK pathway
Regulation of dopamine biosynthesis	Protein phosphatase 2A	Inhibition of tyrosine hydroxylase

#### 1.4. The role of light chain 3 (LC3) in autophagy

Autophagy is a self-degradative process that may protect against neurological disorders such as PD. However, excessive autophagic activation could lead to depletion of essential proteins and it is responsible for programmed cell death (Xiong et al., 2013). Currently, the overexpression of  $\alpha$ -synuclein protein significantly activates the process of autophagy (Cuervo et al., 2004; Vogiatzi et al., 2008; Xiong et al., 2009). Previous studies demonstrated that the early-stage of autophagy activation can response to protective effects and the late-stage of this process might result in cell death or neurotoxic effects (Xiong et al., 2013).

Light chain 3 (LC3), an autophagosomal marker protein in mammals, which is cleaved at its COOH terminus by the protease, resulting in the production of cytoplasmic LC3-I form. Conversion of LC3-I to LC3-II is tightly associated with the autophagosomal membrane probably through conjugation to phosphatidylethanolamine (Kabeya, 2004, 2000).



Autophagy is initiated by the formation of the phagophore (known as isolation membrane). The complex process of autophagy pathway was shown in Figure 58. The major steps of this scheme are the interaction between p62 and LC3-II. The outer membrane of the autophagosome fuses with the lysosome and forms an autophagolysosome. The sequestered material is then degraded inside the autophagolysosome (vesicle breakdown and degradation) and recycled (Choi and Kim, 2013).

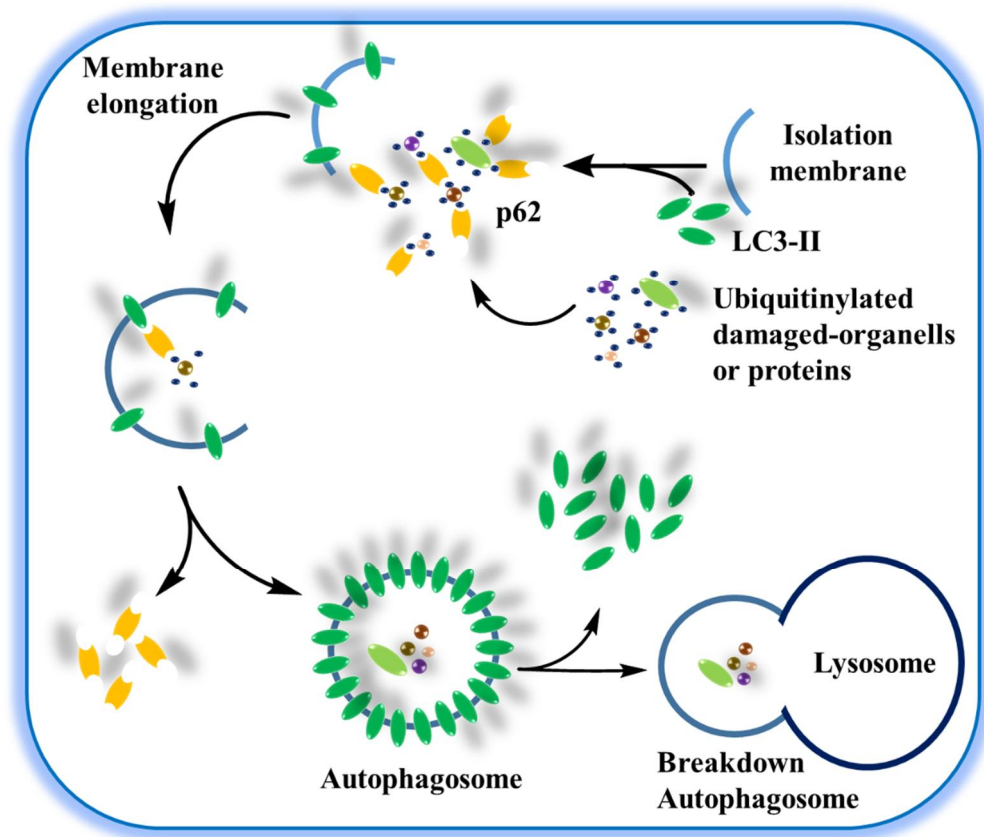


**Figure 58.** Schematic diagram illustrating the steps of autophagy (Choi and Kim, 2013).

### 1.5. *Camellia japonica*

The plant *C. japonica* L., which belongs to the Theaceae family (Figure 59), is widely cultivated in Korea, China, and Japan (Nakamura et al., 2012; Tamaru et al., 2013). In addition to its use as an ornamental or garden tree, *C. japonica* has important uses in traditional medicine. The flower buds of this plant has been used for treating vomiting of blood and bleeding, and showed anti-inflammatory, tonic, and stomatic activities (Nakamura et al., 2012). Previous phytochemical studies in our lab have found potential on protein tyrosine phosphatase 1B (PTP1B) inhibitors (Uddin et al., 2014) and anti-PEDV (porcine epidemic diarrhea virus) active compounds (Yang et al., 2015) from the fruit peels and flowers of this plant, respectively. Bioassay-guided fractionation using a rotenone-induced Parkinson's disease model resulted in the isolation of six new 3,4-*seco*-28-nor-oleanane triterpenoids (**11–16**) from the flowers of *C. japonica*. In this report, we will describe the isolation and structural elucidation of the purified compounds **11–16**, as well as their protective effects on SH-SY5Y neuronal cells in a rotenone model of Parkinson's disease.

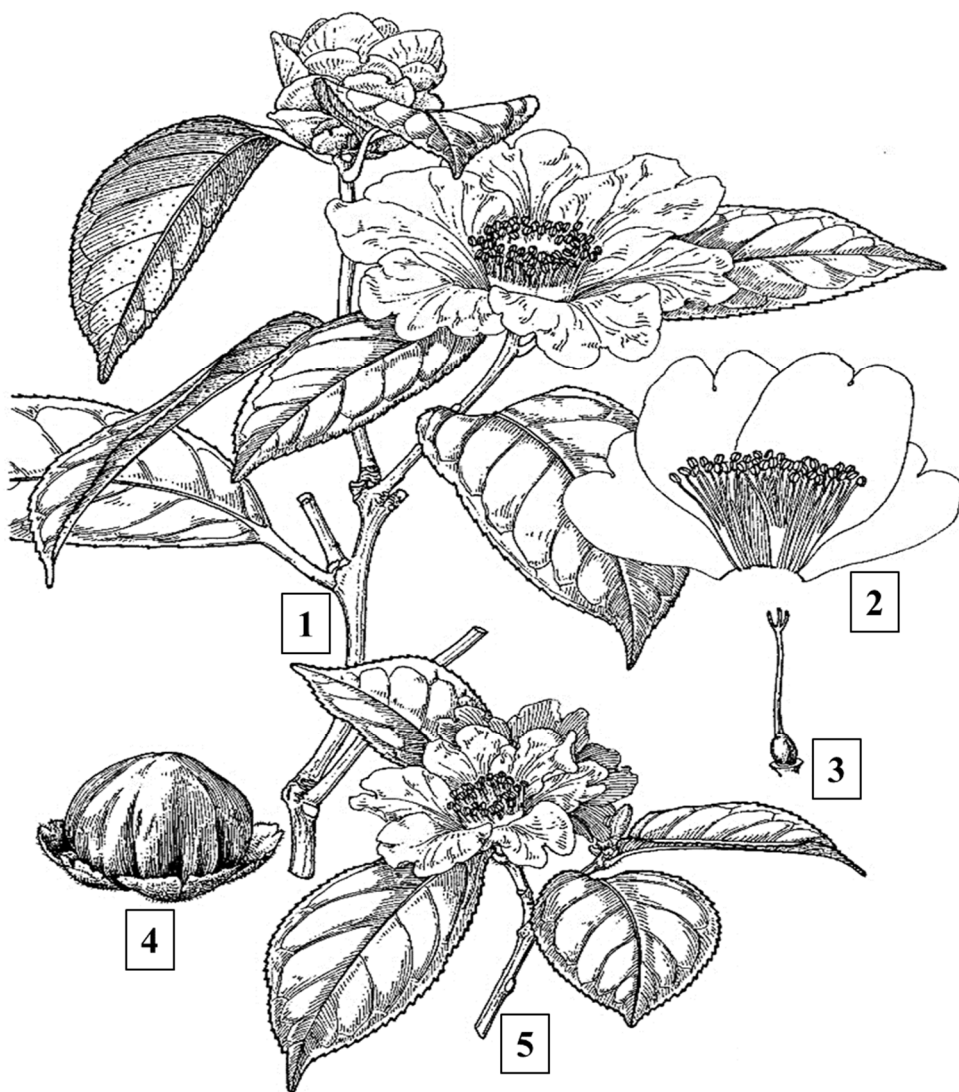
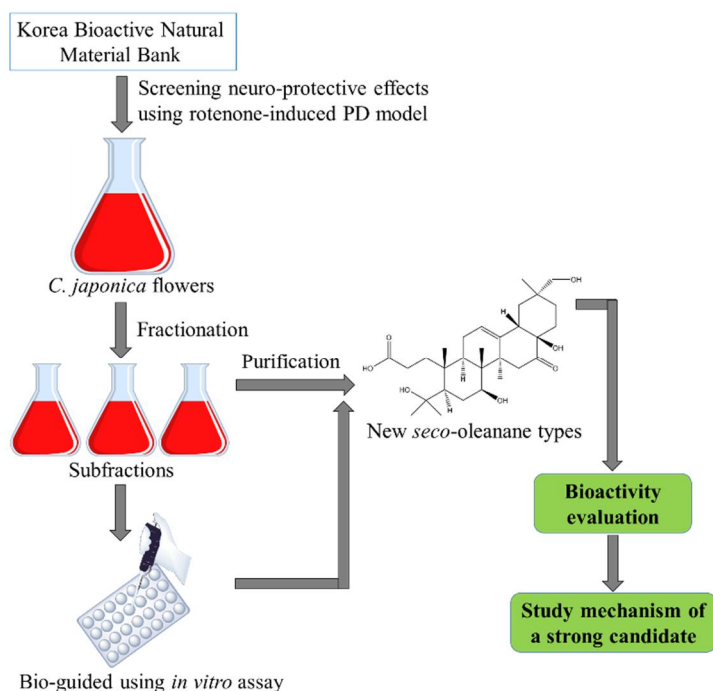


**Figure 59.** *Camellia japonica* Linnaeus var. *japonica*: (1) flowering branch, (2) petals and stamens, (3) pistil, (4) young capsule. (5) *Camellia japonica* var. *rusticana* (Wu et al., 2007).

## 1.6. Purpose of research

The purpose of this study isolated new bioactive chemical entities using bio-guided strategy. During the process to screen the fractions from KBNMB using a rotenone-induced Parkinson's disease model for treating PD, *Camellia japonica* flowers could be protective effects on SH-SY5Y cells in rotenone-induced neurotoxicity. Triterpenoid, a major secondary metabolite of *C. japonica*, was chosen as target compounds. This thesis is organized as follows: (1) isolation of new *seco*-oleanane types based on the bio-guided assay, (2) study the effects of the strongest candidate on the accumulation of  $\alpha$ -synuclein and ROS levels and the condensation of chromosome a rotenone-induced Parkinson's disease. The schematic representation of bio-guided isolation strategy is shown in Scheme 4.



**Scheme 4.** The bio-guided isolation strategy of *C. japonica* flowers.

## 2. Materials and methods

### 2.1. Plant materials

The flowers of *Camellia japonica* were collected from Gwangju city in February, 2013, and were authenticated by Prof. Oh Won Keun at Seoul National University. A voucher specimen (SNU2013-02) was deposited at the College of Pharmacy, Seoul National University, Seoul, Republic of Korea.

### 2.2. Chemicals, reagents and chromatography

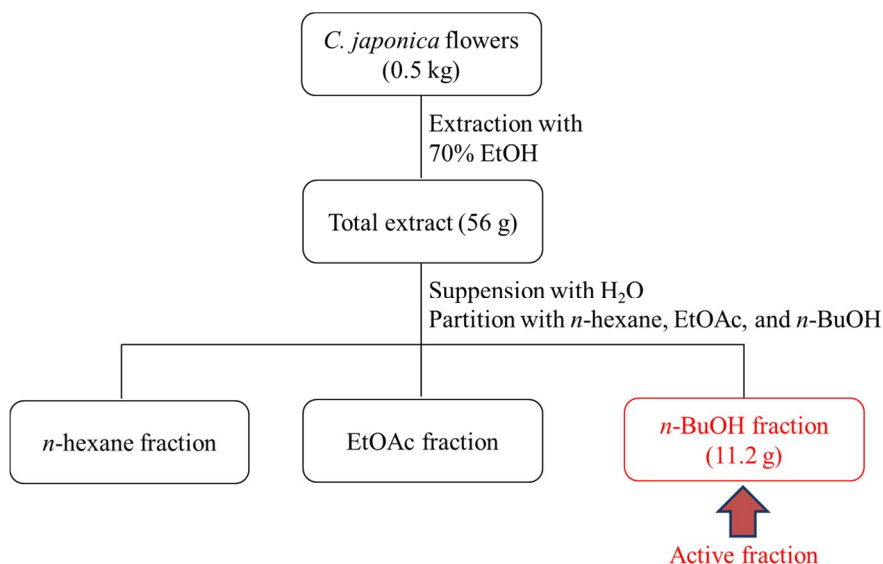
Almost chemical and bioassay reagents, and experimental instruments in Part 2 were used similarly to Part 1. However, there have other chemicals and equipment in this part, including:

- Random primer (iNtRON Biotechnology, INC, Korea)
- Maxima SYBR Green qPCR master mix 2X (Thermo sci., Rockford, IL, USA)
- $\alpha$ -synuclein antibody (SC-12767, Santa Cruz Biotechnology, INC.)
- DCFDA (D6883, Sigma-Aldrich, St. Louis, MO, USA)
- DAPI (Invitrogen, Eugene, OR, USA)
- Mounting medium (Vector, Burlingame, CA, USA)
- StepOnePlus Real-Time PCR System (Applied Biosystems)
- Carl Zeiss LSM710 confocal microscope (Carl Zeiss, Oberkochen, Germany).

### 2.3. Extraction and isolation schemes

*C. japonica* flowers (0.5 kg) were dried and extracted with 70% ethanol three times (each for 2 days) at room temperature. A concentrated crude residue (56 g) was

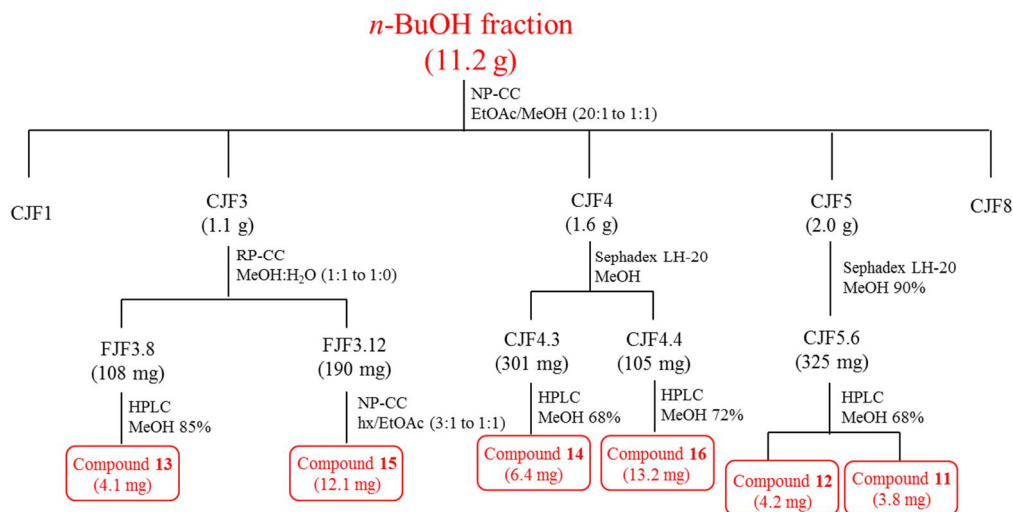
first suspended in deionized water (3 L, 40°C) and then successively partitioned against *n*-hexane, EtOAc, and *n*-BuOH. Screening in a rotenone model of Parkinson's disease indicated that the *n*-BuOH fraction exhibited potential protective effects on SH-SY5Y neuronal cells, and this assay was used in the entire bioactivity-guided fractionation process (Scheme 5).



**Scheme 5.** Extraction and fractionation of *C. japonica*.

The *n*-BuOH fraction (11.2 g) was chromatographed over silica gel CC (5 × 40 cm) eluting with EtOAc/MeOH (from 20:1 to 1:1) to afford eight subfractions (CJF1–CJF8) according to the TLC profile. Fraction CJF3 (1.1 g) was further subjected to RP-C<sub>18</sub> CC (1.0 × 20 cm) eluting with MeOH:H<sub>2</sub>O (1:1 to 1:0) to afford twenty subfractions (CJF3.1–CJF3.20). Fraction CJF3.8 (106 mg) was purified via HPLC [mobile phase: MeOH:H<sub>2</sub>O (85:15)], affording compound **13** (4.1 mg; *t<sub>R</sub>* = 24.3 min). Fraction CJF3.12 (190 mg) was separated by silica gel CC

(1.0 × 20 cm) eluting with *n*-hexane:EtOAc (3:1 to 1:1) to provide compound **15** (12.1 mg). Fraction CJ4 (1.6 g) was fractionated by Sephadex LH-20 CC (2.0 × 60 cm) eluting with EtOH to afford six subfractions (CJF4.1–CJF4.6). Compounds **14** (6.3 mg;  $t_R$  = 39.2 min) and **16** (13.2 mg;  $t_R$  = 36.1 min) were purified from CJF4.3 [301 mg; HPLC condition: mobile phase: MeOH:H<sub>2</sub>O (68:32)] and CJF4.4 [105 mg; HPLC condition: mobile phase: MeOH:H<sub>2</sub>O (72:28)], respectively. Fraction CJF5 (2.0 g) was separated using a Sephadex LH-20 CC (2.0 × 60 cm) eluting with 90% MeOH in H<sub>2</sub>O to yield ten subfractions (CJF5.1–CJF5.10). Fraction CJF5.6 (325 mg) was purified using HPLC [mobile phase: MeOH:H<sub>2</sub>O (58:42)] to afford compound **12** (4.2 mg;  $t_R$  = 40.6 min), and compound **11** (3.8 mg;  $t_R$  = 27.6 min) was obtained from CJF5.7 (169 mg) via HPLC [mobile phase: MeOH:H<sub>2</sub>O (55:45)] (Scheme 6).



**Scheme 6.** Isolation scheme of *n*-BuOH fraction of *C. japonica*.

## 2.4. Chemical and spectral properties of isolated compounds

### 2.4.1. Compound **11**

Compound **11** was obtained as a white amorphous powder;  $[\alpha]_{\text{D}}^{25} -20.6$  (*c* 0.1, MeOH); IR (KBr)  $\nu_{\text{max}}$  3390, 2981, 1710, 1624, 1181, 910  $\text{cm}^{-1}$ ;  $^1\text{H}$  and  $^{13}\text{C}$  NMR data, Table 6; HRESIMS  $m/z$  529.3140  $[\text{M} + \text{Na}]^+$  (calcd for  $\text{C}_{29}\text{H}_{46}\text{O}_7\text{Na}$ , 529.3136).

### 2.4.2. Compound **12**

Compound **12** was obtained as a white amorphous powder;  $[\alpha]_{\text{D}}^{25} -24.1$  (*c* 0.1, MeOH); IR (KBr)  $\nu_{\text{max}}$  3394, 2920, 1715, 1631, 1032, 903  $\text{cm}^{-1}$ ;  $^1\text{H}$  and  $^{13}\text{C}$  NMR data, Table 6; HRESIMS  $m/z$  1063.6682  $[2\text{M} + \text{Na}]^+$  (calcd for  $\text{C}_{60}\text{H}_{96}\text{O}_{14}\text{Na}$ , 1063.6692).

### 2.4.3. Compound **13**

Compound **13** was obtained as a white amorphous powder;  $[\alpha]_{\text{D}}^{25} -26.4$  (*c* 0.1, MeOH); IR (KBr)  $\nu_{\text{max}}$  3420, 2958, 1714, 1642, 1008, 851  $\text{cm}^{-1}$ ;  $^1\text{H}$  and  $^{13}\text{C}$  NMR data, Table 6; HRESIMS  $m/z$  569.3819  $[\text{M} + \text{Na}]^+$  (calcd for  $\text{C}_{33}\text{H}_{54}\text{O}_6\text{Na}$ , 569.3813).



#### 2.4.4. Compound **14**

Compound **14** was obtained as a white amorphous powder;  $[\alpha]_{\text{D}}^{25} -34.8$  (*c* 0.1, MeOH); IR (KBr)  $\nu_{\text{max}}$  3442, 2925, 1715, 1665, 1174, 829  $\text{cm}^{-1}$ ;  $^1\text{H}$  and  $^{13}\text{C}$  NMR data, Table 7; HRESIMS  $m/z$  487.3423  $[\text{M} - \text{H}_2\text{O} + \text{H}]^+$  (calcd for  $\text{C}_{30}\text{H}_{47}\text{O}_5$ , 487.3423) and 469.3317  $[\text{M} - 2\text{H}_2\text{O} + \text{H}]^+$  (calcd for  $\text{C}_{30}\text{H}_{45}\text{O}_4$ , 469.3318).

#### 2.4.5. Compound **15**

Compound **15** was obtained as a white amorphous powder;  $[\alpha]_{\text{D}}^{25} -27.2$  (*c* 0.1, MeOH); IR (KBr)  $\nu_{\text{max}}$  3394, 2958, 1730, 1614, 1385, 993  $\text{cm}^{-1}$ ;  $^1\text{H}$  and  $^{13}\text{C}$  NMR data, Table 7; HRESIMS  $m/z$  529.3880  $[\text{M} - \text{H}_2\text{O} + \text{H}]^+$  (calcd for  $\text{C}_{33}\text{H}_{53}\text{O}_5$ , 529.3893).

#### 2.4.6. Compound **16**

Compound **16** was obtained as a white amorphous powder;  $[\alpha]_{\text{D}}^{25} -24.4$  (*c* 0.1, MeOH); IR (KBr)  $\nu_{\text{max}}$  3393, 2925, 1714, 1596, 1027, 951  $\text{cm}^{-1}$ ;  $^1\text{H}$  and  $^{13}\text{C}$  NMR data, Table 7; HRFABMS  $m/z$  473.3283  $[\text{M} + \text{H}]^+$  (calcd for  $\text{C}_{29}\text{H}_{45}\text{O}_5$ , 473.3267).

**Table 6.** NMR spectroscopic data for compounds **11**–**13**.

	<b>11<sup>a</sup></b>		<b>12<sup>b</sup></b>		<b>13<sup>c</sup></b>	
	$\delta_{\text{H}}$ ( <i>J</i> in Hz)	$\delta_{\text{C}}$	$\delta_{\text{H}}$ ( <i>J</i> in Hz)	$\delta_{\text{C}}$	$\delta_{\text{H}}$ ( <i>J</i> in Hz)	$\delta_{\text{C}}$
<b>1</b>	3.05, m	35.5, CH <sub>2</sub>	2.34, m	35.2, CH <sub>2</sub>	2.33, m	35.4, CH <sub>2</sub>
	2.21, m		1.66, m		1.66, m	
<b>2</b>	3.06, m	29.1, CH <sub>2</sub>	2.50, m	29.7, CH <sub>2</sub>	2.53, m	29.2, CH <sub>2</sub>
	2.66, m		2.08, m		2.19, m	
<b>3</b>		177.5, C		176.9, C		176.8, C
<b>4</b>		74.8, C		75.5, C		76.0, C
<b>5</b>	1.94, dd (10.0, 3.1)	50.5, CH	1.53, dd (11.3, 3.0)	50.9, CH	1.42, dd (10.8, 3.2)	52.9, C
<b>6</b>	2.05, m	34.5, CH <sub>2</sub>	1.52, overlap	33.8, CH <sub>2</sub>	1.45, overlap	33.5, CH <sub>2</sub>
	1.99, m		1.30, overlap		1.29, overlap	
<b>7</b>	4.19, dd (11.0, 4.5)	72.9, CH	3.74, dd (11.3, 4.1)	73.4, CH	3.59, dd (12.0, 4.8)	74.7, CH
<b>8</b>		46.0, C		46.2, C		40.9, C
<b>9</b>	2.07, br d (12.0)	39.6, CH	1.64, dd (10.0, 4.5)	40.0, CH	1.39, dd (11.2, 4.1)	39.5, CH
<b>10</b>		42.3, C		42.3, C		42.2, C
<b>11</b>	2.29, overlap	24.3, CH <sub>2</sub>	2.06, overlap	24.3, CH <sub>2</sub>	2.06, m	24.4, CH <sub>2</sub>
	2.05, overlap		1.96, dt (16.2, 5.0)		1.96, dt (15.0, 5.0)	
<b>12</b>	5.69, t (3.5)	125.4, CH	5.51, t (3.0)	126.2, CH	5.45, t (3.6)	126.1, CH
<b>13</b>		142.6, C		141.9, C		141.6, C
<b>14</b>		50.5, C		50.6, C		50.1, C
<b>15</b>	4.38, d (14.0)	47.6, CH <sub>2</sub>	3.52, d (14.0)	47.4, CH <sub>2</sub>	3.30, d (13.2)	43.4, CH <sub>2</sub>
	3.06, d (14.0)		2.20, d (14.0)		1.66, d (13.2)	
<b>16</b>		216.6, C		217.6, C		216.6, C
<b>17</b>		77.1, C		77.4, C		78.4, C
<b>18</b>	3.30, dd (14.5, 4.0)	53.2, CH	2.80, dd (14.3, 3.9)	52.1, CH	2.78, dd (14.4, 4.2)	53.1, CH
<b>19</b>	2.06, overlap	43.6, CH <sub>2</sub>	1.51, overlap	43.3, CH <sub>2</sub>	1.41, overlap	47.5, CH <sub>2</sub>
	1.72, t (3.0)		1.33, overlap		1.38, overlap	
<b>20</b>		37.1, C		36.9, C		31.8, C
<b>21</b>	2.23, dd (13.5, 4.5)	32.7, CH <sub>2</sub>	2.15, overlap	32.9, CH <sub>2</sub>	1.59, overlap	36.7, CH <sub>2</sub>
	1.57, overlap		1.55, overlap		1.32, overlap	
<b>22</b>	2.56, overlap	31.4, CH <sub>2</sub>	2.11, overlap	30.7, CH <sub>2</sub>	1.60, overlap	30.2, CH <sub>2</sub>
	1.92, overlap		1.52, overlap		1.35, overlap	
<b>23</b>	1.50, s	34.0, CH <sub>3</sub>	1.28, s	32.3, CH <sub>3</sub>	1.27, s	32.8, CH <sub>3</sub>
<b>24</b>	1.48, s	29.1, CH <sub>3</sub>	1.26, s	28.4, CH <sub>3</sub>	1.26, s	28.4, CH <sub>3</sub>
<b>25</b>	1.34, s	20.7, CH <sub>3</sub>	1.12, s	20.4, CH <sub>3</sub>	1.12, s	20.3, CH <sub>3</sub>
<b>26</b>	1.68, s	11.6, CH <sub>3</sub>	1.11, s	11.0, CH <sub>3</sub>	0.91, s	17.6, CH <sub>3</sub>
<b>27</b>	1.55, s	27.4, CH <sub>3</sub>	1.23, s	26.7, CH <sub>3</sub>	1.13, s	26.7, CH <sub>3</sub>
<b>29</b>	3.60, s	74.1, CH <sub>2</sub>	3.16, d (11.0)	74.2, CH <sub>2</sub>	0.90, s	30.2, CH <sub>3</sub>
			3.13, d (11.0)			
<b>30</b>	1.25, s	19.9, CH <sub>3</sub>	0.96, s	19.3, CH <sub>3</sub>	1.15, s	18.0, CH <sub>3</sub>
<b>OMe</b>			3.63, s	52.9, CH <sub>3</sub>		

<b>OBu 1'</b>	4.04, t (6.6)	65.4, CH <sub>2</sub>
<b>OBu 2'</b>	1.39, m	20.2, CH <sub>2</sub>
<b>OBu 3'</b>	1.59, m	31.8, CH <sub>2</sub>
<b>OBu 4'</b>	0.95, t (7.2)	14.1, CH <sub>3</sub>

<sup>a</sup> Recorded in piridine-*d*<sub>5</sub> and at 500 MHz; <sup>b</sup> Recorded in methanol-*d*<sub>4</sub> and at 500 MHz; <sup>c</sup> Recorded in methanol-*d*<sub>4</sub> and at 600 MHz.

**Table 7.** NMR spectroscopic data for compounds **14–16**.

	<b>14<sup>a</sup></b>		<b>15<sup>b</sup></b>		<b>16<sup>a</sup></b>	
	$\delta_{\text{H}}$ ( <i>J</i> in Hz)	$\delta_{\text{C}}$	$\delta_{\text{H}}$ ( <i>J</i> in Hz)	$\delta_{\text{C}}$	$\delta_{\text{H}}$ ( <i>J</i> in Hz)	$\delta_{\text{C}}$
<b>1</b>	2.46, m	35.2, CH <sub>2</sub>	2.33, m	35.4, CH <sub>2</sub>	2.10, m	34.8, CH <sub>2</sub>
	1.52, m		1.65, m		1.57, m	
<b>2</b>	2.58, m	29.8, CH <sub>2</sub>	2.54, m	30.2, CH <sub>2</sub>	2.40, m	30.6, CH <sub>2</sub>
	2.17, m		2.18, m		2.09, m	
<b>3</b>		175.2, C		176.7, C		174.9, C
<b>4</b>		75.4, C		76.0, C		148.3, C
<b>5</b>	1.41, dd (11.0, 3.0)	52.3, CH	1.39, overlap	53.1, CH	2.07, overlap	50.8, CH
<b>6</b>	1.55, m	23.1, CH <sub>2</sub>	1.50, m	23.2, CH <sub>2</sub>	1.69, m	25.3, CH <sub>2</sub>
	1.49, m		1.47, m		1.38, m	
<b>7</b>	1.60, m	33.2, CH <sub>2</sub>	1.61, m	32.9, CH <sub>2</sub>	1.55, m	32.4, CH <sub>2</sub>
	1.52, m		1.39, m		1.26, m	
<b>8</b>		40.5, C		40.9, C		40.3, C
<b>9</b>	1.81, dd (10.5, 6.5)	39.0, CH	1.78, dd (10.4, 6.0)	39.5, C	1.82, dd (10.8, 6.2)	37.9, CH
<b>10</b>		41.9, C		42.2, C		39.9, C
<b>11</b>	2.03, overlap	24.1, CH <sub>2</sub>	2.06, m	24.4, CH <sub>2</sub>	2.10, overlap	24.0, CH <sub>2</sub>
	2.01, overlap		1.95, dt (15.8, 4.8)		1.94, dt (14.8, 4.2)	
<b>12</b>	5.43, t (3.5)	124.9, CH	5.45, t (3.6)	125.7, CH	5.42, t (3.5)	124.4, CH
<b>13</b>		142.6, C		142.5, C		143.0, C
<b>14</b>		49.2, C		49.8, C		49.1, C
<b>15</b>	3.29, d (13.2)	43.2, CH <sub>2</sub>	3.33, d (13.2)	43.8, CH <sub>2</sub>	3.30, d (13.1)	43.3, CH <sub>2</sub>
	1.62, d (13.2)		1.67, d (13.2)		1.63, d (13.1)	
<b>16</b>		213.9, C		216.7, C		213.9, C
<b>17</b>		77.2, C		77.7, C		77.1, C
<b>18</b>	2.82, dd (14.0, 4.0)	52.6, CH	2.82, dd (14.4, 3.6)	52.6, CH	2.83, dd (14.0, 4.0)	52.6, CH
<b>19</b>	1.49, overlap	43.3, CH <sub>2</sub>	1.46, overlap	43.4, CH <sub>2</sub>	1.45, overlap	43.2, CH <sub>2</sub>
	1.27, overlap		1.26, overlap		1.21, overlap	
<b>20</b>		36.6, C		36.9, C		36.6, C
<b>21</b>	1.62, m	32.2, CH <sub>2</sub>	1.61, overlap	32.4, CH <sub>2</sub>	1.58, m	32.2, CH <sub>2</sub>
	1.50, m		1.57, overlap		1.52, m	
<b>22</b>	1.50, m	30.8, CH <sub>2</sub>	1.41, overlap	30.9, CH <sub>2</sub>	1.51, m	30.8, CH <sub>2</sub>
	1.48, m		1.35, overlap		1.48, m	
<b>23</b>	1.29, s	34.1, CH <sub>3</sub>	1.27, s	33.5, CH <sub>3</sub>	4.89, br s	114.0, CH <sub>2</sub>
					4.74, br s	
<b>24</b>	1.24, s	28.1, CH <sub>3</sub>	1.26, s	28.4, CH <sub>3</sub>	1.78, br s	24.4, CH <sub>3</sub>
<b>25</b>	1.15, s	20.3, CH <sub>3</sub>	1.13, s	20.4, CH <sub>3</sub>	0.98, s	19.8, CH <sub>3</sub>
<b>26</b>	1.14, s	17.9, CH <sub>3</sub>	1.15, s	18.0, CH <sub>3</sub>	1.18, s	17.9, CH <sub>3</sub>
<b>27</b>	1.16, s	26.8, CH <sub>3</sub>	1.17, s	26.9, CH <sub>3</sub>	1.19, s	27.1, CH <sub>3</sub>
<b>29</b>	3.16, br s	73.9, CH <sub>2</sub>	3.16, d (10.8)	74.2, CH <sub>2</sub>	3.17, d (10.0)	73.8, CH <sub>2</sub>
			3.13, d (10.8)		3.14, d (10.0)	
<b>30</b>	0.96, s	19.4, CH <sub>3</sub>	0.97, s	19.3, CH <sub>3</sub>	0.96, s	19.4, CH <sub>3</sub>

<b>OH-4</b>	3.22, br s			
<b>OH-17</b>	4.28, br s			
<b>OMe</b>	3.57, s	51.4, CH <sub>3</sub>		
<b>OBu 1'</b>			4.04, t (6.6)	65.4, CH <sub>2</sub>
<b>OBu 2'</b>			1.39, m	20.2, CH <sub>2</sub>
<b>OBu 3'</b>			1.59, m	31.8, CH <sub>2</sub>
<b>OBu 4'</b>			0.95, t (7.8)	14.1, CH <sub>3</sub>

---

<sup>a</sup> Recorded in acetone-*d*<sub>6</sub> and at 500 MHz; <sup>b</sup> Recorded in methanol-*d*<sub>4</sub> and at 600 MHz

## 2.5. Cytotoxicity assay

SH-SY5Y cells (human dopaminergic neuroblastoma cell line) were cultured in Dulbecco's Modified Eagle's Medium (DMEM) and Ham's F12 Nutrient Mixture (F12) (1:1, v:v) supplemented with 10% fetal bovine serum (FBS) (Gibco, NY, USA), 100 U/mL penicillin and 100 µg/mL streptomycin and incubated at 37°C under 5% CO<sub>2</sub>. The cytotoxicity assay was performed by staining with (3-(4,5-dimethyl-2-thiazolyl)-2,5-diphenyl-2H-tetrazolium bromide (MTT) to measure cell viability. Briefly, Cells were seeded onto 48-well plates and grown to 70-80% confluence. Subsequently, the cells were pretreated with various concentrations of compounds **11–16** dissolved in low-serum medium supplemented with 5% FBS for 24 h, and then 2.5 µM rotenone was added to the cells for 12 h. Then, 40 µL of a 2 mg/mL MTT solution was added to each well and incubated for 4 h at 37°C in the dark. After discarding the medium, 250 µL of DMSO was added to each well to dissolve the MTT formazan crystals. The absorbance was measured at 550 nm using an absorbance microplate reader (VersaMax<sup>TM</sup>, Randor, PA, USA).

## 2.6. Quantitative real-time PCR

Cells were seeded onto a 6-well plate and incubated for 1-2 days. When the cell confluence reached approximately 70-80%, the growth medium was replaced with low-serum medium in the presence of various concentrations of compound **15**. After 24 h, the cells were treated with 2.5  $\mu$ M rotenone and incubated for 12 h. Total RNA was isolated from the cells using the TRIzol method. The total RNA was reverse transcribed using random primer (iNtRON Biotechnology, INC, Korea) according to the manufacturer's instruction. Real-time PCR was performed using selective primers for  $\alpha$ -synuclein (forward: 5'-AAG GAC CAG TTG GGC AAG AA-3', reverse: 5'-CCA CAG GCA TAT CTT CCA GAA TTC-3') and 18S ribosomal RNA (forward: 5'-GCT TAA TTT GAC TCA ACA CGG GA-3', reverse: 5'-AGC TAT CAA TCT GTC AAT CCT GTC-3') and conducted using 2  $\mu$ L of cDNA and Maxima SYBR Green qPCR master mix 2X (Thermo sci., Rockford, IL, USA). The cycling conditions for real-time PCR were as follows: 95°C for 10 min, followed by 40 cycles of 95°C for 15 s and 60°C for 1 min. Real-time PCR was conducted using a StepOnePlus Real-Time PCR System (Applied Biosystems). The data were analyzed using StepOne software v2.3.

## 2.7. Western blot analysis

The cultures were prepared using methods similar to those for quantitative real-time PCR. After 12 h, the cells were washed with cold PBS and stored at -80°C. For whole cell lysate, the cells were lysed on ice in 100  $\mu$ L lysis buffer [50 mM Tris-HCl (pH 7.6), 120 mM NaCl, 1 mM EDTA, 0.5% NP-40, and 50 mM NaF] and centrifuged at  $14,000 \times g$  for 20 min. Supernatants were collected from the lysates, and protein concentrations were determined using a protein assay kit (Bio-Rad Laboratories, Inc., CA, USA). Aliquots of lysates were boiled for 5 min and electrophoresed on 15% SDS-polyacrylamide gels. Protein in the gels were electronically transferred to nitrocellulose membranes (PVDF 0.45  $\mu$ m, Immobilon-P, USA). The membranes were then incubated with primary antibodies  $\alpha$ -synuclein (SC-12767, Santa Cruz Biotechnology, INC.) or mouse monoclonal actin antibody. The membranes were further incubated with secondary antibodies. Finally, they were detected using an enhanced chemiluminescence western blot detection kit (Thermo sci., Rockford, IL, USA) and quantified by LAS 4000 luminescent image analyzer (Fuji Film, Tokyo, Japan).

## 2.8. Measurement of intracellular ROS levels

The fluorescent probe 2',7'- dichlorofluorescein diacetate (DCFDA), a well-known ROS indicator, was used to monitor intracellular ROS production in SH-SY5Y cells. Briefly, SH-SY5Y cells were seeded onto 96-well plates and grown to 70-80%

confluence. Then, the growth medium was replaced with low-serum medium supplemented with 5% of FBS in the presence or absence of various concentrations of compound **15**. After 24 h of incubation, the cells were treated with 2.5  $\mu$ M rotenone and incubated for 12 h at 37°C. The cells were then incubated with 20  $\mu$ M of DCFH-DA (D6883, Sigma-Aldrich, St. Louis, MO, USA) for 30 min at 37°C in PBS supplemented with 0.5% FBS and then washed twice with PBS. The fluorescence intensity of the cells were monitored using a fluorescence microplate reader (Spectra Max GEMINI XPS, Molecular Devices, Sunnyvale, CA, USA) with excitation at 488 nm and emission at 530 nm.

## 2.9. Confocal immunostaining

HEK293 cells were grown in DMEM supplemented with 10% FBS (Gibco, Grand Island, NY, USA). A HEK293 stable cell line expressing GFP-LC3 was generated as described previously (LeBel et al., 1992) using a GFP-LC3 plasmid provided by T. Yoshimori (Yoon et al., 2012). For immunostaining, cells were grown on sterilized glass coverslips. After drug treatment, the cells were fixed with 4% paraformaldehyde. The slides were stained with 1  $\mu$ g/mL 4',6-diamidino-2-phenylindole (DAPI) and mounted in mounting medium (Vector, Burlingame, CA, USA). Images were captured using a Carl Zeiss LSM710 confocal microscope (Carl Zeiss, Oberkochen, Germany).

## 2.10. Statistical analysis

Statistical calculations were examined by analysis of variance (ANOVA), followed by Tukey's range test, conducting in SPSS Statistics 20 (SPSS, Inc., Chicago, IL, USA). The results are presented as the means  $\pm$  SD of two to three independent

experiments (\*  $p < 0.05$ , \*\*  $p < 0.01$ , and \*\*\*  $p < 0.001$  compared to the rotenone treatment).

### 3. Results and discussion

#### 3.1. Structural elucidation of isolated compounds (11–16)

##### 3.1.1. Compound **11**

Compound **11** was isolated as a white amorphous powder with  $[\alpha]_D^{25} -20.6$  ( $c$  0.1, MeOH). Its molecular formula was assigned as  $C_{29}H_{46}O_7$ , as determined from the HRESIMS peak at  $m/z$  529.3140  $[M + Na]^+$  (calcd 529.3136), which suggested seven degrees of unsaturation. The IR absorptions indicated the existence of hydroxy ( $3390\text{ cm}^{-1}$ ), carbonyl ( $1710\text{ cm}^{-1}$ ), and olefin ( $1624\text{ cm}^{-1}$ ) functionalities. The  $^1\text{H}$  and  $^{13}\text{C}$  NMR data (Table 6) showed one oxygenated methene ( $\delta_H$  3.60, 2H, s;  $\delta_C$  74.1 ( $\text{CH}_2$ )), one oxymethine group ( $\delta_H$  4.19, 1H, dd,  $J = 11.0, 4.5\text{ Hz}$ ;  $\delta_C$  72.9 (CH)), two oxygenated quaternary carbons ( $\delta_C$  77.1 (C) and 74.8 (C)), one trisubstituted double bond ( $\delta_H$  5.69, 1H, t,  $J = 3.5\text{ Hz}$ ;  $\delta_C$  142.6 (C) and 125.4 (CH)), one ketone group ( $\delta_C$  216.6 (C)), and one carboxylic carbon signal ( $\delta_C$  177.5 (C)). Moreover, there were 6 carbon signals in the  $^{13}\text{C}$  NMR spectrum assigned to methyl signals, which correspond to the  $^1\text{H}$  NMR peaks at  $\delta_H$  1.68, 1.55, 1.50, 1.48, 1.34, and 1.25 (all s, each 3H) (Figure 60). The above results indicated that compound **11** was a 3,4-*seco*-28-nor-oleanane triterpene (Uddin et al., 2014). Compared with camelliaolean B (Uddin et al., 2014), there were no methoxyl



signals in the NMR spectra of compound **11** (Table 6), which indicated that a carboxylic group should be connected to C-2 in compound **11**. This proposal was also confirmed by HMBC correlations from H<sub>2</sub>-1 ( $\delta_{\text{H}}$  3.05, 2.21) and H<sub>2</sub>-2 ( $\delta_{\text{H}}$  3.06, 2.66) to C-3 ( $\delta_{\text{C}}$  177.5 (C)). In addition, the existence of one oxygenated methene group ( $\delta_{\text{H}}$  3.60, 2H, s;  $\delta_{\text{C}}$  74.1 (CH<sub>2</sub>)) in compound **11**, together with the molecular formula, indicated the presence of one additional hydroxy group, which was bonded to C-29 ( $\delta_{\text{C}}$  74.1 (CH<sub>2</sub>)) on the basis of HMBC correlations from H<sub>2</sub>-29 ( $\delta_{\text{H}}$  3.60) and H<sub>3</sub>-30 ( $\delta_{\text{H}}$  1.25) to C-19 ( $\delta_{\text{C}}$  43.6), C-20 ( $\delta_{\text{C}}$  37.1), and C-21 ( $\delta_{\text{C}}$  32.7), as well as ROESY correlations from H-18 ( $\delta_{\text{H}}$  3.30) to H<sub>3</sub>-30 ( $\delta_{\text{H}}$  1.25). The assignments of the other functionalities were determined based on HMBC and ROESY experiments (Figures 61 and 62). The ROESY correlations from H-7 ( $\delta_{\text{H}}$  4.19) to H-5 ( $\delta_{\text{H}}$  1.94) and H-27 ( $\delta_{\text{H}}$  1.55), together with the coupling patterns of H-5 (dd,  $J$  = 10.0, 3.1 Hz) and H-7 (dd,  $J$  = 11.0, 4.5 Hz), determined the  $\alpha$ -orientation of H-5 and  $\beta$ -orientation of OH-7. The chemical shifts of C-16, C-17, C-18, and C-22 ( $\delta_{\text{C-16}}$  215.3,  $\delta_{\text{C-17}}$  76.0,  $\delta_{\text{C-18}}$  52.2, and  $\delta_{\text{C-22}}$  30.3 in CDCl<sub>3</sub>), which were similar to those of camelliaolean B ( $\delta_{\text{C-16}}$  215.1,  $\delta_{\text{C-17}}$  76.3,  $\delta_{\text{C-18}}$  52.5, and  $\delta_{\text{C-22}}$  30.1 in CDCl<sub>3</sub>) (Uddin et al., 2014), were used to determine the  $\beta$ -orientation of OH-17. Finally, compound **11** was elucidated as 4,7 $\beta$ ,17 $\beta$ ,29-tetrahydroxy-16-oxo-3,4-*seco*-28-nor-olean-12-en-3-oic acid.

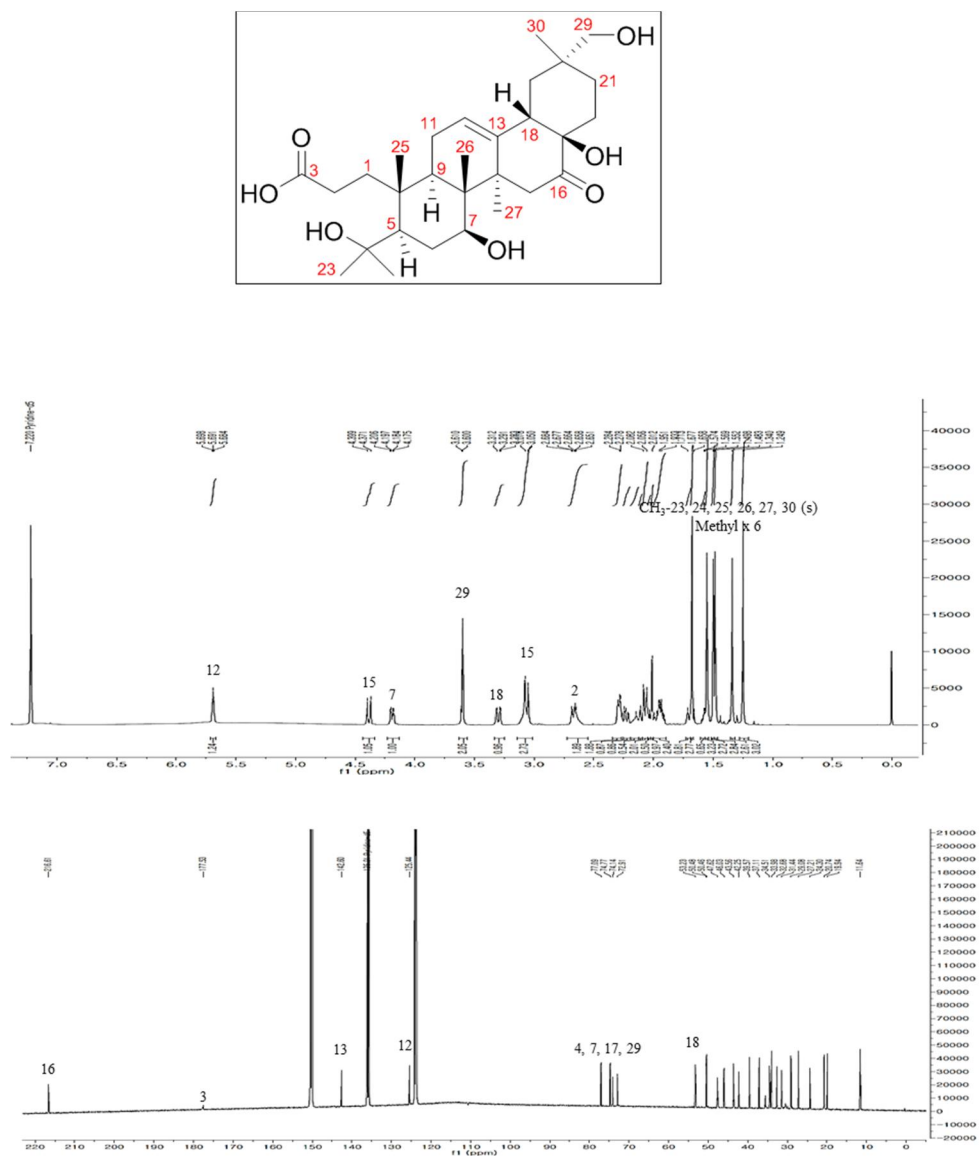


**Figure 60.**  $^1\text{H}$  and  $^{13}\text{C}$  NMR of compound **11** (Pyridine- $d_5$ , 500 MHz/125 MHz).

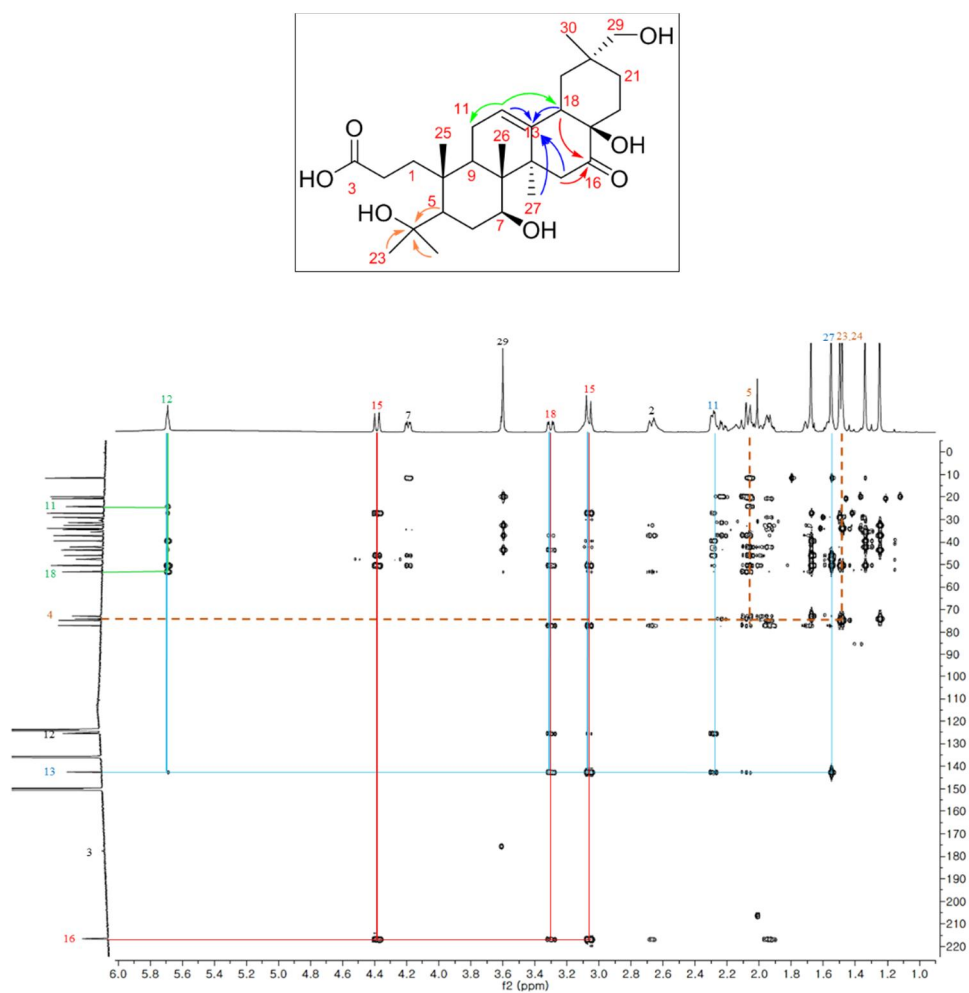


**Figure 61.** HMBC of compound **11** (Pyridine- $d_5$ , 500 MHz).

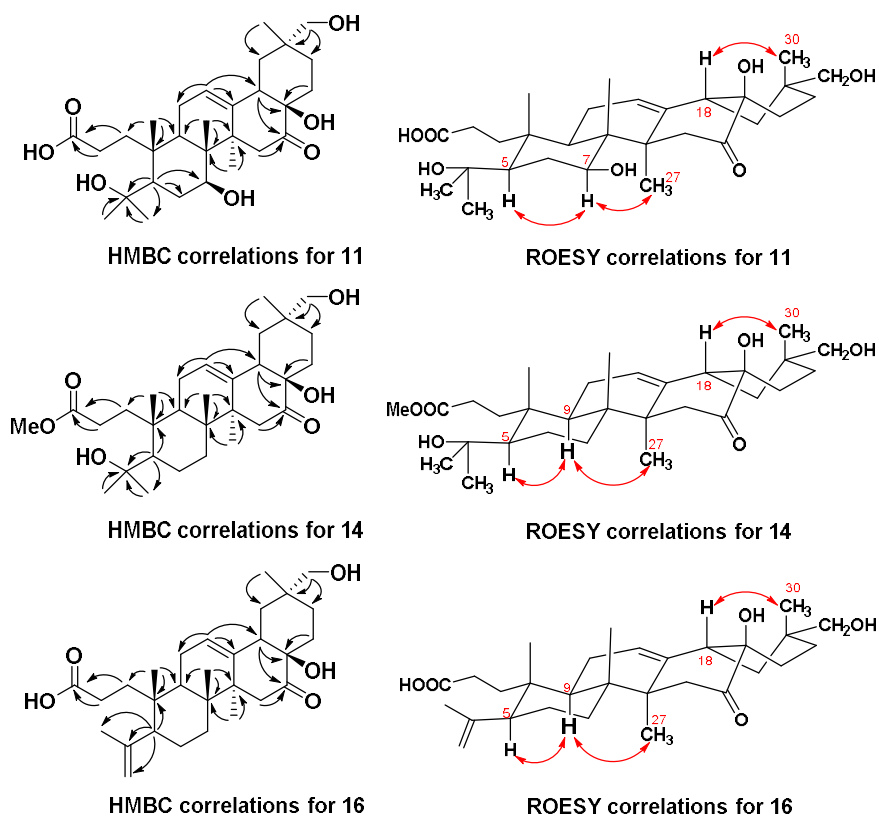


**Figure 62.** Key HMBC (H→C) and ROESY correlations for compounds **11**, **14**, and **16**.

### 3.1.2. Compound **12**

Compound **12**, a white amorphous powder with  $[\alpha]_D^{25} -24.1$  ( $c$  0.1, MeOH), was assigned a molecular formula of  $C_{30}H_{48}O_7$  based on a quasi-molecular ion at  $m/z$  1063.6682  $[2M + Na]^+$  (calcd 1063.6692) in the positive HRESIMS, which indicated seven degrees of unsaturation. The IR spectrum of **12** showed peaks that are characteristic of hydroxy ( $3394\text{ cm}^{-1}$ ), carbonyl ( $1715\text{ cm}^{-1}$ ), and olefin ( $1631\text{ cm}^{-1}$ ) functionalities. With similar NMR patterns as found in compound **11**, the  $^1\text{H}$  and  $^{13}\text{C}$  NMR data of compound **12** (Table 6) showed one oxygenated methene ( $\delta_{\text{H}}$  3.16 (1H, d,  $J = 11.0\text{ Hz}$ ), 3.13 (1H, d,  $J = 11.0\text{ Hz}$ );  $\delta_{\text{C}}$  74.2 ( $\text{CH}_2$ )), one oxymethine group ( $\delta_{\text{H}}$  3.74, 1H, dd,  $J = 11.3, 4.1\text{ Hz}$ ;  $\delta_{\text{C}}$  73.4 (CH)), two oxygenated quaternary carbons ( $\delta_{\text{C}}$  77.4 (C) and 75.5 (C)), one trisubstituted double bond ( $\delta_{\text{H}}$  5.51, 1H, t,  $J = 3.0\text{ Hz}$ ;  $\delta_{\text{C}}$  141.9 (C) and 126.2 (CH)), and one ketone carbon signal ( $\delta_{\text{C}}$  217.6 (C)) (Figure 63). An obvious difference was that compound **12** possessed one methoxyl group ( $\delta_{\text{H}}$  3.63 (3H, s);  $\delta_{\text{C}}$  52.9 ( $\text{CH}_3$ )), which was connected to C-3 based on an HMBC correlation from the proton at  $\delta_{\text{H}}$  3.63 (3H, s) to C-3 ( $\delta_{\text{C}}$  176.9). Similar to compound **11**, the  $\alpha$ -orientation of H-5 and  $\beta$ -orientation of OH-7 was determined from the coupling patterns of H-5 (dd,  $J = 11.3, 3.0\text{ Hz}$ ) and H-7 (dd,  $J = 11.3, 4.1\text{ Hz}$ ) and from ROESY correlations from H-7 ( $\delta_{\text{H}}$  3.74) to H-5 ( $\delta_{\text{H}}$  1.53) and H-27 ( $\delta_{\text{H}}$  1.23). The ROESY correlations from H-18 ( $\delta_{\text{H}}$  2.80) to H<sub>3</sub>-30 ( $\delta_{\text{H}}$  0.96) supported the hydroxylation of Me-29. The chemical shifts of C-16, C-17, C-18, and C-22 ( $\delta_{\text{C-16}}$  215.5,  $\delta_{\text{C-17}}$  76.9,  $\delta_{\text{C-18}}$  51.9, and  $\delta_{\text{C-22}}$  30.2 in  $\text{CDCl}_3$ ), which were similar to those of camelliaolean B ( $\delta_{\text{C-16}}$

215.1,  $\delta_{C-17}$  76.3,  $\delta_{C-18}$  52.5, and  $\delta_{C-22}$  30.1 in  $CDCl_3$ ) (Uddin et al., 2014), were used to determine the  $\beta$ -orientation of OH-17 (Figure 64). Therefore, compound **12** was determined to be 4,7 $\beta$ ,17 $\beta$ ,29-tetrahydroxy-16-oxo-3,4-*seco*-28-nor-olean-12-en-3-oic acid methyl ester.

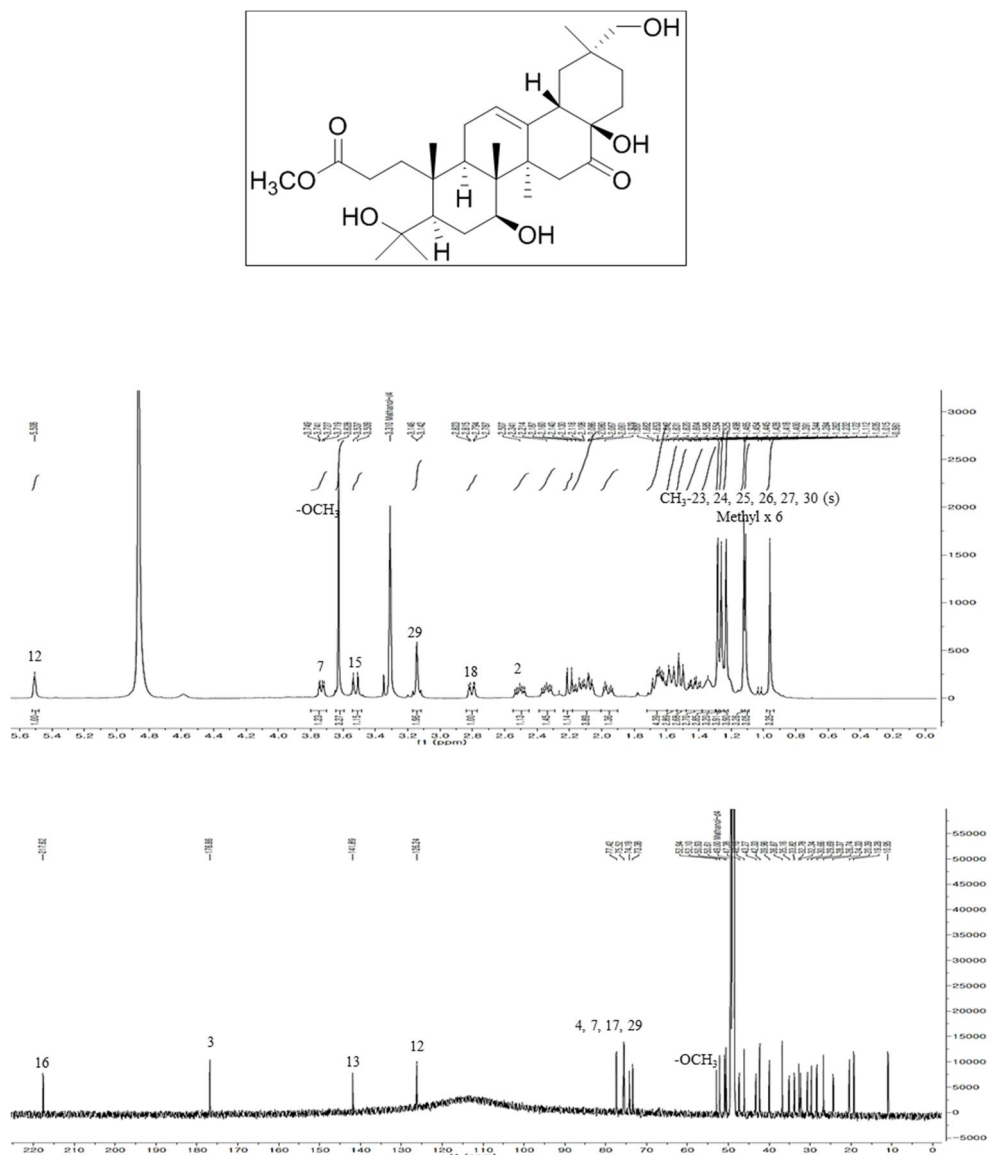


**Figure 63.**  $^1H$  and  $^{13}C$  NMR of compound **12** (methanol- $d_4$ , 500 MHz/125 MHz).

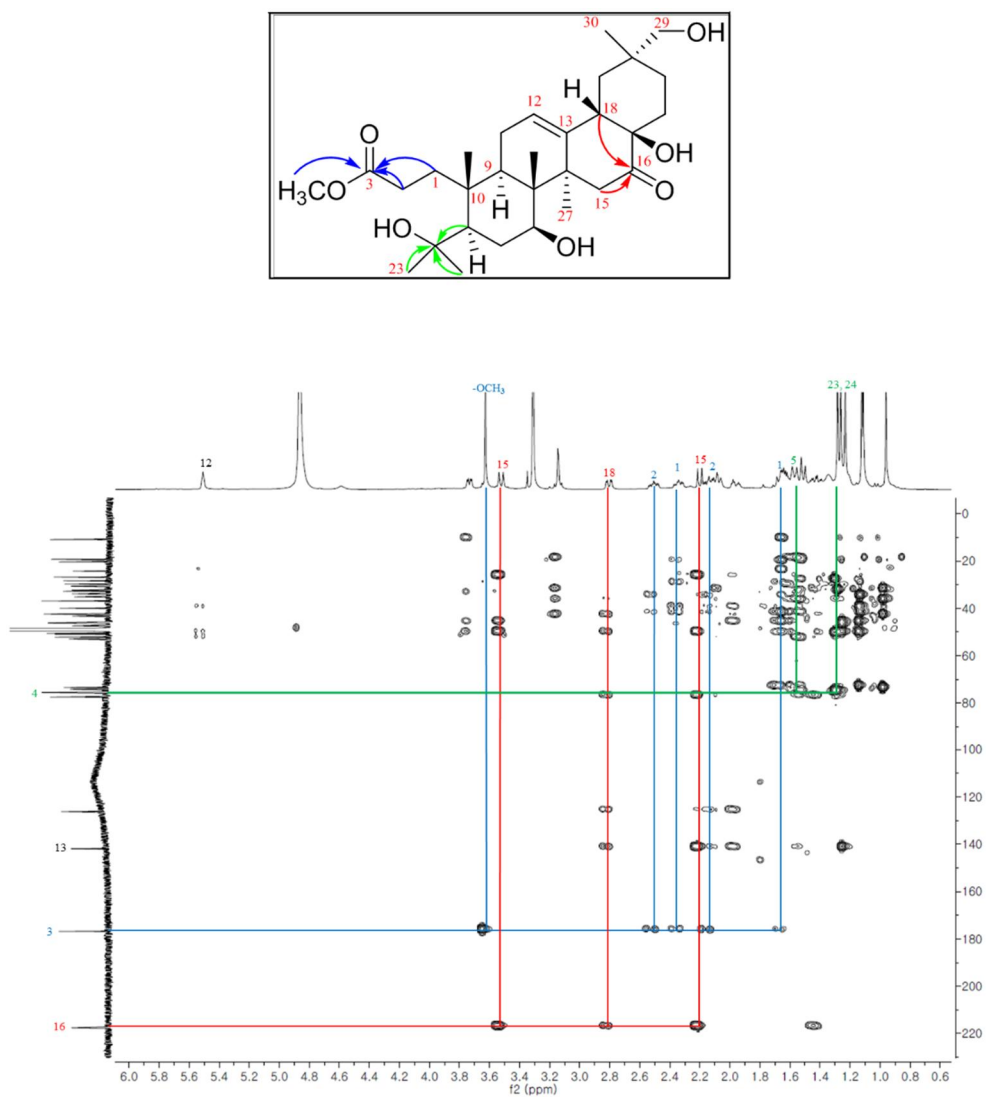


**Figure 64.** HMBC of compound **12** (methanol- $d_4$ , 500 MHz).

### 3.1.3. Compound **13**

Compound **13** was obtained as a white amorphous powder with  $[\alpha]_D^{25} -26.4$  (*c* 0.1, MeOH), and its molecular formula was determined to be  $C_{33}H_{54}O_6$  based on a positive HRESIMS ion at  $m/z$  569.3819  $[M + Na]^+$  (calcd 569.3813). The IR absorptions at 3420, 1714, and  $1642\text{ cm}^{-1}$  were characteristic of hydroxy, carbonyl, and olefin functionalities, respectively. The  $^1\text{H}$  and  $^{13}\text{C}$  NMR data of compound **13** (Table 6) were very similar to those of compounds **11** and **12**. The primary differences were the disappearance of the hydroxylation at Me-29 and the presence of an oxygenated *n*-butyl in compound **13** ( $\delta_{\text{H}}$  4.04 (2H, t,  $J = 6.6$  Hz), 1.59 (2H, m), 1.39 (2H, m), 0.95 (3H, t,  $J = 7.2$  Hz);  $\delta_{\text{C}}$  65.4 ( $\text{CH}_2$ ), 31.8 ( $\text{CH}_2$ ), 20.2 ( $\text{CH}_2$ ), and 14.1 ( $\text{CH}_3$ )) (Figure 65). An HMBC experiment revealed that this oxygenated *n*-butyl group was connected to C-3 based on the correlation of  $\text{H}_2\text{-1'}$  ( $\delta_{\text{H}}$  4.04 (2H, t,  $J = 6.6$  Hz) to C-3 ( $\delta_{\text{C}}$  176.8). Other functionalities were also determined as analyzed by HMBC correlations. Following the same procedure as for compounds **11** and **12**, the orientation of both H-5 and H-7 was deduced from the coupling patterns of H-5 (dd,  $J = 10.8, 3.2$  Hz) and H-7 (dd,  $J = 12.0, 4.8$  Hz) and from ROESY correlations between H-7 ( $\delta_{\text{H}}$  3.59) to H-5 ( $\delta_{\text{H}}$  1.42) and H-27 ( $\delta_{\text{H}}$  1.13). The similarity of the chemical shifts of C-16, C-17, C-18, and C-22 in compound **13** and camelliaolean B was used to determine the  $\beta$ -orientation of OH-17 (Figure 66). Thus, compound **13** was identified as 4,7 $\beta$ ,17 $\beta$ -trihydroxy-16-oxo-3,4-*seco*-28-nor-olean-12-en-3-oic acid *n*-butyl ester.



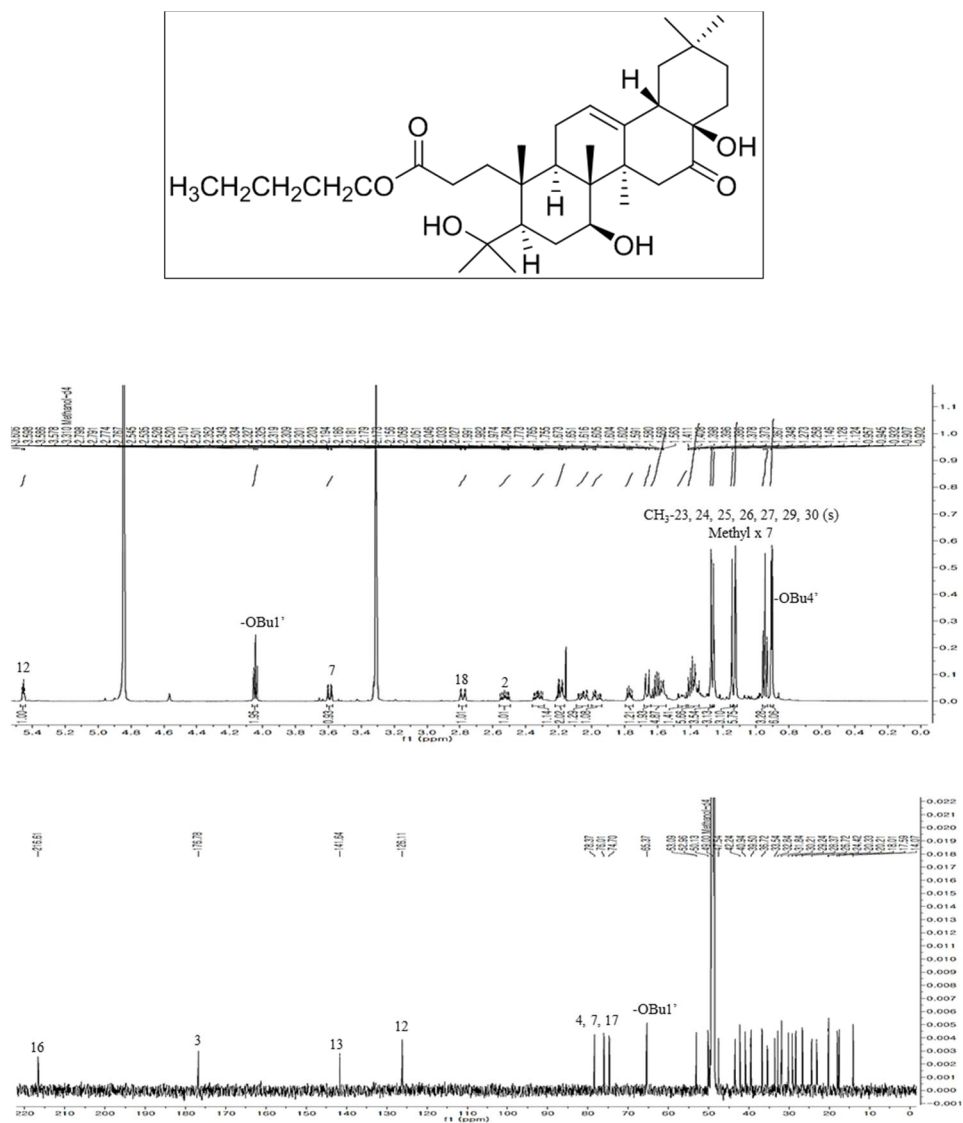


**Figure 65.**  $^1\text{H}$  and  $^{13}\text{C}$  NMR of compound **13** (methanol- $d_4$ , 600 MHz/150 MHz).

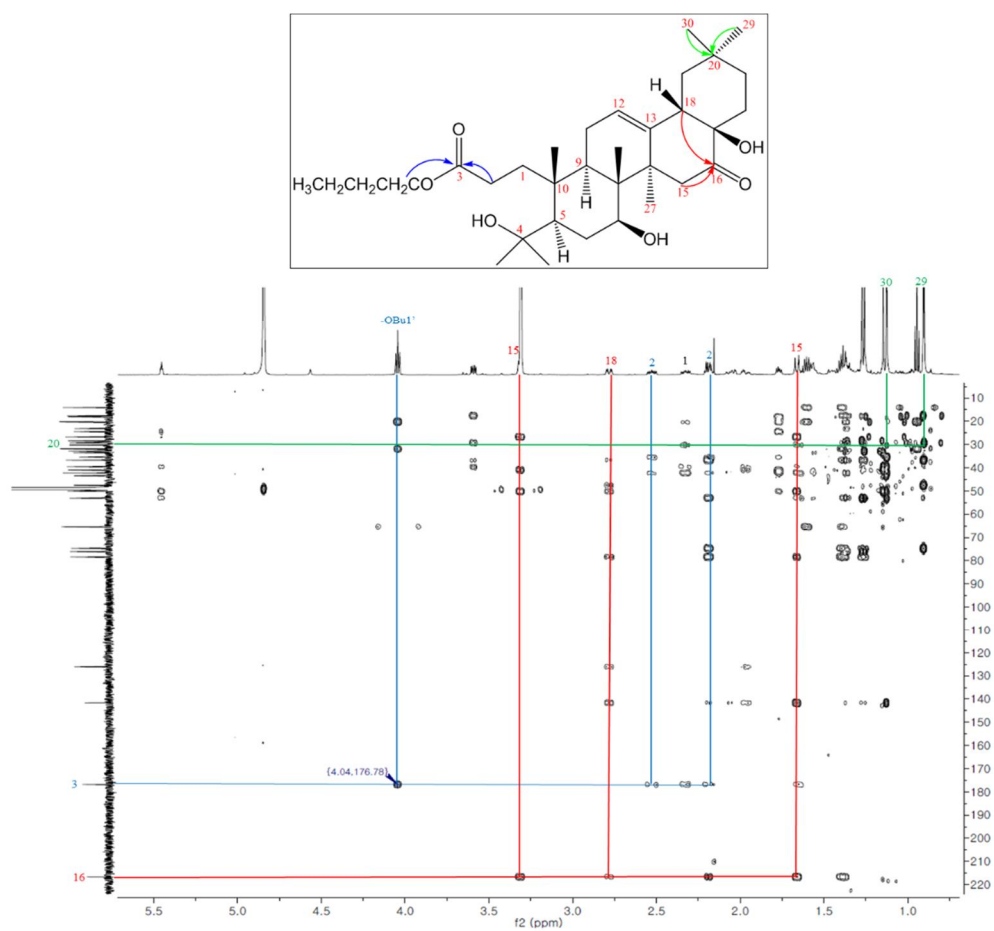
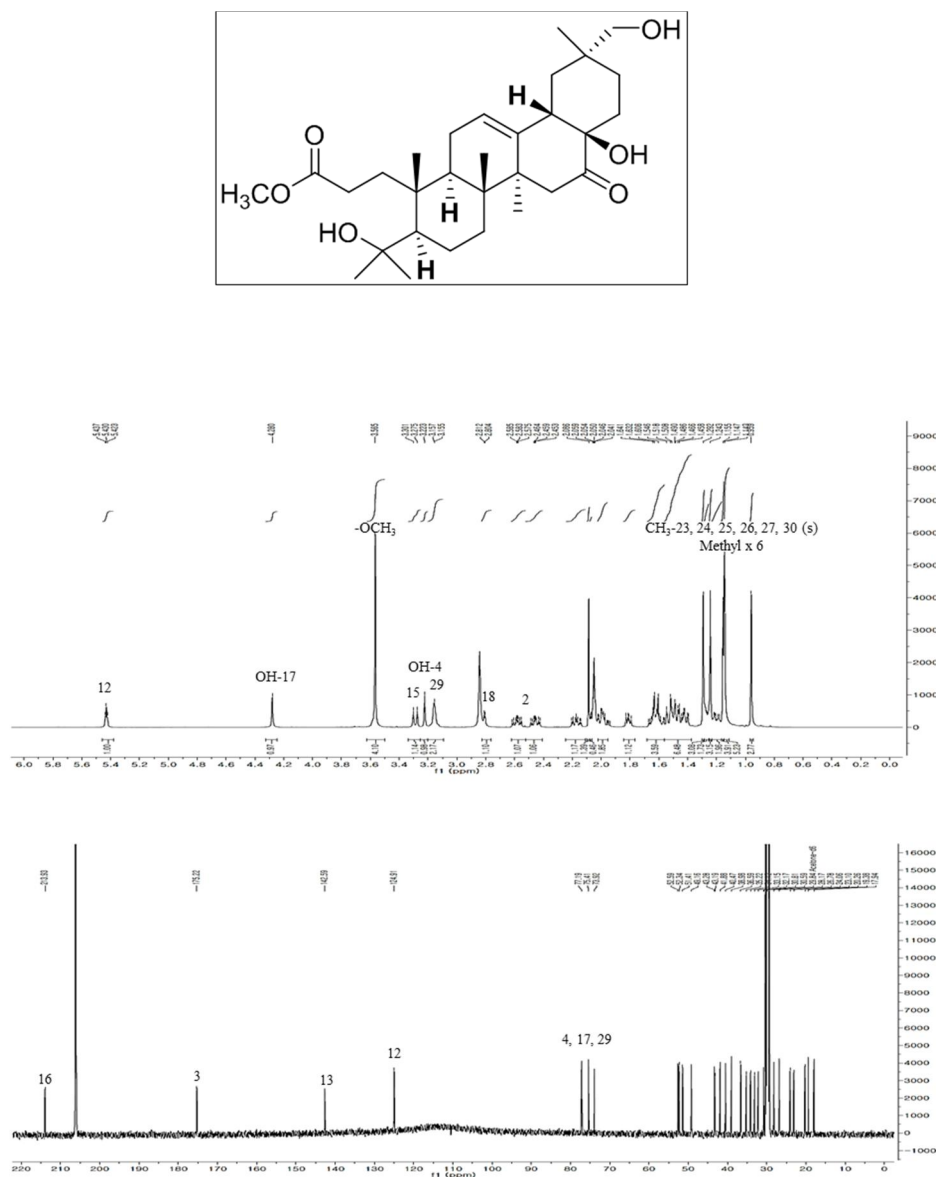


Figure 66. HMBC of compound **13** (methanol- $d_4$ , 600 MHz).

### 3.1.4. Compound **14**

Compound **14**, a white amorphous powder with  $[\alpha]_D^{25} -34.8$  ( $c$  0.1, MeOH), possessed a molecular formula of  $C_{30}H_{48}O_6$ , as suggested by HRESIMS peaks at  $m/z$  487.3423  $[M - H_2O + H]^+$  (calcd 487.3423) and 469.3317  $[M - 2H_2O + H]^+$  (calcd 469.3318). The IR spectrum of compound **14** presented absorptions that are characteristic of hydroxy ( $3442\text{ cm}^{-1}$ ), carbonyl ( $1715\text{ cm}^{-1}$ ), and olefin ( $1665\text{ cm}^{-1}$ ) functionalities. Its  $^1H$  and  $^{13}C$  NMR data (Table 7) showed an oxymethene ( $\delta_H$  3.16, brs;  $\delta_C$  73.9 ( $CH_2$ )), two oxygenated quaternary carbons ( $\delta_C$  77.2, 75.4), one trisubstituted double bond signal ( $\delta_H$  5.43, t,  $J = 3.5\text{ Hz}$ ;  $\delta_C$  142.6, 124.9), and two carbonyl carbons ( $\delta_C$  213.9, 175.2) (Figure 67). These observations indicated that compound **14** shared a similar structure with compound **12**. The only difference was the disappearance of the oxymethine signals ( $\delta_H$  3.74, 1H, dd,  $J = 11.3, 4.1\text{ Hz}$ ;  $\delta_C$  73.4 ( $CH$ )) in compound **12**, suggesting the absence of OH-7 in compound **14**. Other functionalities were determined based on HSQC and HMBC experiments. The relative configuration of compound **14** was determined through a ROESY experiment and comparison of NMR data with analogues. The ROESY correlations from H-18 ( $\delta_H$  2.82) to H<sub>3</sub>-30 ( $\delta_H$  0.96) indicated the attachment of one hydroxy group to C-29 ( $\delta_C$  73.9 ( $CH_2$ )). The  $\beta$ -orientation of OH-17 was supported by the similarity of the chemical shifts of C-16, C-17, C-18, and C-22 ( $\delta_{C-16}$  215.0,  $\delta_{C-17}$  76.1,  $\delta_{C-18}$  52.3, and  $\delta_{C-22}$  30.2 in  $CDCl_3$ ) of compound **14** and those of camelliaolean B ( $\delta_{C-16}$  215.1,  $\delta_{C-17}$  76.3,  $\delta_{C-18}$  52.5, and  $\delta_{C-22}$  30.1 in  $CDCl_3$ ) (Uddin et al., 2014). The similar chemical shifts of C-4/5/6/10 in compound **14** ( $\delta_C$  75.4/52.3/23.1/41.9 in acetone- $d_6$ ) and camelliaolean A ( $\delta_C$  75.4/52.4/23.2/41.8 in

acetone- $d_6$ ) (Uddin et al., 2014) were used to determined H-5 as  $\alpha$ -oriented, which was also supported by the coupling pattern of H-5 (dd,  $J = 11.0, 3.0$  Hz) and the ROESY correlations from H-9 ( $\delta_H$  1.81) to H-5 ( $\delta_H$  1.41) and H<sub>3</sub>-27 ( $\delta_H$  1.16) (Figures 62 and 68). Thus, compound **14** was determined to be 4,17 $\beta$ ,29-trihydroxy-16-oxo-3,4-*seco*-28-nor-olean-12-en-3-oic acid methyl ester.



**Figure 67.**  $^1H$  and  $^{13}C$  NMR of compound **14** (acetone- $d_6$ , 500 MHz/125 MHz).

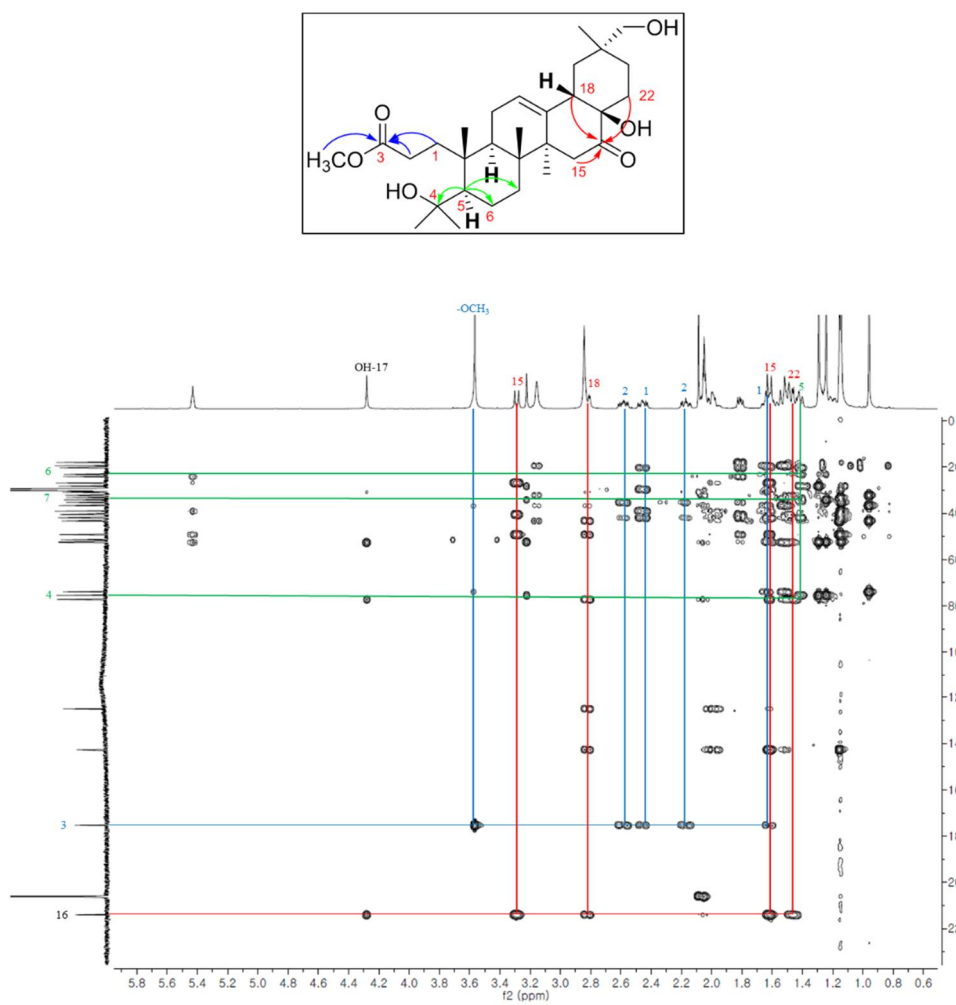


**Figure 68.** HMBC of compound **14** (acetone- $d_6$ , 500 MHz).

### 3.1.5. Compound **15**

Compound **15** was obtained as a white amorphous powder with  $[\alpha]_D^{25} -27.2$  (*c* 0.1, MeOH) and was assigned a molecular formula of  $C_{33}H_{54}O_6$  on the basis of a positive HRESIMS peak at  $m/z$  529.3880  $[M - H_2O + H]^+$  (calcd 529.3893). The IR peaks at 3394, 1730, and 1614  $cm^{-1}$  suggested the presence of hydroxy, carbonyl, and olefin functionalities, respectively. Compound **15** shared a similar NMR pattern (Table 7) with compound **14**. The characteristic difference is the replacement of the methoxyl group in **14** ( $\delta_H$  3.57, s;  $\delta_C$  51.4 (CH<sub>3</sub>)) by an oxygenated *n*-butyl group in **15** ( $\delta_H$  4.04, 2H, t,  $J = 6.6$  Hz), 1.59 (2H, m), 1.39 (2H, m), 0.95 (3H, t,  $J = 7.8$  Hz);  $\delta_C$  65.4 (CH<sub>2</sub>), 31.8 (CH<sub>2</sub>), 20.2 (CH<sub>2</sub>), and 14.1 (CH<sub>3</sub>)), indicating *n*-butyl esterification of the carboxylic group at C-3 (Figure 69). This proposal was further supported by the HMBC correlation from H<sub>2</sub>-1' ( $\delta_H$  4.04) to C-3 ( $\delta_C$  176.7). Following the same procedure as compound **14**, other functionalities and the relative configuration of **15** were determined via by HSQC and HMBC experiments. The ROESY correlations from H-9 ( $\delta_H$  1.78) to H-5 ( $\delta_H$  1.39) and H<sub>3</sub>-27 ( $\delta_H$  1.17) and from H-18 ( $\delta_H$  2.82) to H<sub>3</sub>-30 ( $\delta_H$  0.97) indicated the  $\alpha$ -orientation of H-5 and the hydroxylation at Me-29, respectively. The  $\beta$ -orientation of OH-17 was supported by the similar chemical shifts of C-16/17/18/22 ( $\delta_{C-16}$  215.2,  $\delta_{C-17}$  76.3,  $\delta_{C-18}$  52.3, and  $\delta_{C-22}$  30.1 in CDCl<sub>3</sub>) of compound **15** and those of camelliaolean B ( $\delta_{C-16}$  215.1,  $\delta_{C-17}$  76.3,  $\delta_{C-18}$  52.5, and  $\delta_{C-22}$  30.1 in CDCl<sub>3</sub>) (Figures 62 and 70) (Uddin et al., 2014). Finally, compound **15** was elucidated as 4,17 $\beta$ ,29-trihydroxy-16-oxo-3,4-*seco*-28-nor-olean-12-en-3-oic acid *n*-butyl ester.

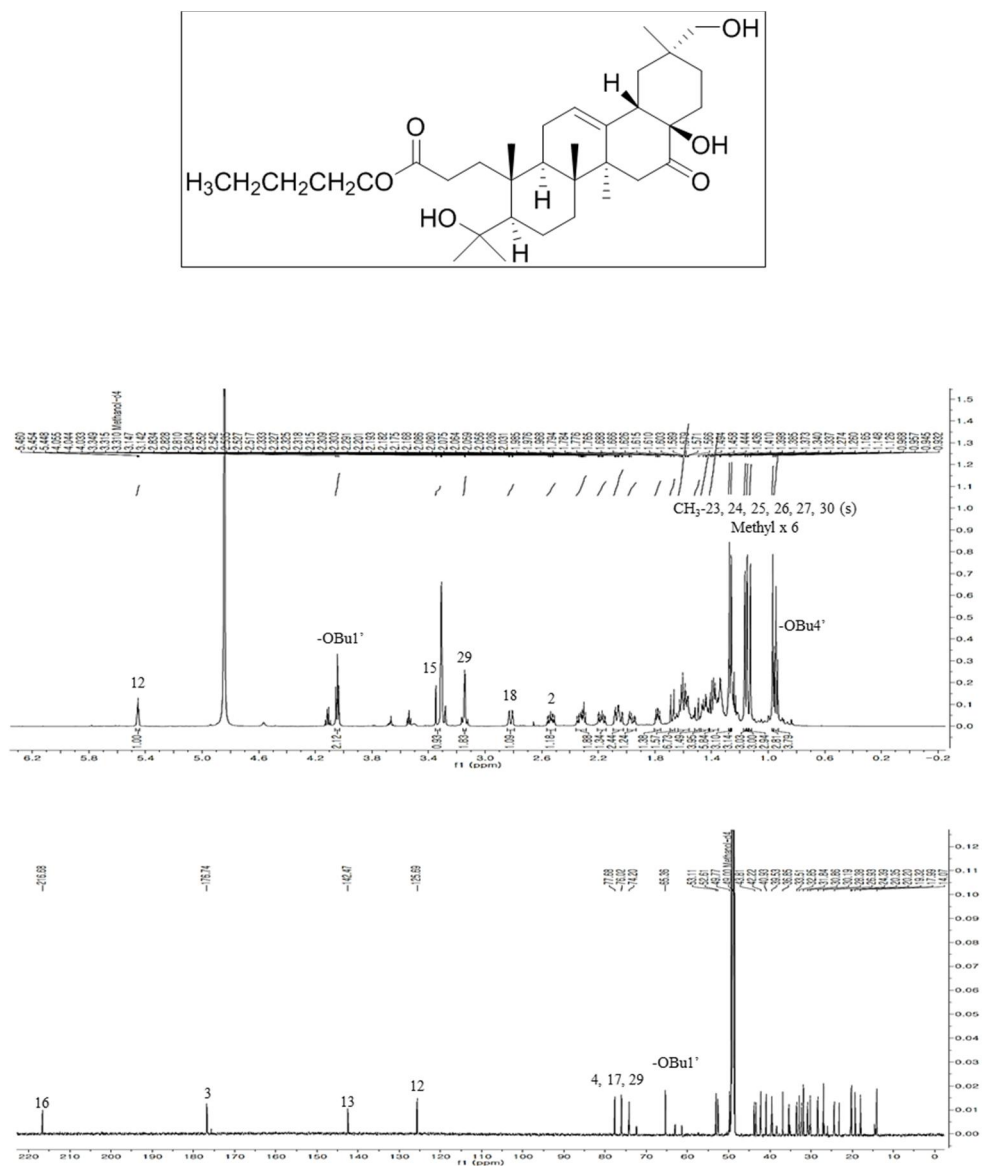


**Figure 69.**  $^1\text{H}$  and  $^{13}\text{C}$  NMR of compound **15** (methanol- $d_4$ , 600 MHz/150 MHz).

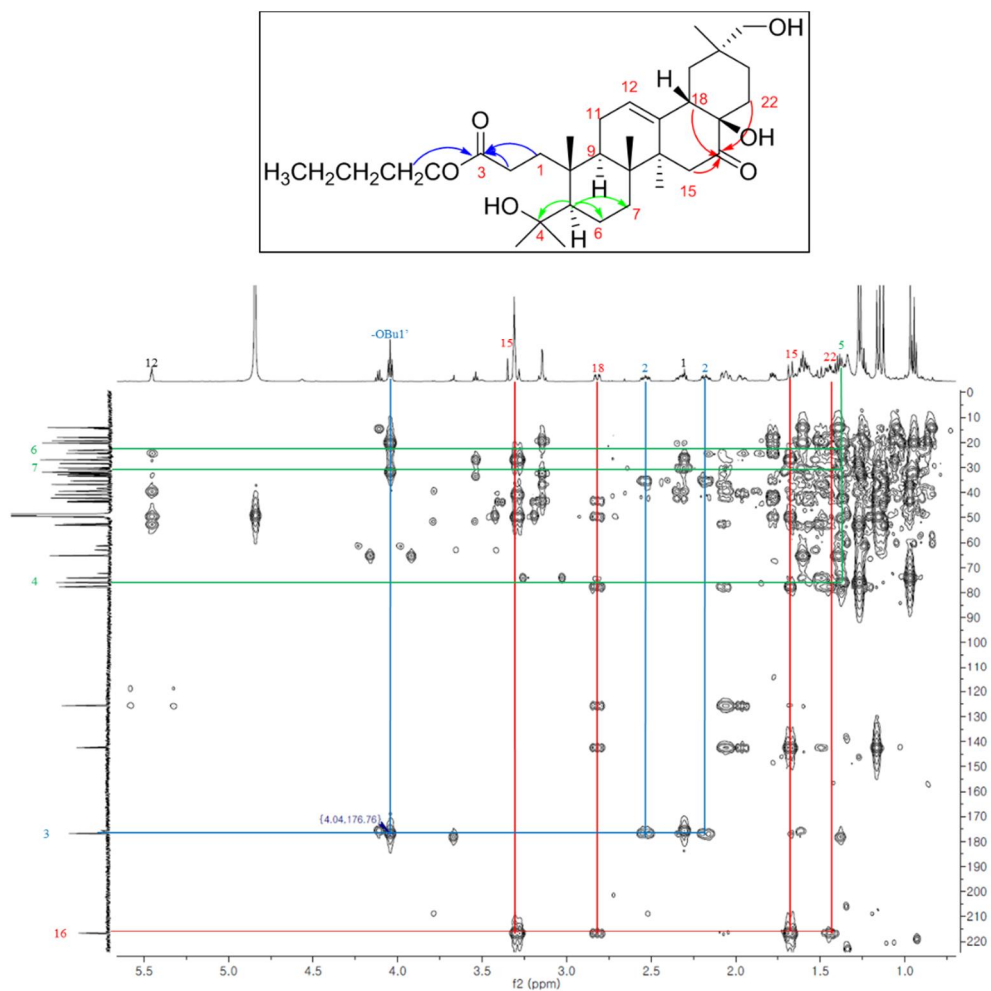


**Figure 70.** HMBC of compound **15** (methanol- $d_4$ , 600 MHz).



### 3.1.6. Compound **16**

Compound **16** was isolated as a white amorphous powder with  $[\alpha]_D^{25} -24.4$  (*c* 0.1, MeOH), and it had a molecular formula of  $C_{29}H_{44}O_5$  based on a positive HRFABMS peak at  $m/z$  473.3283  $[M + H]^+$  (calcd 473.3267). The IR absorptions indicated the presence of hydroxy ( $3393\text{ cm}^{-1}$ ), carbonyl ( $1714\text{ cm}^{-1}$ ), and olefin ( $1596\text{ cm}^{-1}$ ) functionalities. The  $^1\text{H}$  and  $^{13}\text{C}$  NMR spectra showed one oxymethene group ( $\delta_{\text{H}}$  3.17 (1H, d,  $J = 10.0$  Hz), 3.14 (1H, d,  $J = 10.0$  Hz);  $\delta_{\text{C}}$  73.8 (CH<sub>2</sub>)), one oxygenated quaternary carbon ( $\delta_{\text{C}}$  77.1), one trisubstituted olefin system ( $\delta_{\text{H}}$  5.42, 1H, t,  $J = 3.5$  Hz;  $\delta_{\text{C}}$  143.0, 124.4), one terminal double bond ( $\delta_{\text{H}}$  4.89 (br s), 4.74 (br s);  $\delta_{\text{C}}$  148.3 (C), 114.0 (CH<sub>2</sub>)), and two carbonyl carbons ( $\delta_{\text{C}}$  213.9, 174.9). Further analysis indicated that the NMR patterns of compounds **11** and **16** were similar. However the CH-7 signals ( $\delta_{\text{H}}$  4.19, 1H, dd,  $J = 11.0, 4.5$  Hz;  $\delta_{\text{C}}$  72.9) and the C-4 signal at  $\delta_{\text{C}}$  74.8 in compound **11** disappeared, whereas one terminal double bond ( $\delta_{\text{H}}$  4.89 (br s), 4.74 (br s);  $\delta_{\text{C}}$  148.3 (C), 114.0 (CH<sub>2</sub>)) was observed in compound **16**, which suggested the absence of OH-7 and the presence of a  $\Delta^{4,23}$  olefin system in **16** (Table 7 and Figure 71). This proposal was confirmed by HSQC and HMBC experiments, which also determined other functionalities in compound **16**. The *a*-orientation of H-5, the hydroxylation of Me-29, and the relative configuration at C-17 was determined similar to those of compounds **11**, **12**, **14**, and **15**, as analyzed by the ROESY correlation from H-9 ( $\delta_{\text{H}}$  1.82) to H-5 ( $\delta_{\text{H}}$  2.07) and H<sub>3</sub>-27 ( $\delta_{\text{H}}$  1.19), and from H-18 ( $\delta_{\text{H}}$  2.83) to H<sub>3</sub>-30 ( $\delta_{\text{H}}$  0.96) and comparing the chemical shifts of C-16/17/18/22 with those of compounds **11**, **12**, **14**, **15** and camelliaolean B (Figures 62 and 72). Therefore, compound **16** was

determined to be 17 $\beta$ ,29-dihydroxy-16-oxo-3,4-*seco*-28-nor-olean-4(23),12-dien-3-oic acid.

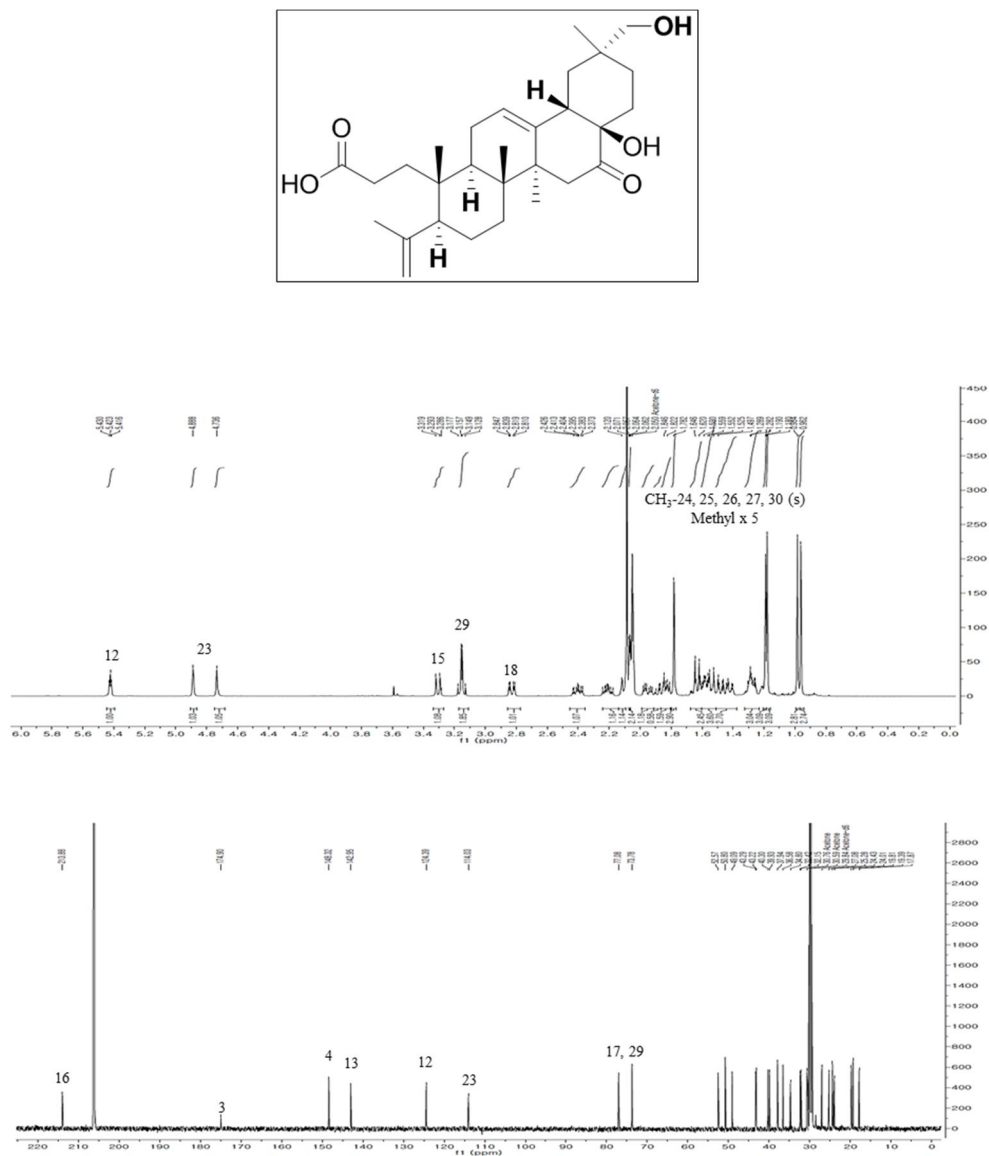


**Figure 71.**  $^1\text{H}$  and  $^{13}\text{C}$  NMR of compound **16** (acetone- $d_6$ , 500 MHz/125 MHz).

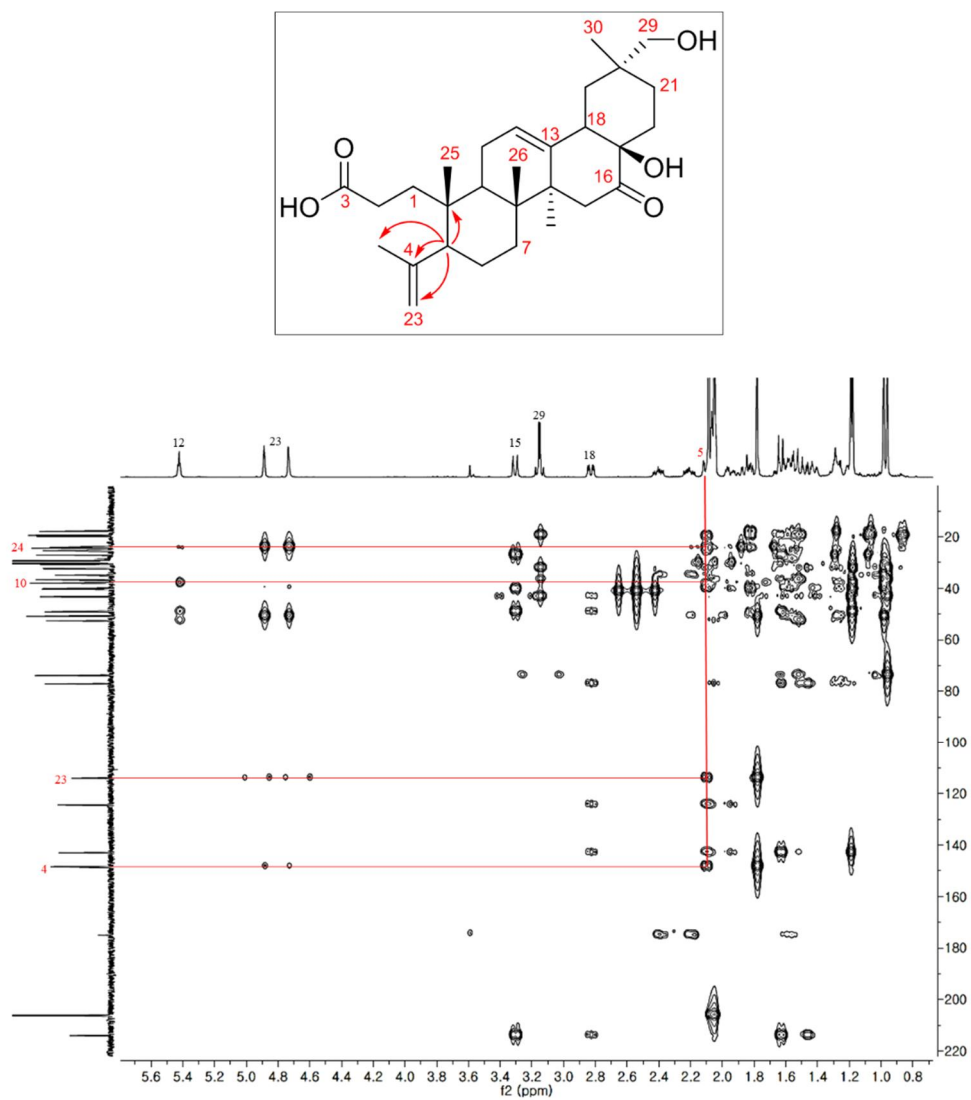


**Figure 72.** HMBC of compound 16 (acetone- $d_6$ , 500 MHz).

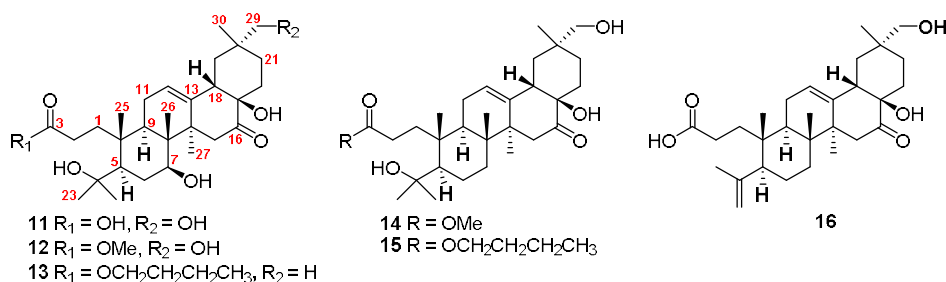


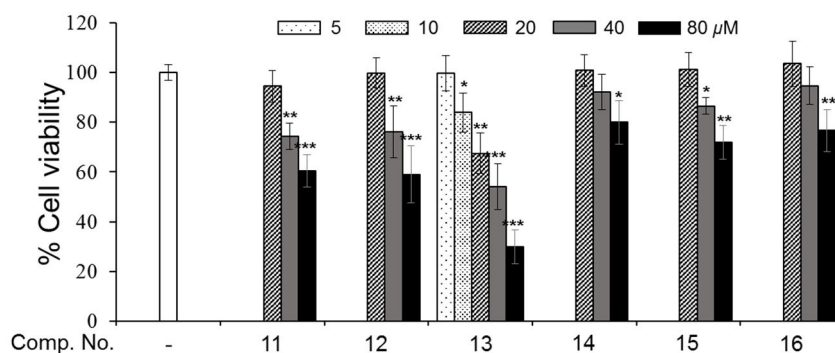
Figure 73. Six 3,4-*seco*-28-nor-oleanane triterpenoids (**11–16**) from *C. japonica*.

### 3.2. Neuroprotective effect of compounds 11–16 on rotenone-induced neurotoxicity of SH-SY5Y cells

A number of studies have demonstrated that a rotenone model of Parkinson's disease has been established to search for candidates to treat PD (Ryu et al., 2013; Sala et al., 2013), in which human dopaminergic SH-SY5Y cells are exposed to 2.5  $\mu$ M of rotenone, a mitochondrial complex I inhibitor. The protection against neurotoxicity of compounds **1–6** was examined with this model.

In the first step, the cytotoxicities of all isolated compounds **11–16** (Figure 73) were determined to estimate the optimum concentrations that are not toxic to SH-SY5Y cells. Consequently, cytotoxicity was not observed when cells were treated with less than 20  $\mu$ M of compounds **11**, **12**, and **14–16**, except for compound **13**, as shown in Figure 74A. Compound **13** was used at low concentrations of less than 10  $\mu$ M because of its cytotoxicity to evaluate protective action against rotenone-induced dopaminergic cell death in SH-SY5Y cells. Therefore, 5–20  $\mu$ M of compounds **11**, **12**, **14–16** and 1–5  $\mu$ M of compound **13** were used to evaluate their neuroprotective effects on a rotenone model. As shown in Figure 74B, pretreatment of compounds **13–16** for 24 h increased cell viability against cell death resulting from treatment by 2.5  $\mu$ M rotenone in a concentration-dependent manner.

(A)



(B)

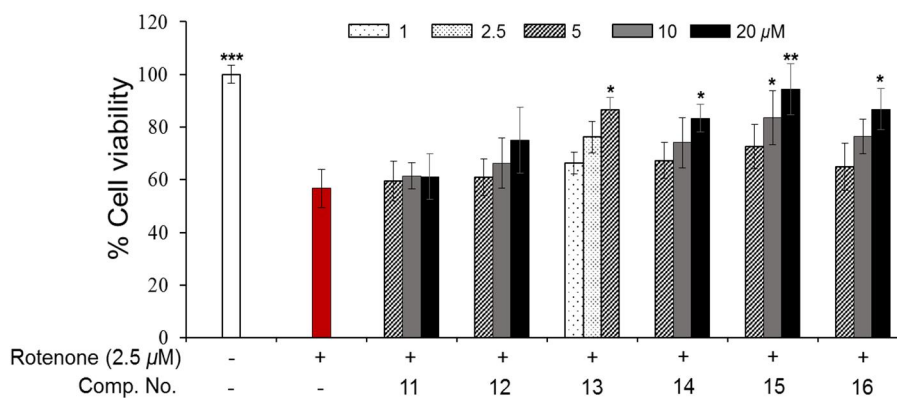
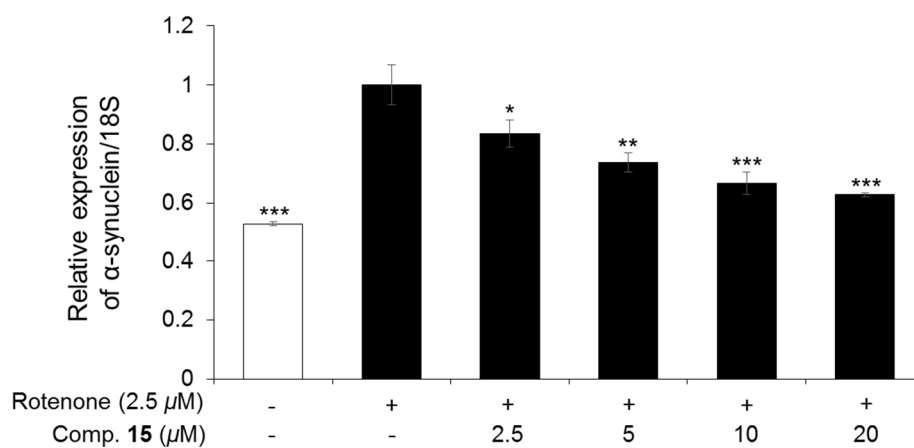


**Figure 74.** Effects of compounds **11–16** on rotenone-induced cytotoxicity in SH-SY5Y cells. (A) Effect of 3,4-*seco*-28-nor-oleanane triterpenoids **11–16** on the viability of SH-SY5Y cells. Each value expressed as the mean  $\pm$  SD ( $n=2$ ), \*  $p < 0.05$ , \*\*  $p < 0.01$ , and \*\*\*  $p < 0.001$  compared to the vehicle. (B) Protective effect of compounds **11–16** on the neurotoxicity of SH-SY5Y cells in a rotenone model of Parkinson's disease. Each value expressed as the mean  $\pm$  SD ( $n=2$ ), \*  $p < 0.05$ , \*\*  $p < 0.01$ , and \*\*\*  $p < 0.001$  compared only to the rotenone treatment group.

### 3.3. Effects of compounds 15 on $\alpha$ -synuclein expression induced by rotenone treatment

An abnormal accumulation of  $\alpha$ -synuclein in the brain is a major feature of Parkinson's disease (Dadakhujiev et al., 2010; Luk et al., 2012). Therefore,  $\alpha$ -synuclein could be a promising target for treating PD (Lee et al., 2014; Maries et al., 2003; T Rohn, 2012; Venda et al., 2010). In this study, we focused on the change of  $\alpha$ -synuclein expression in the presence or absence of triterpenoids from *C. japonica* in SH-SY5Y cells using Western blot analysis and Real-time PCR method. Considering the cytotoxicities of compounds **11–16** and their protection against neurotoxicity, compound **15** was selected for further evaluation on rotenone-induced neurotoxicity in SH-SY5Y cells. As shown in Figures 75 and 76, treatment with rotenone elevated the mRNA and protein expression level of  $\alpha$ -synuclein in SH-SY5Y cells, whereas pretreatment with compound **5** significantly attenuated the increase of  $\alpha$ -synuclein induced by rotenone treatment in a concentration-dependent manner.

(A)



(B)

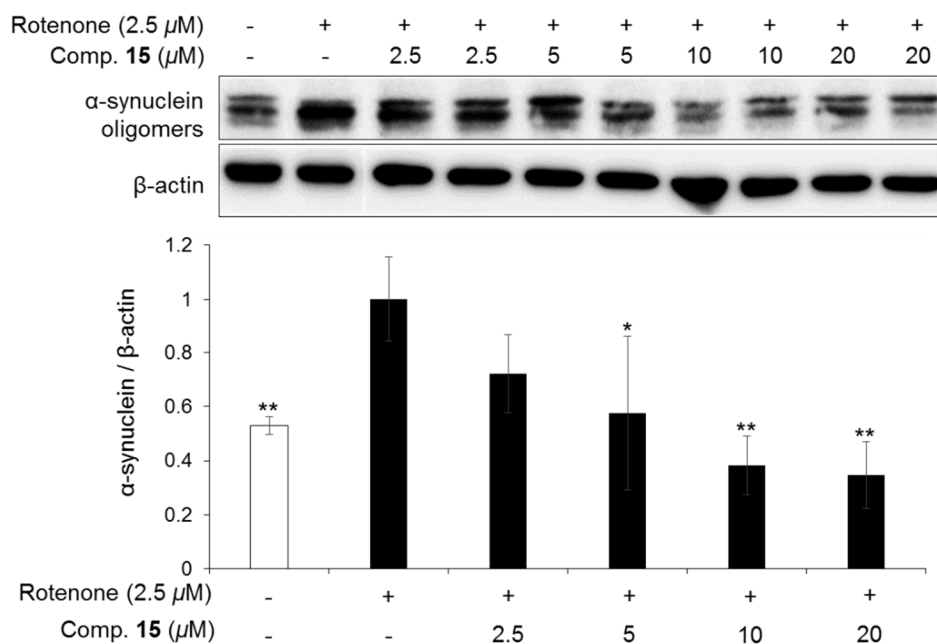


**Figure 75.** Relative mRNA and protein expression levels of  $\alpha$ -synuclein against SH-SY5Y cells.

The cells were pre-incubated with or without compound **15** at different concentrations for 24 h. Then, the cells were treated with 2.5  $\mu$ M rotenone and

incubated for 12 h. (A) Compound **15** decreased the mRNA levels of  $\alpha$ -synuclein induced by rotenone treatment in SH-SY5Y cells as assessed by real-time PCR. Results were calculated as the mean  $\pm$  SD ( $n = 3$ ), \*  $p < 0.05$ , \*\*  $p < 0.01$ , and \*\*\*  $p < 0.001$  compared to the rotenone treatment group. (B) Compound **15** reduced the protein expressions of  $\alpha$ -synuclein analyzed by Western blot. Data present as the mean  $\pm$  SD ( $n = 2-4$ ), \*  $p < 0.05$ , \*\*  $p < 0.01$ , and \*\*\*  $p < 0.001$  compared to the rotenone treatment group.



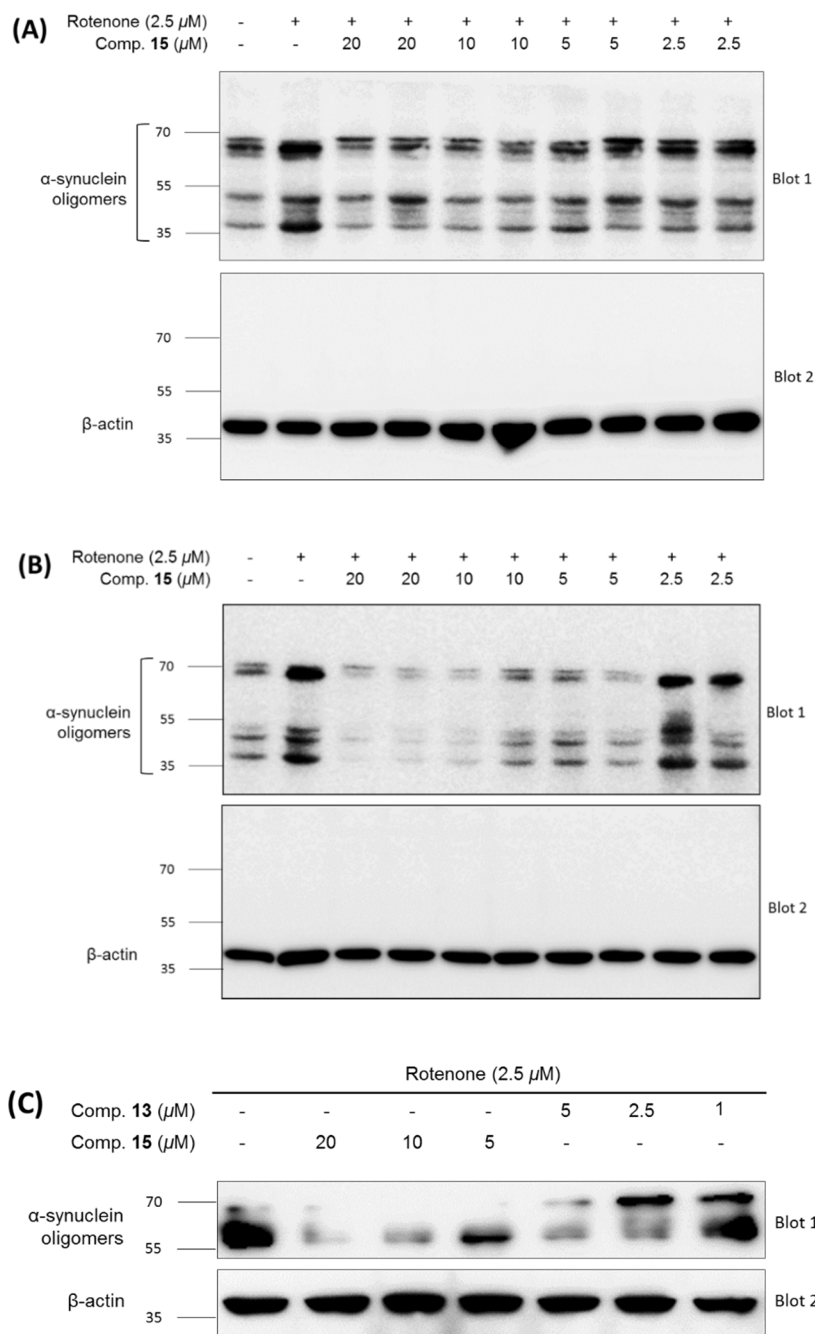


**Figure 76.** Effects of compound **13** and **15** on the protein expressions of  $\alpha$ -synuclein; original uncropped blots.

The cells were pre-incubated with or without test compounds at various concentrations for 24 h. The cells were then exposed to 2.5  $\mu$ M rotenone for 12 h.

Protein lysates were collected as described in experimental sections. Equal amounts of proteins were loaded on SDS-polyacrylamide gels. After transferred to PVDF membranes, they were blocked with 5% of skim milk solution. Then, different blots were incubated with  $\alpha$ -synuclein or  $\beta$ -actin antibodies. All bands were detected using LAS 4000 luminescent image analyzer. Figure A was included in the final analysis (Figure 75).

### 3.4. Effects of compound **15** on intracellular ROS production in a rotenone treatment model

Multiple studies have shown that over-expression of  $\alpha$ -synuclein is potentially related with the increase of reactive oxygen species (ROS) by mitochondrial dysfunction, finally leading to neuronal cell death (Maries et al., 2003; Stefanis, 2012). To examine the inhibitory action of ROS by compound **15**, intracellular ROS generation was determined using a 2',7'-dichlorofluorescein diacetate (DCFH-DA) assay in SH-SY5Y cells, as presented in Figure 77 (Gomes et al., 2005; LeBel et al., 1992). Treatment with rotenone significantly induced the ROS production compared with the non-treatment group. However, pretreatment with compound **15** at various concentrations effectively decreased the ROS production induced by rotenone treatment in a concentration-dependent manner.

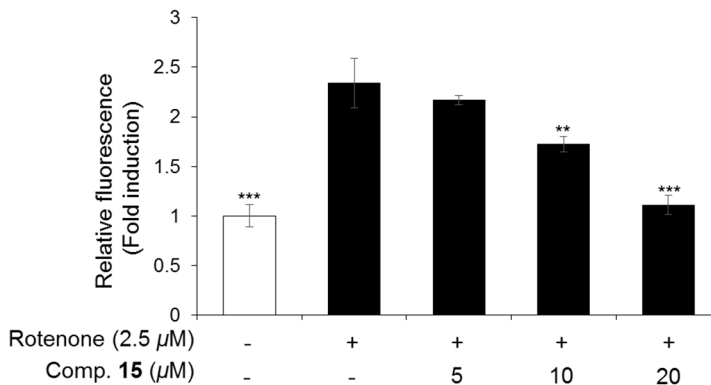
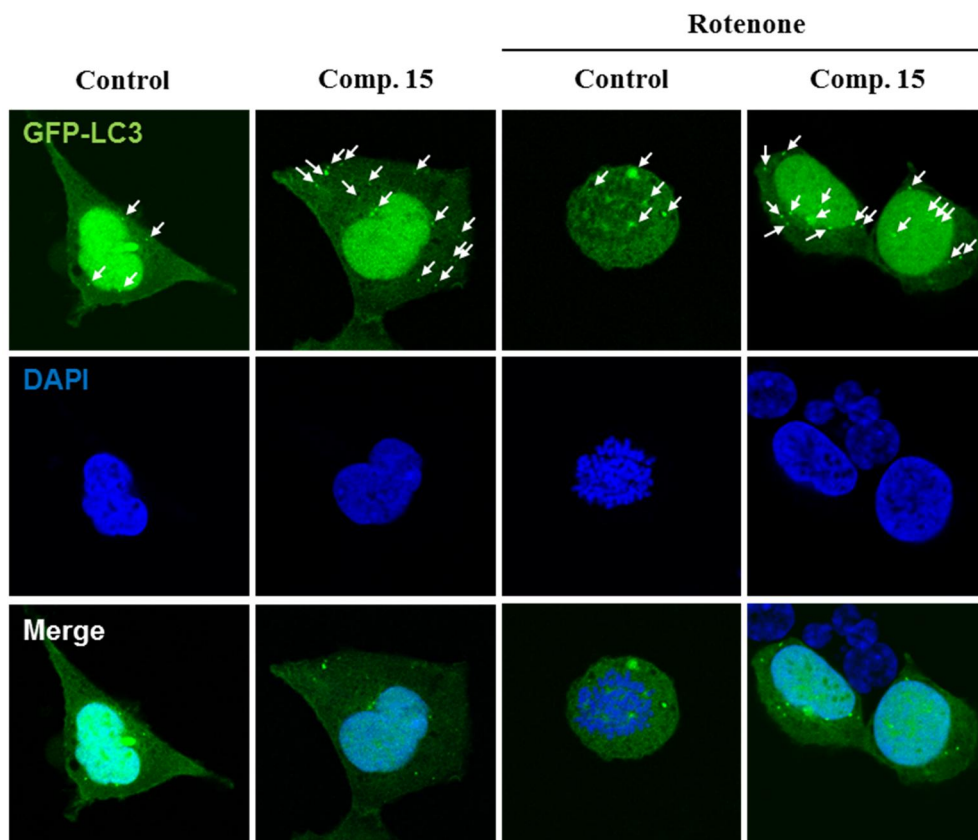


Figure 77. Inhibition of intracellular ROS production by Compound **15**. SH-SY5Y cells were pre-treated with or without compound **15** for 24 h. Rotenone (2.5  $\mu$ M) was added to the cells and incubated for 12 h at 37°C. The cells were then incubated with 20  $\mu$ M of DCFH-DA for 30 min. Values are expressed as the mean  $\pm$  SD ( $n = 3$ ), \*  $p < 0.05$  and \*\*  $p < 0.01$ , and \*\*\*  $p < 0.001$  compared only to the rotenone treatment group.

### 3.5. Compound **15** reduced the condensation of chromosome induced by rotenone treatment

Furthermore, we examined the autophagy regulation by rotenone and compound **15**. Several studies have recently reported that autophagy is responsible for the clearance of  $\alpha$ -synuclein induced by rotenone treatment. Considering that the autophagosomes which possess the LC3 in the membrane of vacuoles colocalized with  $\alpha$ -synuclein-overexpressed aggregation as well as autophagic vacuoles were increased in rotenone-induced PD models (Xiong et al., 2013), autophagy induced by the treatment of compound **15** might contribute to the reduction of the  $\alpha$ -synuclein expression. The cells used in this study were stably transfected with GFP-LC3 vector, a commonly used autophagy marker (Kabeya, 2000; Yoon et al., 2012), and sequentially treated with compound **15** and rotenone. While rotenone treatment caused chromosome condensation, compound **15** recovered rotenone-induced chromosome condensation. Moreover, the formation of autophagosomes was observed upon treatment with compound **15**, suggesting that autophagy is modulated by the treatment with compound **15** (Figures 78 and 79).



**Figure 78.** Compound **15** reduced the condensation of chromosome induced by rotenone treatment in HEK293 cells stably expressing GFP-LC3 measured by the immunocytochemistry method.

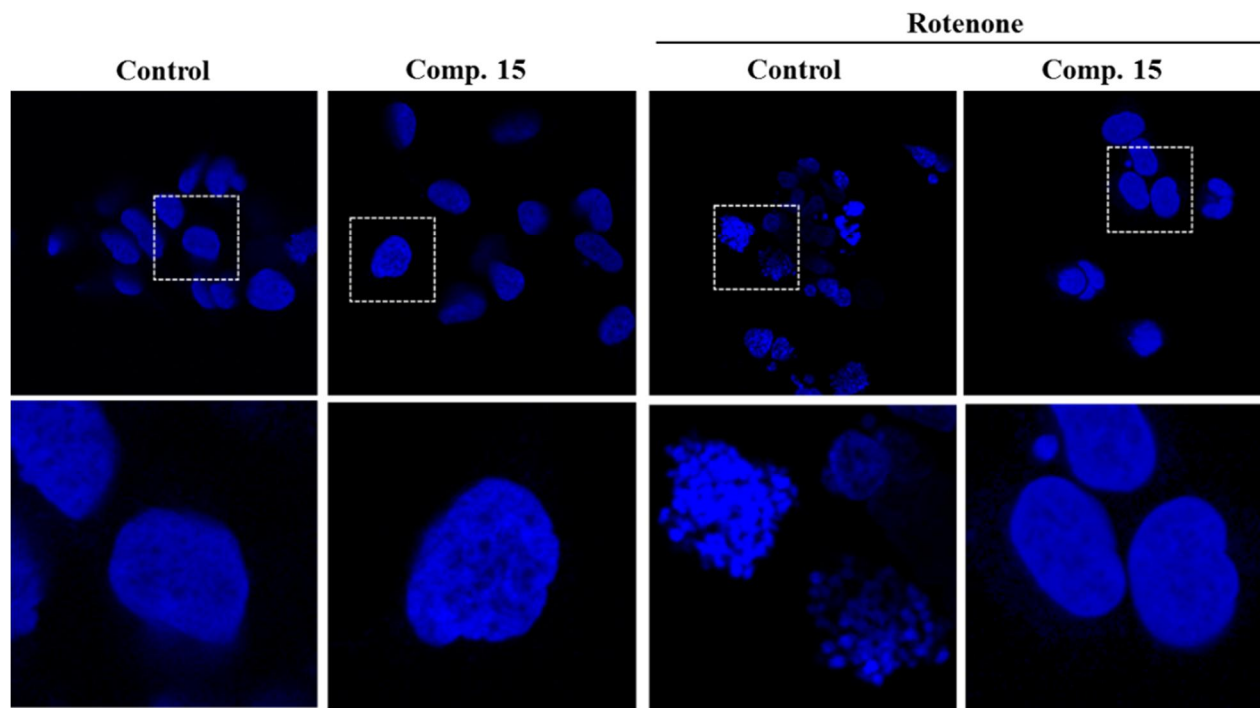


**Figure 79.** Compound **15** ( $20\ \mu\text{M}$ ) reduced the condensation of chromosome induced by rotenone treatment in HEK293 cells.

#### 4. Conclusions

Parkinson's disease shows accumulation of abnormal aggregated protein ( $\alpha$ -synuclein) in neuronal cells, its clearance has been focused on as a treatment marker of this disease (Pan et al., 2009). Until present, there have been only two 3,4-*seco*-28-nor-oleanane triterpenoids reported from *Camellia* without activity, and they were isolated from the fruit peel of *C. japonica* by our group in 2013 (Uddin et al., 2014). Herein, six new 3,4-*seco*-28-nor-oleanane triterpenoids (**11**–**16**) were isolated from the flowers of *C. japonica*, including (**11**) 4,7 $\beta$ ,17 $\beta$ ,29-Tetrahydroxy-16-oxo-3,4-*seco*-28-nor-olean-12-en-3-oic acid, (**12**) 4,7 $\beta$ ,17 $\beta$ ,29-Tetrahydroxy-16-oxo-3,4-*seco*-28-nor-olean-12-en-3-oic acid methyl ester, (**13**) 4,7 $\beta$ ,17 $\beta$ -Trihydroxy-16-oxo-3,4-*seco*-28-nor-olean-12-en-3-oic acid n-butyl ester, (**14**) 4,17 $\beta$ ,29-Trihydroxy-16-oxo-3,4-*seco*-28-nor-olean-12-en-3-oic acid methyl ester, (**15**) 4,17 $\beta$ ,29-Trihydroxy-16-oxo-3,4-*seco*-28-nor-olean-12-en-3-oic acid n-butyl ester, (**16**) 17 $\beta$ ,29-Dihydroxy-16-oxo-3,4-*seco*-28-nor-olean-4(23),12-dien-3-oic acid.

Among isolated triterpenoids, compounds **13**–**16** exhibited potential protective effects on SH-SY5Y neuronal cells in a rotenone model of Parkinson's disease.

Compound **15** significantly inhibited the accumulation of  $\alpha$ -synuclein and ROS levels in the rotenone-treated SH-SY5Y cells.

Compound **15** clearly reduced the condensation of chromosome which induced by rotenone treatment in HEK293 cells with stable expression of the GFP-LC3 reporter protein.

## References

- ADA-American Diabetes Association, 2017. Classification and diagnosis of diabetes. *Diabetes Care* 40, S11-S24.
- Anderson, J.P., Walker, D.E., Goldstein, J.M., De Laat, R., Banducci, K., Caccavello, R.J., Barbour, R., Huang, J., Kling, K., Lee, M., Diep, L., Keim, P.S., Shen, X., Chataway, T., Schlossmacher, M.G., Seubert, P., Schenk, D., Sinha, S., Gai, W.P., Chilcote, T.J., 2006. Phosphorylation of Ser-129 is the dominant pathological modification of  $\alpha$ -synuclein in familial and sporadic lewy body disease. *J. Biol. Chem.* 281, 29739–29752.
- Anh, P.T., Ky, P.T., Cue, N.T., Nhiem, N.X., Yen, P.H., Ngoc, T.M., Anh, H.L.T., Tai, B.H., Trang, D.T., Minh, C. Van, Kiem, P. Van, 2015. Damarane-type Saponins from *Gynostemma longipes* and their Cytotoxic Activity. *Nat. Prod. Commun.* 10, 1351–1352.
- Ardisson Korat, A. V., Willett, W.C., Hu, F.B., 2014. Diet, Lifestyle, and Genetic Risk Factors for Type 2 Diabetes: A Review from the Nurses' Health Study, Nurses' Health Study 2, and Health Professionals' Follow-Up Study. *Curr. Nutr. Rep.* 3, 345–354.
- Bellamy, L., Casas, J.P., Hingorani, A.D., Williams, D., 2009. Type 2 diabetes mellitus after gestational diabetes: a systematic review and meta-analysis. *Lancet* 373, 1773–1779.
- Chen, L., Magliano, D.J., Zimmet, P.Z., 2012. The worldwide epidemiology of type 2 diabetes mellitus - Present and future perspectives. *Nat. Rev.*



*Endocrinol.* 8, 228–236.

- Choi, B.-K., Choi, M.-G., Kim, J.-Y., Yang, Y., Lai, Y., Kweon, D.-H., Lee, N.K., Shin, Y.-K., 2013. Large  $\alpha$ -synuclein oligomers inhibit neuronal SNARE-mediated vesicle docking. *Proc. Natl. Acad. Sci.* 110, 4087–4092.
- Choi, T.G., Kim, S.S., 2013. Autophagy in Redox Signalling. *Hanyang Med. Rev.* 33, 83.
- Colla, E., Jensen, P.H., Pletnikova, O., Troncoso, J.C., Glabe, C., Lee, M.K., 2012. Accumulation of Toxic  $\alpha$ -Synuclein Oligomer within Endoplasmic Reticulum Occurs in  $\alpha$ -Synucleinopathy In Vivo. *J. Neurosci.* 32, 3301–3305.
- Cuervo, A.M., Stafanis, L., Fredenburg, R., Lansbury, P.T., Sulzer, D., 2004. Impaired degradation of mutant  $\alpha$ -synuclein by chaperone-mediated autophagy. *Science*. 305, 1292–1295.
- Dadakhjaev, S., Noh, H.S., Jung, E.J., Cha, J.Y., Baek, S.M., Ha, J.H., Kim, D.R., 2010. Autophagy protects the rotenone-induced cell death in  $\alpha$ -synuclein overexpressing SH-SY5Y cells. *Neurosci. Lett.* 472, 47–52.
- Danaei, G., Finucane, M.M., Lu, Y., Singh, G.M., Cowan, M.J., Paciorek, C.J., Lin, J.K., Farzadfar, F., Khang, Y.H., Stevens, G.A., Rao, M., Ali, M.K., Riley, L.M., Robinson, C.A., Ezzati, M., 2011. National, regional, and global trends in fasting plasma glucose and diabetes prevalence since 1980: Systematic analysis of health examination surveys and epidemiological studies with 370 country-years and 2.7 million participants. *Lancet* 378, 31–40.
- Dawson, T.M., Dawson, V.L., 2003. Molecular Pathways of Neurodegeneration in Parkinson's Disease. *Science*. 302(5646), 819-822.

- DeFronzo, R.A., Ferrannini, E., Groop, L., Henry, R.R., Herman, W.H., Holst, J.J., Hu, F.B., Kahn, C.R., Raz, I., Shulman, G.I. and Simonson, D.C., 2015. Type 2 diabetes mellitus. *Nature reviews Disease primers*, 1, 15019
- Dorsey, E.R., Bloem, B.R., 2018. The Parkinson pandemic - A call to action. *JAMA Neurol.* 75(1), 9–10.
- Emamzadeh, F.N., 2016. Alpha-synuclein structure, functions, and interactions. *J. Res. Med. Sci.* 21–29.
- Exner, N., Lutz, A.K., Haass, C., Winklhofer, K.F., 2012. Mitochondrial dysfunction in Parkinson's disease: Molecular mechanisms and pathophysiological consequences. *EMBO J.* 31(14), 3038–3062.
- Fang, Z.P., Zeng, X.Y., 1996. Structure of gypentonoside a from *Gynostemma pentaphyllum* Makino. *Yaoxue Xuebao* 31, 680–683.
- Feigin, V.L., Abajobir, A.A., Abate, K.H., Abd-Allah, F., Abdulle, A.M., Abera, S.F., Abyu, G.Y., Ahmed, M.B., Aichour, A.N., Aichour, I. and Aichour, M.T.E., 2017. Global, regional, and national burden of neurological disorders during 1990-2015: a systematic analysis for the global burden of disease study 2015. *Lancet. Neurol.* 16, 877–897.
- Gomes, A., Fernandes, E., Lima, J.L.F.C., 2005. Fluorescence probes used for detection of reactive oxygen species. *J. Biochem. Biophys. Methods* 65, 45–80.
- Guo, X.L., Wang, T.J., Bian, B.L., 1997. Studies on the chemical constituents of *Gynostemma longipes* C.Y. Wu. *Yaoxue Xuebao* 32, 524–529.

- Hardie, D.G., Ross, F.A., Hawley, S.A., 2012. AMPK: A nutrient and energy sensor that maintains energy homeostasis. *Nat. Rev. Mol. Cell Biol.* 13, 251–262.
- Hardie, D.G., Ross, F.A., Hawley, S.A., 2012b. AMP-activated protein kinase: A target for drugs both ancient and modern. *Chem. Biol.* 19(10), 1222–1236.
- Herman, M.A., Kahn, B.B., 2006. Glucose transport and sensing in the maintenance of glucose homeostasis and metabolic harmony. *J. Clin. Invest.* 116(7), 1767–1775.
- Hsieh, W.T., Chiang, B.H., 2014. A well-refined in vitro model derived from human embryonic stem cell for screening phytochemicals with midbrain dopaminergic differentiation-boosting potential for improving Parkinson's disease. *J. Agric. Food Chem.* 62, 6326–6336.
- Huang, S., Czech, M.P., 2007. The GLUT4 Glucose Transporter. *Cell Metab.* 5(4), 237–252.
- Jackson-Lewis, V., Przedborski, S., 2007. Protocol for the MPTP mouse model of Parkinson's disease. *Nat. Protoc.* 2, 141–151.
- Kabeya, Y., 2004. LC3, GABARAP and GATE16 localize to autophagosomal membrane depending on form-II formation. *J. Cell Sci.* 117, 2805–2812.
- Kabeya, Y., 2000. LC3, a mammalian homologue of yeast Apg8p, is localized in autophagosome membranes after processing. *EMBO J.* 19, 5720–5728.
- Kahn, B.B., Alquier, T., Carling, D., Hardie, D.G., 2005. AMP-activated protein kinase: Ancient energy gauge provides clues to modern understanding of metabolism. *Cell Metab.* 1(1), 15–25.

- Kim, J., Yang, G., Kim, Y., Kim, J., Ha, J., 2016. AMPK activators: Mechanisms of action and physiological activities. *Exp. Mol. Med.* 48, e224.
- Kim, M., Wands, J.R., 2010. Insulin pathway. *Signaling Pathways in Liver Diseases* (Berlin Heidelberg: Springer-Verlag). 229–241.
- Krook, A., Wallberg-Henriksson, H., Zierath, J.R., 2004. Sending the signal: Molecular mechanisms regulating glucose uptake. *Medicine and Science in Sports and Exercise.* 36(7), 1212–1217.
- Kwon, D.Y., Kim, Y.S., Ryu, S.Y., Choi, Y.H., Cha, M.R., Yang, H.J., Park, S., 2012. Platyconic acid, a saponin from *Platycodi radix*, improves glucose homeostasis by enhancing insulin sensitivity in vitro and in vivo. *Eur. J. Nutr.* 51, 529–540.
- Kwon, J., Hiep, N.T., Kim, D.W., Hwang, B.Y., Lee, H.J., Mar, W., Lee, D., 2014. Neuroprotective xanthenes from the root bark of *Cudrania tricuspidata*. *J. Nat. Prod.* 77, 1893–1901.
- LeBel, C.P., Ischiropoulos, H., Bondy, S.C., 1992. Evaluation of the probe 2', 7'-dichlorofluorescein as an indicator of reactive oxygen species formation and oxidative stress. *Chem. Res. Toxicol.* 5, 227–231.
- Lee, C., Lee, J.W., Jin, Q., Jang, H., Jang, H.J., Rho, M.C., Lee, M.K., Lee, C.K., Lee, M.K., Hwang, B.Y., 2015. Isolation and characterization of dammarane-type saponins from *Gynostemma pentaphyllum* and their inhibitory effects on IL-6-induced STAT3 activation. *J. Nat. Prod.* 78, 971–976.
- Lee, H.J., Bae, E.J., Lee, S.J., 2014. Extracellular  $\alpha$ -synuclein-a novel and crucial factor in Lewy body diseases. *Nat. Rev. Neurol.* 10, 92–98.
- Lee, S.M., Kim, S.C., Oh, J., Kim, J.H., Na, M., 2013. 20(R)-Ginsenoside Rf: A

- new ginsenoside from red ginseng extract. *Phytochem. Lett.* 6, 620–624.
- Liao, P.Y., Wang, D., Zhang, Y.J., Yang, C.R., 2008. Dammarane-type glycosides from steamed notoginseng. *J. Agric. Food Chem.* 56, 1751–1756.
- Lin, Y.P., Chen, T.Y., Tseng, H.W., Lee, M.H., Chen, S.T., 2012. Chemical and biological evaluation of nephrocizin in protecting nerve growth factor-differentiated PC12 cells by 6-hydroxydopamine-induced neurotoxicity. *Phytochemistry* 84, 102–115.
- Lotharius, J., Brundin, P., 2002. Pathogenesis of parkinson's disease: Dopamine, vesicles and  $\alpha$ -synuclein. *Nat. Rev. Neurosci.* 3, 932–942.
- Luk, K.C., Kehm, V., Carroll, J., Zhang, B., O'Brien, P., Trojanowski, J.Q., Lee, V.M.Y., 2012. Pathological  $\alpha$ -synuclein transmission initiates Parkinson-like neurodegeneration in nontransgenic mice. *Science* (80). 338, 949–953.
- Maries, E., Dass, B., Collier, T.J., Kordower, J.H., Steece-Collier, K., 2003. The role of  $\alpha$ -synuclein in Parkinson's disease: insights from animal models. *Nat. Rev. Neurosci.* 4, 727.
- Marín-Peñalver, J.J., Martín-Timón, I., Sevillano-Collantes, C., Cañizo-Gómez, F.J. del, n, C.S.-C.F.J. del C.-G., mez, 2016. Update on the treatment of type 2 diabetes mellitus. *World J. Diabetes* 7, 354.
- Meissner, W.G., Frasier, M., Gasser, T., Goetz, C.G., Lozano, A., Piccini, P., Obeso, J.A., Rascol, O., Schapira, A., Voon, V., Weiner, D.M., Tison, F., Bezard, E., 2011. Priorities in Parkinson's disease research. *Nat. Rev. Drug Discov.* 10, 377–393.
- Mihaylova, M.M., Shaw, R.J., 2012. The AMP-activated protein kinase (AMPK)

- signaling pathway coordinates cell growth, autophagy, & metabolism. *Nat. Cell Biol.* 13, 1016–1023.
- N., L., P., T.K., P.D., M., N., L., P., K., P.M.D., M.M., S.B., B., H., S.H., H., 2017. Neuroprotective propensity of PTUPB, a dual inhibitor of sEH and COX-2 against rotenone induced neurotoxicity in cell line and *Drosophila* model of Parkinson's disease. *Mov. Disord.* 32, 861–862.
- Nakamura, S., Moriura, T., Park, S., Fujimoto, K., Matsumoto, T., Ohta, T., Matsuda, H., Yoshikawa, M., 2012. Melanogenesis inhibitory and fibroblast proliferation accelerating effects of noroleanane- and oleanane-type triterpene oligoglycosides from the flower buds of *Camellia japonica*. *J. Nat. Prod.* 75, 1425–1430.
- Nasir Uddin, M., Sharma, G., Choi, H.S., Lim, S. IL, Oh, W.K., 2013. AMPK activators from natural products: A patent review. *Nat. Prod. Sci.* 19, 1–7.
- Newman, D.J., Cragg, G.M., 2016. Natural Products as Sources of New Drugs from 1981 to 2014. *J. Nat. Prod.* 79(3), 629–661.
- Nguyen, P.H., Gauhar, R., Hwang, S.L., Dao, T.T., Park, D.C., Kim, J.E., Song, H., Huh, T.L., Oh, W.K., 2011. New dammarane-type glucosides as potential activators of AMP-activated protein kinase (AMPK) from *Gynostemma pentaphyllum*. *Bioorganic Med. Chem.* 19, 6254–6260.
- O'Neill, H.M., 2013. AMPK and exercise: Glucose uptake and insulin sensitivity. *Diabetes Metab. J.* 37(1), 1–21.
- Pan, T., Rawal, P., Wu, Y., Xie, W., Jankovic, J., Le, W., 2009. Rapamycin

- protects against rotenone-induced apoptosis through autophagy induction. *Neuroscience* 164, 541–551.
- Pham, H.T.T., Hoang, M.C., Ha, T.K.Q., Dang, L.H., Tran, V.O., Nguyen, T.B.T., Lee, C.H., Oh, W.K., 2018. Discrimination of different geographic varieties of *Gymnema sylvestre*, an anti-sweet plant used for the treatment of type 2 diabetes. *Phytochemistry* 150, 12–22.
- Richter, E.A., Ruderman, N.B., 2009. AMPK and the biochemistry of exercise: implications for human health and disease. *Biochem. J.* 418, 261–275.
- Rocha, E.M., De Miranda, B., Sanders, L.H., 2018. Alpha-synuclein: Pathology, mitochondrial dysfunction and neuroinflammation in Parkinson's disease. *Neurobiol. Dis.* 109, 249–257.
- Ruderman, N.B., Carling, D., Prentki, M., Cacicedo, J.M., 2013. AMPK, insulin resistance, and the metabolic syndrome. *J. Clin. Invest.* 123 (7), 2764–2772.
- Ryu, H.W., Oh, W.K., Jang, I.S., Park, J., 2013. Amurensin G induces autophagy and attenuates cellular toxicities in a rotenone model of Parkinson's disease. *Biochem. Biophys. Res. Commun.* 433, 121–126.
- Sala, G., Arosio, A., Stefanoni, G., Melchionda, L., Riva, C., Marinig, D., Brighina, L., Ferrarese, C., 2013. Rotenone upregulates alpha-synuclein and myocyte enhancer factor 2D independently from lysosomal degradation inhibition. *Biomed Res. Int.* 2013.
- Sashidhara, K. V., Modukuri, R.K., Jadiya, P., Rao, K.B., Sharma, T., Haque, R., Singh, D.K., Banerjee, D., Siddiqi, M.I., Nazir, A., 2014. Discovery of 3-

- arylcoumarin-tetracyclic tacrine hybrids as multifunctional agents against Parkinson's disease. *ACS Med. Chem. Lett.* 5, 1099–1103.
- Stanford, K.I., Goodyear, L.J., 2014. Exercise and type 2 diabetes: molecular mechanisms regulating glucose uptake in skeletal muscle. *Adv. Physiol. Educ.* 38, 308–314.
- Stefanis, L., 2012.  $\alpha$ -Synuclein in Parkinson's disease. *Cold Spring Harb. Perspect. Med.* 2, a009399.
- Tamaru, S., Ohmachi, K., Miyata, Y., Tanaka, T., Kubayasi, T., Nagata, Y., Tanaka, K., 2013. Hypotriglyceridemic potential of fermented mixed tea made with third-crop green tea leaves and camellia (*camellia japonica*) leaves in sprague-dawley rats. *J. Agric. Food Chem.* 61, 5817–5823.
- T Rohn, T., 2012. Targeting alpha-synuclein for the treatment of Parkinson's disease. *CNS Neurol. Disord. Targets* (Formerly Curr. Drug Targets-CNS Neurol. Disord.) 11, 174–179.
- Tu, L., Zhao, Y., Yu, Z.Y., Cong, Y.W., Xu, G., Peng, L.Y., Zhang, P.T., Cheng, X. and Zhao, Q.S., 2008. Six new dammarane triterpenoids from *Viburnum cylindricum*. *Helvetica Chimica Acta*, 91(8), 1578-1587.
- Uddin, M.N., Sharma, G., Yang, J.L., Choi, H.S., Lim, S. Il, Kang, K.W., Oh, W.K., 2014. Oleanane triterpenes as protein tyrosine phosphatase 1B (PTP1B) inhibitors from *Camellia japonica*. *Phytochemistry* 103, 99–106.
- Venda, L.L., Cragg, S.J., Buchman, V.L., Wade-Martins, R., 2010.  $\alpha$ -Synuclein and dopamine at the crossroads of Parkinson's disease. *Trends Neurosci.* 33,



559–568.

- Vogiatzi, T., Xilouri, M., Vekrellis, K., Stefanis, L., 2008. Wild type  $\alpha$ -synuclein is degraded by chaperone-mediated autophagy and macroautophagy in neuronal cells. *J. Biol. Chem.* 283, 23542–23556.
- Wrangel, C. von, Schwabe, K., John, N., Krauss, J.K., Alam, M., 2015. The rotenone-induced rat model of Parkinson's disease: Behavioral and electrophysiological findings. *Behav. Brain Res.* 279, 52–61.
- Wu, Z.Y., Raven, P.H., Hong, D.Y., 2007. Flora of China. Vol. 12: Hippocastanaceae through Theaceae.
- Xiong, N., Huang, J., Zhang, Z., Zhang, Z., Xiong, J., Liu, X., Jia, M., Wang, F., Chen, C., Cao, X., Liang, Z., Sun, S., Lin, Z., Wang, T., 2009. Stereotaxical infusion of rotenone: A reliable rodent model for Parkinson's disease. *PLoS One* 4, 11, e7878.
- Xiong, N., Xiong, J., Jia, M., Liu, L., Zhang, X., Chen, Z., Huang, J., Zhang, Z., Hou, L., Luo, Z., Ghoorah, D., Lin, Z., Wang, T., 2013. The role of autophagy in Parkinson's disease: rotenone-based modeling. *Behav. Brain Funct.* 9, 13.
- Yamamoto, N., Yamashita, Y., Yoshioka, Y., Nishiumi, S., Ashida, H., 2016. Rapid preparation of a plasma membrane fraction: Western blot detection of translocated glucose transporter 4 from plasma membrane of muscle and adipose cells and tissues. *Curr. Protoc. Protein Sci.* 2016, 29.18.1–29.18.12.
- Yang, F., Shi, H., Zhang, X., Yu, L., 2013. Two novel anti-inflammatory 21-nordammarane saponins from tetraploid jiaogulan (*Gynostemma pentaphyllum*). *J. Agric. Food Chem.* 61, 12646–12652.

- Yang, J.L., Ha, T.K.Q., Dhodary, B., Pyo, E., Nguyen, N.H., Cho, H., Kim, E., Oh, W.K., 2015. Oleanane triterpenes from the flowers of *camellia japonica* inhibit porcine epidemic diarrhea virus (PEDV) replication. *J. Med. Chem.* 58, 1268–1280.
- Yoon, J.-H., Her, S., Kim, M., Jang, I.-S., Park, J., 2012. The expression of damage-regulated autophagy modulator 2 (DRAM2) contributes to autophagy induction. *Mol. Biol. Rep.* 39, 1087–1093.
- Zhang, X., Chiu, V.M., Stoica, G., Lungu, G., Schenk, J.O., Hill, H.H., 2014. Metabolic analysis of striatal tissues from parkinson's disease-like rats by electrospray ionization ion mobility mass spectrometry. *Anal. Chem.* 86, 3075–3083.
- Zimmet, P., Alberti, K.G.M.M., Shaw, J., 2001. Global and societal implications of the diabetes epidemic. *Nature.* 414, 782–787.

# 국문초록

## Part 1

천연물은 새로운 당뇨치료제 개발에 있어서 유용한 자원이라 할 수 있으며 각지에서 과거로부터 민족의학적으로 유용하게 사용되어온 식물 중에서 과학적으로 기전과 효능이 평가되지 못한 식물이 많다. 약용식물로부터 당뇨치료를 위한 소재를 발굴하는 연구를 진행하는 가운데, 전통적으로 베트남에서 제 2형 당뇨병치료에 사용되어 왔던 *Gynostemma longipes* 잎의 95% EtOH 추출물이 2-NBDG를 사용한 assay에서 glucose uptake를 유의적으로 증가시키는 것을 확인하였다. *G. longipes*의 생리활성과 화학성분에 대한 연구가 거의 되어 있지 않았기 때문에 본 연구는 항당뇨 생리활성을 나타내는 단일물질의 분리를 목적으로 수행되었다. *Gynostemma longipes* C.Y.Wu는 박과 (Cucurbitaceae) 에 속하는 다년생 덩굴성식물로서 베트남의 Ha Giang 지방의 허브농장에서 재배되어 수집되었다. 본 연구를 통하여 3,4-*seco* dammarane계열 3종 (1-3), hexanordammarane glycoside 계열 2종 (4-5), dammarane 계 glycoside 계열 5종 (6-10) 을 포함하여 총 10종의 신규물질을 분리하였으며 분리된 화합물의 구조는 UV, IR, NMR, MS/MS를

포함한 이화학적 및 분광학적 분석과 기존문헌들과의 비교를 통하여 동정하였다. 분리된 화합물 10종에 대하여 분화된 3T3-L1 adipocyte에서 2-NBDG를 사용한 glucose uptake에 미치는 활성을 평가하였을 때, 화합물 **1, 2, 4** 및 **8**이 Glucose transporter type 4 (GLUT4) 전위 (translocation)을 통하여 강한 glucose uptake 촉진효과를 보였다. 세포 내로의 2-NBDG uptake 촉진효과의 기전을 확인하기 위하여 glucose uptake 조절에 중요한 역할을 한다고 알려진 AMPK pathway에 미치는 활성을 검색하였을 때, 화합물 **1, 2, 4, 8** 및 **10**이 mouse C2C12 근관세포 (myotube)에서 인산화된 AMPK와 ACC의 발현을 상향조절하는 것을 확인하였다. 위 결과들은 당뇨병 치료제로서의 *G. longipes*의 전통적인 용례와도 일치함을 알 수 있다.

## Part 2

*Camellia japonica* L. 은 차나무과 (Theaceae)에 속하는 상록수로서 한국, 중국, 일본에서 널리 자생하며 또한 재배되기도 한다. 전통적으로 *C. japonica* 의 꽃봉오리는 상혈 (vomiting of blood), 출혈에 사용되었으며 강장, 항염증의 목적으로도 사용되어왔다. 본 연구는 파킨슨병의 rotenone model 에서 신경보호효과를 검색하는 assay 를 수행하였을 때 *C. japonica* 꽃의

70% EtOH 추출물이 강력한 신경보호효능을 나타내는 후보군으로 선정되었기에 본 활성을 나타내는 단일화합물 분리를 목적으로 실험을 수행하였으며 6 종의 신규 3,4-*seco*-28-noroleanane 계열 triterpenoid (**11-16**)를 분리하였다. 분리된 화합물의 구조는 UV, IR, NMR, MS/MS 를 포함한 이화학적 및 분광학적 분석과 기존문헌들과의 비교를 통하여 동정하였다. 분리된 화합물에 대하여 신경보호활성을 평가하였을 때, 화합물 **13-16** 이 human dopaminergic SH-SY5Y 세포에서 효과적으로 신경독성에 대한 보호효과를 나타내었다. 특히 화합물 **15**의 경우,  $\alpha$ -synuclein 발현과 rotenone 처리에 의한 세포 내 활성산소발생을 억제함으로 강력한 세포보호활성을 나타내었다. 더욱이 이 화합물은 autophagy marker 로 알려진 microtubule-associated protein 1A/1B light chain 3 (LC3)을 유도하며 rotenone 처리에 의해 유도된 염색체 응축을 감소시켰다. 위 결과들을 종합하였을 때, 본 연구를 통하여 파킨슨 질병의 치료제개발에 있어 유용한 후보물질을 제시하였다고 사료된다.

주요어: *Gynostemma longipes*, 당뇨병, triterpenes, *Camellia japonica*, 신경보호효과, 파킨슨질병.

학번: 2015-30776

## Scientific Publication

No.	Name of paper	Name of journal	Year published	Author
1	12,23-Dione dammarane triterpenes from <i>Gynostemma longipes</i> and their muscle cell proliferation activities via activation of the AMPK pathway	Scientific Reports	accepted	Co-first author
2	Insulin Mimetic Activity of 3,4-Seco and Hexanordammarane Triterpenoids Isolated from <i>Gynostemma longipes</i>	Journal of Natural Products	2018	Co-first author
3	Hypoglycemic triterpenes from <i>Gynostemma pentaphyllum</i>	Phytochemistry	2018	Co-first author
4	Flavone glycosides from <i>Sicyos angulatus</i> and their inhibitory effects on hepatic lipid accumulation	Phytochemistry	2018	Co-author
5	Piperlongumine activates Sirtuin1 and improves cognitive function in a murine model of Alzheimer's disease	Journal of Functional Foods	2018	Co-author
6	Discrimination of different geographic varieties of <i>Gymnema sylvestre</i> , an anti-sweet plant used for the treatment of type 2 diabetes	Phytochemistry	2018	Co-author
7	Sesquiterpenoids with Various Carbocyclic Skeletons from the Flowers of <i>Chrysanthemum indicum</i>	Journal of Natural Products	2017	Co-author
8	Polyoxygenated Steroids from the Sponge <i>Clathria gombawuiensis</i>	Journal of Natural Products	2017	Co-author
9	C-Methylated Flavonoid Glycosides from <i>Pentarhizidium orientale</i> Rhizomes and Their Inhibitory Effects on the H1N1 Influenza	Journal of Natural Products	2017	Co-author

Virus

No.	Name of paper	Name of journal	Year published	Author
10	Anti-influenza effect of the major flavonoids from <i>Salvia plebeia</i> R.Br. via inhibition of influenza H1N1 virus neuraminidase	Natural Product Research	2017	Co-author
11	<b>Antiviral escin derivatives from the seeds of <i>Aesculus turbinata</i> Blume (Japanese horse chestnut)</b>	<b>Bioorganic &amp; Medicinal Chemistry Letters</b>	<b>2017</b>	<b>Co-first author</b>
12	<b>PTP1B inhibitors from the seeds of <i>Iris sanguinea</i> and their insulin mimetic activities via AMPK and ACC phosphorylation</b>	<b>Bioorganic &amp; Medicinal Chemistry Letters</b>	<b>2017</b>	<b>Co-first author</b>
13	Anthraquinones from <i>Morinda longissima</i> and their insulin mimetic activities via AMP-activated protein kinase (AMPK) activation	Bioorganic & Medicinal Chemistry Letters	2017	Co-author
14	<b>Antiviral phenolics from the leaves of <i>Cleistocalyx operculatus</i></b>	<b>Fitoterapia</b>	<b>2016</b>	<b>First author</b>
15	<b>3,4-seco-28-Nor-oleanane triterpenes from <i>Camellia japonica</i> protect from neurotoxicity in a rotenone model of Parkinson's disease</b>	<b>Tetrahedron</b>	<b>2016</b>	<b>Co-first author</b>
16	Microwave assisted synthesis and cytotoxic activity evaluations of new benzimidazole derivatives	Tetrahedron Letters	2016	Co-author

17	Chemical constituents from <i>Melicope pteleifolia</i> leaves	Phytochemistry	2016	Co-author
----	---	----------------	------	-----------

No.	Name of paper	Name of journal	Year published	Author
18	Protein Tyrosine Phosphatase 1B Inhibitors from the Stems of <i>Akebia quinata</i>	Molecules	2016	Co-author
19	Antiviral activities of compounds from aerial parts of <i>Salvia plebeian</i> R. Br	Journal of Ethnopharmacology	2016	Co-author
20	Discovery of inhibitory materials against PEDV corona virus from medicinal plants	Japanese Journal of Veterinary Research	2016	Co-author
21	<b>Oleanane Triterpenes from the Flowers of <i>Camellia japonica</i> Inhibit Porcine Epidemic Diarrhea Virus (PEDV) Replication</b>	<b>Journal of Medicinal Chemistry</b>	<b>2015</b>	<b>Co-first author</b>
22	Antiviral Indolosesquiterpenoid Xiamycins C–E from a Halophilic Actinomycete	Journal of Natural Products	2015	Co-author
23	Jubanines F–J, cyclopeptide alkaloids from the roots of <i>Ziziphus jujuba</i>	Phytochemistry	2015	Co-author
24	Three new coumarins from <i>Saposhnikovia divaricata</i> and their porcine epidemic diarrhea virus (PEDV) inhibitory activity	Tetrahedron	2015	Co-author
25	Dammarane triterpenes as potential SIRT1 activators from the leaves of <i>Panax ginseng</i>	Journal of Natural Products	2014	Co-author



## ACKNOWLEDGEMENT

Undertaking this doctoral research has been a truly life-changing experience for me and it would not have been possible without Seoul National University. First and foremost, I would like to express my sincere gratitude to my supervisor, Professor Oh Won Keun, for all the support and encouragement during last 6.5 years I studied in Korea. Without his guidance, motivation, and immense knowledge, this PhD would not have been achievable.

I would also like to thankfulness to Professor Kim Jinwoong, Professor Sung Sang Hyun, Professor Kang Keon Wook, and all professors in College of Pharmacy for their support and great lectures. In addition, my sincere thanks to Professor Park Junsoo, Professor Darren R. Williams, Professor Lee Chul-Ho, and Professor Tran Van On for helping and providing the idea when I performed the experiment.

I am grateful to all the faculty, staff members and lab technicians in College of Pharmacy, whose services turned my research a success.

This PhD study would not have been possible without the corporation and support of team members. I am also very grateful to my seniors, especially Professor Yang Jun-Li, Dr. Dao Trong Tuan, Kim Jayeon for their assistance when I was a freshman in the lab. Moreover, a very special thank you to all our lab members Dr. Lee Dong Young, Dr. Huh Jung Moo, Dr. Kim Hyeon Woo, Dhodary Basanta, An Jin Pyo, Lee Heeju, Lee Ba Wool, Cho Hyomoon, Woo Sun Min, Ryu Byeol, Park Eun Jin, Park Jung Geun, Han Sohee, Lee Yae Rin and Professor Kang's members (Dr. Nguyen Thuy Phuong, Dr. Bui Thu Quyen, Kim Jiwon). I would like to say a heartfelt thank you to Pham Ha Thanh Tung, Nguyen Ngoc Hieu, Doan Thi Phuong, Dang Lan Huong for always encouraging me.

I would like to thank all colleagues in the College of Natural Sciences and Department of Chemistry. Special thanks to Professor Bui Thi Buu Hue for her support and continuous encouragement throughout my years of study.

Cuối cùng, con chân thành biết ơn gia đình, ba Hà Văn Khi, mẹ Lê Thị Thu, anh trai Hà Duy Quý, Hà Duy Quang, chị Lê Thị Hà Giang, cháu Hà Lê Kim Thy luôn bên cạnh chia sẻ vui buồn, động viên, và ủng hộ con trong suốt 6.5 năm học ở Korea. Chúc gia đình luôn mạnh khỏe và bình an trong Chúa, Đức Mẹ và Ông Trên./.



RightsLink®



ACS Publications  
Most Trusted. Most Cited. Most Read.

**Title:** Insulin Mimetic Activity of 3,4-Seco and Hexanordammarane Triterpenoids Isolated from *Gynostemma longipes*  
**Author:** Ha Thanh Tung Pham, Thi Kim Quy Ha, Hyo Moon Cho, et al  
**Publication:** Journal of Natural Products  
**Publisher:** American Chemical Society  
**Date:** Nov 1, 2018  
Copyright © 2018, American Chemical Society

**PERMISSION/LICENSE IS GRANTED FOR YOUR ORDER AT NO CHARGE**

This type of permission/license, instead of the standard Terms & Conditions, is sent to you because no fee is being charged for your order. Please note the following:

- Permission is granted for your request in both print and electronic formats, and translations.
- If figures and/or tables were requested, they may be adapted or used in part.
- Please print this page for your records and send a copy of it to your publisher/graduate school.
- Appropriate credit for the requested material should be given as follows: "Reprinted (adapted) with permission from (COMPLETE REFERENCE CITATION). Copyright (YEAR) American Chemical Society." Insert appropriate information in place of the capitalized words.
- One-time permission is granted only for the use specified in your request. No additional uses are granted (such as derivative works or other editions). For any other uses, please submit a new request.



# Tetrahedron

*Certificate of publication for the article titled:*  
"3,4-seco-28-Nor-oleanane triterpenes from *Camellia japonica* protect  
from neurotoxicity in a rotenone model of Parkinson's disease "

---

*Authored by:*  
Jun Li Yang  
Thi Kim Quy Ha

---

*Published in:*  
Volume 72, Issue 23 (2016), Pages 3240-3249